Calibration and quality assessment of DESCARTES—grabsampler for stratospheric tracers

Johan Arvelius

IRF Scientific Report 286
September 2005

ISSN 0284-1703
ISBN 91-7305-945-5

INSTITUTET FÖR RYMDFYSIK
Swedish Institute of Space Physics

Kiruna, Sweden

Calibration and quality assessment of DESCARTES

—grabsampler for stratospheric tracers

Johan Arvelius
Swedish Institute of Space Physics
Kiruna

7th September 2005

Doktorsavhandling vid Institutet för rymdfysik
Doctoral thesis at the Swedish Institute of Space Physics
Calibration and quality assessment of DESCARTES —grabsampler for stratospheric tracers.
Online version and errata at: `http://www.irf.se/publications/SciReports/`
Typeset by the author in LaTeX.
Kiruna, September 2005
Rev. 1

IRF Scientific Report 286
ISSN 0284-1703
ISBN 91-7305-945-5 pp. 182 pages
Printed at the Swedish Institute of Space Physics
Box 812
SE-981 28, Kiruna, Sweden
September 2005

Sammanfattning

DESCARTES är ett lätt ballongburet provtagningsinstrument för stratosfäriska spårgaser. Det är utvecklat vid universitetet i Cambridge. DESCARTES-teamet vid Institutet för rymdfysik (IRF) i Kiruna har under åren 1997–2000 genomfört 33 flygningar med två olika versioner av instrumentet från nordliga latituder.

Det generella intresset av långlivade stratosfäriska spårgaser är att studera den globala cirkulationen i stratosfären och utbytet av luft mellan stratosfären och troposfären. För studier av den kemiska ozonnedbrytningen i stratosfären spelar långlivade spårgaser en avgörande roll som referens för att skilja mellan variation i ozonkoncentrationen av kemiskt och dynamiskt ursprung.

Denna avhandling fokuserar på kalibrering och kvalitetssäkring av mätningar gjorda med den tredje versionen av DESCARTES-instrumentet hemmahörande vid IRF. Två i grunden olika kalibreringsförfaranden för instrumentet behandlas. Osäkerhetsuppskattningar är gjorda för båda dessa metoder och resultaten är prövade i laboratorietester. Dessutom jämförs resultaten från två versioner av DESCARTES och andra instrument. Analyserade data från samtliga lyckade flygningar presenteras.

Den grundläggande principen för instrumentet är att pumpa luftprover genom en fälla som innehåller en bädd av det kemiska adsorptionsmaterialet Carboxen, som adsorberar ett antal spårgaser. När instrumentet hämtats tillbaka efter en flygning gasas de adsorberade ämnena i fällan ut genom att fällan upphettas på elektrisk väg. De utgasade ämnena analyseras med gaskromatografi. I praktiken kan endast CFC-11 analyseras.

Den slutgiltiga bestämningen av blandningsförhållandet från instrumentet är direkt beroende av att adsorptionen i fällorna för de ämnen man vill undersöka är fullständig. En serie laboratorieexperiment har genomförts där två likadana fällor kopplats efter varandra. På så sätt har tillförlitligheten av den första fällan kunnat studeras genom att uppmäta hur mycket som bryter igenom till den andra fällan. En modell har utvecklats för att förstå resultatet av dessa tester och kunna kompensera för eventuella genombrott vid provtagning under flygningar. Modellen visade att adsorptionen i fällorna inte kan förklaras med enkel kromatografisk teori. Resultaten ger endast möjlighet att bedöma osäkerheten i mätningarna till följd av risken för genombrott.

Nyckelord: Adsorption, Ballong, Carboxen, CFC, Halogeniserade kolväten, Klor-Flourkarbon, Spårgas, Stratosfärisk spårgas.

Abstract

DESCARTES is a light-weight, balloon-borne grab sampler for stratospheric long-lived tracers developed at the University of Cambridge. 33 flights have been performed with two versions of the instrument at northern latitudes by the DESCARTES team at the Swedish Institute of Space Physics (IRF) in Kiruna during the years 1997–2000.

The general interest in long-lived stratospheric tracers is to study the general global circulation of air in the stratosphere and the exchange between the stratosphere and troposphere. In the study of chemical ozone depletion in the stratosphere, long-lived tracers serve as an important reference to distinguish between the variations in ozone of dynamical and chemical origin.

This thesis focuses on calibrations and quality assessment of the measurements made with the third version of the DESCARTES instrument based at IRF. Two different general approaches to make calibrations are discussed. Uncertainty estimations for both of these methods are made and the results are tested by laboratory methods and by comparisons to other instruments, including comparisons between two versions of DESCARTES. Analyzed and calibrated flight data for all successful flights are presented.

The basic principle of the instrument is to chemically adsorb a number of tracers (in practice only CFC-11 is measured) in an adsorption bed of Carboxen in a micro trap through which the sampled air is driven by a pump. After recovery the adsorbed species in the trap is desorbed by electrical heating of the trap and analysed by gas chromatography.

The resulting estimated mixing ratios from the instrument are directly dependent on the adsorption of the sampled species being quantitative in the traps. Laboratory experiments are described using two traps in series, where the performance of the first is tested by sampling the breakthrough by the second. A model is developed to recreate these tests in order to be able to compensate for breakthrough during flights. The model showed that the adsorption in the traps is not explained by simple chromatographic theory and the results allow us only to give an estimation of the uncertainty due to breakthrough.

Keywords: Adsorption, Balloon, Carboxen, CFC, Chloro-Fluoro Carbon, Grab sampling, Halocarbon, Molecular sieve, Stratospheric tracer, Tracer.

Contents

1 Stratospheric tracers **1**
1.1 Dynamical tracers 1
1.2 Chemical tracers 1
1.2.1 Chemical tracers with stratospheric source 2
1.2.2 Chemical tracers with tropospheric source 2
1.2.3 Chemical tracers with neither stratospheric source nor sink 3
1.3 Combination of tracers 4
1.4 Polar vortex 5
1.5 CFCs in the stratosphere 5

2 Working principles **7**
2.1 Sampling 9
2.1.1 Storing flight data 11
2.2 Adsorbent Carboxen 13
2.3 Heating system 13
2.4 Chromatographic analysis 14
2.5 Reference to other parameters 16

3 Calibrations **19**
3.1 Calibration standards 20
3.2 Flow meter calibrations 22
3.2.1 Calibration function 23
3.3 Direct air standard absolute calibrations 23
3.3.1 Sample boxes individuality 24
3.3.2 Flight data quality concerns 25
3.4 Indirect calibration method 26
3.4.1 ECD response 26
3.4.2 Individual trap response 27
3.4.3 Inter flight analysis response changes 30
3.4.4 Sample boxes individuality 37
3.4.5 Absolute calibration 39
3.4.6 Calculation of sample mixing ratio 42
3.5 Test of calibrations 42
3.6 Other species than CFC-11 42
3.6.1 CFC-113 44
3.6.2 Methyl chloroform and carbon tetrachloride 47
3.7 Discussion 47

3.8 Conclusions 51

4 Simulation of trap adsorption **53**
4.1 Introduction 53
4.2 Quantitative estimation 57
4.3 Experiments 58
4.3.1 Results 60
4.4 General model description 62
4.5 Distribution approach 64
4.5.1 Inflow distribution 66
4.5.2 Desorption redistribution 66
4.5.3 Model performance monitoring 67
4.5.4 Algorithm 68
4.6 Serial approach 69
4.6.1 Differential adsorption strength 70
4.6.2 Langmuir isotherm 72
4.7 Model validity 73
4.7.1 Physical errors 73
4.7.2 Numerical errors 74
4.8 Interpretation 74
4.9 Qualitative model checks 74
4.10 Simulation results 76
4.10.1 Langmuir isotherm 78
4.10.2 No desorption 78
4.10.3 Different binding strength 80
4.11 Quantitative breakthrough estimation 81
4.11.1 Sample volume estimation 84

5 Uncertainty estimations **89**
5.1 Flow estimation 89
5.2 Representativeness of samples 90
5.3 Chromatogram peak integration 90
5.4 Breakthrough 92
5.5 Direct calibration method 93
5.5.1 Precision 93
5.5.2 Absolute uncertainty 94
5.6 Indirect calibration method 94
5.6.1 ECD response function 95
5.6.2 Precision 95
5.6.3 Absolute uncertainty 97
5.7 Tests of uncertainties 97
5.7.1 Test on calibrations 98
5.7.2 Low pressure 98
5.7.3 Double flights 98
5.7.4 Tropospheric samples on ground 101
5.7.5 Tropospheric samples during flights 102
5.8 Conclusions 104

6 Possible future improvements **105**
6.1 Choice of material . . . 105
6.2 Traps . . . 105
6.3 Heating system . . . 106
6.4 Calibration . . . 106
6.5 Determination of sample sizes . . . 106
6.6 Breakthrough control . . . 107

7 Measurement activities **109**
7.1 1997, ILAS validation campaign . . . 109
7.2 1999, THESEO and SKERRIES campaigns . . . 111
7.3 1999–2000, Several campaigns . . . 116
7.3.1 In vortex flights . . . 116
7.3.2 Comparisons to other instruments . . . 118
7.3.3 Comments to flights . . . 120
7.4 Published data . . . 129

A Practical treatment of DESCARTES **131**
A.1 Sample box . . . 131
A.2 Analysis software . . . 132
A.2.1 Quick start . . . 136
A.3 Heater box . . . 136
A.4 Gas chromatograph . . . 138
A.5 Updates on instrument . . . 138

B Detailed flight instructions **143**
B.1 Before leaving . . . 143
B.2 Bring to flight . . . 143
B.3 Before flight . . . 144
B.4 Delivery time . . . 146
B.5 After recovery . . . 147
B.6 Analysis . . . 148
B.7 After analysis . . . 149

C Calibration constants **151**

D Flight checklist **153**

Bibliography **159**

Index of acronyms **169**

Index of notation **171**

Index **175**

List of Figures

1.1 Tracers in the atmosphere with a polar vortex formed in the winter polar area. 2

2.1 DESCARTES III.2 with a mounted sample box. 8
2.2 Sample box. 8
2.3 Schematic illustration of DESCARTES sampling and analysis . . . 9
2.4 Sample traps. 10
2.5 Schematic of DESCARTES instrument 10
2.6 Example of data file from onboard computer 12
2.7 Schematic of the sampling box and GC system during analysis. . . 15
2.8 Example of chromatograms from both heatings of an analysis of one sample in a flight. 16

3.1 Inter-comparison between the two different absolute air standards used. 21
3.2 Example of flow meter calibration. 22
3.3 Example of direct absolute calibration curve. 24
3.4 All direct absolute calibration curves. 25
3.5 Example of ECD response calibration Box I, CFC-11. 28
3.6 Example of trap individuality tests for box I. 28
3.7 The ECD response calibration compensated for trap individuality . 31
3.8 Results of test samplings performed in all analysis 33
3.9 Relationship between the mean response of test runs and median response of calibration runs during repeatability tests. 34
3.10 Calibration results as function of R values for calibration runs sampled by DESCARTES. 34
3.11 ECD response calibration compensated for analysis response as well as trap individuality. 36
3.12 Details of absolute calibrations, with and without compensation for analysis response. 37
3.13 ECD response for all boxes 38
3.14 ECD response for all boxes compensated for analysis response . . . 39
3.15 Example of calibration for absolute response factor α. 40
3.16 Calibrations for absolute response factor α, all boxes 41
3.17 Results of calibrations from the direct absolute calibration method 43
3.18 Results of calibrations from the indirect absolute calibration method 43
3.19 Calibration curve for CFC-113 the same way as figure 3.7. 44

3.20 Direct method absolute calibration curve for CFC-113. 45
3.21 Correlations between chromatographic peak areas of CFC-11 and CFC-113 sampled through different sample lines. 46
3.22 Dynamco Dash-1 switch and pressure meter. 47
3.23 Direct method absolute calibration curve for CFC-113. 48
3.24 Direct method absolute calibration curve for CFC-113. 49
3.25 Calibration test for box II. Similar to the top panels of figures 3.17 and 3.18. 50
3.26 Calibration test for box IV. 51

4.1 Theoretical breakthrough according to *Yoon and Nelson* [1984] . . 56
4.2 Theoretical breakthrough according to *Senum* [1981] 57
4.3 Accumulated breakthrough of CFC-11 for different flow speeds . . 60
4.4 Comparison between the experimental accumulated breakthrough and the two theories discussed. 61
4.5 Accumulated breakthrough of CFC-11 for low-pressure experiment 61
4.6 Histogram representation of the model. 63
4.7 Contents in model bins after some iterations and trap exchange. . 64
4.8 The principle of the algorithm for the distribution approach. . . . 65
4.9 The principle of the algorithm for the serial approach. 70
4.10 The principle of the algorithm with two types of adsorption sites. . 71
4.11 The principle of the algorithm with correction for Langmuir isotherm. 73
4.12 Time series of distribution of CFC in the trap. 75
4.13 Breakthrough at different flow velocities, see text for details. . . . 76
4.14 Linear relationship as predicted by *Yoon and Nelson* [1990]. 77
4.15 Breakthrough at different flow velocities 77
4.16 Results with Langmuir isotherm added. 79
4.17 Results with Langmuir isotherm higher desorption coefficients. . . 79
4.18 Results from test with no adsorption in the investigated species only saturation of adsorption sites. 80
4.19 Results with some of the adsorption sites giving 10 times lower desorption. 81
4.20 Measured breakthrough from double trap experiments. From *Roslin* [2003]. 82
4.21 Direct proportionality coefficients of breakthrough as a function of sampled mass or volume from double trap experiments assuming direct proportionality of breakthrough to sampled mass or volume. 83
4.22 Pressure parameter ϕ as a function of mass flow for DESCARTES II flights. 85
4.23 Sample volumes and volume flows for tests, calibrations and flights. 87

5.1 Integration test made manually and independent by three operators. 91
5.2 Direct absolute calibration curve common to all boxes. 93
5.3 ECD response function with conf. interval of the curve fit 96
5.4 Uncertainty estimations of the direct absolute calibration approach applied to calibration runs as presented in figure 3.17. 99
5.5 Uncertainty estimations of the indirect calibration approach applied to calibrations as presented in figure 3.18. 99

5.6 Results of low pressure test from the direct absolute calibration method. . . . 100
5.7 Results of low pressure test from the indirect absolute calibration method. . . . 100
5.8 Flight profiles from flight 000515. DESCARTES III.2 profile in blue and DESCARTES II in green. . . . 101
5.9 Flight profile from flight 001117. . . . 102
5.10 Results from samplings done with DESCARTES of ambient air on ground analyzed with the direct absolute calibration method. . . . 103
5.11 Same tests as in figure 5.10 analyzed with the indirect calibration method. . . . 103

7.1 Example of chromatogram from the flight 981117 from Andøya. . . . 112
7.2 Flight profile from flight 990127. . . . 113
7.3 Flight profile from flight 990212 114
7.4 Flight profile from flight 990218. . . . 114
7.5 Flight profile from flight 990420 115
7.6 Flight profile from flight 990826. . . . 115
7.7 Ozone and potential temperature measurements interpolated to CFC levels from DESCARTES measurements. . . . 117
7.8 Flight profiles of CFC-11 inside vortex winter and spring 1999–2000. 118
7.9 Correlations of CFC-11 and ozone inside vortex winter and spring 1999–2000. . . . 119
7.10 Flight profile from flight 991203. Comparison parameters measured by accompanying radio sonde and ozone sonde. . . . 123
7.11 Flight profile from flight 991215. . . . 123
7.12 Flight profile from flight 000128. Pressure and temperature measurements from radio sonde and ozone from SAOZ. . . . 124
7.13 Flight profile from flight 000209. Pressure and temperature measurements from radio sonde and ozone from SAOZ. . . . 124
7.14 Flight profile from flight 000301. . . . 125
7.15 Flight profile from flight 000305. . . . 125
7.16 Flight profile from flight 000307. Pressure and temperature measurements from radio sonde and ozone from SAOZ. . . . 126
7.17 Flight profile from flight 000403. Pressure and temperature measurements from radio sonde and ozone from SAOZ. . . . 126
7.18 Flight profile from flight 000404. . . . 127
7.19 Flight profiles from flight 000616. . . . 127
7.20 Flight profile from flight 000814. DESCARTES III.2 in blue and DESCARTES II in green. . . . 128
7.21 Flight profile from flight 000922. . . . 128
7.22 Flight profile from flight 001211. . . . 129

A.1 Trap heater switch, when valco valve is in trap position 11. . . . 132
A.2 Connection to valve 3 in the GC 137

List of Tables

3.1 Analysed mixing ratios of used standards. 20

7.1 Flights during the ILAS Validation Campaign 1997 109
7.2 Flights 1998 to 2000 110

A.1 Explanations of Chemstation methods for use with DESCARTES . 133
A.2 Descriptions of Chemstation sequences to use for DESCARTES analysis. 134
A.3 Temperature parameters for heating methods. 135

C.1 Calibration constants for flow meter calibration 1999-10-13 used for flights to that date. 151
C.2 Calibration constants for flow meter calibration 1999-10-14 used for flights after that date. 151
C.3 Calibration constants for flow meter calibration of DESCARTES II 2000-09-19. 152
C.4 Calibration constants for ECD response functions. 152

Chapter 1

Stratospheric tracers

Tracers are of great use for studies of both dynamical and indirectly also chemical processes in the atmosphere. A tracer is some property of an airmass that labels it i. e. something that is conserved under the dynamical processes to be studied in an airmass and which distinguishes it from other airmasses. Processes with different time scales need tracers that are conserved under these time scales. To be useful, tracers also need to have significant spatial variations over appropriate length scales. So a tracer with the right balance between temporal and spatial variations has to be found for the specific processes to be studied. For example extremely long-lived tracers always get smeared out with time and do not give the large gradients needed to resolve small scale phenomena. Tracers commonly used for stratospheric processes are of two types, dynamical and chemical.

1.1 Dynamical tracers

Tracers in this text are used to study dynamical phenomena and are thereby in some sense dynamical tracers, but the term dynamical tracer will here be used for dynamical features of the airmass that can be used as tracers.

In the stratosphere where the air is stratified the potential temperature (θ) acts as a good dynamical tracer. As most transport is adiabatic and conserves potential temperature (θ) deviations from this pattern are easily seen. The only sources and sinks of θ are radiative heating/cooling and turbulent mixing of airmasses.

The other important dynamical tracers that are used are potential vorticities. There are different potential vorticities defined, each conserved under different transports.

1.2 Chemical tracers

All truly conservative gases in the atmosphere are well mixed and not useful as tracers. Species that have sources and sinks in different regions of the atmosphere will give a gradient between these regions. This gradient makes it possible to use the gas as a tracer. Depending on the location of these regions the tracers can be used for different purposes.

1.2.1 Chemical tracers with stratospheric source

Gases that undergo chemical reactions in the stratosphere leave products that might be useful tracers. Reactions that are irreversible in the stratosphere like photolysis of Chloro Fluoro Carbons (CFCs) give tracers that might be used to study large scale phenomena like Brewer-Dobson circulation. In the example with CFCs the fluorine reacts with hydrogen to form an inert tracer; hydrogen fluoride, while the chlorine takes part in many chemical reactions and only the sum of all inorganic chlorine can be viewed as an inert tracer. The different chlorine species might be used as shorter lived tracers. For example after a local chlorine activation event the active chlorine species group can be used to trace this airmass for a while.

1.2.2 Chemical tracers with tropospheric source

Gases such as CFCs that have sinks only in the stratosphere exhibit concentration gradients from the tropical tropopause that acts as the source region. If the sink, as in the CFC case, is high up in the stratosphere (photolysis by UV light) there will be a gradient decreasing with height. As most transport in the stratosphere is adiabatic this gradient is rather similar to the potential temperature gradient all over the globe. This is the case for all tracers that have a lifetime much longer than the time scale of quasi-horizontal transport at the height of interest (weeks to months) and it is said that these tracers are in slope equilibrium.

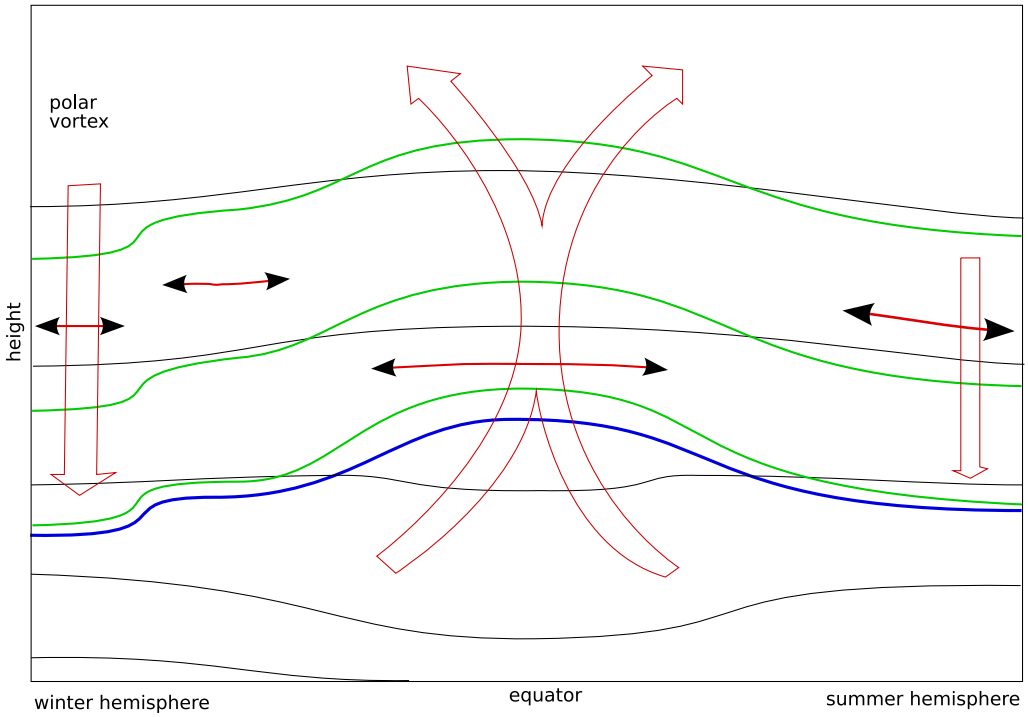

Figure 1.1: Tracers in the atmosphere with a polar vortex formed in the winter polar area. Thin black lines are θ-level iso-surfaces, thick blue line the tropopause, green lines iso-surfaces of a long-lived tracer. Red-black arrows indicate fast adiabatic transports while the hollow red arrows slower diabatic circulation.

If the horizontal transport were infinitely faster than both the vertical transport and the chemical conversion rate, iso-surfaces of such a tracer and potential temperature should coincide completely. As indicated in figure 1.1 the iso-surfaces of a long-lived tracer (such as CFCs) slope on the average more steeply towards the poles than the iso-surfaces of θ. It was shown by *Mahlman et al.* [1986] and *Holton* [1986] that long-lived tracers will all show similar slopes determined by an equilibrium between meridional advection and isentropic quasi-horizontal transport. These are tracers in slope equilibrium. In a little more detail, the barriers to the horizontal flow at the edges of the polar vortex and tropical pipe, can be seen as larger gradients. On the shorter time-scale of one winter the cooling of the polar vortex also is seen as a vertical shift in iso-surfaces of tracers over the vortex edge illustrated in figure 1.1 and can then be used to determine the subsidence.

These properties of the tracers are the major source for understanding of the large-scale global convection.

1.2.3 Chemical tracers with neither stratospheric source nor sink

A very special case is the tracer that is completely inert in the stratosphere. From what has been said earlier this cannot act as a tracer unless the tropospheric abundance is changing over time in a long and stable trend. The abundance of the tracer in the atmosphere in this case gives the time of entry to the stratosphere. When the stratospheric air is mixed, only species that have a linear tropospheric trend can be used to derive the mean age of the airmass in the stratosphere. This is called a chronological tracer and the best example is carbon dioxide, which has increased steadily at 3.3 ± 0.1 Pg/a during the 80's and 3.2 ± 0.1 Pg/a during the 90's [*Houghton et al.*, 2001, p. 190]. However the seasonal growth dependence for plants makes an overlayed one-year oscillation in abundance of carbon dioxide that causes problems in sampling. CF_3-CF_2Cl (CFC-115) and SF_6 are so long-lived in the stratosphere that the tropospheric trend is always dominant and they might also be used as chronological tracers.

From measurements of a chronological tracer the mean age of airmass ($\bar{\Gamma}$) can be derived. It has then been showed by *Volk et al.* [1997] that the lifetime of other trace-gases in the stratosphere can be derived as

$$\tau = -\frac{\bar{\sigma} M_\mathrm{a}}{M_\mathrm{u} C \left.\frac{d\chi}{d\bar{\Gamma}}\right|_{\bar{\Gamma}=0}} \tag{1.1}$$

where $\bar{\sigma}$ is the mass weight average mean atmospheric mixing ratio in the atmosphere, M_a and M_u are the dry mass of the whole atmosphere and the atmosphere above the tropopause, C is a correction factor for nonlinear growth and χ is the actual mixing ratio. Combining equation 1.1 for two different tracers gives a new ratio of their lifetimes

$$\frac{\tau_1}{\tau_2} = \frac{\bar{\sigma}_1}{\bar{\sigma}_2} \frac{C_2}{C_1} \left.\frac{d\chi_2}{d\chi_1}\right|_\mathrm{tp}, \tag{1.2}$$

where tp denotes that the ratio should be taken as the limit value in the stratosphere approaching the tropopause. This eliminates the need to know the masses

and age but unfortunately the $\bar{\sigma}$ and C need a chemical transport model to be calculated.

1.3 Combination of tracers

Tracers that are long-lived compared to quasi-horizontal transport on the global scale are in slope equilibrium. The vertical gradients of these tracer fields are dependent on the lifetime of the species in that height region. This means that a vertical profile for the tracer depends on the strength and distribution of the sink region.

As the gradient of the tracer abundance depends on the sink regions, comparisons of height profiles of different tracers, for example plotting abundance of one as a function of the other, gives information on the sinks and lifetimes of the tracers compared to each other. For two tracers in slope equilibrium such a plot will show a tight correlation curve [*Plumb and Ko*, 1992]. For tracers that are also long lived in comparison with the rapid exchange surfaces in vertical motion this correlation forms a straight line [*Plumb and Ko*, 1992]. If at least one of the components does not fulfil this the correlation curve might be compact but curved. Mixing of air between airmasses from different regions in this tracer space will show up as straight interconnections between these points. From simultaneous measurements of these tracers such anomalous points are an indication of mixing [*Plumb et al.*, 2000; *Waugh et al.*, 1997].

Tracers that have their sink region in the upper stratosphere, are inert just above the tropopause. It has been shown by *Plumb and Ko* [1992] that, in a steady state, the ratio of their stratospheric lifetimes can be derived from the linear relation of their abundances.

$$\frac{\tau_1}{\tau_2} \approx \frac{d\sigma_2}{d\sigma_1} \left.\frac{\sigma_1}{\sigma_2}\right|_{\mathrm{tp}}, \tag{1.3}$$

where τ is the lifetime, σ is the steady state mixing ratio and the indices 1 and 2 refers to the two species.

The model of *Plumb and Ko* [1992] used the assumptions of fast horizontal flows and steady state. However it became clear from measurements that, for example, volcanic aerosols stay in the tropics for a long time and exhibit steeper latitudinal gradients than expected [e.g. *Trepte and Hitchman*, 1992], showing that the latitudinal flow was restricted in a region separating the tropical region from the mid latitudes, a transport barrier. *Plumb* [1996] further showed that, with the approximation of a rigid transport barrier in the lower stratosphere between the tropical region and the mid latitudes, allowing only diffusive transport, there must be net up-draft in the tropical region and a down-welling in the extra tropical region. In this model the tracer–tracer slope coefficient above the tropopause is shown to be equal to the fraction of the net exports from each half of the stratosphere:

$$\left(\left.\frac{d\sigma_1}{d\sigma_2}\right|_{\mathrm{tp}}\right)_{\mathrm{N}} = \frac{\Gamma_{1\mathrm{N}}}{\Gamma_{2\mathrm{N}}}; \left(\left.\frac{d\sigma_1}{d\sigma_2}\right|_{\mathrm{tp}}\right)_{\mathrm{S}} = \frac{\Gamma_{1\mathrm{S}}}{\Gamma_{2\mathrm{S}}}. \tag{1.4}$$

The net export from each half of the stratosphere Γ is, in the case of tracers with only stratospheric sinks, equal to the sinks. The division of the hemispheres is, in this calculation, not the equator but the effective division of the Brewer-Dobson circulation pattern.

It is further shown by *Plumb* [1996] that the ratio of the abundances at the tropopause is likely to be rather similar in the northern and southern extra-tropics and then the ratio of the lifetimes is given by

$$\frac{\tau_1}{\tau_2} \approx \frac{\sigma_1}{\sigma_2}\bigg|_{\mathrm{tp}} \frac{\Gamma_1}{\Gamma_2} = \frac{\sigma_1}{\sigma_2}\bigg|_{\mathrm{tp}} \frac{1}{2}\left\{\left(\frac{d\sigma_1}{d\sigma_2}\bigg|_{\mathrm{tp}}\right)_{\mathrm{N}} + \left(\frac{d\sigma_1}{d\sigma_2}\bigg|_{\mathrm{tp}}\right)_{\mathrm{S}}\right\}. \tag{1.5}$$

1.4 Polar vortex

In the investigations of the polar vortex tracers play an important role. The polar vortex is formed pole-ward and above the sub-tropical jet in the winter [*Schoeberl and Hartmann*, 1991]. This vortex formation is a cold pool in the stratosphere as there is no heating from ozone absorption during the polar night while there is thermal radiation outflow. During the Airborne Antarctic Ozone Experiment (AAOE) *Hartmann et al.* [1989] showed that the vertical motion of the polar vortex air must be downward or zero to explain the measurements of long-lived tracers during the campaign. *Proffitt et al.* [1989] and *Loewenstein et al.* [1989] showed that the temporal trend of the long-lived tracer N_2O during the same campaign indicates that diabatic cooling and vortex subsidence occurred both in and around the polar vortex.

For the Airborne Arctic Stratospheric Expedition (AASE) *Lait et al.* [1990] showed that long-lived stratospheric tracers are well correlated with the dynamical tracers potential vorticity (q) and potential temperature (θ). From simultaneous measurements of long-lived tracers and ozone during spring the ozone concentration can be calculated from model analysis of dynamical parameters for the dynamical parameter region covered by the observations.

1.5 CFCs in the stratosphere

Molina and Rowland [1974] identified already in 1974 a potential threat from CFCs to the ozone layer through photolysis of the molecules and thereafter catalytic cycles including the released chlorine. This triggered a large interest in measurements of these species in the stratosphere. The first stratospheric samples were taken in 1975 [*Schmeltekopf et al.*, 1975] by balloon-borne grab-sampler [*Schmeltekopf et al.*, 1976]. Since then CFCs have been measured by several other grab-samplers on balloon platforms [*Tyson et al.*, 1978; *Honda et al.*, 1996; *Fabian et al.*, 1979] and aircraft [*Tyson et al.*, 1978; *Heidt et al.*, 1989; *Pierotti et al.*, 1980; *Cronn et al.*, 1977] as well as in-situ measurements from balloons [*Robinson et al.*, 2000; *Moore et al.*, 2003; *Riediger*, 2000; *Bujok et al.*, 2001] and aircraft [*Loewenstein et al.*, 1989; *Elkins et al.*, 1996].

The theory from *Molina and Rowland* [1974] has been verified and it is clear that chlorine and bromine released in the photolysis of the halogenated organic species take part in catalytic ozone destruction [World Meterological Organization

(WMO) 2002, 2002]. The use of CFCs and other substances that are known to contribute to ozone depletion is heavily restricted according to the Montreal Protocol from 1986 that has been amended and adjusted several times, the latest in Beijing 1999 [United Nations Environment Program (UNEP) 2000, 2000]. To make predictions of the future trends in ozone the rate of release of these species i. e. the stratospheric lifetime of the organic species must be known [*Montzka et al.*, 2002].

In studies of ozone depletion simultaneous measurements of ozone and long-lived tracers can be used in correlation studies. The primary source region for ozone and the primary loss region for several long-lived tracers, including CFCs and N_2O is in the tropical stratosphere. These species have long photochemical lifetimes outside this area. In general ozone does not have a long enough lifetime to give compact relations to long-lived tracers [*Plumb and Ko*, 1992]. However, in polar regions during wintertime, in time periods with no significant chemical ozone depletion, also ozone is a conservative tracer and forms a tight correlation curve with long-lived tracers in an airmass [*Proffitt et al.*, 1990]. If the airmass is isolated any changes in these tight correlation curves can be used as a measure of chemical ozone depletion [*Proffitt et al.*, 1993]. The condition of sampling the same isolated airmass can be ensured in severeal different ways. The most direct method in the arctic vortex is to use the potential vorticity [*Müller et al.*, 2002], the jet [*Proffitt et al.*, 1990] or a chemical tracer [*Proffitt et al.*, 1993] as a measure of the vortex to get the ozone loss in the vortex. It has been argued for example by *Plumb et al.* [2000] that chemical ozone depletion inferred this way can be misstaken for mixing with mid-latitude air. This is rejected by *Müller et al.* [2001] that argues that if mixing across the vortex edge has occurred this method rather might underestimate the ozone loss. With simultaneous measurements of several tracers with different lifetimes that form a correlation curve that is compact but not linear, the compactness of the tracer–tracer relationship can be used as an indicator of pure vortex air [*Müller et al.*, 2001]. Several other more sophisticated techniques are described in *Harris et al.* [2002].

To track the dynamical situations for those studies 3D modelling is of great use. For these models dynamical parameters like θ and potential vorticity (q) are central and to verify them profiles of long-lived tracers are important [*Bregman et al.*, 2000]. In Chemical Transfer Models (CTMs) a long lived tracer field can be included for more or less direct comparisons with measured profiles [*Bregman et al.*, 2000].

The use of CFCs as tracers in the stratosphere has grown during this time and is now the primary interest of these measurements. In the arctic region these tracers can be used to study the descent of the polar vortex [*Bauer et al.*, 1994; *Ray et al.*, 2002; *Greenblatt et al.*, 2002], mixing processes across the vortex edge [*Ray et al.*, 2002; *Waugh et al.*, 1997] and to the troposphere [*Ray et al.*, 1999; *Bregman et al.*, 2000]. *Morgenstern and Pyle* [2003] showed that, for the technique to study mixing from canonical tracer relationships of tracers, only a few balloon flights are needed during a campaign, but simultaneous measurements of tracers with different lifetimes and an accuracy better than 2%.

Chapter 2

Working principles for the DESCARTES instrument

The Détermination et Séparation par Chroatographie lors de l' Analyse des Résultats des Traceurs Echantillonnés dans la Stratosphère (DESCARTES) instrument was developed over a period of several years at the University of Cambridge. In total five instruments have been built, with two instruments of the third version basically the same. The individual instruments will here be denoted by version numbers I, II, III.1, III.2 and IV. The most recently developed version has been built in Cambridge with larger modifications both to the sampling system and desorption/analysis system but the basic principle of the sampling system still remains the same. Basically only the instrument belonging to IRF, version III.2, shown in figure 2.1 is discussed here with some comparisons to version II which is the version most used. Each of the individual instruments was modified during their use. An article documenting mainly version II was written by *Danis et al.* [2000]. *Stacey* [1996] has made a major characterisation of different parameters of the same version. The general working principle has remained the same. DESCARTES III and the present update of DESCARTES II use the same interchangeable sample boxes one such box is shown in figure 2.2. There are at the moment four such boxes available here numbered I to IV of which only I, II and IV have been used by the Swedish Institute of Space Physics (IRF) DESCARTES team and will be treated in this study.

DESCARTES is a grabsampler for stratospheric trace gases flown up into the stratosphere suspended below a balloon. Samples are taken at predefined pressure levels during the flight by pumping air through small tubes containing the adsorbent carboxen 1000, or carboxen 569 depending on which box, which are strong adsorbents of CFC. (See figure 2.3, sampling flow marked in green.) The instrument contains 16 similar such 'traps' mounted on a 16-position valve seen to the left in figure 2.2. A detail showing a trap is seen in figure 2.4. At the end of the flight the instrument is safely taken down by a controlled drop in a parachute and thereafter recovered. After recovery the content of the traps is analysed in the laboratory. The adsorbed samples are thermally desorbed by running an electrical current through the material of the trap, marked in deep blue in figure 2.3. The traps are heated to about 200 °C for 30 seconds. The samples desorbed from the sample traps are led to a Gas Chromatograph (GC)

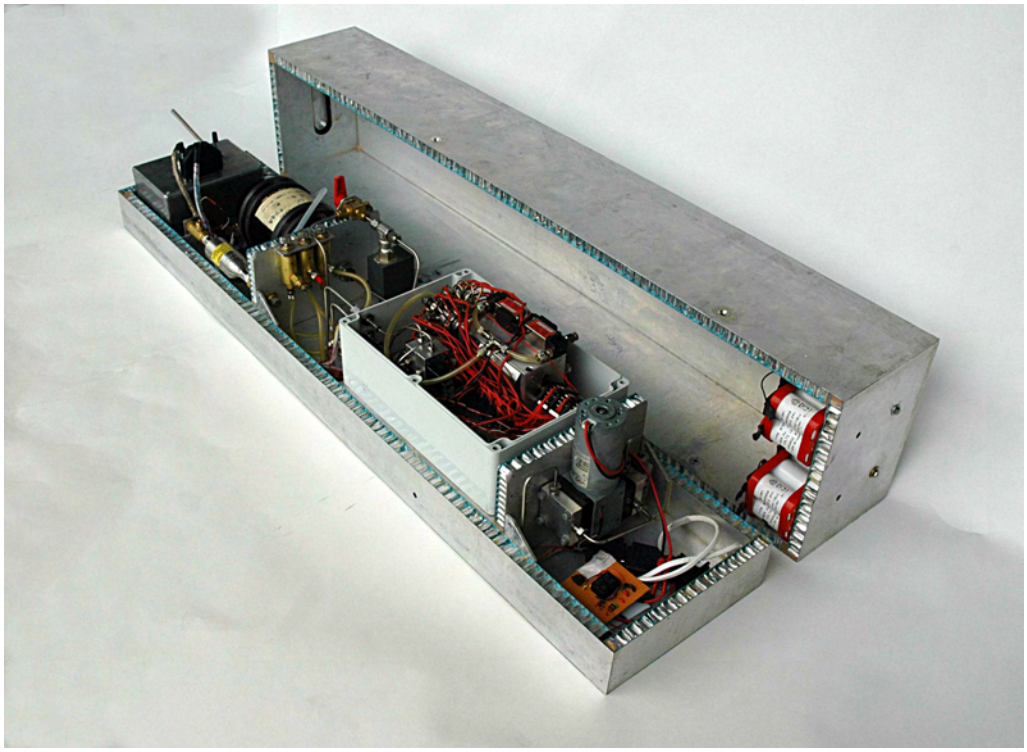

Figure 2.1: DESCARTES III.2 with a mounted sample box.

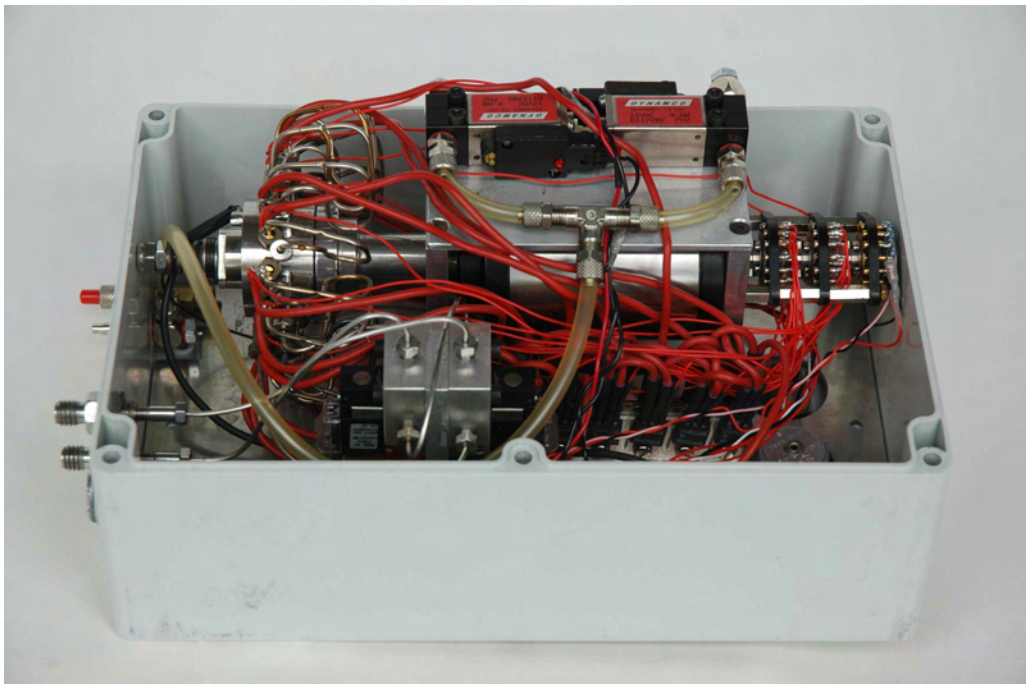

Figure 2.2: Sample box.

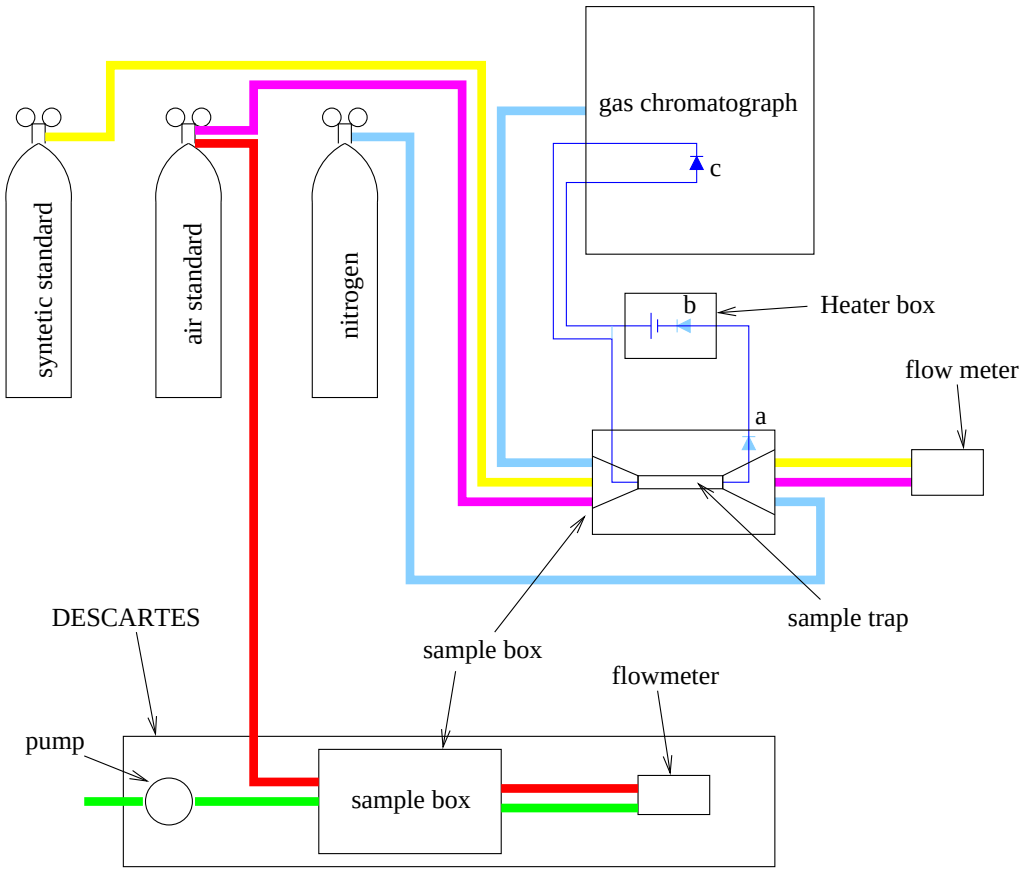

Figure 2.3: Schematic illustration of DESCARTES sampling and analysis. Gas flows colour coded: green – flight sampling, red – air standard absolute calibration with DESCARTES, yellow – synthetic standard calibration, magenta – GC-controlled air standard absolute calibration and blue analysis. In darker blue is also the principle for the electrical circuit for the heating with the temperature sensitive diode marked at different positions.

for analysis (light blue flow in figure 2.3). The instrument is calibrated by letting a measured amount of a standard sample through the traps according to the red, cyan or yellow flow in figure 2.3 and making the analysis in the same way as for the flights.

2.1 Sampling

Sampling is done at preset pressure levels in the flight program triggered by the instruments pressure meters and controlled by an on-board computer. The instrument is presented schematically in figure 2.5 and on photo in figure 2.1. The sampling is performed by pumping air through the system with the pump, first bypassing the traps, using the valves D in figure 2.5, to flush though the system. Then, with the pump running, the flow is redirected, by switching valves D, to the trap, to sample. At the same time the mass flow is measured (flow meters) and integrated (by the on-board computer) until the desired mass has

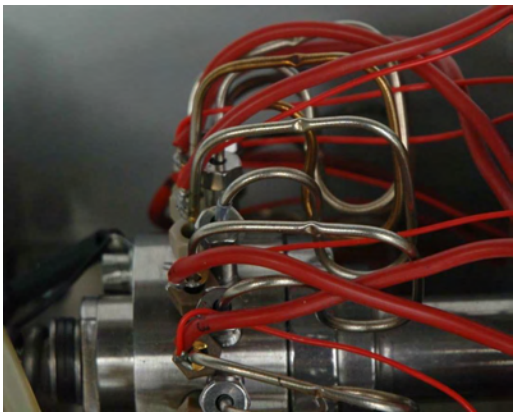

Figure 2.4: Sample traps.

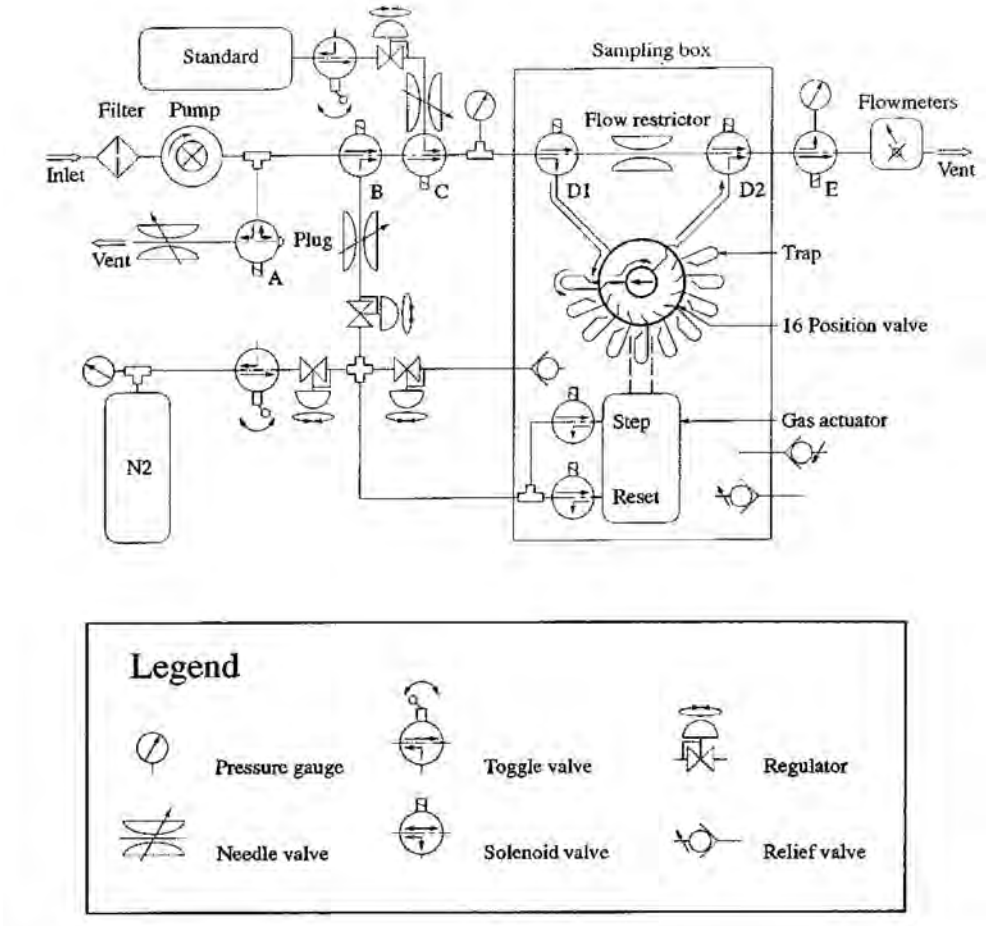

Figure 2.5: Schematic of DESCARTES instrument, reprinted from *Danis et al.* [2000].

been sampled. In order to restrict the flow at higher pressure samples there is an overflow valve installed between the pump and the trap (marked A in figure 2.5) that can be opened to the surrounding air to decrease the pressure given by the pump and thereby the flow.

In detail the sampling follows the following steps. The pressure is read out by a routine until it drops under a predefined level. Then the overflow valve (A) is opened and the pump is started to purge the inlet tube. When the pre-selected sampling pressure is read out from the pressure gauge, the overflow valve is closed if the flow readout from the flow meter is smaller than a defined cut-off value. Otherwise it stays open. After a delay of about 10 s valves D1 and D2 are switched and the flow is redirected to go through the trap and the mass flow integrated.

The integration of the flow is done by a machine code subroutine. This ensures that it is rapidly executed on the slow computer, as needed for accuracy. The routine is executed shortly after the redirection of the flow through the trap. This code integrates the reading for a few seconds and produces a file including the average flow readout. A loop in the flight program reads this file directly to see if the predefined mass has been sampled, otherwise the subroutine is run again. The integration is then not completely continuous but has short interruptions about each 3 seconds. The flow from the readings is taken to be the mean during the whole sampling.

When sampling is done the trap is pressurised. This is done by leaving the switches D in trap position, switching the pressurise valve E from the flowmeter to the pressure guage and switching valve B to let pressure from the nitrogen pressure flask on the system. This pressure is set to ensure that the trap is in over pressure until the analysis is made. In this way the traps are secured against contamination from tropospheric air even for the smallest leakage.

To avoid disturbing other instruments, the pump has its own power circuit, not even sharing ground with the rest of the instrument. That is the reason for the zero reading of the pump voltage at most times.

2.1.1 Storing flight data

All parameters measured during a flight are stored in local memory in the onboard computer. These data are then extracted to an ascii datafile called `data.dat` after recovery (see sec B.5). To fully understand this file it is important to know how it is created, since the intuitive way to read it can be misleading in several aspects.

For each sample there is a block in the file starting with the string `Sample` and a number, see example of file in figure 2.1.1. The following row, starting with `REQUESTED SAMPLE` is data taken from the parameters file `fr_prms.h` at the time of file generation. If the parameters file transferred to DESCARTES on board computer is not the same as the one used for compilation of the flight program these data might be wrong.

The measured parameters then appear in six rows per sample taken. The sensors are read one at a time to a temporary file by a machine code subroutine called from the flight program called `AtoDall`. In a similarly called function `AtoD_all` this file is then read to primary memory. The writing of the data to the storage memory is done by yet another function in the program called

FLIGHT DATE: ..../..../.... FLIGHT TIME: ....:....:.... LOCATION: ....

	Ambient	Temps degC				Pressures mB			N2	Trap	Mass Flow	Valve States					Battery mV	
Time UT	mBar	degC	Pump	Vlco	Flow	Line	Vbox	Prss	psi	no.	thru trap	IN-OUT	VN2	Stnd	OvFlw	Prss	Comp.	Pump.
Launch!!																		
08:14:25	993	0	2	8	1	-1	1040	0	192	2	2884/ 2864	OFF	OFF	OFF	OFF	OFF	13080	13298
Ascent!!																		
10:41:19	596	0	0	1	1	-2	605	285	195	2	2970/ 2893	OFF	OFF	OFF	OFF	OFF	12471	13369
10:45:22	498	0	0	1	1	-1	483	319	197	2	2936/ 2894	OFF	OFF	OFF	OFF	OFF	12463	13364
10:50:00	399	0	0	1	0	-2	364	335	199	2	2933/ 2893	OFF	OFF	OFF	OFF	OFF	12454	13364
Sample 01																		
REQUESTED SAMPLE: STRATOS at 250 hPa, mass: 30 scc, max. wait: 200 sec. and max. time sample: 35 sec.																		
	Ambient	Temps degC				Pressures mB			N2	Trap	Mass Flow	Valve States					Battery mV	
Time UT	mBar	degC	Pump	Vlco	Flow	Line	Vbox	Prss	psi	no.	thru trap	IN-OUT	VN2	Stnd	OvFlw	Prss	Comp.	Pump.
10:53:08	343	0	3	1	0	749	296	342	197	2	24915/17768	OFF	OFF	OFF	ON	OFF	12369	0
10:53:25	336	0	3	1	0	749	296	342	197	4	24905/17714	OFF	OFF	OFF	ON	OFF	12369	0
10:53:29	324	0	3	1	0	749	296	342	197	4	24894/18604	ON	OFF	OFF	ON	OFF	12369	0
10:53:33	323	0	3	1	0	749	296	342	197	4	24889/18536	ON	OFF	OFF	ON	OFF	12369	0
10:54:21	305	0	3	1	0	697	296	708	197	4	2752/ 2704	ON	ON	OFF	ON	ON	12369	0
10:54:35	309	0	3	1	0	697	296	708	197	4	2836/ 2842	OFF	OFF	OFF	ON	ON	12369	0
through traps: average MF60 = 24891 counts and MF200 = 18570 counts. Duration in 100th of sec.: 747																		
Sample 02																		
REQUESTED SAMPLE: STRATOS at 220 hPa, mass: 30 scc, max. wait: 100 sec. and max. time sample: 40 sec.																		

Figure 2.6: Example of data file from onboard computer, from start of file to second sample

`StoreState`. The first command in `StoreState` is to read the time, i. e. the time in the final file is the time when data was written to storage memory. Due to limitations in memory size, sometimes only parts of the data are stored. In the write instructions that go to the first and fifth rows all the parameters on the row are written. The second to fourth and sixth rows show readings of the time, ambient pressure, flowmeters and the booleans (`IN-OUT`, `VN2`, `Stnd`, `OvFlw` and `Prss`) from the same `AtoDall` run. The rest of the data on those lines are simply repetitions of the parameters on the line above. In the write instruction that gives the sixth row, also the mean flow meter readings and duration time are written, presented in the seventh row. In version II of DESCARTES the datafile is generated from the primary memory where all data on each row are from the same `AtoDall` run.

2.2 Adsorbent Carboxen

Carboxen 569 is expected to adsorb quantitatively if the flow linear velocity is less then 500 cm/min. Our samples are taken at low pressure and hence the volume flow is larger. A numerical estimation in section 4.2 of our sampling shows that we exceed this flow. This is of major concern for the instrument and is further investigated in chapter 4.

2.3 Heating system

The heating system is based on ohmic heating of the material of the trap. This high power circuit is schematically indicated in deep blue in figure 2.3. The heating power is regulated by pulsation of the current through the trap. The resistance of the trap is estimated during heating as a measure of the trap temperature and used as a switching point for the pulsating voltage over the trap. The change in resistance from the temperature change in the trap is small compared to the total resistance in the electrical circuit used for the measurement. To measure this signal in all possible noises in the system and thereby regulate the heating of the trap is probably a problem that limits the desorption efficiency.

The heating power to get the wanted temperature of the traps is set by changing the resistance switching point individually for each trap. Test runs with samples in the traps are analyzed and then a second similar heating is performed on the same trap. The temperature is raised until the remnants coming out in the second heating are negligable.

The largest source of change in the response of this measurement was found to be a zener diode used to stabilise the heating in the circuit that was found to have a large temperature dependence of its zener voltage. In an earlier version there were separate diodes for each trap mounted in the sample box (a in figure 2.3) and they were not protected against temperature variations. They were mounted very close to the current regulating transistor that was warmed up during the heating and thus produced an unwanted feedback effect. The circuit was redesigned by François Danis (University of Cambridge) in a way that all the diodes where replaced with one diode. This diode was first placed in the heater box (b), later

on moved to the temperature regulated oven of the GC (c). This is one of the larger changes to the system noted in appendix A.5.

Earlier a system with traps wound with a nichrome wire was tested. In that system the heating current was sent through the nichrome wire and the temperature was estimated by measuring the resistance of the wire. This method gives a better signal due to the fact that the resistivity of the material has a large temperature dependence and the resistance is larger. However, this is not necessarily a measurement of the right parameter as it assumes that the thermal conduction to the trap is similar between traps and over time. See further discussion on possible improvements in chapter 6.

2.4 Chromatographic analysis

The samples desorbed from the sample traps are led to a Hewlett Packard (HP) 8690 GC for analysis. In order to work with DESCARTES analysis the GC is specially equipped, the principle is shown in figure 2.7. The column is a Chrompac CP-Sil 5 CB Wall-Coated Open Tubular (WCOT) column 0.53 mm i.d. and 5 µm that is split into two parts, one pre-column 10 m long and one main column of 40 m. The flow is reversed in the pre-column (as indicated in figure 2.7b) when the species of interest has passed by to avoid the risk that slow moving species might overlap in time with the next analysis. The flushing makes sure they do not stay in the column.

During the desorption of the trap a gas flow of pure N_2 is going through the trap and the chromatographic column (figure 2.7a). While the trap is heated the flow is kept low in order to avoid getting the desorbed quantitiy diluted too much by the carrier gas. After the desorption the flow is raised to optimize chromatography.

The desorption and analysis is run by the macro `trap`*trap*`.m` (where the italic *trap* shall be exchanged with the trap number) on the analysis computer. This macro includes communication to the heater box to heat the traps and is further explaind in appendix A.2. There are individual macros for the traps with different parameters to the heater box. The flow is adjusted to the flow rate of the desorption, the 10 port valve (valve 1) is set on (figure 2.7a) and the nitrogen flow is changed from bypass to the trap (valve 3) at the initiation of the macro. After 0.7 min of flushing the heater is turned on (valve 8) for 0.5 min. After 1.7 min the flow is raised and after 3 min the trap is closed. After 8 min the pre-column back flushing starts (valve 1 off) as indicated in figure 2.7b. The chromatogram is recorded for 24 min.

Two heating cycles with chromatographic analysis of the desorbed species are normally made to analyse the contents of a DESCARTES trap. The detector signal from the last heating cycle is first used to confirm that the heating has worked properly i. e. there are no remnants left of the relevant species in the second chromatogram. When this is confirmed this signal is used as a blank run to subtract from the signal from the first run to isolate the signature from other chromatographic disturbances (which are generally present). An example of two successive chromatograms from an analysis of a flight sample is given in figure 2.8.

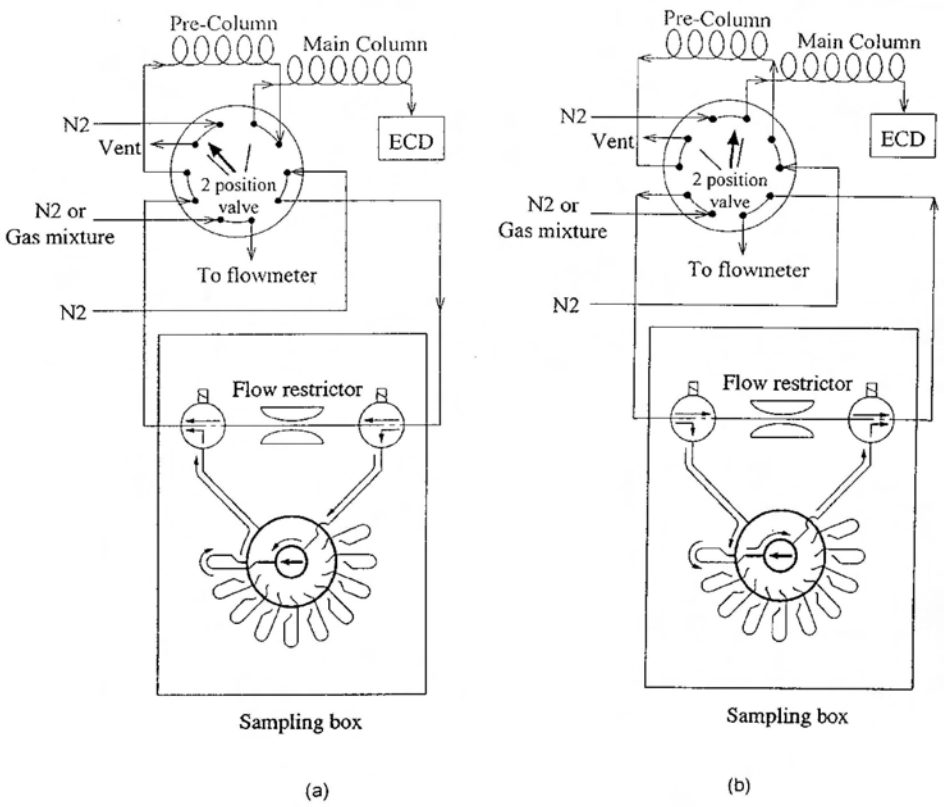

Figure 2.7: Schematic of the sampling box and GC system during analysis. Reprinted from *Danis et al.* [2000]

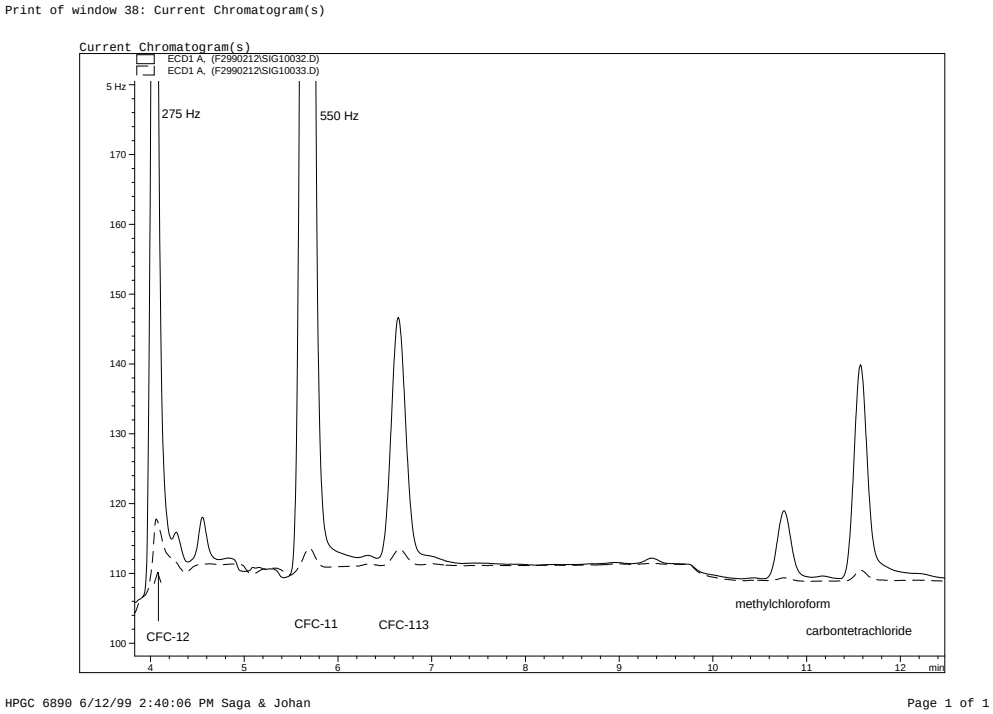

Figure 2.8: Example of chromatograms from both heatings of an analysis of one sample in a flight.

In order to make the analysis less subjective and less time consuming automatic integration of the chromatograms has been tried. This has proved to be of limited use due to the fact that the chromatographic peaks differ over a large span in size between samples from different heights during a flight. The best automatic integration is used together with a manual inspection and adjustment.

For time saving the oven temperature of the GC has been raised during the analysis from 50 °C to 85 °C so that the peaks due to methyl chloroform and carbon tetrachloride appear sooner. But, as problems were found to arise with noise from previous analysis appearing in chromatograms this ramping was not generally used.

2.5 Reference to other parameters

In order to correlate other parameters measured by other instruments on the same or more or less simultaneous payloads a common parameter with good presision is needed. The time is set manually at boot time for the computer, care has been taken to set this time to 1 s precision from Global Positioning System (GPS) in order to syncronise with other instruments. The pressure sensors for surrounding pressure are found not to give reliable readings with good enough uncertainty. During flight these are used by the onboard computer to trigger the sampling but pressures from other instruments (always been present on the payload) have been used in presenting results.

In practice there is also almost always temperature data taken by other instrumentation in the payload, giving the possibility to calculate the potential temperature (θ). As the humidity is always low in the stratosphere the potential temperature is calculated without corrections for humidity as

$$\theta = T \cdot \left(\frac{p}{1 \text{ bar}}\right)^{-0.288}. \tag{2.1}$$

Height information has been taken from the official Flight Trajectory Data (FTD) from the launch facility. Comparisons to other parameters have been interpolated to the time of DESCARTES sampling when the time resolution has been courser than the DESCARTES sampling length and calculated as the arithmetic mean for data points taken during the DESCARTES sampling when possible.

Chapter 3

Calibrations

Calibration of the instrument has been performed using two different approaches. One approach, presented in section 3.3, is to emulate a flight in the laboratory to get the total system response. The other approach, presented in section 3.4, is to calibrate each of the subsystems independently in the laboratory. As the flow meters show strongly nonlinear response, the flow meter calibration (section 3.2) must be done independently in both cases. In the first approach the flows are measured with the same flow-meters during calibrations and flights, so the generalisation of the results depends only on the form of the calibration curve. In the second approach flows are measured by a lab flow-meter during calibrations and the results are directly dependent on the absolute calibrations of the flow-meters.

Unfortunately the two approaches show a significant absolute difference of about 12%.

There are several different subsystems in the instrument that have unknown response: the flow meters, the adsorption and desorption efficiencies, the Electron Capture Detector (ECD) in the GC and there might even be uncontrolled adsorption and desorption effects in the system.

For consistency, the latest calibration of box I and curves only for CCl_3F (CFC-11) has been used for most examples in this chapter. Box I shows by far the worst trap individuality of the boxes used (discussed in section 3.4.2), thereby the spread in calibration curves is larger for this box and differences are more easily spotted. The qualitative conclusions are however similar for the other boxes. Sampling of $CCl_2F\text{-}CClF_2$ (CFC-113) suffers from uncontrolled adsorption effects, this is discussed in section 3.6.1. The quality of the measurements of the other species are discussed in section 3.6.

For practical reasons calibrations have not been performed in a low pressure environment, such as that which prevails in the stratosphere. Setups with internally lower pressure in the gas system have been tried but this gives abnormal pressure differences and possible leaks into parts of the system that can not be adequately accounted for. That our calibrations have been performed in room temperature and pressure gives uncertainties of how representative they are to flight conditions.

3.1 Calibration standards

Several different gas standards, both compressed air and synthetic mixtures in nitrogen, are used. These, with contents according to table 3.1 are:

1. Gravimetric mix in nitrogen. From SIP Analytical Ltd, diluted at University of Cambridge to unknown concentrations.

2. New synthetic standard. Mix in nitrogen from SIP Analytical Ltd of grade 'Diamond' (±1%), cylinder serial no C219626. An order of magnitude too concentrated, diluted with pure nitrogen according to section A.5 to unknown concentrations.

3. Cryogenic natural air sample from Weybourne beach 1992-03-27 calibrated at University of East Anglia (UEA) against the Advanced Global Atmospheric Gases Experiment (AGAGE) standard mixture [*Cunnold et al.*, 1997].

4. Compressed air standard from National Oceanic and Atmospheric Administration (NOAA). A natural dried air sample from Niwot Ridge, Colorado analysed for N_2O, SF_6, CFC-11, CCl_2F_2 (CFC-12), CFC-113, CH_3CCl_3, CCl_4 and Halon-1211. Calibrated at Climate Monitoring and Diagnostic Laboratory (CMDL) against NOAA working standards in August 2000. Cylinder ID: ALM-67702.

Standard number		1	2	3	4	
species name	formula	concentration				unit
CFC-11	CCl_3F	271	664	277.81	263.0 ± 2.6	ppt
CFC-113	$CCl_2F\text{-}CClF_2$	81	202	86.18	82.6 ± 0.8	ppt
methyl chloroform	CH_3CCl_3			172.28	44.1 ± 0.9	ppt
carbon tetrachloride	CCl_4			112.15	98.5 ± 2.0	ppt
Halon-1211	$CBrClF_2$				4.30 ± 0.2	ppt
nitrous oxide	N_2O				316.1 ± 0.7	ppb
sulfur hexaflouride	SF_6				4.69 ± 0.2	ppt
CFC-12	CCl_2F_2			533.39	535.7 ± 1.6	ppt
chloroform	$CHCl_3$			15.01		ppt
tetrachloroethylene	C_2Cl_4			12.70		ppt

Table 3.1: Analysed mixing ratios of used standards. Concentrations of synthetic standards derived from absolute calibrations of DESCARTES

The concentrations of the diluted synthetic standards are derived by correlation to the air standard 3 in the absolute calibrations described in section 3.4.5.

As there are two absolute standards, there is a good possibility to test these against each other. This was done in the way that one box was filled with both standards under similar circumstances. To compare the results from both analysis they were compensated for the nonlinear response of the ECD as described in

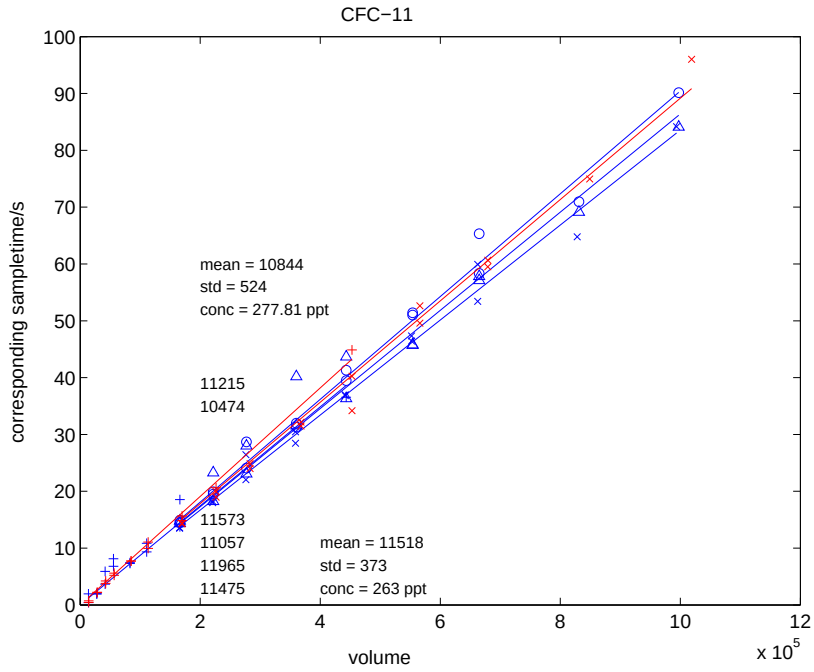

Figure 3.1: Inter-comparison between the two different absolute air standards used. Standard 4 in red and standard 3 in blue. See text for details.

section 3.4. In figure 3.1 the result for this test is plotted. The red marks and lines and the numbers above the line refers to standard 3 while the blue marks and lines as well as the numbers below the line refers to standard 4. The numbers are the direct proportionality coefficients*. These coefficients are proportional to the concentrations in the samples. The ratio of these constants is $\alpha_4/\alpha_3 = 11518/10844 \approx 1.06$ and the ratio of the concentrations of CFC-11 is $c_{a4}/c_{a3} = 277.81/263.0 \approx 1.06$. This test shows that the concentrations given in table 3.1 are consistent with each other to the precision of our measurements.

The reason for the many standards is that they have become available at different times in the project. From the very beginning a synthetic standard of CFCs in pure nitrogen was used as a relative standard to monitor the response of the system. Then the profiles that had no absolute calibration were normalised by setting a tropospheric sample to an estimate of the tropospheric concentration. A large improvement was an analysed air sample that could be used as an absolute standard. This was available in a very limited amount and was only used to scale an absolute value for the calibrations made by the synthetic standard. The last and superior is the latest well calibrated standard of compressed air that can be used for a one step absolute calibration of the total system response.

*This is the same coefficients that will be presented in section 3.4.5 with the difference that the both tests are divided by the same standard concentrations. The absolute value has thereby not a direct physical meaning for both standards, but the only important aspect at the moment is that they are directly proportional to the concentrations in the standards.

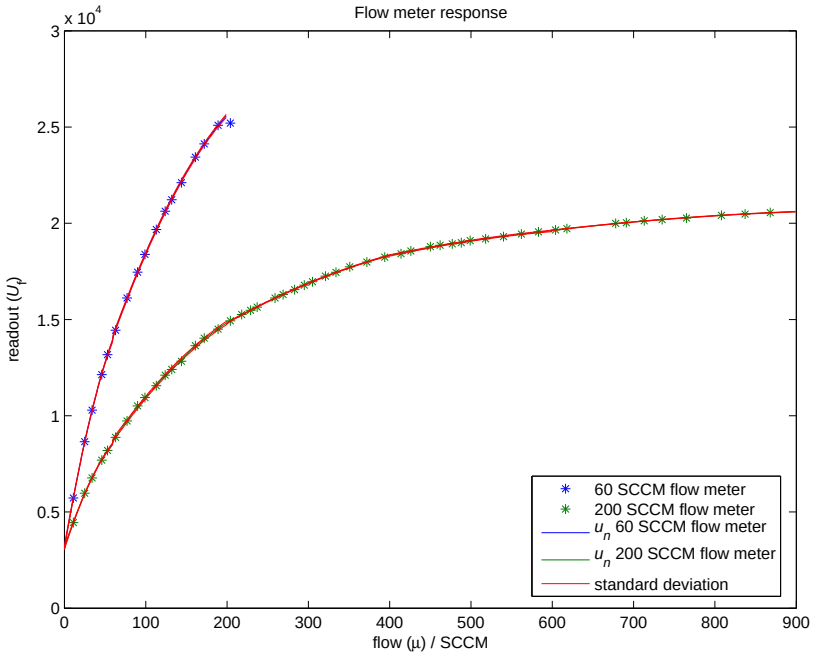

Figure 3.2: Example of flow meter calibration. DESCARTES reading of output from built in flow meters versus calibration flow set by lab flow controller.

3.2 Flow meter calibrations

The flow meter calibration is performed by coupling another, well calibrated lab flow controller in series after the on board flow meters. Air is let through the system by connecting a vacuum pump to the flow controller. A calibration curve, shown in figure 3.2, is taken by setting the flow with the flow controller.

There are two flow meters on-board DESCARTES which each should take one interval of the flow measurements. In practice it has turned out that both cover almost the whole interval of flows appearing in a flight. This gives an opportunity to compare flow meters to each other during flight.

Even though the flow meters show low noise the absolute value of their output voltage is varying. It has been observed that it is disturbed for example when a computer running on AC power is connected. Calibrations run with a computer connected indicate that this is a stable offset. During flight zero readings (z_f) are taken from the flow-meters, i. e. the signal is read out when there is no flow. These zero readings are then used to adapt the calibration curve for the present measurement.

The flow controllers used for the calibrations are two Aera FC-2600 for the flows up to 60 SCCM[†] and 200 SCCM respectively. They are both calibrated by the manufacturer in April 1999 as seen in section A.5 on page 139.

By accident sampling was made with much larger flows in one flight. To cover this, the flow meter was calibrated to a Tylan FC-2900 in the same way with a

[†]SCCM: standard cubic centimetre per minute, is a mass flow unit corresponding to 1/60 cm^3/s of the gas in question at standard temperature and pressure (1 °C and 1 atm)

range up to 1000 SCCM. Inter-comparisons of the flow meter calibrations with different flow controllers shows good agreement.

Another approach to make the flow meter calibration has also been tested. To do this, we pushed air with the DESCARTES on board pump to the flow controller, placing the on board flow meters last. This turned out to be problematic since a steady flow was hard to reach.

3.2.1 Calibration function

The signal read out from the flow meters seems to have a low noise during one calibration session and is not easily represented by a simple function within the noise level. The range for each flow meter is therefore split up in N parts to which a second degree polynomial $u_n(\mu) = u_{n1} + u_{n2}\mu + u_{n3}\mu^2$ fits the flow meter voltage readout (U_f) as a function of the mass flow μ from the flow controller in the region $n \in [1, N]$. The number of parts (N) varies from 1 in calibration up to 60 SCCM to 5 for the calibration up to 1000 SCCM.

To make the absolute values agree between different calibrations a zero reading z_f is read from the flow meter when there is no flow and the constant term is changed to $u^*_{n1} = u_{n1} - u_{11} + z_\mathrm{f}$ where u_{11} is the constant term for the lowest flow part of the calibration, i. e. the scale is shifted to the zero reading.

The mass flow during flight sampling μ is then estimated by one solution to the extraction of the flow from u_n, here called f_n,

$$\mu = f_n(U_\mathrm{f}, z_\mathrm{f}) = -\frac{1}{2\,u_{n3}}\left(u_{n2} - \sqrt{u_{n2}^2 - 4\,u^*_{n1}\,u_{n3} + 4\,u_{n3}\,U_\mathrm{f}}\right). \tag{3.1}$$

As the function u_n fits the response U_f to the flow μ the intervals for the individual polynomials are defined to an interval in μ ($\mu_{\mathrm{max},n-1}$,$\mu_{\mathrm{max},n}$]. However during a flight the flow is the searched variable and the readout U_f is the known, therefore readouts from the flow meters $U_{\mathrm{max},n}$, corresponding to $\mu_{\mathrm{max},n}$ are calculated as

$$U_{\mathrm{max},n} = u_{n+1}(\mu_{\mathrm{max},n}). \tag{3.2}$$

These are only defined for the on-board flow meter measuring the larger flow interval. These values are then used to choose the right calibration factors for the flow measures taken during flights.

All calibration constants as well as the values for U_max for these functions are listed in tables C.1 to C.3 on pages 151–152.

3.3 Direct air standard absolute calibrations

The first approach to make calibrations is to use the flight software to sample standard samples with DESCARTES using the same program as during flights. In this way we avoid introducing new procedures not present during flights. By keeping all procedures the same systematic errors present in both flights and calibration will tend to cancel each other.

The flow is calculated according to the flow meter calibration and then the sampled amount is calculated as the mean flow multiplied with the sample length

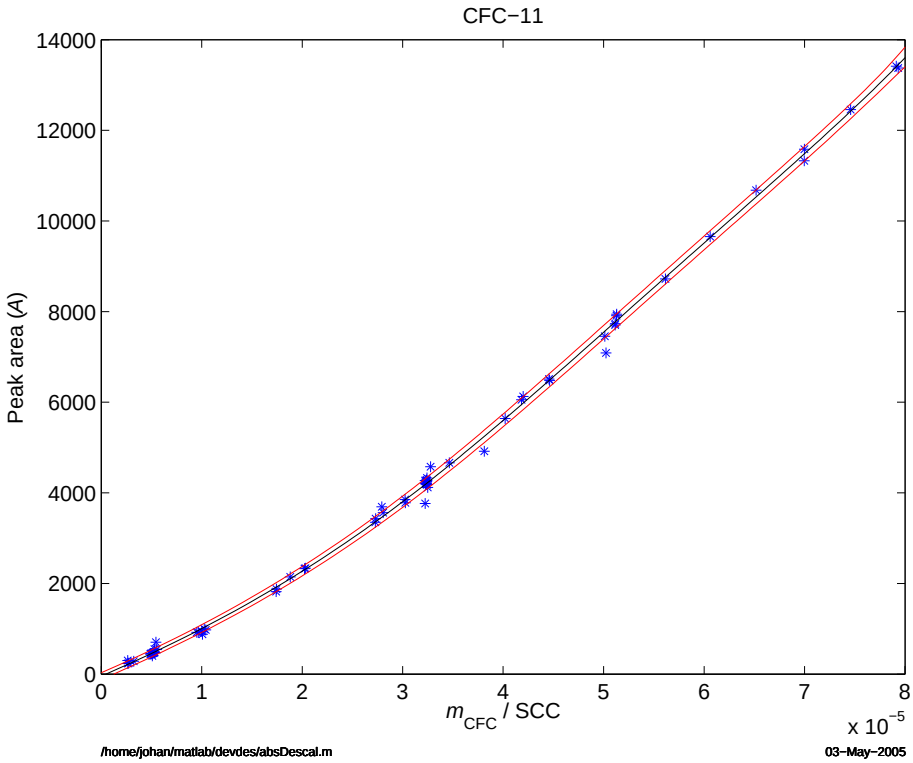

Figure 3.3: Example of direct absolute calibration curve. CFC-11 in box I. Fourth order polynomial fit, $h(A)$, (black) with one standard deviation (red).

and the standard concentration,

$$m_{\mathrm{CFC}} = f_n(U_{\mathrm{f}}, z_{\mathrm{f}})\, t_{\mathrm{s}}\, c_{\mathrm{a}}{}^{\ddagger}. \tag{3.3}$$

Flow and time readings are read from DESCARTES flight log (section 2.1.1) and concentrations from table 3.1. A detector response function is obtained by a fourth order polynomial h,

$$m_{\mathrm{CFC}} = h(A) \tag{3.4}$$

fitted to the sampled amount of CFC as a function of the detector response as shown in figure 3.3. The mixing ratio of the sample is then calculated as

$$c = \frac{h(A)}{f_n(U_{\mathrm{f}}, z_{\mathrm{f}})\, t_{\mathrm{s}}}. \tag{3.5}$$

3.3.1 Sample boxes individuality

In order to achieve the best possible fit of a response function to the data a large statistical basis is required. Calibration runs are made for all three boxes

[‡]This product is a measure of the mass of CFC in the sample. Under assumption of the ideal gas law and in units used here the result is in SCC. Note that the SCC as a mass unit is dependent on the normal density of the species and differs from species to species. It can be converted to mass or amount of substance by multiplication and division with the molar masses for the CFC and air. The important thing at the moment is that it is a measure of the mass.

considered in this work. The boxes are hand made and not exactly similar, the largest difference is the different adsorbents used. It is not obvious if all the calibration data from all boxes should be joined to one dataset for one common response function or if the fitting of such a function should be done individually for each box. Figure 3.4 shows all calibration data colour coded for the boxes. From this figure we empirically decided to fit a common response functions for all the boxes. Coefficients for the polynomial h are found in equation C.2 on page 152 and for f_n in tables C.1 to C.3 on pages 151–152.

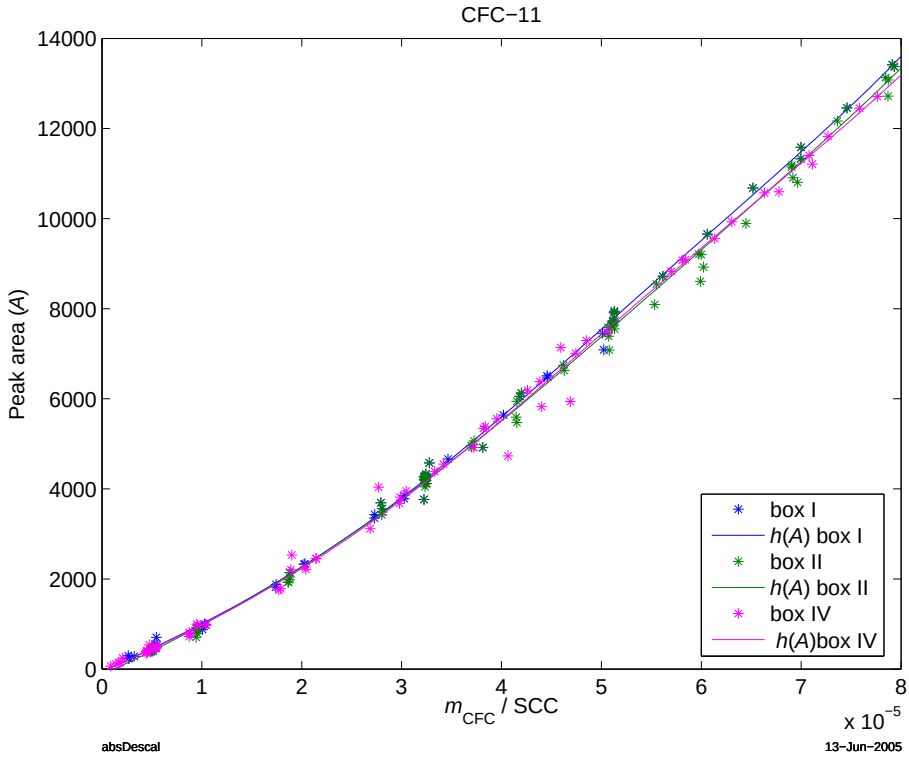

Figure 3.4: Direct absolute calibration curves, $h(A)$for CFC-11 and all boxes. Fourth order polynomial fits are used. Standard deviation is not plotted to increase readability.

3.3.2 Flight data quality concerns

Environmental properties such as the pressure and temperature of both the hardware and the gas stream are different and might still be reasons for concern. This might give differences due to adsorption and desorption of the gases to the surfaces of the gas system and the carboxen as well as changing the response of the flow meters. The calibration gas flow is connected to the sample line after the pump (and a couple of other switches as seen in figure 3.22) as taking the samples through the pump raises practical problems. Since the pump includes a rubber diaphragm while all other surfaces in contact with the gas samples are made of stainless steel and aluminium with some graphite ferrules this is of concern for uncontrolled adsorption effects, see further discussion in section 3.6.1. Also there might be non-plug flow effects as discussed in section 5.2 while using the pump.

Both calibration approaches have limitations in that only one standard sample with known mixing ratios is available (in principle two but their concentrations are rather similar) so the flow, sampling time and sample size can not be changed independent to each other. By using the same system as during a flight most possible errors are thought to cancel. As there is only one standard there is an implicit assumption to both methods that calibrations with different sample sizes but one concentration give the same result as sampling different concentrations. This also means that the estimation of the sample volume is assumed to be at least proportional to the truth. The time reading is thought to be linear but the flow meter reading is not. This means that even in this approach the flow meter response must be calculated. In this approach of calibration the flow is measured by the on-board flow meters and calculated by the same calibration function as during a real flight. This means that the only function of the flow meter calibration in this case is to linearise the flow meter response, an absolute offset will not effect the results. The method is less sensitive to absolute errors than the one described in section 3.4.

3.4 Indirect calibration method

In the other calibration approach a response function of the ECD is taken on a synthetic standard, using the GC to control the sampling (section 3.4.1). Absolute calibration is achieved by sampling an air standard similarly (section 3.4.5). Stable flows are achieved by regulation of the pressure on the outlet valve on the GC. The outflow from vent during these samples is measured regularly with a calibrated flow-meter.

The amount of CFC in the sample is calculated taking the ECD signal, mapping it through the response function of the ECD and multiplying with an absolute calibration factor from the absolute calibration. The mixing ratio is calculated by division of this result with the integrated flow from DESCARTES.

3.4.1 ECD response

The ECD used for the analysis does not have a linear response to the amount of the species analysed. When calibrating the subsystems independently, characterisation of the ECD response is made by letting samples of a synthetic standard mixture of CFCs in nitrogen with a stable flow, measured by the Aera flow controller, pass the trap for a predefined time. The sample is analysed and by many of these measurements a calibration curve for the ECD response is obtained.

This could in principle be handled by fitting a nonlinear response function to the absolute calibration standard of pressurised air. As mentioned in section 3.1, at the beginning of the project a very limited amount of well calibrated air standard was available. To achieve a better statistical basis for the nonlinear fitting calibration was made in separate linearity tests with the synthetic standard instead.

The linearity function g_l for small samples is calculated as a first order linear regression of the logarithms of the sampling time and the peak areas from the analysis. The chromatogram peak area is a parameter output from the analysis

that is completely dependent on the hardware and settings of the instrument. For this work we consider it a dimensionless parameter. The time reading on the other hand must be normalised to the logarithm. To make sense, we measure the time in seconds and use the numerical value, i. e. formally divide the time by $t_0 = 1\,\mathrm{s}$. Due to noise in the chromatographic curve the behaviour of the function for very small values is not obvious. It turned out that the statistical values for the parameters improved by the addition of an offset term to the time. Therefore the fitting is done iteratively to get a constant offset term γ_l for which the best total fit is possible. The function is given by

$$g_\mathrm{l}(x) = g_{\mathrm{l}1}x + g_{\mathrm{l}2},$$

where $g_{\mathrm{l}1}$ and $g_{\mathrm{l}2}$ are the coefficients that fit $g_\mathrm{l}(\ln A)$ to $\ln(\frac{t_\mathrm{s}-\gamma_\mathrm{l}}{t_0})$ best in a least square sense, where A are integrated peak areas, t_s are the sampling times for the calibration and γ_l is the offset term that gives the best fit. For larger samples the response of the detector seems more linear and the uncertainty, which is mainly from the sampling process (see section 3.4.2), does not seem to grow exponentially. For these larger samples a linear regression g_h is made to fit $g_\mathrm{h}(A)$ to t_s. This gives then a modified response $g(A)$ as a function of the raw integrated areas A,

$$g(A) \equiv \begin{cases} \gamma_\mathrm{l} + e^{g_\mathrm{l}(\ln A)}\, t_0 = \gamma_\mathrm{l} + A^{g_{\mathrm{l}1}}\, e^{g_{\mathrm{l}2}}\, t_0 & \text{for } A \le A_\mathrm{lim}, \\ g_\mathrm{h}(A) = g_{\mathrm{h}1}A + g_{\mathrm{h}2}, & \text{for } A > A_\mathrm{lim}. \end{cases} \tag{3.6}$$

The breakpoint A_lim is chosen from a by eye determination of the calibration data. An example of theses fittings and the data they are fitted to is shown in figure 3.5. As in figure 3.3 the red curves indicate one standard deviation. Each type of marker corresponds to one calibration run.

3.4.2 Individual trap response

The individual traps in the sample box show slightly different responses in the calibrations. The first step is to investigate if this is an ECD, analysis or sampling effect.

The traps have, for longer or shorter time periods, given reproducible but individual responses to tests where similar samples have been fed to all traps in a box and then analysed. As seen in the example figure 3.6 this effect is overlayed on the signature of another effect of different response of the whole calibration runs from run to run that will be further discussed in section 3.4.3. The sampling has been performed the same way as for the linearity test described in section 3.4.1 with the only difference that all samples are equal size. The legend in figure 3.6 shows the dates of the individual calibration runs. It is worth noting that the last calibration is made one year after most of the others. In this run the two traps 10 and 12 do not show the earlier, rather reproducible, low response.

This variation in trap response is measured empirically but the cause of this variation is not obvious. For the interpretation of the results the different possibilities can be of three different origins:

Heating The trap individuality might originate in the desorption mechanism from the trap, for example the temperature of the traps differ. If this is

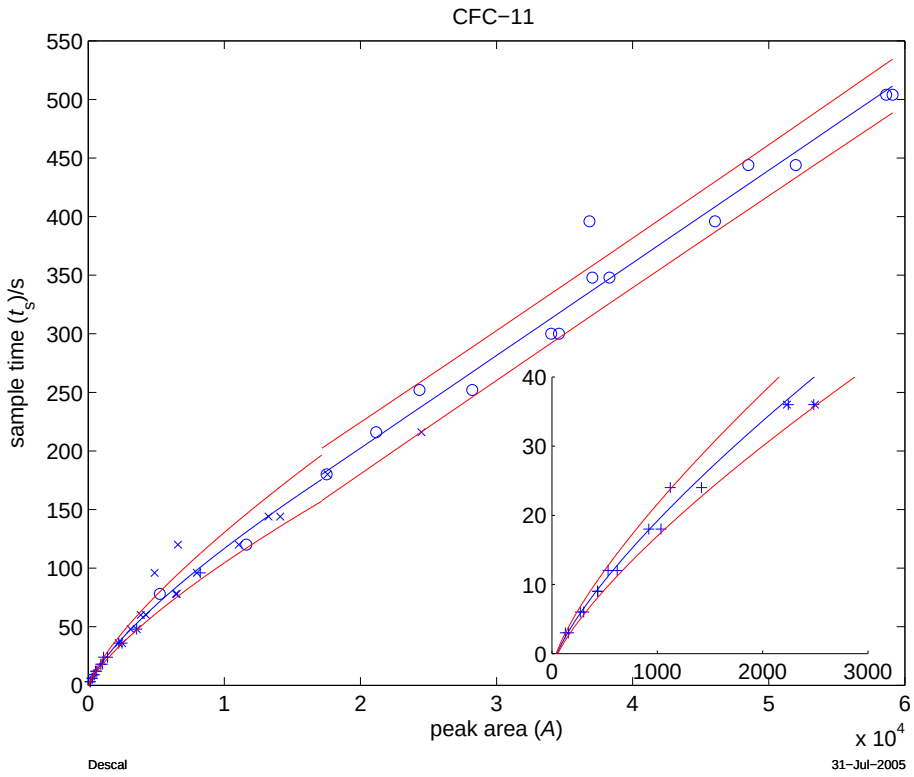

Figure 3.5: Example of ECD response calibration box I, CFC-11. Blue lines are the response function $g(A)$ and the red lines show one standard deviation.

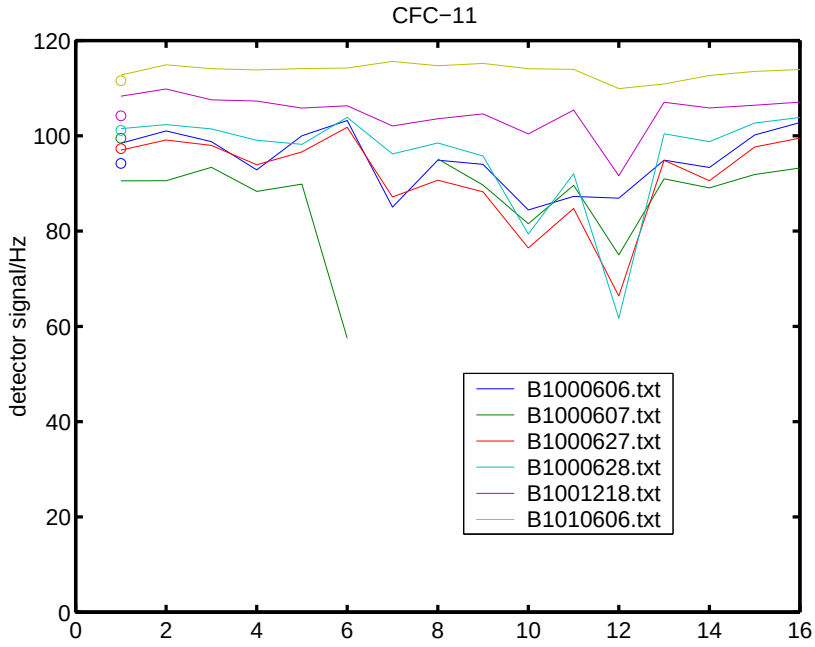

Figure 3.6: Example of trap individuality tests for box I. The direct chromatogram peak area without modifications plotted for six tests for the traps 1–16.

the case, the same signature is to be expected for all samples and a multiplicative correction factor can be applied to all calibrations and analysis runs. As mentioned in section 2.3, the heating of the traps is adjusted individually. Problems with the heating mechanism are likely to be seen in the second heating of the traps.

Adsorbent The adsorbent bed may differ, either in the amount of adsorber or contamination to the trap that changes the efficiency. If this is the case, the variation in response comes from different amounts of adsorbent is leaking out of the trap during sampling, an effect called breakthrough, further discussed in chapter 4. Then a correction function of the sampled amount should be applied to all calibrations and analysis runs. The problem should show up independent of sampling mechanism but (possibly) depending on the flow speed through the trap and/or the sampled volume.

Sampling The sampling mechanism of these tests might give rise to the effect, for example if the flow is not the same trough all the traps. Then the trap individuality would be an effect seen only during calibrations and the response to real flight samples would not be affected. Thus no correction should be done to the analysis of flight data.

From a quick look at the calibration samples presented in figure 3.5 (synthetic standard sampled by the GC) and figure 3.3 (natural air standard sampled by DESCARTES) it is obvious that the spread is much larger for the first combination. From figure 3.3 it is obvious that the analysis system is not responsible for the majority of the spread in the calibration curve. As the calibration curve for the analysis system is not linear and the analysis system is not responsible for the trap individuality, the correction factor must be calculated for, and applied to the sample size rather than the detector response.

The only control that has been made to see the flow during sampling is for the absolute calibration sampling. This is done the same way as these repeatability test samplings but with a compressed air standard. During those fillings the same Aera flow controller as used for the flow meter calibration was attached to the outflow from the GC and the flow was controlled manually. These readings showed fast dips or spikes in the flow when the trap was opened and the pressure stabilising. These fluctuation was from +2% to -5% of the steady flow and only lasting for a few seconds and does not show a correlation with the individual trap response. This is not enough to explain the large difference in the individual traps responses, even the steady state flows manually read from the flow controller does not show the variability of this magnitude.

A final individuality factor r for each trap and species is calculated as the mean over all sequences of the response $g(A)$ (equation 3.6) relative to the mean response of the sequence,

$$r = \frac{1}{\#\text{seq}} \sum_{\text{seq}} \frac{g(A)}{\langle g(A) \rangle}, \tag{3.7}$$

where $\langle g(A) \rangle$ is the mean response of the sequence

$$\langle g(A) \rangle = \frac{1}{\#\text{traps}} \sum_{\text{traps}} g(A).$$

In some calibration runs results from some of the traps are missing. As there are differences in the response both from trap to trap in the same calibration run and systematically between the calibration runs, the missing values are replaced using the rest of the calibration data in a process of 3 steps:

1. For each trap the mean detector response is calculated.
2. A preliminary response factor is calculated by dividing the response for each individual heating with the mean for all traps in the sequence.
3. Missing values are then artificially replaced by the mean value for the sequence times the mean response of the trap from all other sequences contained in the calibration.

The same individual response of the traps applies to the ECD response calibration. This is seen by dividing the sample sizes of the ECD response calibration data from figure 3.5, by r. The result is shown in figure 3.7. The spread is obviously smaller after this correction. It is interesting to note that the standard deviation is smaller both in the high and the low region of the calibration curve. It is also obvious that changes of similar magnitude to the calibration curve taken by the DESCARTES instrument in figure 3.3 would give larger spread. From this we can conclude that the trap individuality, is most likely an artifact of the sampling system of GC controlled sampling and therefore the correction factor is applied in the calculation of the response function $g(A)$ but not to the flight analysis.

As there are differences in the response both individually and flight to flight an ECD response test procedure was implemented. These tests were performed after the two heatings of the samples. The bypass (the tube connecting valves D1 and D2 in figure 2.5 without going through the trap) was filled with a synthetic standard, this volume was then injected to the GC column giving a chromatogram that could be integrated for the response (method `newbypas.m` see table A.1). Later in the project the differences in the response were not thought to be from the ECD, according to the discussion above, making this test unnecessary. It was removed from the analysis sequence (in the change from `newpos`*wp*`.s` to `analys`*wp*`.s` analysis sequence see table A.2) to speed up the analysis and also to prevent the traps from being contaminated in the process if there for some reason could be a need for a third heating to verify that the trap was clean.

3.4.3 Inter flight analysis response changes

There is an effect that the response of whole calibration runs is changing as previously noted in the repeatability tests described in section 3.4.2. It is important for the performance of the instrument to investigate if this influences the measurements and if it can be compensated for.

In the analysis procedure of DESCARTES there are calibration samples taken in the waiting position[§] before and after the analysis of the traps containing samples. In total four samples, two before the analysis of the other samples and

[§]The trap that is in position when the analysis starts. It is not used for sampling, neither in calibrations or flights due to risk of contamination.

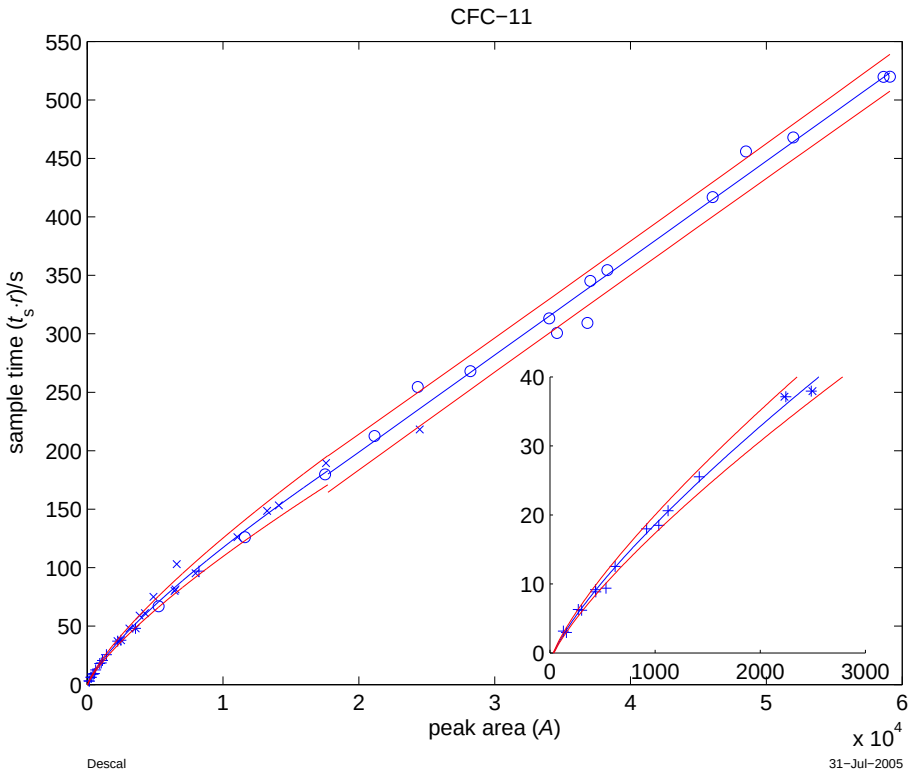

Figure 3.7: The ECD response calibration presented in figure 3.5 with the sample times compensated for trap individuality, Box I, CFC-11

two after are taken with the same sampling technique as for the repeatability tests. These analyses have been integrated in the same way as the other samples and the results have been followed for the period 1999-12-03 to 2001-06-19. Results are shown in figure 3.8. A long term trend seems to appear in box I, in the other boxes there seem to be no similar effects. The large discrepancy in box II is discussed later.

That this response is, at least to some extent, the same as seen during repeatability tests (described in section 3.4.2) is clear from a comparison between the test and calibration samples during these tests. These were made with the same sampling procedure and standard and as clearly seen in figure 3.6 on page 28 they also shows the change in system response as the overall response between calibration runs. Figure 3.9 on page 34 that shows the integrated chromatographic peak areas from the repeatability tests, as the mean of the four test runs (as in figure 3.8) vs. the median of repeatability test (indicated by circles in figure 3.6). All boxes show the same tendency but the relation for box II is shifted relative to the others.

To investigate this the mean peak area of all the test samples for all analysis of each box are calculated. The fraction between mean peak area of the four test samples during an analysis and the overall mean is called R. If the test sample response is representative for the whole analysis this R parameter can be used to compensate for the analysis run response.

The nature of these changes is not obvious. The problem is fully in analogy with the trap individualities discussed in section 3.4.2 and the same three different possible sources are interesting to distinguish: heating, adsorbent or sampling.

If this effect is a heating or an adsorbent effect influencing also the measurements, it should be investigated whether it can be compensated for.

A way to test if it should be compensated for in flight analysis would be to make a plot similar to figure 3.9 with calibrations taken by DESCARTES. However the sampling procedure for the instrument, described in section 2.1, is not designed to take samples of exact predefined sizes. The calibration runs made for the calibrations according to the direct calibration method described in section 3.3 can however be used for the same purpose. As these are of different sizes the simple approach used for repeatability tests can not be used. But, if the effect has an influence on the analysis that should be compensated for, and if this is not done, there would be a positive correlation between the estimated volume mixing ratio c and the value of R inferred from the test samples for the flight. Figure 3.10 shows a plot of these parameters for analysis made with both analysis methods. In this figure the calibrations containing only low-flow samples are excluded as they have proved troublesome, as will be shown in section 3.5. There seems to be no particular trend in these data. From this we can conclude that flight data should not be compensated for analysis specific response.

Following similar argumentation to that regarding the trap individuality in section 3.4.2, it is clear that, if the problem does not show up in the analysis, it is not likely to be due to the detector and thereby any compensation should be applied to the sampled amount during the calibrations. As seen in figure 3.9 the differences in response from time to time are on the order of 10%. The analysis method has proved to be much more accurate than this, for example during the

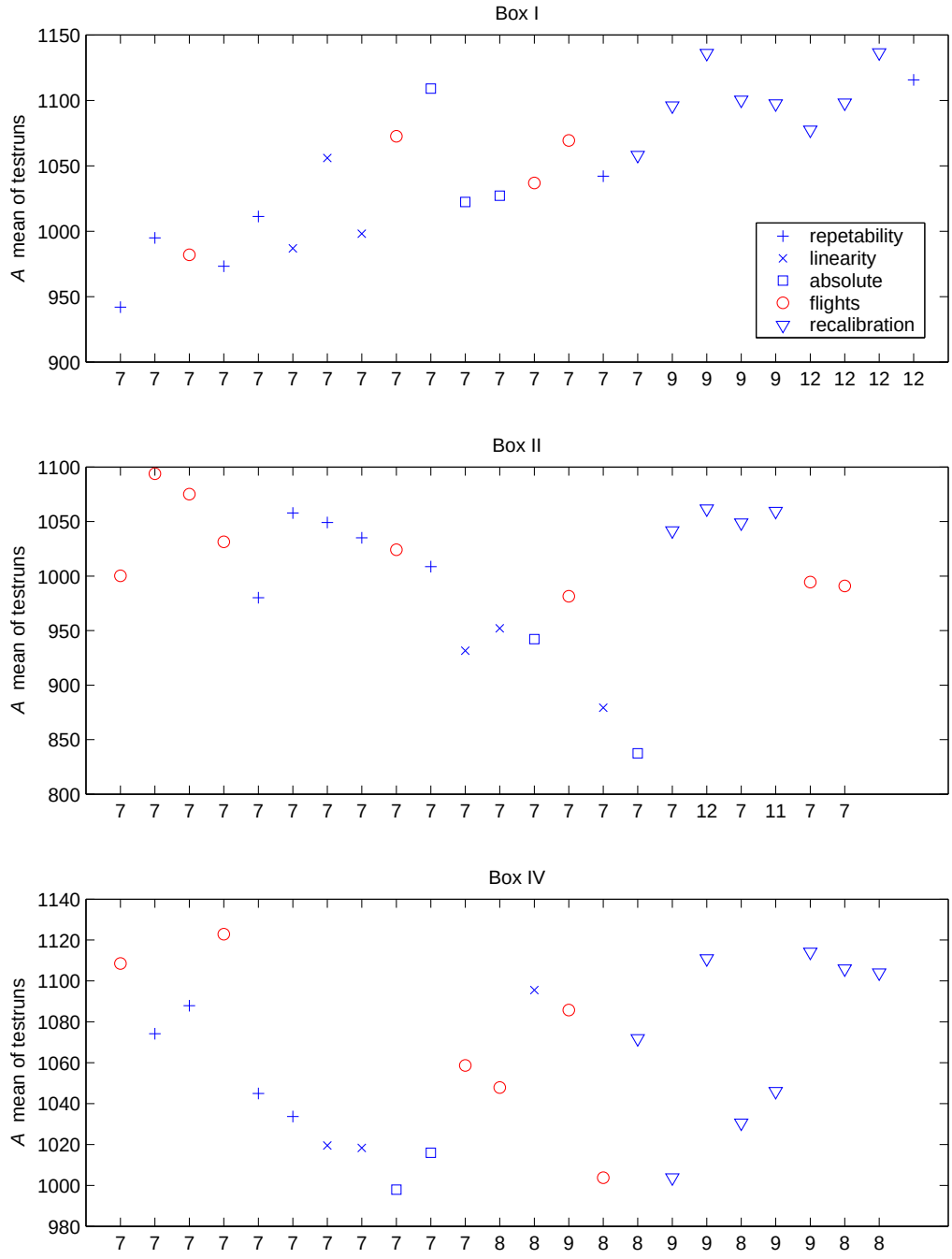

Figure 3.8: Results of test samplings performed in all analysis. Mean of chromatogram areas for the four samples. Placed in chronological order for each box. Numbers at the bottom of the plots are trap number used.

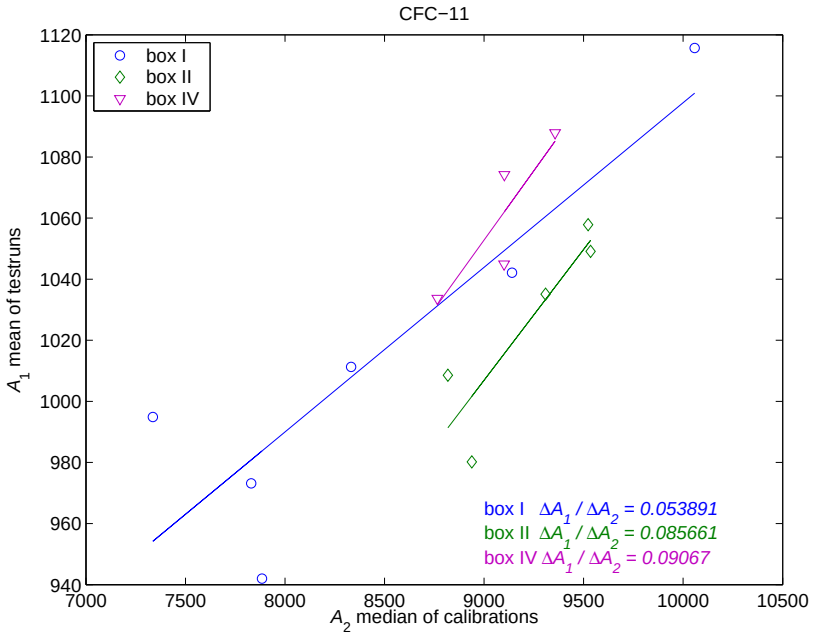

Figure 3.9: Relationship between the mean response of test runs and median response of calibration runs during repeatability tests.

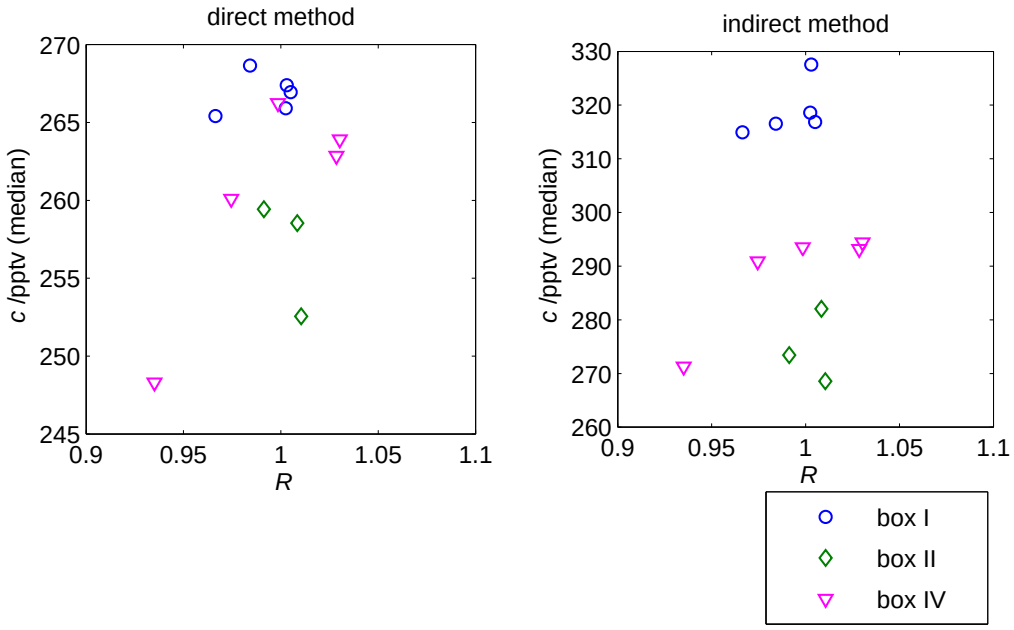

Figure 3.10: Calibration results as function of R values for calibration runs sampled by DESCARTES. c from direct absolute calibration method in the left panel and from indirect method in the right panel.

calibrations described in section 3.3. This indicates a sampling problem and the investigation will focus on adjustments to the sample sizes for calibrations and the estimated amounts in results. From this we can also draw the conclusion that the uncertainty should not affect the flight results as the flight samples are taken by DESCARTES.

To investigate this we have to relate the measured change in chromatogram area to the amounts of CFC entering the detector. The data shall be adjusted by the same factor as the response of the test sample. The discrepancy is seen as a change in detector response (peak area (A)). Here we denote the difference from analysis to analysis ΔA. The relative response of the estimated volume ($\Delta V/V$) is wanted, where ΔV is the analysis to analysis discrepancy in estimated CFC amount expressed as volume of calibration standard. To achieve this we will do a local linearisation of the calibration curve around the sample. These changes are approximately

$$\Delta A \approx \frac{\partial A}{\partial V}\Delta V \tag{3.8}$$

$$\frac{\Delta A}{A} \approx \frac{\partial A}{\partial V}\frac{V}{A}\frac{\Delta V}{V} \tag{3.9}$$

for the test runs, where $\frac{\partial A}{\partial V}$ is the instrument response to sampled volume at the sample size in question from a calibration curve i. e. in the notation of section 3.4.1 $\left(\frac{\partial g(A)}{\partial A}\right)^{-1}$. The assumption here is that the relative change from the long term average in V i. e. $\Delta V/V$ is similar for all samples in the box for the calibration regardless the different sizes of samples. This gives the possibility to use the test heating for the flight and derive the $\Delta V/V$ deviation from equation 3.9. From the ECD response function without correction presented in figure 3.7 a value for the relational constant at the size of the test samples is estimated to

$$\left(\frac{\partial A}{\partial V}\frac{V}{A}\right)\Bigg|_{\text{test size}} \approx 1.19,$$

i. e. slightly higher than a direct proportionality that should have given the value 1. This assumption is hard to test in other ways than comparing statistical properties of the determination of the fittings, when using these corrections in the calibrations. One test that can be done is to look at the deviations in the repeatability calibrations that are all performed at the internally same sample size, which is different from the size of the test runs. According to equation 3.9 this assumption leads to

$$\Delta A \propto \frac{\partial A}{\partial V}V \tag{3.10}$$

i. e.

$$\frac{\Delta A_1}{\Delta A_2} = \frac{\frac{\partial A}{\partial V}\big|_1 V_1}{\frac{\partial A}{\partial V}\big|_2 V_2} \approx 0.11 \tag{3.11}$$

where indices 1 and 2 denotes test runs and repeatability runs respectively and the constants are taken from the uncorrected ECD response function as before. This value can be compared to regression of this relationship from figure 3.9. This test has large uncertainties but at least indicates that this is not a large overcorrection.

As with the trap individuality in section 3.4.2 the calculated analysis response correction can be tested on the ECD response calibration curve. In analogy with figures 3.5 and 3.7, figure 3.11 shows the same calibrations compensated for analysis response as well as trap individuality. This test turns out to give no guidance at all, the situation is neither better or worse than without the compensation for the analysis response. The standard deviation of the linear part of the calibration curve has changed from 15.52 s to 15.33 s i. e. not significantly.

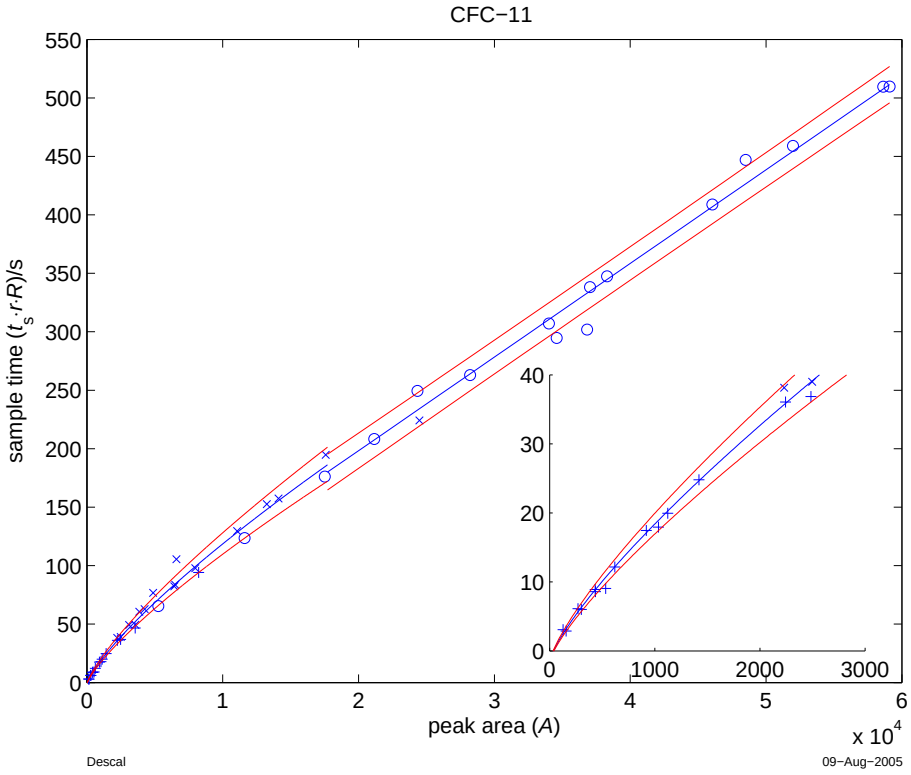

Figure 3.11: The ECD response calibration from figures 3.5 and 3.7 with sample times compensated for analysis response as well as trap individuality.

When compensation for analysis response is tested against absolute calibration, one major discrepancy is found. One of the calibrations of box II has the lowest ever measured test sample as seen in figure 3.8, second panel. Details of the two absolute calibrations of box II are shown in figure 3.12. The absolute calibration will be described in section 3.4.5. For now we can be satisfied with that the calibration is made with the same procedure as the ECD response tests. The calibration results is then linearised by $g(A)$ to give direct proportionality coefficient determined by the concentrations in the calibration standards. To clearly show the effects, the proportionality fittings are done individually for the two calibration runs. As expected from the calibration runs, one of these results in an unusual calibration factor. As seen in figure 3.12 the calibrations were rather consistent with each other without compensation for the analysis response (left panel). However the very low response of the test run seems to be an artifact for that single trap during that analysis as compensating for this in the calibration

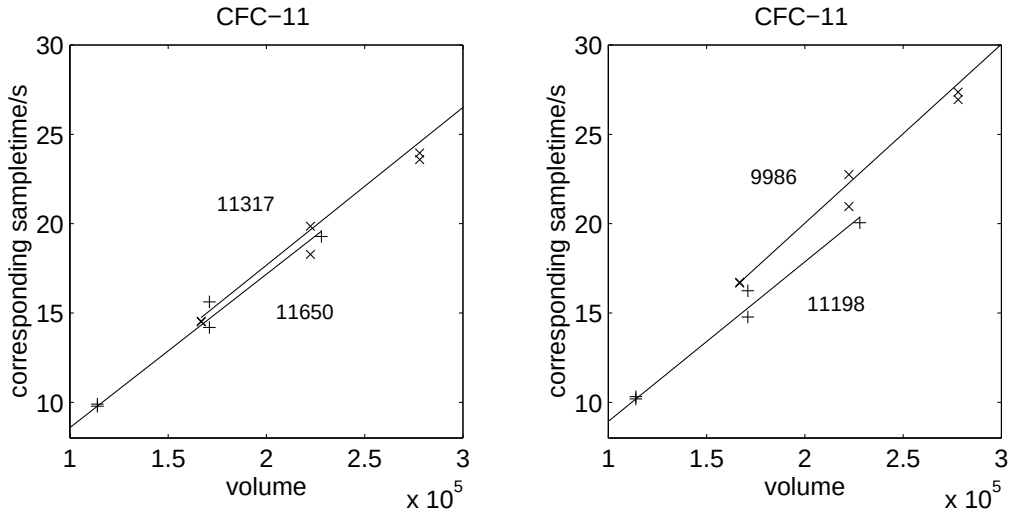

Figure 3.12: Absolute calibrations for Box II. Details of calibration line similar to figure 3.15, but with individual proportionality fittings for the two calibration runs. Left panel is compensated for the analysis response.

makes a large discrepancy between the two runs (right panel). This indicates that these test samples should be used with care to avoid large systematic fluctuations for whole flights. The calibrations are made with the test sample by the same trap most of the times.

As concluded earlier, compensation for analysis efficiency should not be used in flight analysis. For trap individuality calibrations it makes no sense. For linearity and absolute calibrations there seems to be no significant improvement to the statistics but a potential danger to introduce systematic errors. It is therefore concluded not to use compensation for analysis response at all.

3.4.4 Sample boxes individuality

There are two possible methods to calibrate the three boxes, either merge the datasets to a common calibration or individual for each box. As indicated already by the trap individuality tests (section 3.4.2, figure 3.9) there there might be differences in the responses between the individual boxes. In the approach of individual subsystem calibrations this can be easily understood as for example differences in flow resistance. On the other hand the calibrations also show scattering. There is no obvious advantage for either of the methods and we will here take an empirical approach to choose the method to use.

For the ECD response calibrations, calibration curves similar to figure 3.7 are plotted for all boxes in one common plot in figure 3.13 on the following page. The standard deviations are left out to increase readability but the calibration curves do not fall within one standard deviation from each other.

A last chance for the correction algorithm for inter flight analysis response change (described in section 3.4.3) could be if it led to the individual boxes forming common calibration curves. If the individual response of the boxes comes from their flow resistance they will give similar response changes to both ECD

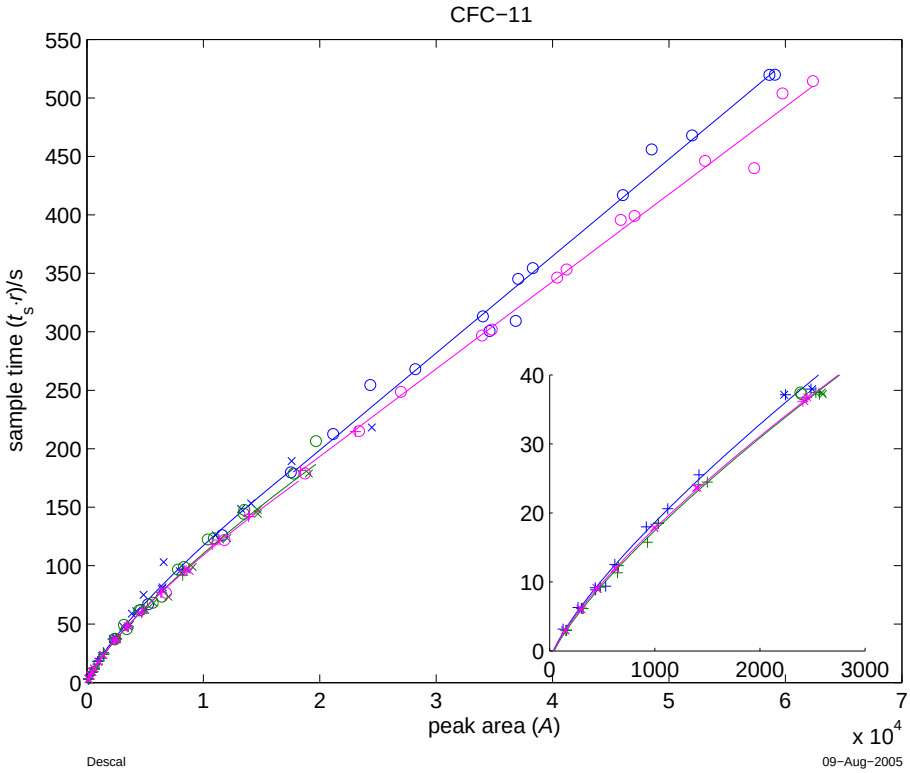

Figure 3.13: ECD response similar to figure 3.7 for all boxes. Box I in blue, box II in green and box IV in magenta. Standard deviation curves not plotted to increase readability.

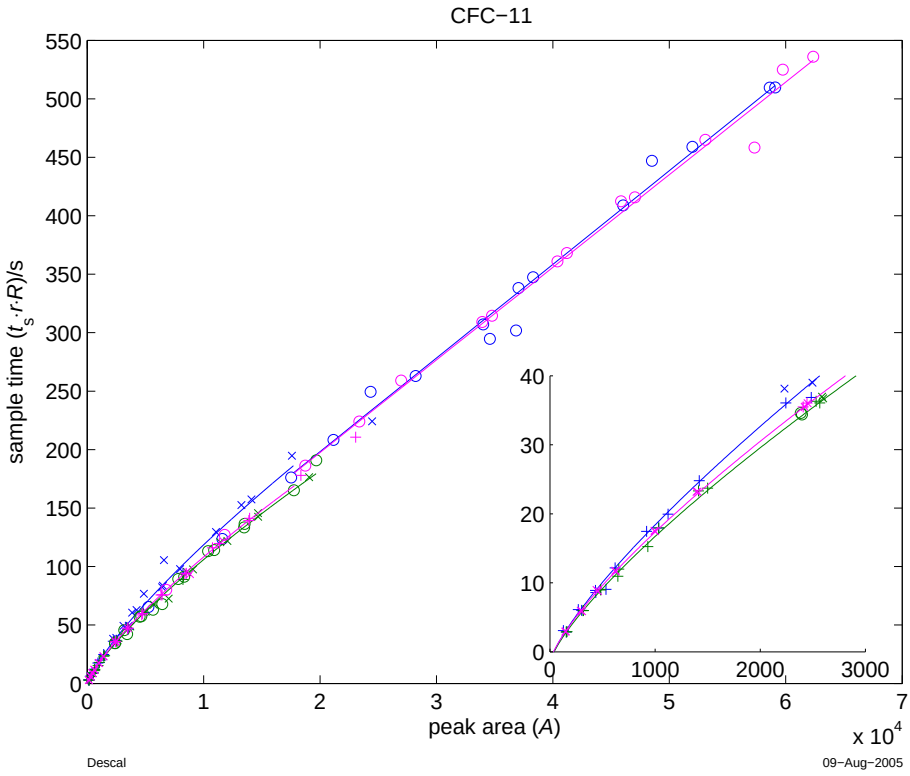

Figure 3.14: ECD response for all boxes similar to figure 3.13 but compensated for analysis response like figure 3.11.

response calibrations and to absolute calibrations, as they are performed the same way. If this correction were to provide the boxes with a common calibration, it would have to be applied inter box, i. e. the calibration runs should be compared to the mean of all analysis of all boxes. Figure 3.14 shows all ECD response calibrations compensated in this way. (This is the way this compensation has been applied the whole time even if it has not been important earlier.) A fast look at the figure might give the impression that the different boxes are more tightly correlated but a closer look at the part below 200 s, where most of both the calibration and flight samples are, shows that there is no improvement. The idea of compensation for the inter analysis response change is thereby finally discarded.

3.4.5 Absolute calibration

Absolute calibrations are performed in the same way as for the linearity tests. The absolute calibration is then performed by fitting a direct proportionality factor between the sample sizes of an air standard of known composition to the linearised detector response.

Measured chromatogram areas (A) can from the ECD response function calculated in section 3.4.1 give a measure of the amount of sample in the trap in the unknown unit of "equivalent time" of synthetic standard sample $g(A)$ for comparison with absolute standard samples. As the flow is (or at least is meant

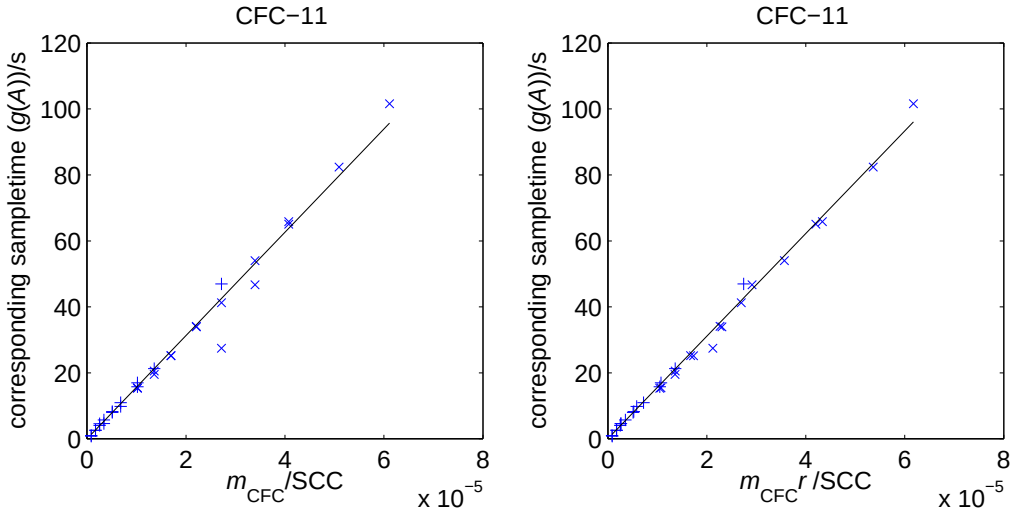

Figure 3.15: Example of calibration for absolute response factor α. Both panels showing the same calibration data, the right panel is compensated for the trap individuality by multiplication of the trap individuality factor r to the sampled amount. Box I, CFC-11

to be) constant during the experiments in section 3.4.1, $g(A)$ is proportional to the amount of CFC in the sample $m_{\mathrm{CFC}} = c\, t_{\mathrm{s}}\, \mu$[¶], where c is the mixing ratio of species and μ the sampling mass-flow. $g(A)$ is the time of standard sampling corresponding to measured chromatogram peak area.

As $g(A) \propto c\, t_{\mathrm{s}}\, \mu$,

$$\alpha \equiv \frac{g(A)}{c\, t_{\mathrm{s}}\, \mu} = \frac{g(A)}{m_{\mathrm{CFC}}} \tag{3.12}$$

defines the proportionality constant α.

In figure 3.15 the absolute calibration data and the best direct proportionality fit with slope α is plotted. Even in this test we can clearly see that the spread is smaller while compensating for the trap individuality shown in the right panel. The sampling procedure in this test is similar to the one used for both the ECD response calibration in section 3.4.1 and the trap individuality in section 3.4.2. The only difference is the standard used. The same individuality in trap response is seen here also, strengthening the idea that it is a sampling artifact.

In the same manner as section 3.4.4, the question whether the boxes should have common or individual calibration constants is solved empirically. Figure 3.16 on the next page shows the calibration data for all calibrations together. Ideally this plot should have a proportionality fit that is fully determined from the concentrations of the two calibration gases. From the figure it is also clear that a single common calibration curve for all boxes is preferred.

[¶]see footnote on page 24

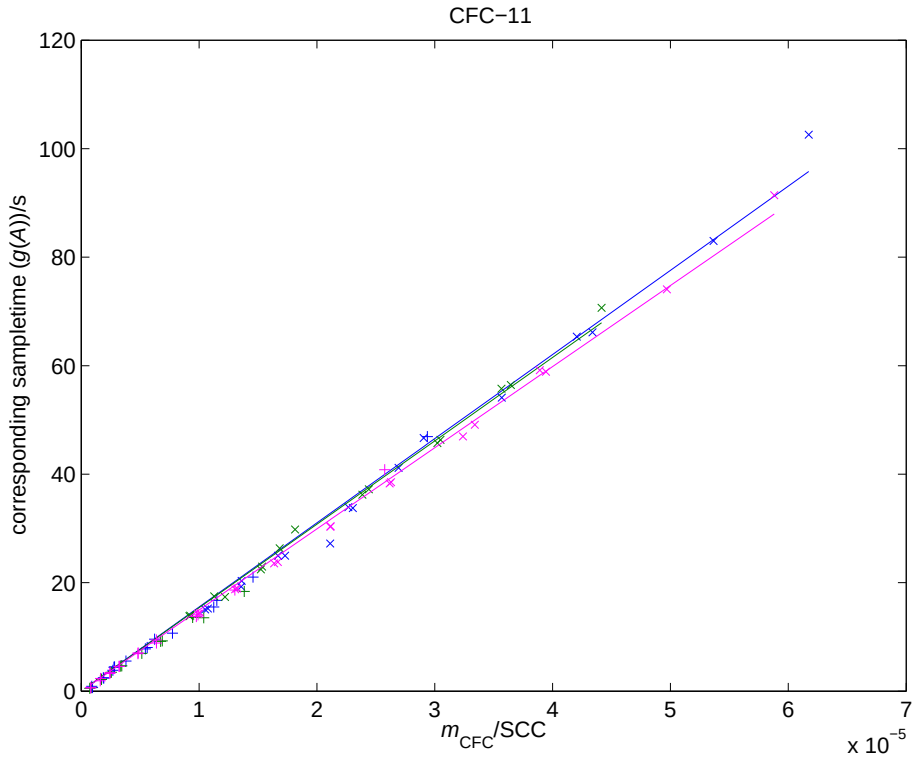

Figure 3.16: Calibrations for absolute response factor α, compensated for trap individuality like right panel of figure 3.15. Data points for all boxes with individual fittings, colour coded after boxes, box I is blue, box II green and box IV magenta. The different marks are for different calibration runs.

3.4.6 Calculation of sample mixing ratio

The final expression for the mixing ratio of the species is then

$$c = \frac{g(A)}{\alpha\,\mu\,t_\mathrm{s}} = \begin{cases} \dfrac{\gamma_\mathrm{l} + e^{g_\mathrm{l}(\ln A)}\,t_0}{\alpha\,f_n(U_\mathrm{f}, z_\mathrm{f})\,t_\mathrm{s}} & \text{for } A \le A_\mathrm{lim}, \\ \dfrac{g_\mathrm{h}(A)}{\alpha\,f_n(U_\mathrm{f}, z_\mathrm{f})\,t_\mathrm{s}} & \text{for } A > A_\mathrm{lim}. \end{cases} \tag{3.13}$$

Calibration constants for the functions g, f_n and α are found in appendix C.

The ECD linearity function g is calculated individually for each box with compensation for individual trap response factor r as described in section 3.4.2 but not compensated for inter flight response changes as discussed in section 3.4.3. The absolute calibration factor α is calculated as one common function for all boxes, compensated for individual trap response as discussed in section 3.4.5.

3.5 Test of calibrations

The samples taken by DESCARTES in the absolute calibrations (section 3.3) give all necessary data to be analysed as a normal flight. This can be used to investigate and compare the results from the different calibration methods. Plotting the results as functions of different parameters allows remaining systematic errors to be identified. In figures 3.17 and 3.18 the calculated absolute standard mixing ratio (c_a) from the analysis of the same set of calibration runs is analysed according to the two different calibration methods described in sections 3.3 and 3.4.

The mean of the estimated volume mixing ratio for the direct method, shown in figure 3.17, is per definition the target value as this is the same data as used for the calibration. As seen in the figure there is a problem in very low flows (probably due to the fact that the flow readings are close to the noise level of the flow meters) and runs with flow less then 10 SCCM are excluded from the calibration. This is indicated by the dotted line in the figure. A mean offset to the indirect method presented in figure 3.18 is easily seen. It is also clear that both methods have their worst precision in the case of low flows.

3.6 Other species than CFC-11

In the chromatograms four distinct peaks corresponding to the species CFC-11, CFC-113, methyl chloroform (CH_3CCl_3) and carbon tetrachloride (CCl_4) are recognised as seen in the sample chromatogram in figure 2.8 on page 16. As the instrument has been developed with primary focus on CFC-11 the calibrations method has also been developed, as dicussed in the previous parts in this chapter, for CFC-11. Exactly same procedure is however possible to adopt for the other species. In the following two sections the results are presented.

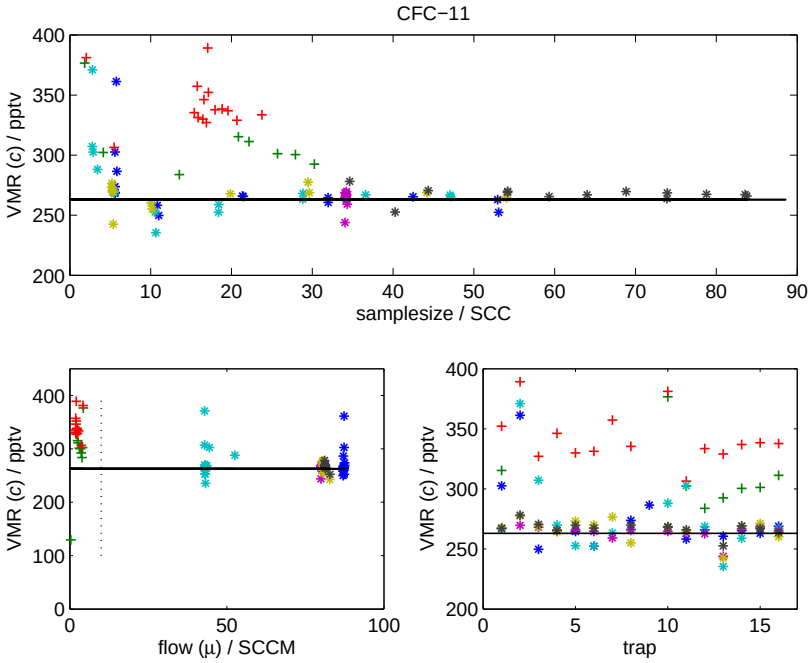

Figure 3.17: Results of calibrations from the direct absolute calibration method described in section 3.3. The black line indicates the known concentration of the calibration standard, $c_a = 263$ pptv. Each colour is one calibration run. Flows lower than 10 SCCM are not used in the fitting of the calibration function, those samples are marked by plus signs.

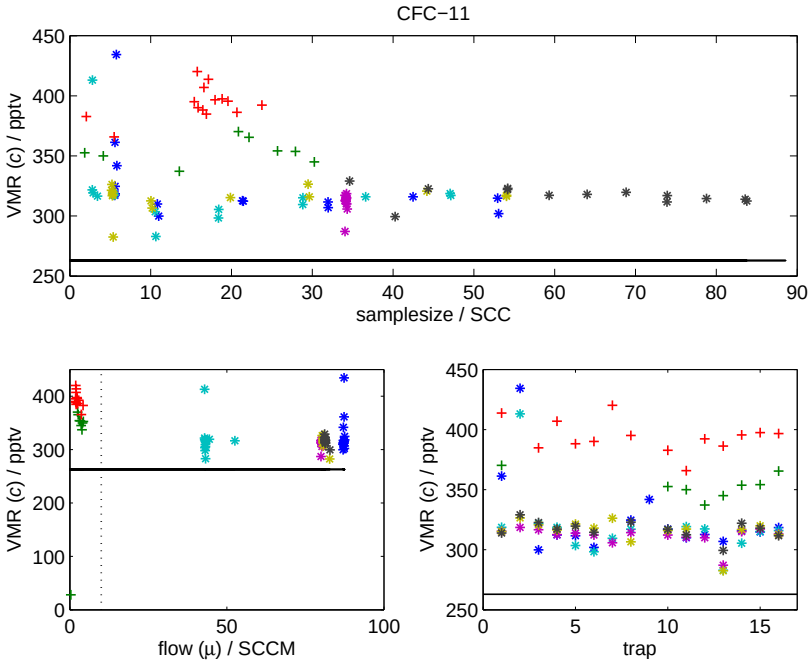

Figure 3.18: Results of calibrations from the indirect absolute calibration method described in section 3.4. Similar to figure 3.17. The y-axis covers not the same but equally sized intervals as in figure 3.17

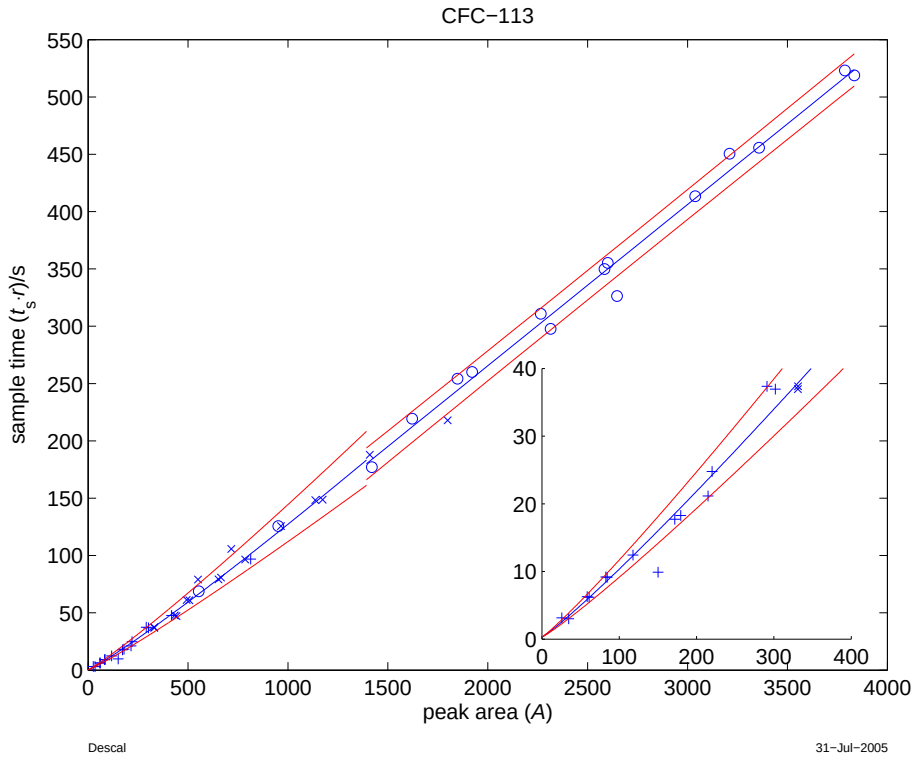

Figure 3.19: Calibration curve for CFC-113 the same way as figure 3.7.

3.6.1 CFC-113

Calibrations made by sampling a gas mixture by control of the GC show reliable results for CFC-113 as shown in figure 3.19 (to be compared to figure 3.7 on page 31). The largest uncertainty and contribution to the spread in these calibration is thought to be the assumption of stable flow.

As shown in section 3.3, controlling the sampling by the instrument ensures a good flow integration. As seen in figure 3.20 the calibration then fails completely for CFC-113.

As the mixing ratios of the species in the standards are fixed, scatter plots of the two species against each other eliminate all flow integration uncertainty. Figure 3.21 shows these scatter plots for samples taken in different ways. NOAA and UEA denote two different compressed natural air standards (NOAA means standard no. 4 and UEA no. 3 in table 3.1), while DESCARTES and GC denote the sampling methods. From a comparison of the upper right and the lower left panel we can see that the different standards both perform well, forming tight correlations, when sampling through the GC. The scatter in the top left panel shows that sampling with DESCARTES gives large uncertainty.

The sampling line of the instrument contains a two stage rubber diaphragm pump and a couple of switches leading the flow into the core sample box. Sampling calibration standards with the instrument goes through the last of those as illustrated in figure 3.22. This means that calibrations circuit for the direct absolute calibration also includes a Dynamco Dash-1 switch on the DESCARTES

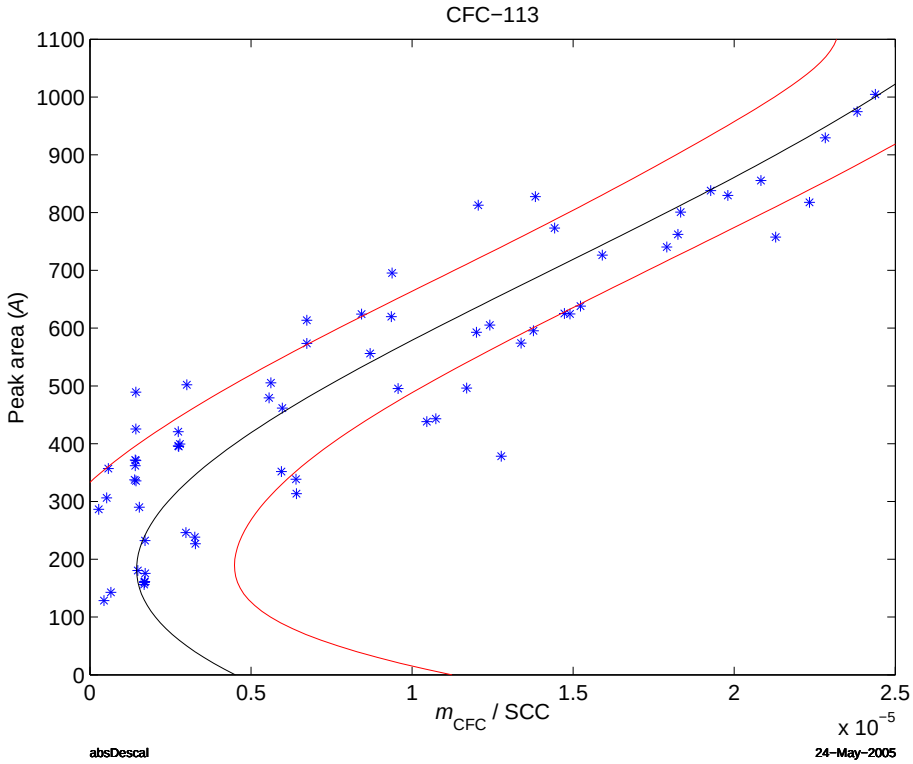

Figure 3.20: Direct method absolute calibration curve $h(A)$, for CFC-113 the same way as figure 3.3.

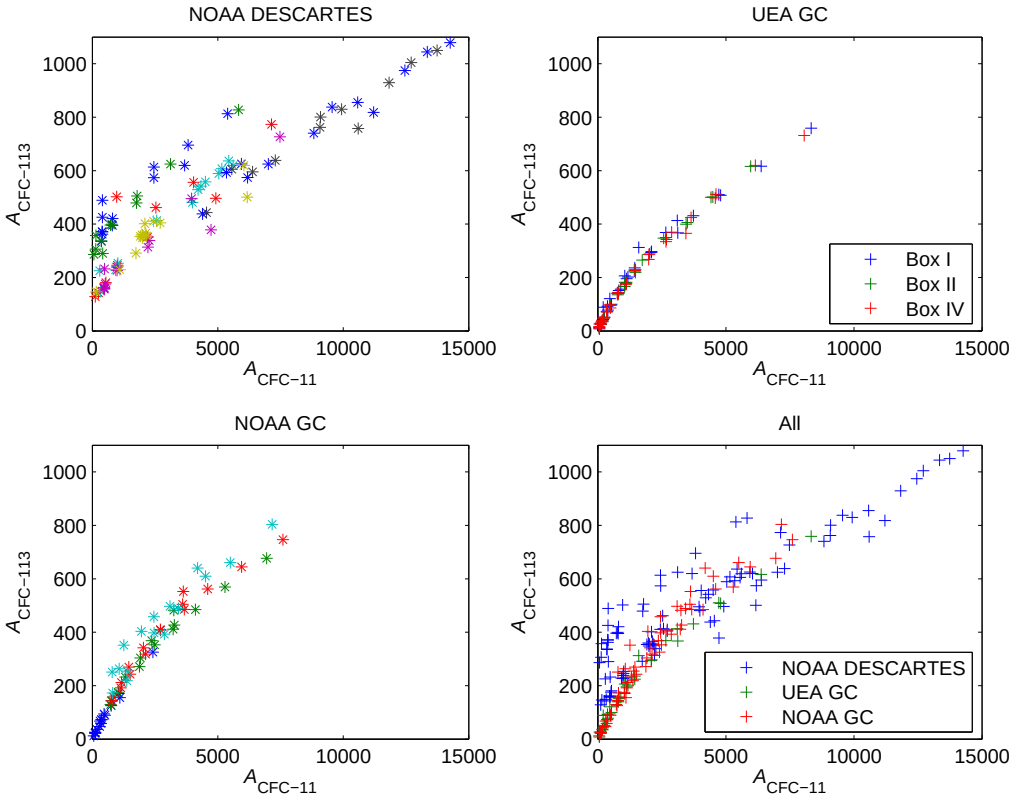

Figure 3.21: Correlations between chromatographic peak areas of CFC-11 and CFC-113 sampled through different sample lines.

instrument shown in figure 3.22 that the indirect sampling controlled by the GC does not. In the sample box the flow is let through another switch to a 16 position Valco valve onto which the trap is mounted. Except for the plastic and brass parts seen in figure 3.22, and the pump, the whole sample line is stainless steel. The regulators of the standard bottles also differ. The regulator of the synthetic standard is an ordinary brass regulator while the regulator for the compressed air standard used for the calibration is a special high purity regulator in electropolished stainless steel that is not thought to give adsorption processes. Appearently the problems sampling CFC-113 is due to the fact that the samples are passing the Dynamco Dash-1 switch.

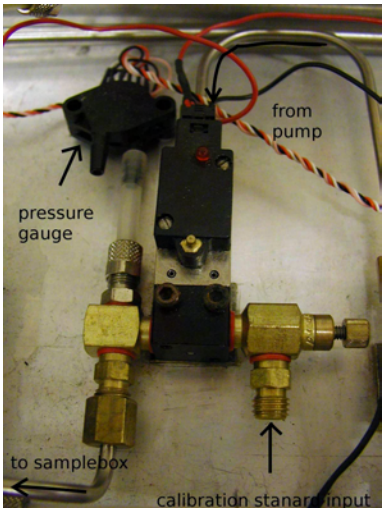

Figure 3.22: Dynamco Dash-1 switch and pressure meter. While sampling in the stratosphere the flow is going in the top of the switch while sampling standard enters the needle valve on the right.

3.6.2 Methyl chloroform and carbon tetrachloride

The two species methyl chloroform and carbon tetrachloride show similarly bad calibration results as CFC-113. In this case even the indirect calibration results (not presented) look similarly bad as the direct method presented in figures 3.23 and 3.24. The reason for the bad performance of the instrument to these species is not further investigated and no analysis of the flight data is presented for these species.

3.7 Discussion

The direct absolute calibration described in section 3.3 gives much smaller spread of calibration points than the indirect and much more complicated method described in section 3.4. This calibration is made in a way that, to a large extent, is similar to the samplings during flight which is also to it's favour. That this is the more reliable, and superior of the two is in no doubt. However as this method has not been used during the whole period that the instrument has made scientific measurements there is a question of which calibration method should be used for flights prior to the NOAA compressed air calibration standard becoming available. As seen in the test of the calibrations on the same data (presented in section 3.5), the calibrations show a significant absolute response difference. There are two possible origins for this difference:

System response change over time. The calibrations have been performed in two major calibration campaigns each rather concentrated in time. There is a possibility that the real system response of the analysis system has changed during the time between these two calibration campaigns. If this is

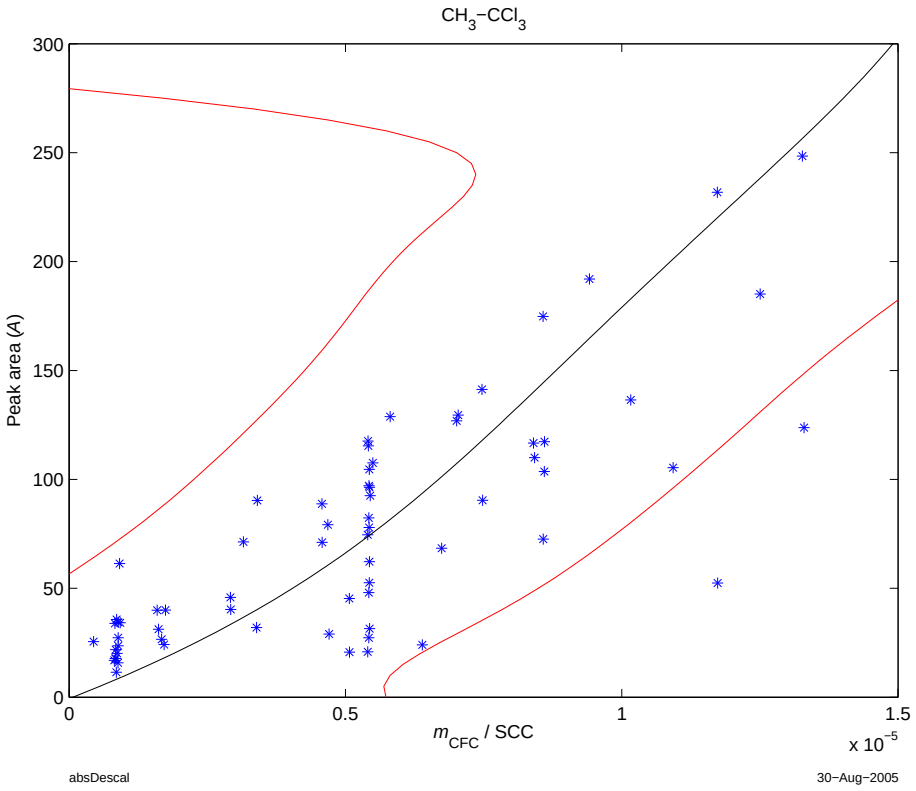

Figure 3.23: Direct method absolute calibration curve $h(A)$, for methyl chloroform the same way as figure 3.3.

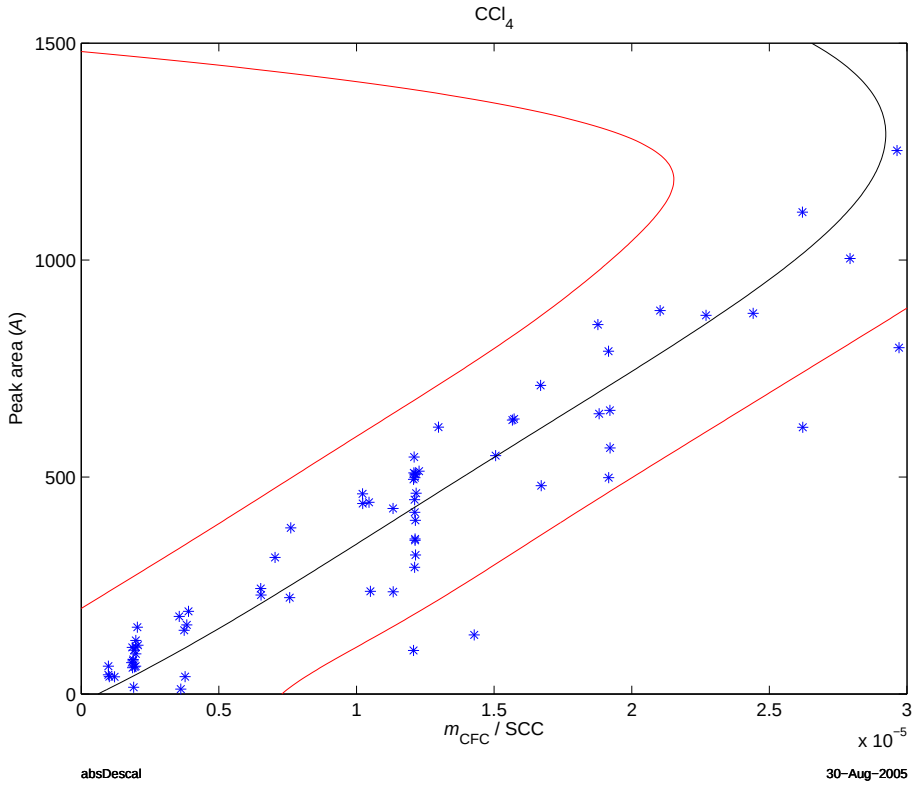

Figure 3.24: Direct method absolute calibration curve $h(A)$, for carbon tetrachloride the same way as figure 3.3.

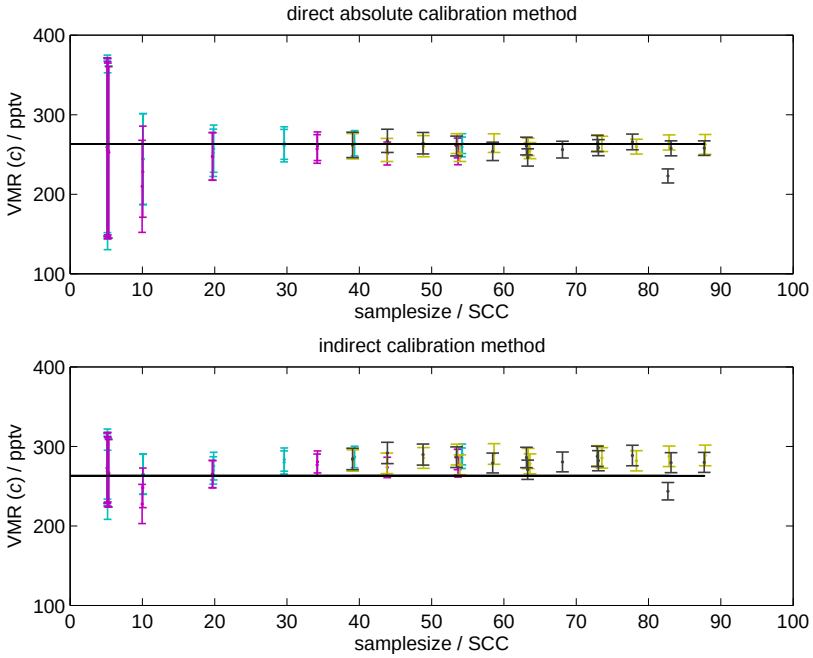

Figure 3.25: Calibration test for box II. Similar to the top panels of figures 3.17 and 3.18.

the case the calibration that is performed closest in time to the measurement should be used.

Systematic errors in calibrations. The two calibration methods follow two rather different approaches to the calibration problem. There might be systematic errors in either of the methods. From this point of view the direct absolute calibration method is thought to be the most reliable as it has large similarities to the flights and thereby it is thought that most systematic errors tend to cancel. If this is the case this approach should be used for all flights, even before the calibration had started.

The overall trend in the response for box I seen in figure 3.8 on page 33, together with the tests of the calibrations in figures 3.17 to 3.18 on page 43, might seem like an indication that this is a system response over time. However the other two boxes investigated show no such trend but, never the less, show the same discrepancy as shown in figures 3.25 and 3.26. The samples with large uncertainties are, as in calibrations of box I, associated with low flows.

Two different instruments have been used for the measurements: DESCARTES version II and version III.2. For the indirect calibration method the only dependence of the instrument is the flow meter calibration as most of the calibrations are performed directly on the sample boxes that are interchangeable between the instruments. The basic idea of the direct absolute method on the other hand is to use the instrument as much as possible to make systematic errors cancel. The question to ask is then if the instruments are similar enough to use the direct absolute calibrations from DESCARTES III.2 directly on DESCARTES II. The version II instrument has not been available in Kiruna for such a calibration with

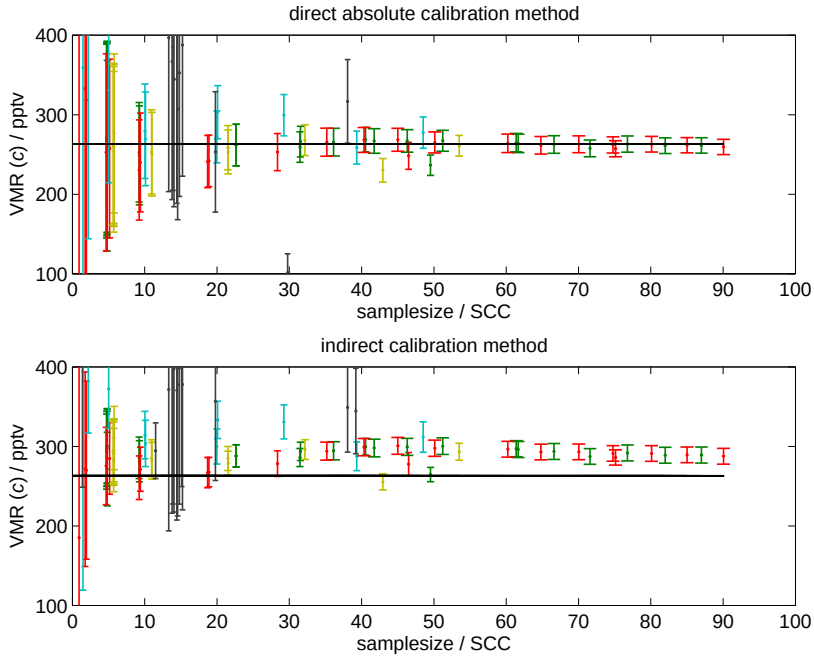

Figure 3.26: Calibration test for box IV.

our boxes and analysis system since the NOAA calibration standard has been available.

3.8 Conclusions

The sampling procedure using the GC is not trustworthy. It is the largest source of uncertainties in the project and the indirect calibration is complicated. Any true system response change over time of the order of magnitude that differs between the calibrations should have been seen overlayed on the individual trap response and the individual calibration response as an overall trend in for example the test samples presented in figure 3.8. As the difference in response between the calibrations is roughly similar for all the boxes used and there is no such trend in the calibrations, we have chosen to trust the direct absolute calibration method and say that the true system response is reliable for the whole period of measurements.

The two instruments are, from a hardware point of view, very similar. The pumps in the instruments are the same model, the tube dimensions and material are almost the same. The flow meters differ but the flow is anyway calibrated in a separate flow meter calibration. This was done at the same occasion with the same reference flow controller by the same operating personnel. The computers differ, the flight software is migrated from the version II instrument to the version III with adaptation of the code to work on the other computer. Anyway the actual flow meter readouts are performed by a machine code subroutine that is called in both the manual readouts during the flow meter calibration and during flights. These circumstances all speak in favour of the hypothesis that the instruments are

similar enough to use the direct absolute calibrations taken with the instrument version III.2 even for the version II.

The compensations for individual trap response and response of analysis is not used in the direct absolute calibration method. One common calibration response function is used for all boxes.

Unless especially noted, all the flight data presented in the following is analysed with the direct absolute calibration method.

Chapter 4

Simulation of trap adsorption

According to chromatographic theory there is for each adsorber–adsorbent pair in a packed column system a specific retention volume. Abnormal high flow speed may give considerably faster breakthrough. The sampling traps in the instrument work as short chromatographic columns with high adsorption. As DESCARTES during a flight is sampling at steadily decreasing pressure, both the linear flow speed through the trap and the volume of the air get higher.

This indicates that an investigation of the possibility for breakthrough to occur in CFC in the traps must be performed. Due to the low concentration of the species of interest a special technique with double traps had to be developed. The results are presented in section 4.3. In order to interpret the results from those experiments, and predict breakthrough in flight sampling, a simple model of the trap is needed. This model has previously been presented with first results in *Arvelius et al.* [2004].

The trap model constructed for this study is only a model of the trap behaviour on macroscopic level to see if the measured breakthrough in a double trap experiment can be explained by simple parameterisations of adsorption and desorption processes. For detailed understanding of those processes a microphysical model like e.g. *MacElroy et al.* [1997] is needed but that is beyond the scope of this text.

4.1 Introduction

The DESCARTES traps are pipes filled with a chemical adsorbent for CFCs - carboxen. Two physical processes determine how the CFCs in the air passing the traps are distributed in the adsorption bed. First the CFCs are adsorbed in a first step. As the adsorbent bed is homogeneous the chance for a particle to be absorbed per unit time is constant and the distribution will fall off exponentially. Meanwhile there is an continuous desorption going on of the already adsorbed CFCs. These will redistribute inside the trap, according to the same exponential fall-off.

As the adsorbent is meant to give quantitative adsorption, the ideal adsorbent would have infinite adsorption coefficient (κ_{a}) and zero desorption coefficient (κ_{d}). The time-scales for the adsorption and desorption processes are set by these constants. The adsorption is much faster and must happen on a time-scale shorter

than the time for an air parcel to pass the trap. The desorption is on a much longer time-scale. This is used for the modelling of the desorption in the trap which is made in two steps according to these two physical processes.

In order to make direct injection to the gas chromatograph during the analysis, without further pre-concentration steps, the size of the adsorption bed should preferably be as small as possible. This must be balanced against the fact that the breakthrough of the trap has to be under control. The traps of the DESCARTES instrument are rather small and this study aims to investigate which sample sizes might be considered safe under different conditions including different flow rates and pressures.

Adsorption of gases to a surface is a competitive situation in that the molecules adsorb to the surface more easily than to other adsorbed molecules. For adsorption up to the limit where a mono-layer of adsorbed molecules is formed there is a theory that adsorption efficiency is proportional to the unoccupied area, called Langmuir theory. The adsorbents used are the hydrofobic molecular sieves Carboxen 569 and 1000. A molecular sieve is an adsorbent that has a large micro porosity with pore sizes of the same order of size as the molecules of interest. Smaller molecules will enter strong adsorption sites in the pores while larger molecules only can adsorb on the outer surface, the sieve effect [*Harper*, 2000]. Molecular sieves also exhibit an effect called ultramicropore filling i. e. the pores get filled with the adsorbent [*Sing and Williams*, 2004]. The most interesting feature is thought to be the porosity volume rather than the surface area, even though they seems to be described by Langmuir isotherm theory and the porosity volume is difficult to measure [*Harper*, 2000]. The pore volume of Carboxen 569 and 1000 used in our traps is estimated to be of the same order of magnitude for the three intervals micro-pore ($0.3 - 2$ nm), meso-pore ($2 - 50$ nm) and macro-pore (> 50 nm) with about double volumes for Carboxen 1000 [*O'Doherty et al.*, 1993a]. Others claim that the adsorption in micro pores is not strictly Langmuirian but increases strongly for low concentrations [*Bertoni et al.*, 1981; *Namiesnik et al.*, 1981]. *Comes et al.* [1993] claims that Langmuir isotherms might need to be considered at concentrations above 1 ppm i. e. much higher than levels considered here.

As the traps are not perfect it is an interesting task to characterise their behaviour. The obvious interesting thing is the time when the adsorbate is flowing out from the trap. This is called the breakthrough time consistently with chromatography retention time. According to standard chromatography theory this shall happen when a certain volume of carrier gas has passed the column, the retention volume, and in analogy there shall be a breakthrough volume (V_b) when the trap starts to bleed it's adsorbates. To make samples in a safe way different definitions on a safe sample volume have been proposed.

Many attempts has been made to characterise and determine the breakthrough volume. In analogy with chromatography for example *Vidal-Madjar et al.* [1978] proposed that the breakthrough volume should be defined as the retention volume. In accordance with chromatographic theory it should then be possible to define a specific retention volume for the adsorbate-adsorber pair independent of bed geometry. This was used by *Bertoni et al.* [1981]; *Vidal-Madjar et al.* [1978] and *O'Doherty et al.* [1993a] in their studies to determine the spe-

cific retention volume with a chromatographic column packed with the adsorber. *Bertoni et al.* [1981] compared to direct breakthrough measurements on traps and showed good agreement for lighter compounds (C_1-C_5) but no agreement at all for heavier on Carbopak B and Tenax GC. The same study also showed that several compounds at the same time gives shorter retention time for the slower compounds due to competition for adsorption sites.

This approach has been criticised from many sources [*Harper*, 2000] to be unrealistic mainly due to the fact that the concentration of the adsorbate in the trap is higher during a constant sampling and the adsorption follows the Langmuir adsorption isotherm. Traps must be tested directly and with real sample concentrations. *Riba et al.* [1991] came up with a method of sampling well known volumes of well known standards to a trap, desorbing the trap and analysing the contents. The breakthrough volume is defined as the end of the proportional part of the relation volume-content. This method was developed by *Bertoni and Tappa* [1997] for low concentrations, referencing a second standard in the sample with much larger breakthrough volume. In the same article an indirect method for small samples is also developed based on a system with two traps in series where the sample is loaded to the first and, after elution by a carrier gas, both are analysed.

Later most studies has been performed by using the trap as a chromatographic column, looking continuously at the outflow with a chromatographic detector [*Harper*, 1993; *Betz et al.*, 1989; *Seshadri and Bozzelli*, 1983; *Comes et al.*, 1996, 1993; *O'Doherty et al.*, 1993a; *Namiesnik et al.*, 1981]. The breakthrough volume in these cases is expressed as the volume when either the outflow concentration is a certain fraction of the inflow concentration or when the integrated outflow is a certain fraction of the inflow. To be able to compare these *Harper* [1993] estimated that 5% breakthrough level (ratio between incoming and outgoing concentrations) corresponds to 0.25% breakthrough sample loss (the integrated outflow compared to the integrated inflow, in the following called cumulative breakthrough) and 33% breakthrough corresponds to 5% breakthrough sample loss. *Namiesnik et al.* [1981] consider breakthrough from the detection limit.

Yoon and Nelson [1990] claim that the ratio of out-flowing concentration from a trap to the ingoing (breakthrough level) evolves over time if the trap is fed by a homogeneous gas stream is given by

$$P = \frac{1}{1 + e^{k'(\tau - t)}} \tag{4.1}$$

which can be rewritten

$$\ln \frac{P}{1 - P} = -k'(\tau - t), \tag{4.2}$$

where k' is a rate constant, τ the time required for 50% breakthrough level, and t the time.

The function $P(t)$ in equation 4.1 is plotted in figure 4.1 left panel. To be able to compare these with the results of the experimental studies of *Roslin* [2003] even the cumulative breakthrough of the trap according to the same theory is calculated and plotted in the right panel.

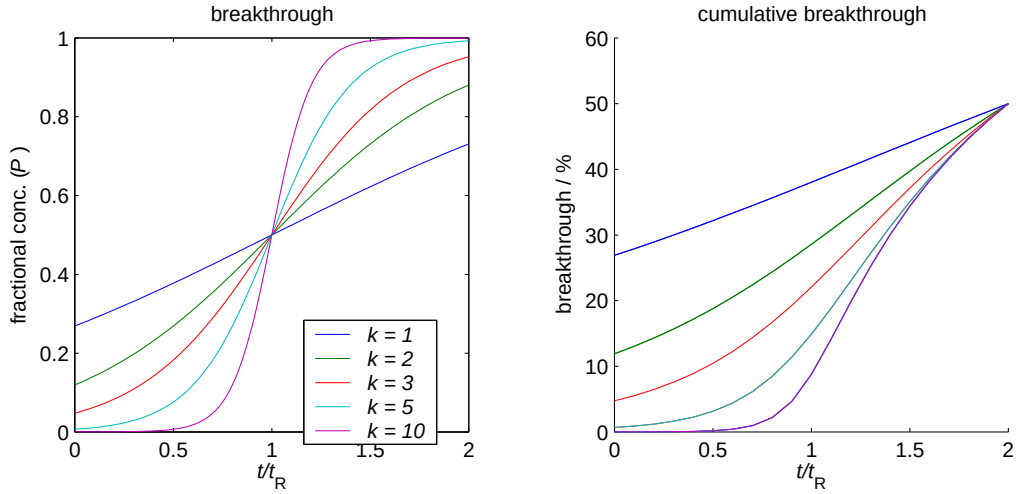

Figure 4.1: Theoretical breakthrough according to *Yoon and Nelson* [1984] for different values of k'

According to *Reilly et al.* [1962] the same physical quantity is given by

$$P(t) = \frac{1}{2} + \frac{1}{2}\,\mathrm{erf}\left(\frac{t - t_\mathrm{R}}{\sqrt{2}\,\sigma}\right) \tag{4.3}$$

where erf is the error function, t_R is the retention time and σ is the standard deviation of the peak. This is the same as [*Senum*, 1981]:

$$P(t) = \frac{1}{2}\,\mathrm{erfc}\left(\frac{t_\mathrm{R} - t}{\sqrt{2}\,\sigma}\right) + \frac{1}{2}\,\mathrm{erfc}\left(\frac{t_\mathrm{R} + t}{\sqrt{2}\,\sigma}\right), \tag{4.4}$$

where erfc is the complementary error function. This can be rewritten as a function of the sampled volume

$$P(V) = \frac{1}{2}\,\mathrm{erfc}\left(\sqrt{\frac{N}{2}}\left(1 - \frac{V}{V_\mathrm{R}}\right)\right) + \frac{1}{2}\,\mathrm{erfc}\left(\sqrt{\frac{N}{2}}\left(1 + \frac{V}{V_\mathrm{R}}\right)\right), \tag{4.5}$$

where V_R is the retention volume and N is the number of theoretical plates of the adsorbent [*Senum*, 1981]. The number of theoretical plates is a measure of the ability to separate species in chromatography. Assuming Gaussian peaks in the chromatogram it is defined as

$$N = \left(\frac{t_\mathrm{R}}{\sigma}\right)^2. \tag{4.6}$$

In the same manner as figure 4.1 the function $P(V)$ in equation 4.5 is plotted in figure 4.2 left panel. Plotting against the volume and time is fully comparable as a stable flow is assumed. However in figure 4.1 the plots are to double τ, that is the time of 50% breakthrough, while in figure 4.2 the plots are to double retention volume, corresponding to retention time that is not obviously the same as τ.

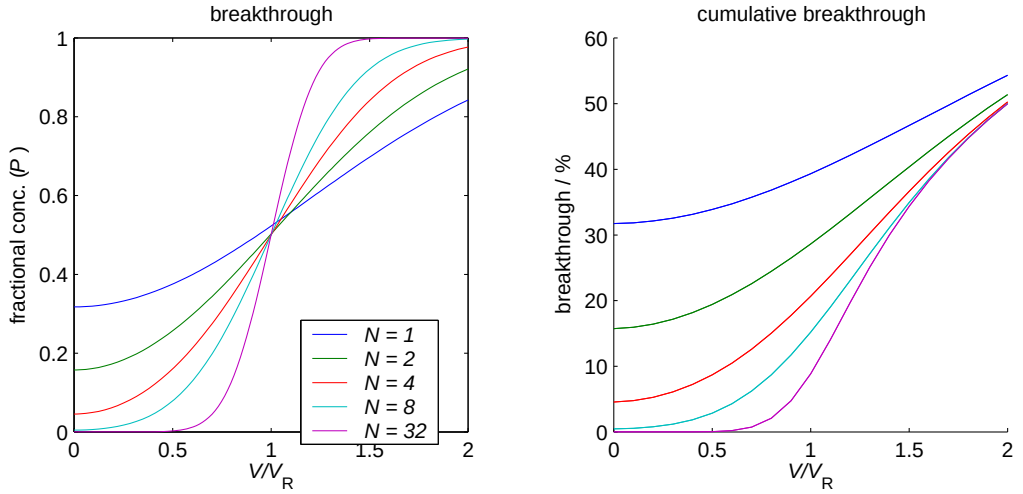

Figure 4.2: Theoretical breakthrough according to *Senum* [1981] for different values of N.

One way to ensure quantitative desorption is to divide the adsorber bed in two parts and analyse both. This is done with one main trap followed by a similar of half the length. The results from the analysis can be added as long as the sample in the second trap is $< 25\%$ of the sample in the first [*Harper*, 1993]. *Pankow* [1989] states the criterion that sample efficiency is $>90\%$ for volumes $\leq V_R/2$. Other estimations of the safe sample volume include

$$V_{max} = V_R(1 - 2/\sqrt{N}) \tag{4.7}$$

[*Raymond and Guiochon*, 1975]. This is obviously limited to N values larger than 4, *Vidal-Madjar et al.* [1978] has used it in situations where N is on the order of magnitude 100. *Senum* [1981] shows that this corresponds to 95% collection efficiency for small N with larger efficiency for larger values of N. This also means that to get better efficiency than 95% the trap must have a value of N larger than 4 for the species in question.

The breakthrough volume has been shown to be independent of flow speed up to a certain limit [*O'Doherty et al.*, 1993a; *Harper*, 1993; *Sturges and Elkins*, 1993] while it is very pronounced for higher flows [*Seshadri and Bozzelli*, 1983; *Sturges and Elkins*, 1993]. Smaller tube diameter for the traps has been shown to increase trap efficiency below 6 mm inner diameter [*Harper*, 1993]. Unfortunately there are only a few [*O'Doherty et al.*, 1993b,a] studies that have been published on such small traps as those investigated here (1.27 mm diameter).

4.2 Quantitative estimation

Carboxen 569 is expected to adsorb quantitatively if the flow linear velocity is less then 500 cm/min. The inner dimension of the sample traps in DESCARTES is 0.050 inch $\approx$ 1.27 mm which means that the maximum mass-flow allowed is

$$\mu_{max} = v\pi r^2 m/V.$$

where v is the linear flow velocity, r the inner dimension radius of the tube, m is the sampled mass and V the sampled volume. In terms of standard cubic centimeter (SCC), the ideal gas law becomes

$$m = \frac{KVp}{T} \tag{4.8}$$

where p is the pressure and the proportionality constant

$$K = \frac{1\ \text{SCC} \cdot 273.15\ \text{K}}{1\ \text{cm}^3 \cdot 1\ \text{atm}}.$$

The maximum flow is then

$$\frac{\mu_{\max} T}{p} = Kv\pi r^2 = 273.15 \cdot 500 \cdot \pi \cdot 0.127^2 \frac{\text{SCCM K}}{\text{atm}} = 6920 \frac{\text{SCCM K}}{\text{atm}}. \tag{4.9}$$

The largest flow is at the beginning of the sampling where the air pressure is 250 hPa and maximum temperature is about 220 K which means

$$\mu_{\max} = \frac{6920\,p}{T} \frac{\text{SCCM K}}{\text{atm}} \approx \frac{6920 \cdot 0.25}{220} \text{SCCM} \approx 8\,\text{SCCM}.$$

This limit is far below the mass flows during a normal sampling in a flight.

According to Scientific Instrument Services the breakthrough volume (V_b) of CFC-11 to Carboxen 569 is 5 L/g at 0 °C. DESCARTES traps are filled with $m_\text{c} = 15$ mg of Carboxen. For quantitative adsorption, no more gas than $V_\text{b}/2$ must go through the trap. The maximum volume for the sampling is then given by

$$V_{\max} = V_\text{b} m_\text{c}/2 = 5 \cdot 15/2\ \text{cm}^3 \approx 40\ \text{cm}^3. \tag{4.10}$$

The largest samples are taken at the highest altitudes (air pressure $\sim$ 10 hPa) with DESCARTES and the limit for these is then

$$m_{\max} = \frac{KV_{\max} p}{T} = \frac{273 \cdot 40 \cdot 0.01}{260}\ \text{SCC} \approx 0.4\ \text{SCC}. \tag{4.11}$$

The sample size during stratospheric flights at that height is significantly higher. This rough estimation implies that a special study on our system is needed. In the design of the instrument breakthrough experiments were performed under atmospheric pressure showing that 4 mg was enough for quantitative adsorption. To allow for the effects of reduced ambient pressure on the trapping efficiency the amount was increased to 15 mg [*Danis et al.*, 2000]. The situation is thereby thought to be better than could be feared from the quick calculations above.

4.3 Experiments

As mentioned above, the most common way to determine breakthrough is by direct detection with a detector after a trap. This approach can only be used for simple mixes where it is obvious which is the species breaking through and when the concentration of that species is large enough so that a fraction of it is detectable. The samples of our interest (CFCs in air) fulfil none of these requirements. Instead an approach inspired by the *Bertoni and Tappa* [1997] was

adopted. The principle was to put two similar traps in series, leading samples through the traps while integrating the flow and then to analyse the second of these traps to see if breakthrough had occurred in the first. To get a quantitative estimation of the sample size to breakthrough the first of these traps has been the same throughout the experiment but the second has been switched between different traps. In this way each of them samples the breakthrough from the first trap during one part of the experiment. Cumulative sums of the analysed contents of these give the total sample loss from the start of the experiment.

A series of experiments of this kind to see how the breakthrough effects could be quantified in the traps of DESCARTES was performed by *Roslin* [2003]. These were of four different kinds:

1. Flow-rate experiment where the flow rate was changed in a systematic way between the experiments, all performed at ambient pressure.

2. Low pressure experiment in a vacuum chamber where the DESCARTES instrument was adapted to do the double-trap experiment and sampled the air in low surrounding pressure.

3. Nitrogen purging experiment, where an air sample was taken during two minutes to initiate a sample in the first trap and then the flow was shifted to nitrogen.

4. Test flight, where the same setup was flown on a balloon for the same purpose.

The flow-rate experiment was made with the well known air standard, while the low pressure experiment and test flight sampled the ambient air with DESCARTES on-board pump. The mixing ratio of CFCs in these samples was assumed to be global average as measured by NOAA's Halocarbons and other Atmospheric Trace Species (HATS) group [*Hall et al.*, 2002] and previous flights under similar circumstances. As the parameter of prime interest is the volume sampled before breakthrough rather then the actual concentration in the second trap, the experiment does not depend critically on this uncertainty.

One of the primary goals with the work was to distinguish the effects of mass flow speed from volume flow speed. There is no pressure measurement in the trap which makes it difficult to compare these. Most of the pressure drop in the system is thought to appear in or very close to the trap. As these parts of the gas system are almost symmetric around the trap from a gas flow point of view, and there are measurements of the pressure before the trap as well as in the surroundings, the pressure is interpolated linearly between these values. For the double trap experiments the pressure is assumed to drop similarly over both traps. The temperature in the trap is assumed to be similar to the temperature of the flow measured before the trap and the volume flow is calculated according to the ideal gas law. [*Roslin*, 2003, pages 12–14]

One test in this study was to initialise the trap with an air sample and then flush the trap with pure nitrogen. A similar effect was achieved in the flight experiment by taking the first sample in the troposphere.

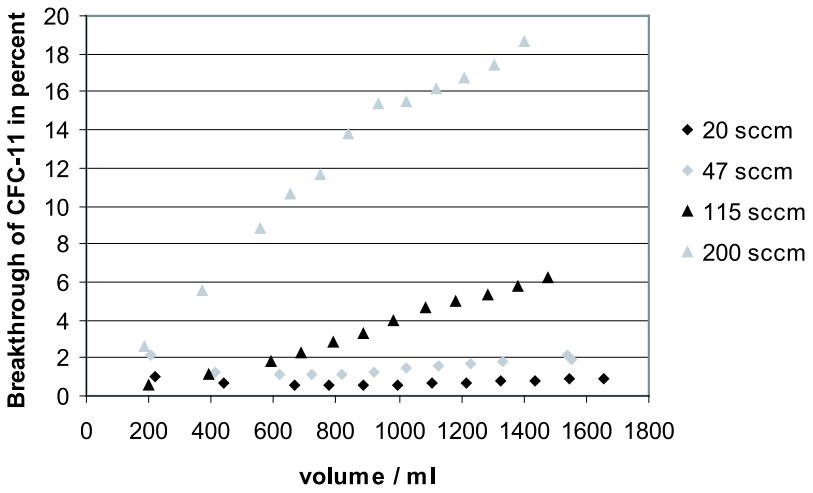

Figure 4.3: Accumulated breakthrough of CFC-11 as a function of sampled volume for different flow speeds. Reprinted from *Roslin* [2003] Figure 10.

4.3.1 Results

The flow-rate experiment showed a clear influence of the flow speed on the breakthrough. It was also clear from this test that this influence is stronger than a direct proportionality. Figure 4.3 shows the ratio of the cumulative sums of the amounts of CFCs in the second traps to the cumulative amounts of CFCs in the sample expressed in percent. Notice that the difference in flow speed between the two fastest tests are less then two-fold while the difference in breakthrough is about tree-fold.

For these experiments it is not obvious how large the breakthrough volume is. By comparison with the theoretical curves presented in figure 4.2 the number of theoretical plates and breakthrough volumes should be possible to deduce from the best theoretical fit. Figure 4.4 shows some of the same functions from figures 4.1 and 4.2 but stretched along the x axis to fit the end values of each of the experimental series. As seen in the figure these theories give rather similar solutions but make no success in describing the experiment results.

The experiment in vacuum tank sampled the air inside the tank, the under lying assumption being that the mixing ratio in the tank is stable and similar to the surroundings. This should in principle answer the question of whether the breakthrough is linearly dependent on the volume flow speed. A few tests were made but only one was technically successful. The result is shown in figure 4.5, plotted in the same way as figure 4.3. The mass-flows were about 25 SCCM and 390 SCCM respectively while the volume flows were estimated to 160 ml/min and 270 ml/min respectively [*Roslin*, 2003]. In comparison with figure 4.3 one can see that the breakthrough of the 50 hPa test is about threefold the 20 SCCM test but half the 115 SCCM that has a smaller volume flow speed. From these tests is it obvious that the simplest hypothesis, that the breakthrough is directly proportional to the volume flow speed, is not correct. As these results do not predict the breakthrough in general, a numerical simulation was proposed with the aim to reproduce the experiments and give a general understanding.

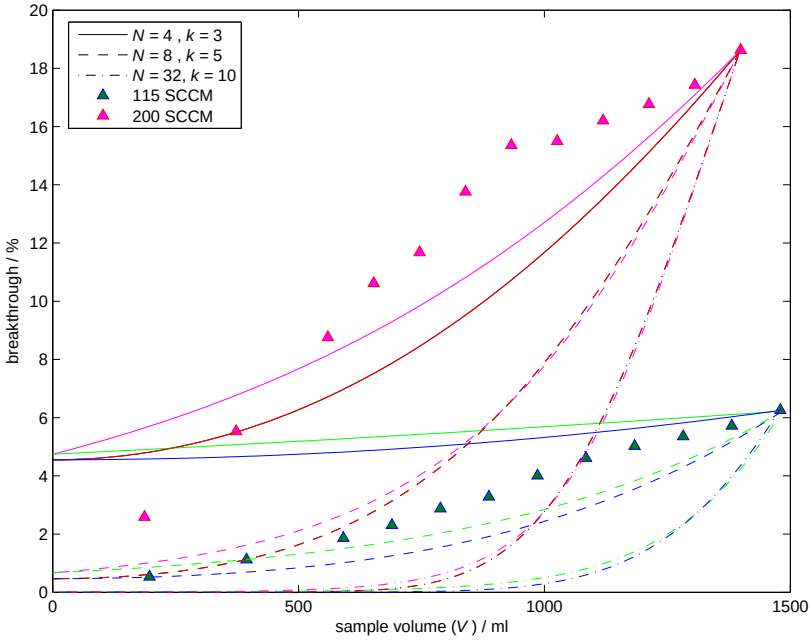

Figure 4.4: Comparison between the experimental accumulated breakthrough from figure 4.3 with chosen theoretical solutions of the two theories discussed. Experimental results are marked with triangles. The theory of *Yoon and Nelson* [1984] from figure 4.1 is plotted in magenta and green while the theory of *Reilly et al.* [1962] from figure 4.2 is plotted in red and blue.

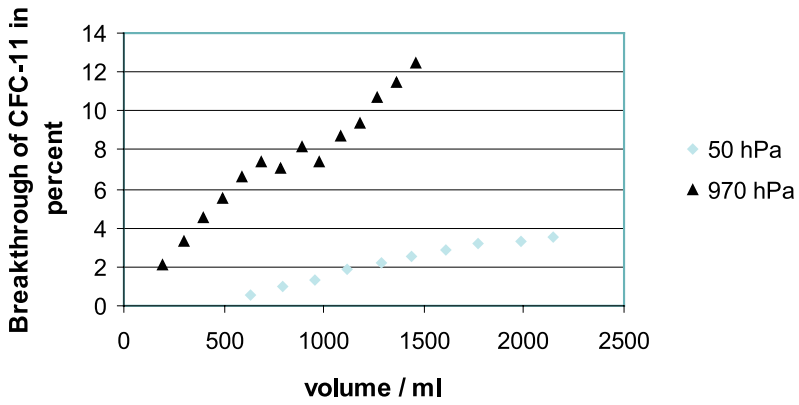

Figure 4.5: Accumulated breakthrough of CFC-11 as a function of sampled volume for low-pressure experiment and normal pressure reference. Reprinted from *Roslin* [2003] Figure 12.

The nitrogen purging experiment showed that adsorbent was continuously purged off the trap at a constant level, low but significantly above the detection limit.

The launch at the test flight was heavily delayed due to technical problems in other parts of the flight train. Due to this disturbance the experiment ran out of battery power after five samples. In the last of those, however, the sample in the second trap showed that the outflow concentration from the first trap was about 19 pptv [Roslin priv. comm]. This is about 4 times the estimated inflow concentration at that height from other measurements during similar circumstances, showing that the already trapped CFC-11 in the first trap was bleeding off to the second.

The first sample of 433 ml was taken at a mass flow rate of 214 SCCM and a volume flow estimated to 300 ml/min shows a breakthrough of about 8%. This fits rather well with the 200 SCCM flow rate test that was done at atmospheric pressure at an estimated volume flow speed of 186 ml/min [Roslin priv. comm.] indicating that the mass flow speed is the more important parameter.

4.4 General model description

The model developed in this study to investigate the behaviour of the traps is a simple macroscopic model. The basic principle is that the amount of adsorbent in the trap as a function of the depth into the adsorption bed is calculated. The adsorption bed is in the model sliced up in a finite number of bins and a numerical value is assigned to the amount of adsorbent in each bin. The adsorption and desorption processes are parameterised with constant adsorption and desorption coefficients. The adsorption of new adsorbent to the bins as well as the desorption of the previously bound is calculated in time steps according to two different algorithms presented in sections 4.5 and 4.6. The basic principle is shown graphically in figure 4.6.

In the model the trap is divided into b bins evenly distributed in depth of the adsorption bed (x) with width $\Delta x \equiv x_\mathrm{t}/b$, where x_t is the total length of the two traps in the double trap experiment. The fraction of CFC absorbed in one bin while passing is given by $\Delta x\, \kappa_\mathrm{a}/v$ where v is the linear flow velocity. This fraction must of course be small. As this fraction is common in the coming calculations, we can define the new constant

$$K_\mathrm{a} \equiv \frac{\Delta x\, \kappa_\mathrm{a}}{v} \ll 1. \tag{4.12}$$

The first step can be taken for a time Δt which is short compared to the desorption time, then a redistribution is computed for the desorbed parts. The desorbed amount is a fraction of the adsorbed according to

$$\Delta N_\mathrm{d}(n) = -N(n)\, \kappa_\mathrm{d}\, \Delta t \tag{4.13}$$

from which it is obvious that

$$K_\mathrm{d} \equiv \kappa_\mathrm{d}\, \Delta t \ll 1 \tag{4.14}$$

must be fulfilled.

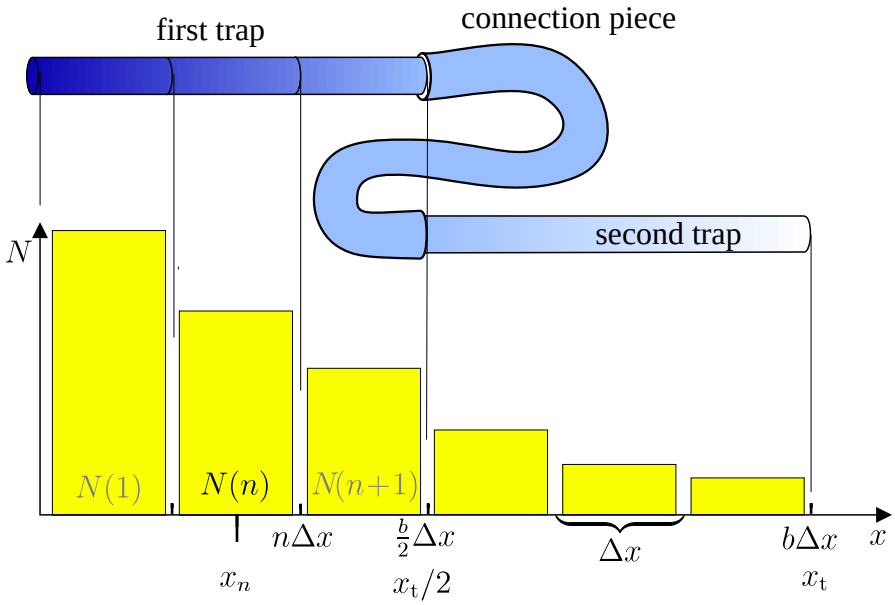

Figure 4.6: Histogram representation of the model. In the model the amount of trapped adsorbents is represented by numbers $N(n)$ plotted in the yellow histogram. Each of these corresponds to a slice of a trap of length Δx in the double trap experiments. The first $b/2$ of the total b bins corresponds to the first trap and the rest to the second.

Test runs have shown that the performance of the model does not change significantly for K_a and K_d lower than 0.1. When a model run shall be performed values for the adsorption and desorption coefficients as well as flow velocity are entered to the model. From the given values of κ_a and v the lowest possible even integer value of b to achieve $K_\mathrm{a} < 0.1$ is calculated and from the given value of κ_d the largest possible time step (Δt) that fulfils $K_\mathrm{d} < 0.1$ is calculated. In this way the computational speed is maximised.

All the laboratory tests (and the test flight) with double traps are performed in a way that the first trap is fixed and the flow of all the samples goes through it while the second trap is shifted after each sample to get a time series of breakthrough from the investigated first trap. To be able to compare the model results with the measured breakthrough in the double trap experiment, the above algorithm makes sure that the number of bins in the model is even. The model is divided in two parts, the first $b/2$ bins are treated as the first trap and the rest as the second trap. In the simulation numerical values of the adsorbent amount contained in each bin (N) are stored in a vector $\mathbf{N}$ covering both traps. For all simulations to be compared to these tests the second half of the vector $\mathbf{N}$ in the model is, at times of this trap being exchanged, copied to another vector and all values replaced by zeros to simulate a new empty trap. An example of the contents in the trap bins in the end state of a simulation is shown in figure 4.7. In this run there are only 32 bins in the model. The blue colour shows the contents in the traps that was in the flow in the last integration step and in red the sum in the previous traps. It can be seen that the second trap has been exchanged, thereby the discontinuity between the 16th and 17th bins. In the sum the dis-

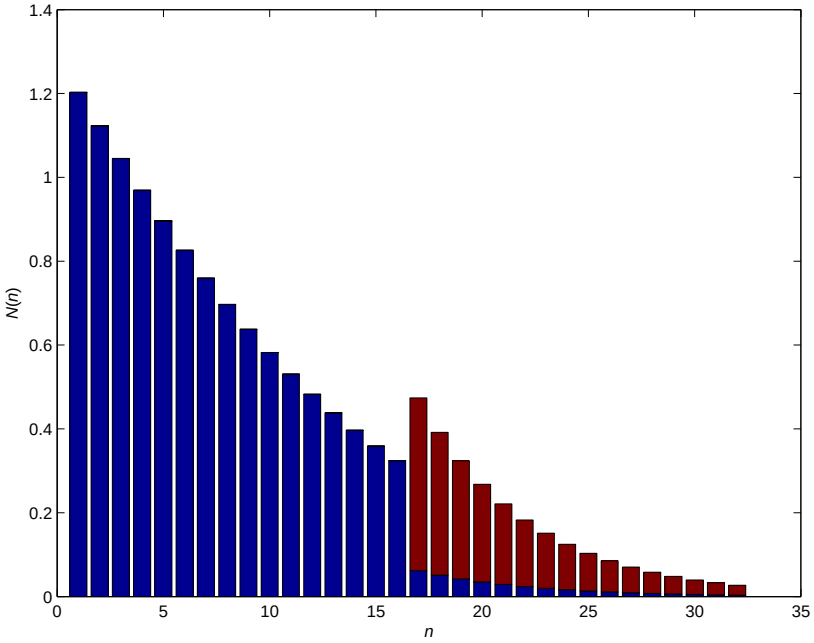

Figure 4.7: Contents in model bins after some iterations and trap exchange. The traps in the flow line are plotted in blue and the traps already shifted away from the second position in red

continuity is positive, i. e. the sum of the contents in the first bin of all the traps that have been in the second position is larger than the contents in the last bin in the first trap. This can be understood as the concentrations in the second traps are preserved when they are moved out of the flow while there is still desorption from the first trap that is in the flow the whole time.

For the iteration of the model two different algorithms has been developed described in sections 4.5 and 4.6. For simulations that both algorithms apply to they should give identical results. Several test-runs in different parts of parameter space confirm that they do. From a programming point of view they are rather different and they share almost no code which is a good indication that the basics of the algorithms are free from major bugs.

4.5 Distribution approach

This approach to the making of an iteration algorithm works in two steps iteratively and is highly vectorised. The underlying assumption is that unbound CFCs will distribute exponentially, i. e. the probability for adsorption per unit length in the trap is constant. The principle is shown graphically in figure 4.8.

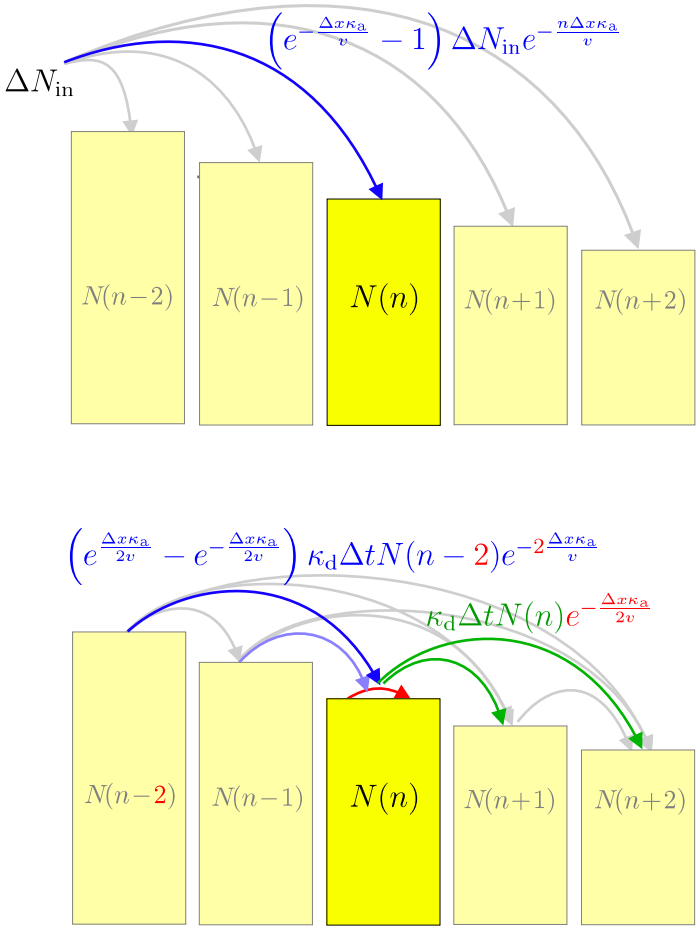

Figure 4.8: The principle of the algorithm for the distribution approach. In the top panel the inflow distribution step where the expression for the contribution to bin n, $\Delta N_{\text{a}}(n)$ is given. In the bottom panel the redistribution step where the inflow from *one* of the other bins, as indicated by the darker blue arrow, is given in blue. The total outflow going to all the subsequent bins and out of the trap is given in green, the exponential factor in the end is due to the self readsorption indicated by the red arrow.

4.5.1 Inflow distribution

If an amount of CFCs ΔN_{in} is entering the trap they will be distributed according to

$$dN(x) = \frac{\Delta N_{\mathrm{in}} e^{-\frac{x\kappa_{\mathrm{a}}}{v}}}{\int_0^\infty e^{-\frac{x'\kappa_{\mathrm{a}}}{v}} dx'} dx. \tag{4.15}$$

Each time step in the model an amount ΔN_{in} is entering the trap. ΔN_{in} may of course change over time. This inflow will be distributed in the discrete bins of the model and make a contribution ΔN_{a} to N according to

$$\begin{aligned}
\Delta N_{\mathrm{a}}(n) &= \frac{\int_{x_n-\frac{\Delta x}{2}}^{x_n+\frac{\Delta x}{2}} \Delta N_{\mathrm{in}}\, e^{-\frac{x\kappa_{\mathrm{a}}}{v}} dx}{\int_0^\infty e^{-\frac{x\kappa_{\mathrm{a}}}{v}} dx} \\
&= \frac{\kappa_{\mathrm{a}}}{v} \int_{x_n-\frac{\Delta x}{2}}^{x_n+\frac{\Delta x}{2}} \Delta N_{\mathrm{in}}\, e^{-\frac{x\kappa_{\mathrm{a}}}{v}} dx \\
&= \Delta N_{\mathrm{in}}\, e^{-\frac{x_n\kappa_{\mathrm{a}}}{v}} \left(e^{\frac{\Delta x\,\kappa_{\mathrm{a}}}{2v}} - e^{-\frac{\Delta x\,\kappa_{\mathrm{a}}}{2v}} \right) \\
&= \left(e^{\frac{K_{\mathrm{a}}}{2}} - e^{-\frac{K_{\mathrm{a}}}{2}} \right) \Delta N_{\mathrm{in}}\, e^{-(n-\frac{1}{2})K_{\mathrm{a}}} \\
&= \left(e^{K_{\mathrm{a}}} - 1 \right) \Delta N_{\mathrm{in}}\, e^{-n\,K_{\mathrm{a}}}.
\end{aligned} \tag{4.16}$$

ΔN_{a} shall be thought of as the change in N due to adsorption, similar nomenclature, ΔN with a subscript will be used for several terms summing up to the total change in N during a time step, ΔN.

4.5.2 Desorption redistribution

Each time step there is desorption from each bin according to equation 4.13. The desorbed CFCs are redistributed according to the same exponential decrease as in equation 4.16. Each bin then gets a contribution from each earlier bin in the trap which shall be summed up according to

$$\Delta N_{\mathrm{r}}(n) = \sum_{i=1}^{n-1} \frac{\int_{x_n-\frac{\Delta x}{2}}^{x_n+\frac{\Delta x}{2}} -\Delta N_{\mathrm{d}}(i)\, e^{-\frac{(x-x_i)\kappa_{\mathrm{a}}}{v}} dx}{\int_0^\infty e^{-\frac{x\kappa_{\mathrm{a}}}{v}} dx}, \tag{4.17}$$

where $-\Delta N_{\mathrm{d}}$ is the amount desorbed from a bin during the time step. After similar steps as in the calculations above this ends up in

$$\begin{aligned}
\Delta N_{\mathrm{r}}(n) &= \left(e^{\frac{K_{\mathrm{a}}}{2}} - e^{-\frac{K_{\mathrm{a}}}{2}} \right) \sum_{i=1}^{n-1} N(i) \kappa_{\mathrm{d}} \Delta t e^{-\frac{(n-i)\Delta x \kappa_{\mathrm{a}}}{v}} \\
&= \left(e^{\frac{K_{\mathrm{a}}}{2}} - e^{-\frac{K_{\mathrm{a}}}{2}} \right) K_{\mathrm{d}} \sum_{i=1}^{n-1} N(i)\, e^{-(n-i)K_{\mathrm{a}}}.
\end{aligned} \tag{4.18}$$

For later use we could also see that for n larger than a few, for any positive integer k smaller than n;

$$\begin{aligned}
&\Delta N_{\mathrm{r}}(n) \\
&= \left(e^{\frac{K_{\mathrm{a}}}{2}} - e^{-\frac{K_{\mathrm{a}}}{2}}\right) K_{\mathrm{d}} \left(\sum_{i=1}^{k} N(i)\, e^{-(n-i)K_{\mathrm{a}}} + \sum_{i=k+1}^{n-1} N(i)\, e^{-(n-i)K_{\mathrm{a}}}\right) \\
&= \left(e^{\frac{K_{\mathrm{a}}}{2}} - e^{-\frac{K_{\mathrm{a}}}{2}}\right) K_{\mathrm{d}} \left(e^{(k-n)K_{\mathrm{a}}} \sum_{i=1}^{k} N(i)\, e^{-(k-i)K_{\mathrm{a}}} + \sum_{i=k+1}^{n-1} N(i)\, e^{-(n-i)K_{\mathrm{a}}}\right).
\end{aligned} \tag{4.19}$$

There is also some self re-adsorption in the bin but as the desorption is distributed over the trap it is assumed to be emitted in the centre of the bin and therefore only half the bin is exposed and the term for $i = n$ is

$$\begin{aligned}
\Delta N_{\mathrm{s}}(n) &= \frac{\int_0^{\frac{\Delta x}{2}} -\Delta N_{\mathrm{d}}(n)\, e^{-\frac{x\kappa_{\mathrm{a}}}{v}} dx}{\int_0^{\infty} e^{-\frac{x\kappa_{\mathrm{a}}}{v}} dx} \\
&= -K_{\mathrm{d}}\, N(n) \left(e^{-\frac{K_{\mathrm{a}}}{2}} - 1\right).
\end{aligned} \tag{4.20}$$

The contribution to bin n in this step is then $\Delta N_{\mathrm{d}}(n) + \Delta N_{\mathrm{r}}(n) + \Delta N_{\mathrm{s}}(n)$. After this step a new contribution from sampling a time interval Δt can be computed according to section 4.5.1 and these steps are then altered iteratively.

4.5.3 Model performance monitoring

To monitor the performance of the model it is interesting to see that the total inflow is either adsorbed or flows out. For this reason the outflow is also calculated in both steps. In the derivation of these formule it is concluded that there is no difference depending on what comes after the trap and that one can therefore calculate as if the tube was filled with carboxen for infinite length.

The total amount of CFC that does not get trapped in the first adsorption step is then

$$\begin{aligned}
\Delta N_{\mathrm{out,a}} &= \int_{x_{\mathrm{t}}}^{\infty} \frac{dN(x)}{dx} dx \\
&= \frac{\int_{x_{\mathrm{t}}}^{\infty} \Delta N_{\mathrm{in}}\, e^{-\frac{x\kappa_{\mathrm{a}}}{v}} dx}{\int_0^{\infty} e^{-\frac{x\kappa_{\mathrm{a}}}{v}} dx} \\
&= \frac{\kappa_{\mathrm{a}}}{v} \Delta N_{\mathrm{in}} \int_{x_{\mathrm{t}}}^{\infty} e^{-\frac{x\kappa_{\mathrm{a}}}{v}} dx \\
&= \Delta N_{\mathrm{in}}\, e^{-\frac{x_{\mathrm{t}}\kappa_{\mathrm{a}}}{v}} \\
&= \Delta N_{\mathrm{in}}\, e^{-bK_{\mathrm{a}}}.
\end{aligned} \tag{4.21}$$

The total outflow during a redistribution step is a sum of contributions from

desorption in all bins similar to equation 4.17,

$$\begin{aligned}\Delta N_{\mathrm{out,r}} &= \sum_{i=1}^{b} \frac{\int_{x_\mathrm{t}-x_i}^{\infty} -\Delta N_\mathrm{d}(i) e^{-\frac{x\kappa_\mathrm{a}}{v}} dx}{\int_0^\infty e^{-\frac{x\kappa_\mathrm{a}}{v}} dx} \\ &= K_\mathrm{d} \sum_{i=1}^{b} N(i) e^{-\frac{(x_\mathrm{t}-x_i)\kappa_\mathrm{a}}{v}} \\ &= K_\mathrm{d} \sum_{i=1}^{b} N(i) e^{-(b-i+0.5)K_\mathrm{a}}.\end{aligned} \tag{4.22}$$

4.5.4 Algorithm

The binning and the time step of the model is set from the limitations in equations 4.12 and 4.14 by setting $K_\mathrm{a} \approx 0.1$ and $K_\mathrm{d} \approx 0.1$.

The calculations of the distribution in the trap are made with a few matrix operations. First the amount of CFC adsorbed in each bin at time t is represented by a vector

$$\mathbf{N}(t) = \begin{pmatrix} N_1 & N_2 & \dots & N_b \end{pmatrix} \tag{4.23}$$

such that $N_n \equiv N(n)$. The calculation of the initial distribution according to equation 4.16 gives

$$\mathbf{N}(t) = \mathbf{N}(t-\Delta t) + \Delta N_\mathrm{in} \begin{pmatrix} e^{-0.5K_\mathrm{a}} & e^{-1.5K_\mathrm{a}} & \dots & e^{-(b-0.5)K_\mathrm{a}} \end{pmatrix} \tag{4.24}$$

starting from an empty trap, the zero vector. The outflow is calculated according to equation 4.21. A vector

$$\mathbf{E} \equiv \begin{pmatrix} e^{-(b-1)K_\mathrm{a}} & e^{-(b-2)K_\mathrm{a}} & \dots & e^{-K_\mathrm{a}} \end{pmatrix} \tag{4.25}$$

is calculated and then the $(b-1) \times b$ matrix

$$\begin{aligned}\mathbf{N}^\top \mathbf{E} &= \begin{pmatrix} N_1 \\ N_2 \\ \vdots \\ N_b \end{pmatrix} \begin{pmatrix} e^{-(b-1)K_\mathrm{a}} & e^{-(b-2)K_\mathrm{a}} & \dots & e^{-K_\mathrm{a}} \end{pmatrix} \\ &= \begin{pmatrix} N_1 e^{-(b-1)K_\mathrm{a}} & N_1 e^{-(b-2)K_\mathrm{a}} & \dots & N_1 e^{-K_\mathrm{a}} \\ N_2 e^{-(b-1)K_\mathrm{a}} & N_2 e^{-(b-2)K_\mathrm{a}} & \dots & N_2 e^{-K_\mathrm{a}} \\ \vdots & \vdots & \ddots & \vdots \\ N_b e^{-(b-1)K_\mathrm{a}} & N_b e^{-(b-2)K_\mathrm{a}} & \dots & N_b e^{-K_\mathrm{a}} \end{pmatrix}.\end{aligned} \tag{4.26}$$

Now the last sum in equation 4.18 can be identified as the sum of the upper right diagonals of the matrix starting with $n = 2$ at the top right element and the last bin as the sum of the diagonal starting in the upper left corner.

When parameters are chosen in a manner that the binning in the model is forced to be very fine, the matrix $\mathbf{N}^\top \mathbf{E}$, that has a size that grows with number of bins squared, may grow larger than the available computer memory allows. Then the problem can be divided by use of equation 4.19 and instead of $\mathbf{N}$ and

E split them into smaller parts by division points k the part between k_i and k_{i+1} is then

$$\mathbf{N}_i(t) = \begin{pmatrix} N_{k_i+1} & N_{k_i+2} & \dots & N_{k_{i+1}} \end{pmatrix} \tag{4.27}$$

where N_k is the same as in equation 4.24 and

$$\mathbf{E}_i = \begin{pmatrix} e^{-(b-k_i-1)K_\mathrm{a}} & e^{-(b-k_i-2)K_\mathrm{a}} & \dots & e^{-(b-k_{i+1})K_\mathrm{a}} \end{pmatrix}. \tag{4.28}$$

The matrix then becomes

$$\begin{aligned} \mathbf{N}_i^\top \mathbf{E}_i &= \begin{pmatrix} N_{k_i+1} \\ N_{k_i+2} \\ \vdots \\ N_{k_{i+1}} \end{pmatrix} \begin{pmatrix} e^{-(b-k_i-1)K_\mathrm{a}} & e^{-(b-k_i-2)K_\mathrm{a}} & \dots & e^{-(b-k_{i+1})K_\mathrm{a}} \end{pmatrix} \\ &= \begin{pmatrix} N_{k_i+1}e^{-(b-k_i-1)K_\mathrm{a}} & N_{k_i+1}e^{-(b-k_i-2)K_\mathrm{a}} & \dots & N_{k_i+1}e^{-(b-k_{i+1})K_\mathrm{a}} \\ N_{k_i+2}e^{-(b-k_i-1)K_\mathrm{a}} & N_{k_i+2}e^{-(b-k_i-2)K_\mathrm{a}} & \dots & N_{k_i+2}e^{-(b-k_{i+1})K_\mathrm{a}} \\ \vdots & \vdots & \ddots & \vdots \\ N_{k_{i+1}}e^{-(b-k_i-1)K_\mathrm{a}} & N_{k_{i+1}}e^{-(b-k_i-2)K_\mathrm{a}} & \dots & N_{k_{i+1}}e^{-(b-k_{i+1})K_\mathrm{a}} \end{pmatrix}. \end{aligned} \tag{4.29}$$

As in the previous case the last sum in equation 4.19 can be identified as the sum of the diagonals in this matrix. The sum from 1 to k is trivial to calculate as well as the exponential factor.

4.6 Serial approach

This approach to the iteration algorithm is to calculate the adsorption and desorption simultaneously in one bin at a time and loop over the bins in geometrical order. An advantage with this approach over the distribution approach is that it is not limited to the exponential distributions between bins and thereby Langmuir theory can be inferred. The principle is shown graphically in figure 4.9.

In each bin the adsorption probability is considered constant. If we call the inflow of CFC to bin n from the previous bin $N_\mathrm{g}(n)$ the amount adsorbed in the bin with width Δx is given by

$$\begin{aligned} \Delta N_\mathrm{a}(n) &= \frac{\int_0^{\Delta x} N_\mathrm{g}(n) e^{-\frac{x\kappa_\mathrm{a}}{v}} dx}{\int_0^{\infty} e^{-\frac{x\kappa_\mathrm{a}}{v}} dx} \\ &= \frac{\kappa_\mathrm{a}}{v} \int_0^{\Delta x} N_\mathrm{g}(n) e^{-\frac{x\kappa_\mathrm{a}}{v}} dx \\ &= -N_\mathrm{g}(n) \left(e^{-\frac{\Delta x \kappa_\mathrm{a}}{v}} - 1 \right) \\ &= \left(1 - e^{-K_\mathrm{a}}\right) N_\mathrm{g}(n). \end{aligned} \tag{4.30}$$

The desorption from a bin is calculated as previously according to equation 4.13 on page 62 and the self readsorption according to equation 4.20 on

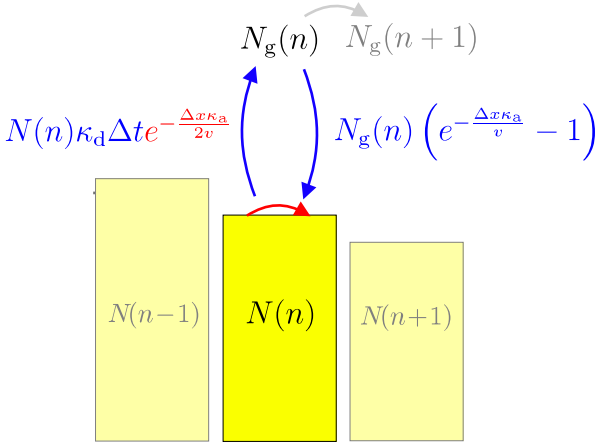

Figure 4.9: The principle of the algorithm for the serial approach. There is an amount of CFC in the model bin n called $N(n)$ and an amount in-flowing to that segment from the previous bin called $N_g(n)$. The exchange between these two marked blue is calculated for each bin sequentially with the value of $N_g(n)$ copied to $N_g(n+1)$ after this exchange. The exponential factor in the expression on the left highlighted in red is due to that some molecules desorbed in the bin are adsorbed in the same bin again, self readsorption, indicated by the red arrow. One time step is finished when the last bin is updated. The value of N_g after that step is added to the outflow and a new time step starts at the first bin with a value of $N_g(1)$ from the feeding of the trap.

page 67. This means the contribution to bin n at time t is given by

$$\begin{aligned} \Delta N(n) &\equiv N(n,t) - N(n,t-\Delta t) \\ &= \Delta N_a(n) + \Delta N_d(n) + \Delta N_s(n) \\ &= N_g(n)\left(1 - e^{-K_a}\right) - K_d N(n,t-\Delta t) e^{-\frac{K_a}{2}} \end{aligned} \tag{4.31}$$

and the same amount is subtracted from the flow out of the bin

$$N_g(n+1) = N_g(n) - \Delta N(n). \tag{4.32}$$

The inflow to the first bin is the inflow to the trap, $N_g(1) = \Delta N_{in}$. The outflow from the second trap is the value of N_g flowing out from the last bin, $\Delta N_{out} = N_g(b) - \Delta N(b)$.

4.6.1 Differential adsorption strength

As indicated by laboratory tests as discussed in section 4.1 the desorbed fraction during trap desorption is not independent of the concentration. This could indicate that different adsorption sites have different adsorption strengths. In the serial approach of the code a system with a finite amount of parallel bins with different adsorption strengths is therefore developed. This is done by letting each bin have several variables containing the concentration of the species each with different desorption coefficients. The principle is shown graphically in figure 4.10. The adsorbed amount in each type of adsorption site m in bin n is then a function

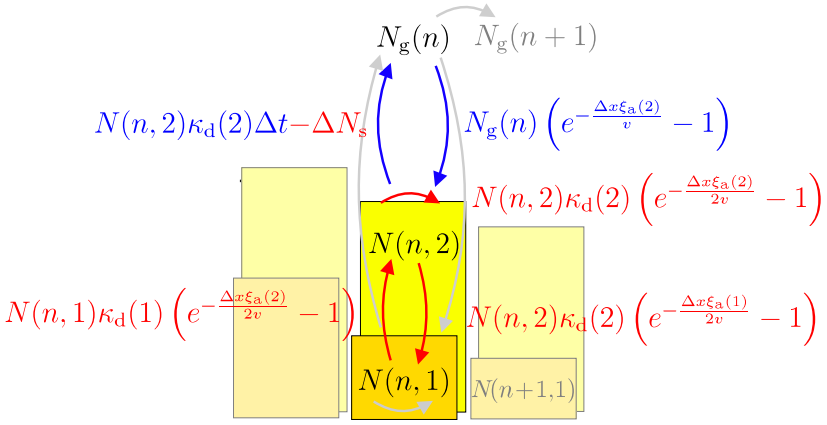

Figure 4.10: The principle of the algorithm with two types of adsorption sites. Similar to the serial approach shown in figure 4.9 except that there are now two values of $N(n)$ both having their exchange with the same $N_g(n)$. The self adsorption term is now slightly more complicated with cross terms between the two types of adsorption sites indicated in red. Expressions for site type number two are given in blue and red. The situation is completely analog for site type number one.

of the adsorption strength and the fraction of adsorption sites that are of this kind. No attempt has been made in the model to separate these two parameters as there is no obvious relation between the adsorption and desorption strengths. Let us for the moment denote the effective adsorption coefficient for the type of adsorption place m $\xi_a(m)$ and the corresponding $\Xi_a(m) \equiv \Delta x\, \xi_a(m)/v$. Then, similar to equation 4.30, the adsorption to adsorption places of type m of bin n can be calculated according to

$$\begin{aligned}
\Delta N_a(n,m) &= \frac{\int_0^{\Delta x} N_g(n) e^{-\frac{x\xi_a(m)}{v}} dx}{\int_0^{\infty} e^{-\frac{x\xi_a(m)}{v}} dx} \\
&= \frac{\xi_a(m)}{v} \int_0^{\Delta x} N_g(n) e^{-\frac{x\xi_a(m)}{v}} dx \\
&= -N_g(n)\left(e^{-\frac{\Delta x \xi_a(m)}{v}} - 1\right) \\
&= \left(1 - e^{-\Xi_a(m)}\right) N_g(n).
\end{aligned} \tag{4.33}$$

The desorption is calculated from each part with their desorption coefficients $\kappa_d(m)$ similar to equation 4.13

$$\Delta N_d(n,m) = -N(n,m)\kappa_d(m)\Delta t. \tag{4.34}$$

For the self readsorption as well as $N_g(n+1)$ it does not matter from which adsorption site the desorbed molecules are coming. The self readsorption term is

similar to equation 4.20

$$\begin{aligned}\Delta N_{\mathrm{s}}(n,m) &= \frac{\int_0^{\frac{\Delta x}{2}} \sum_{m'} -\Delta N_{\mathrm{d}}(n,m') e^{-\frac{x\xi_{\mathrm{a}}(m)}{v}} dx}{\int_0^{\infty} e^{-\frac{x\xi_{\mathrm{a}}(m)}{v}} dx} \\ &= -\sum_{m'} \Delta N_{\mathrm{d}}(n,m') \left(e^{-\frac{\Xi_{\mathrm{a}}(m)}{2}} - 1 \right) \\ &= -\sum_{m'} N(n,m') \kappa_{\mathrm{d}}(m') \Delta t \left(e^{-\frac{\Xi_{\mathrm{a}}(m)}{2}} - 1 \right)\end{aligned} \tag{4.35}$$

where m' is just a summation variable that runs over all m. The exchange of CFC in the bin is then

$$\begin{aligned}\Delta N(n,m) &= \Delta N_{\mathrm{a}}(n,m) + \Delta N_{\mathrm{d}}(n,m) + \Delta N_{\mathrm{s}}(n,m) \\ &= N_{\mathrm{g}}(n) \left(1 - e^{-\Xi_{\mathrm{a}}(m)} \right) - N(n,m) \kappa_{\mathrm{d}}(m) \Delta t \\ &\quad - \sum_{m'} N(n,m') \kappa_{\mathrm{d}}(m') \Delta t \left(e^{-\frac{\Xi_{\mathrm{a}}(m)}{2}} - 1 \right)\end{aligned} \tag{4.36}$$

and the flow out of bin is $N_{\mathrm{g}}(n+1) = N_{\mathrm{g}}(n) - \Delta N(n) = N_{\mathrm{g}}(n) - \sum_{m'} \Delta N(n,m')$.

4.6.2 Langmuir isotherm

As pointed out in section 4.1 (page 54), Langmuir isotherm theory is not thought to be relevant in the small concentrations of CFCs in the air. The largest interest to include Langmuir theory in the code is therefore if there are other substances that could pollute the trap in higher concentrations. The principle is shown graphically in figure 4.11.

In the serial approach of the model a simple code can take the finite number of adsorption places and the Langmuir isotherm into account. At the same time several species have to be handled in the model to allow a pollutant. This is done by setting several variables of concentrations in each bin in the same way as for different adsorption strengths. We denote these m. A parameter for the number of available adsorption places ($N_{\mathrm{L,tot}}$) in the same unit as N must be fed to the model. The number of adsorption places in a bin is then $N_{\mathrm{L}} \equiv N_{\mathrm{L,tot}} \frac{\Delta x}{x}$. Adsorption and self readsorption is modified by a factor $1 - \frac{N(n)}{N_{\mathrm{L}}}$, but as there is one type of adsorption site the ordinary adsorption coefficient (κ_{a}) to be used is now a function of the species (m). The adsorption changes from equation 4.30 to

$$\begin{aligned}\Delta N_{\mathrm{a}}(n,m) &= \left(1 - e^{-K_{\mathrm{a}}(m)} \right) N_{\mathrm{g}}(n) \left(1 - \frac{N(n)}{N_{\mathrm{L}}} \right) \\ &= \left(1 - e^{-K_{\mathrm{a}}(m)} \right) N_{\mathrm{g}}(n) \left(1 - \frac{\sum_{m'} N(n,m')}{N_{\mathrm{L}}} \right),\end{aligned} \tag{4.37}$$

while the desorption is given by equation 4.34 now with the m meaning the species rather than the type of adsorption site.

The different adsorption strength and Langmuir theory may be combined in the model, then the summations over m in section 4.6.1 are made for all m that corresponds to the same species, while the summation over m in equation 4.37 goes over all, including all species.

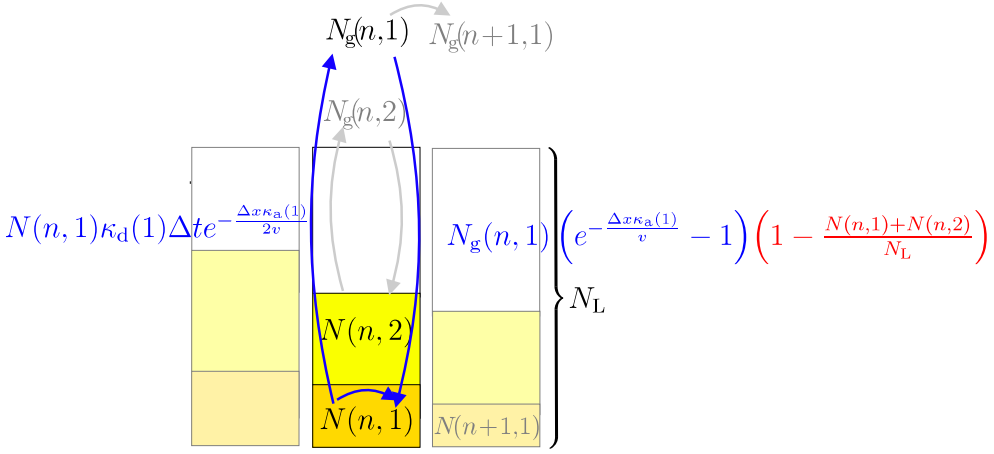

Figure 4.11: The principle of the algorithm with correction for Langmuir isotherm. This is similar to the serial approach shown in figure 4.9 except that there is now a limited number of adsorption sites available, N_L, and the adsorption term on the right is changed with a correction factor highlighted in red according to Langmuir theory. The model runs this only with competing species. As these are different species they interact with different flow variables $N_g(n,m)$ and there are no cross terms for the self readsorption.

4.7 Model validity

There are several approximations made in this model. Here we discuss the main ones.

4.7.1 Physical errors

According to *Comes et al.* [1993], the Langmuir isotherm theory does not have to be considered at concentrations lower than 1 ppm in adsorption beds of this kind. The method for low concentrations (ppb) by *Bertoni and Tappa* [1997] is also based on this assumption. The species of investigation here are sub ppb and thus do not affect each other by competition. There might well be other species in the air that are not caught in our analysis that can have larger concentrations. The calibration of the instrument is performed with both a synthetic standard of CFC in pure nitrogen and dried air. Which of these best represents the stratospheric air in this sense is not obvious.

There are reports that the trap efficiency drops considerable with high flow speed [*Seshadri and Bozzelli*, 1983; *Sturges and Elkins*, 1993]. These effects are of potential relevance for this study and could also form a target for further investigation.

It has been reported that the results depend on the geometry of the trap [*Harper*, 1993]. Such mechanisms are poorly understood and are not included in the model. The adsorption bed consists of balls of Carboxen with small spacings rather than an even bed on a molecular level. This complication is not considered in the model.

The dead volume between the traps in the double trap experiments is not included, but is found to be negligible.

The pressure difference and therefore the velocity difference in different parts of the traps is not considered. Neither is the temperature difference. None of these parameters are well known and are therefore difficult to include realistically.

4.7.2 Numerical errors

There are always errors arising from the numerical resolution of digital models. Here these errors are in both time and position, although the model is constructed in such a way that the amount of input is always conserved regardless of the binning.

The first error appears from the distribution in time. All distribution of molecules to new adsorption sites is modelled as immediate with no delay due to a finite carrier velocity. The carrier velocity is only taken into account to calculate the exposure time of a bin to the particle.

Redistribution is made in time-steps that are limited by equation 4.14. Test runs have showed that a fraction 0.1 is good enough, i. e. shorter time steps have marginal influence on the result.

The binning is limited by equation 4.12 and similarly test runs have shown that 0.1 is good enough, i. e. finer resolution does not change the result. Reemission is considered to appear from the geometrical centre of the bin. When strong gradients are present this is not really true. This is monitored and the centre of gravity for one bin is never more than 10^{-5} trap-sizes from the centre.

4.8 Interpretation

All parameters in the model are quasi-parameters related to normal physical parameters. However to derive real physical measurable parameters from these is not straightforward. There are two measurable parameters to make comparisons to, that is the mass flow and the amount in each trap. The absorbed amount in the trap is also dependent on the calibration with adsorption and desorption and thereby highly dependent on the efficiencies modelled. Pressure is measured in the flow line before the trap and in the surroundings. From symmetry arguments the mean pressure in the trap can be estimated from these [*Roslin*, 2003]. The mixing ratio of CFC in these calibrations is a well-known constant.

The input parameters to the model are: the total sampled volume at trap pressure (`vol`), the velocity of flow (`vel`) and the mixing-ratio of CFC in sample (`conc`). The sample time is then given by `vol/vel`. adsorption coefficient (κ_a) is the probability per unit time for a molecule in gas phase to adsorb to the adsorbent in the trap i. e. molecules are distributed according to the flow velocity independent of the time steps of the model. κ_d is the probability per time unit for desorption from the trap i. e. proportional to the probability per time step in the model independent of the velocity.

4.9 Qualitative model checks

First of all the simulation is based on theory for a chromatographic column. This means that, for very low flow speed, the trap should behave like a column. To

test this a run was made with the flow velocity parameter set to 0.05. A time series of the content of the trap after different times is shown in figure 4.12. The characteristic signature of a column, with the concentration peak broadening during the flow through the column, is clearly seen.

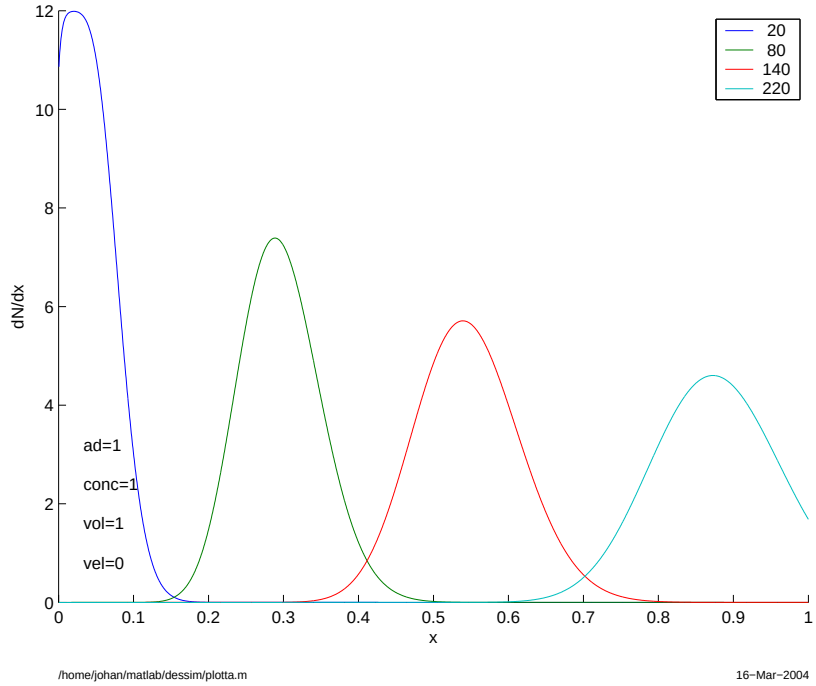

Figure 4.12: Time series of distribution of CFC in the trap. The x-axis is the position in the trap and the y-axis is the concentration. The four lines shows the distribution at four times according to the legend. CFC-mixture of conc 1 has been input for 20 time units and nothing thereafter. Carrier flow constant at 1.

It has been shown by *Seshadri and Bozzelli* [1983]; *Sturges and Elkins* [1993] that too rapid flow can significantly lower the adsorption efficiency of a trap. This is reproduced in the model by a series of runs all with the same sample size, concentration and coefficients but varying velocities as presented in figure 4.13. There the total content in the second trap in a double trap simulation is plotted against the total sample amount. It is easily seen that, for low flows, the breakthrough comes in at almost the same time and is first seen in trap 6. With flows over 0.1 in this simulation the breakthrough is coming a lot earlier. This is understood as, for low flow speed, there is a sharp onset of the breakthrough at the retention volume. It is well known from chromatographic theory that the statistical peak broadening is larger if the flow is too fast. For a continuous inflow, a larger broadening shows as a less sharp breakthrough onset. All curves go asymptotically to total breakthrough. A comparison with figure 4.2 (right panel) shows that the model seems to agree rather well but not completely with the theory of *Senum* [1981].

From the theory of *Yoon and Nelson* [1990] there should be a linear relationship of $\ln \frac{P}{1-P}$ to t. This is met by the model according to figure 4.14. In this model run the trapped amount in the second trap is used to calculate the ratio

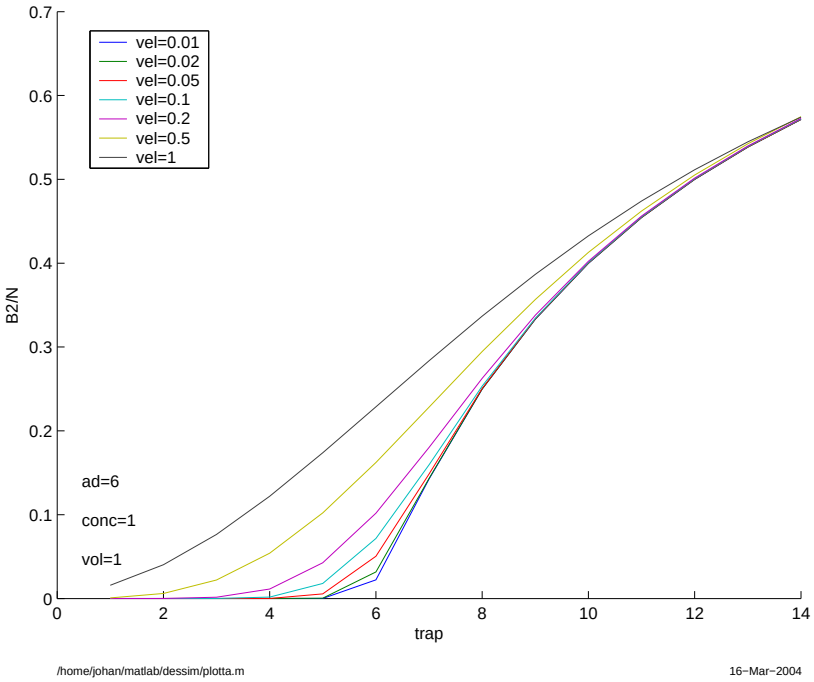

Figure 4.13: Breakthrough at different flow velocities, see text for details.

of the integrated outflow from the first trap during a sample to the integrated inflow as a measure of P. The point in the diagram is plotted in the centre of the integration periods. The lowest value point in the right panel in the figure seems to be off the curve. This is an effect of the fact that the plotted values are simulated amounts in the second bin of a double trap experiment. The first of those in this model run has a much larger sample volume than the following and during this long sample the largest contribution is coming at the end while the point is plotted in the centre of the volume interval.

4.10 Simulation results

The first lab experiment we need to recreate is the flow-rate experiment performed by *Roslin* [2003]. The test was performed as a double trap experiment where a series of samples were taken through one trap. A second trap was changed for each sample to give a series of breakthrough values. The results presented in figure 4.15 show that similar sample sizes give widely different breakthrough values. This is primarily due to the different reaction time available for adsorption. This is shown by the model run. As the relationship of the time and flow rate variables in the model to the absolute values is unknown, solutions with different combinations of these parameters are possible. Model runs with parameters that fitted the highest breakthrough value are shown by red lines in figure 4.15. There is an infinite number of solutions of which three are shown. It is obvious that they have different success in describing the experiment. The model was then run with a flow that was 115/200 times the previous (in the lab test the flows where 200 SCCM and 115 SCCM). The corresponding runs are plotted in blue corresponding

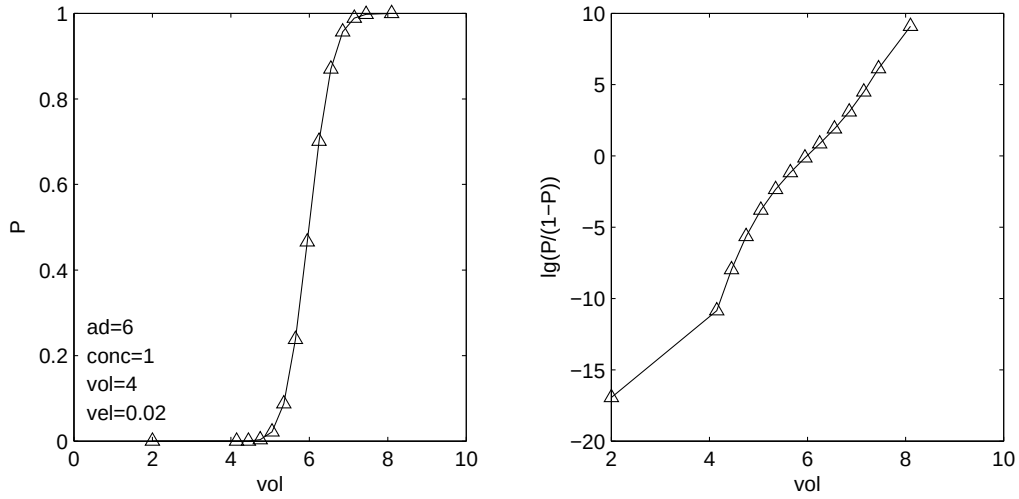

Figure 4.14: Linear relationship as predicted by *Yoon and Nelson* [1990].

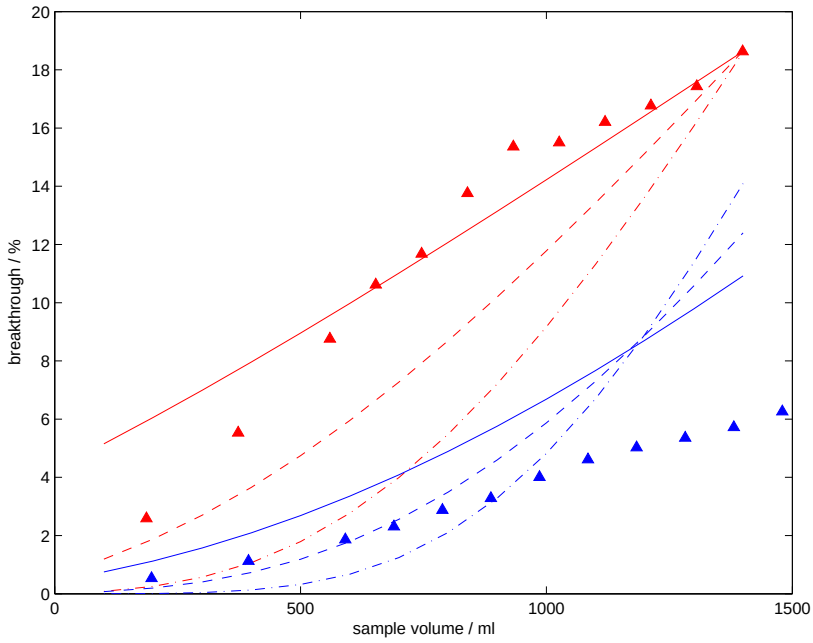

Figure 4.15: Breakthrough at different flow velocities, experimental values indicated by triangles, adopted from *Roslin* [2003], and simulations by lines. 200 SCCM in red and 115 SCCM in blue. The y-axis is the cumulative sum of the analysed amounts in the second trap divided by the known full input.

line style. These are to be compared with the lower flow experiment. As indicated in the figure, all possible solutions overestimated the breakthrough for this flow. This shows that the reaction time cannot fully explain the flow rate dependence. The picture is consistent with even lower flow rates.

4.10.1 Langmuir isotherm

As mentioned earlier, the code has a possibility to include Langmuir isotherm and several species competing for adsorption places. There is of course an infinite parameter space with the new parameters of the new species and the amount of adsorption places, that is also unknown. The solutions including the Langmuir isotherm and competing species can only differ significantly from the solution without if there is a substantial decrease in the number of available adsorption sites. The occupation of these sites must also be by the unknown disturbing species that must be present at a much higher concentration than the one of primary interest (as the concentrations of our species are too low). As none of these concentrations in the trap is possible to compare to experiments, and the only interaction between them is in the competition for the adsorption sites, the magnitude of the amounts or their relation is not important as long as the species of primary interest does not make a significant contribution to the occupation of adsorption sites. For numerical reasons in the model it is better not to make a difference of many orders of magnitude. A ratio in concentrations of 100 is chosen for the simulations.

If the other species has a much slower retention, the species of primary interest would penetrate deeper into the adsorption bed to unaffected parts with all adsorption sites unoccupied and thereby the situation does not change significantly. The situation where the retention speeds of the two species are comparable is potentially interesting. If the other species has a much faster retention the adsorption sites get gradually more occupied with time by the secondary species. This might also be an interesting situation.

Simulation runs with the same desorption coefficients as the investigated species for the disturber, 100 times higher concentration and the adsorption coefficients varying from half to double compared to that of the investigated species is shown in figure 4.16 on the next page. As seen in the figure this makes a marginal difference. The amount of available adsorption places is chosen such that there should be a substantial difference. In the end of the simulation for the case with half adsorption coeffient the fraction of occupied sites is decaying from 50% in the entrance end of the trap to 3% in the rear end. In the case with double adsorption coefficient the other species is more evenly distributed to occupy 17–12% of the adsorption sites. A similar figure with the desorption of the unknown species set to one tenth of the desorption coeffient of the species of the primary is shown in figure 4.17 on the facing page.

4.10.2 No desorption

With no desorption, without competing species, and for low concentrations, the solution is the obvious constant level of outflow concentration. With a large amount of competing species, close to saturation, where the Langmuir theory

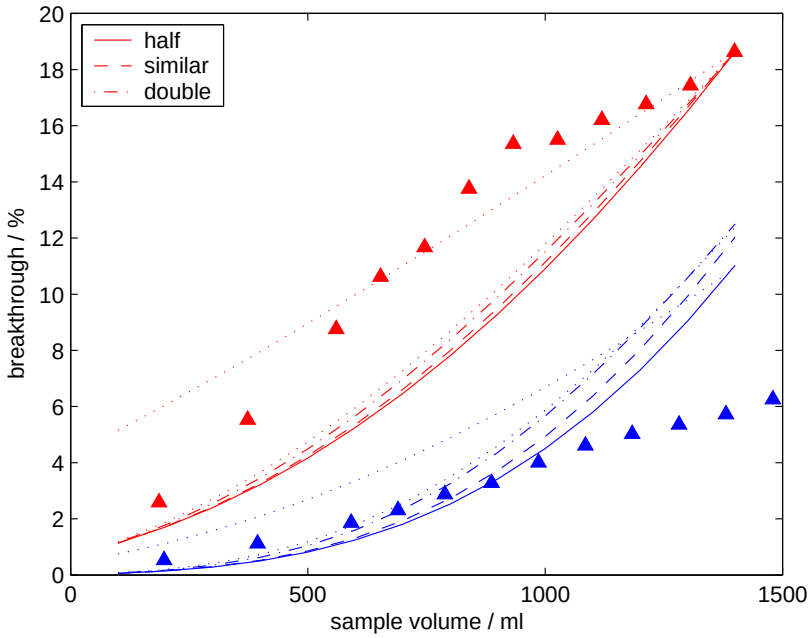

Figure 4.16: Results with Langmuir isotherm added, runs with half, similar and double adsorption coefficient of the unknown species compared to the known, all with 100 times higher concentration and similar desorption. Dotted line similar to figure 4.15 for comparison.

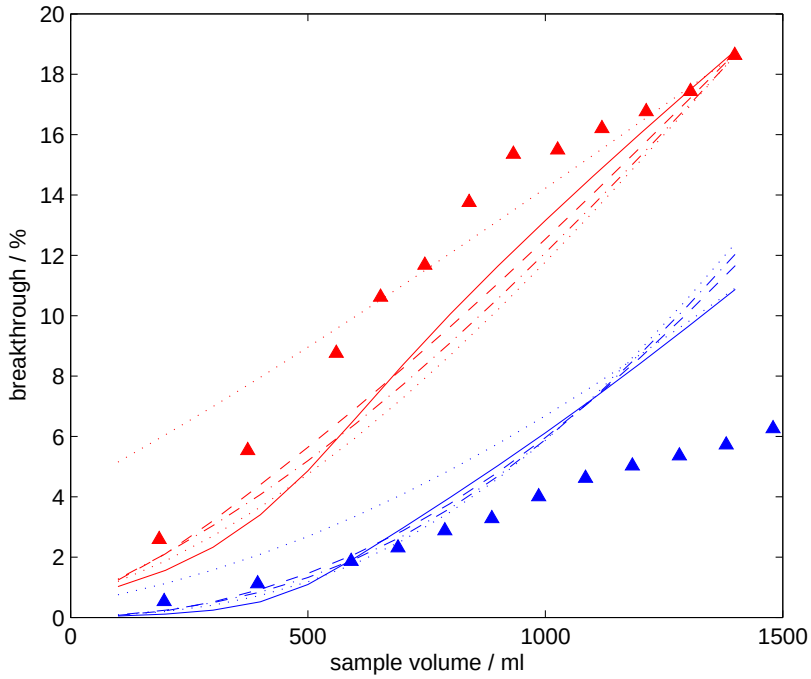

Figure 4.17: Results with Langmuir isotherm added this time with the desorption coefficient of the unknown species 10 times higher than for the one of primary interest. The meanings of the lines similar to figure 4.16.

maybe is not valid, breakthrough curves close to the measured curves can be achieved in model runs. This is highly preliminary as this violates both the criteria for the Langmuir isotherm and the approximations for the chromatography theory on which the model is based. This might anyway indicate this is an interesting part of parameter space for further analysis. Speaking against this solution are other lab tests where the sample has been purged off the trap by pure nitrogen.

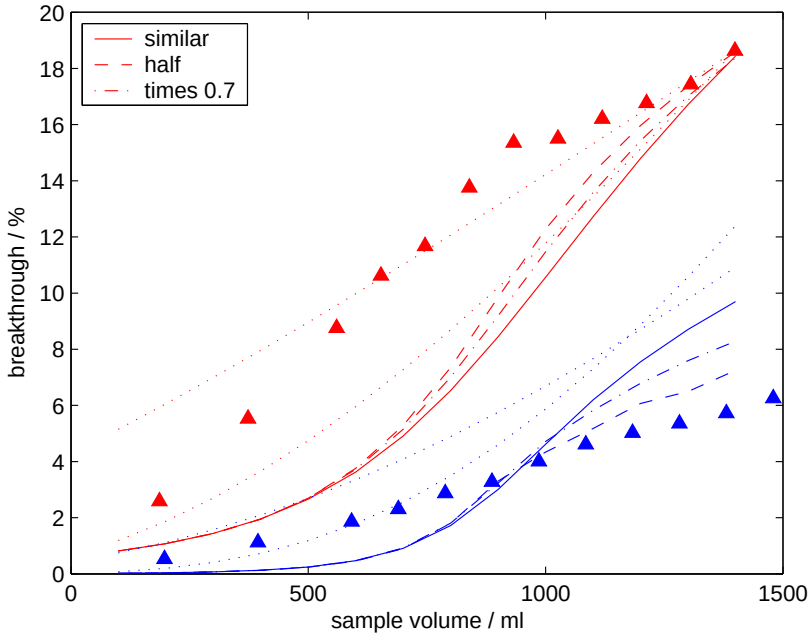

Figure 4.18: Results from test with no adsorption in the investigated species only saturation of adsorption sites. Dotted line similar to figure 4.15 for comparison.

4.10.3 Different binding strength

The possibility to include adsorption sites with a different binding strength (i. e. different desorption coefficient) than the majority is investigated. Even in this case the parameter space is infinite and quantitative estimations on which parts that can give interesting results is needed.

A much smaller binding strength than for the majority does not significantly differ from the case that there is none at all i. e. the adsorbent continues in the flow. This is not an interesting solution. If the binding strength is very much larger than for the majority of sites the adsorbent is effectively removed for the whole time span of the experiment this is not an interesting solution either.

Figure 4.19 on the next page shows the results of simulations performed with different fractions of the adsorption sites with 10 times stronger bindings. As seen in the figure the quantitative effect is in the right direction even if it is quantitatively far too small.

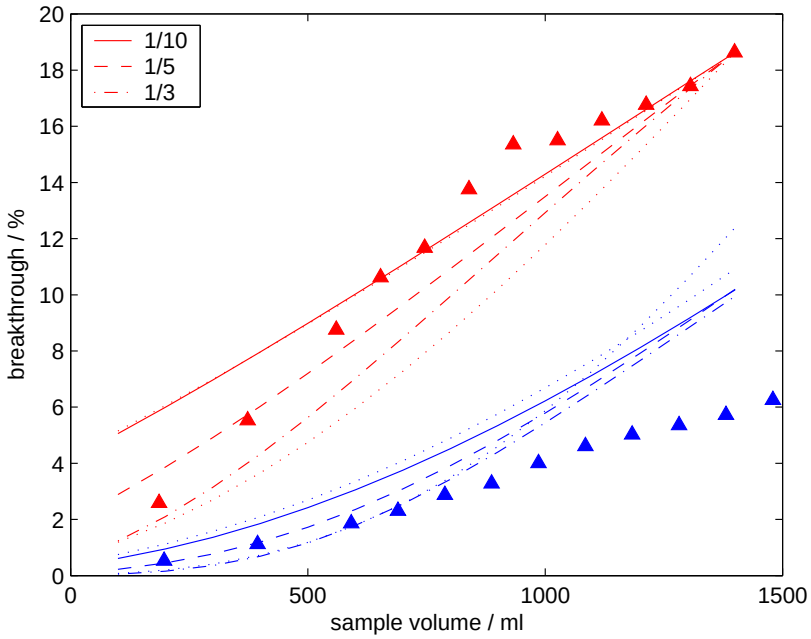

Figure 4.19: Results with some of the adsorption sites giving 10 times lower desorption. The fraction of particles adsorbed to stronger sites given by the legend. Dotted line similar to figure 4.15 for comparison.

4.11 Quantitative breakthrough estimation

As seen in the previous section the breakthrough of the traps are not successfully described by the model which has been based on simple physical principles. To get a quantitative estimation of the breakthrough from the trap the model can be modified in an empirical way to better adopt to measured quantities, for example make the adsorption coefficient velocity dependent with an exponent that reproduces the flow rate test. Another approach is to make a much simpler empirical fit of the data available from the breakthrough tests. The major reason to make the model was to be able to understand the processes and from well grounded physical assumptions make better and safer inter- and extrapolations. If the model takes physically unexplained dependencies into account this advantage is missing and a simple parameterisation of the problem from the measurements will be used to give quantitative estimations of the breakthrough.

The physical background to the breakthrough is obviously not well understood. Therefore, for the empirical approach, we look at both sampled volumes and masses and both volume and mass flows. As earlier seen in figures 4.3 and 4.5 the total breakthrough grows linearly with growing samples. As these are cumulative sums the last point in each series includes all the results. In figure 4.20 on the following page the direct proportionalities for these are shown for all of these plotted as both sampled volumes and masses. In figure 4.21 on page 83 these direct proportionality coefficients are plotted as a function of either the mass- or volume flow. The flow test plotted in the top panels of figure 4.20 and by blue stars in figure 4.21 is taken manually by purging a stable flow of standard regulated by a regulator through the trap. The pressure test (bottom

panels of figure 4.20 and red stars in figure 4.21) is ambient air in the lab sampled by DESCARTES pump. From the flight one sample was taken in tropospheric conditions.

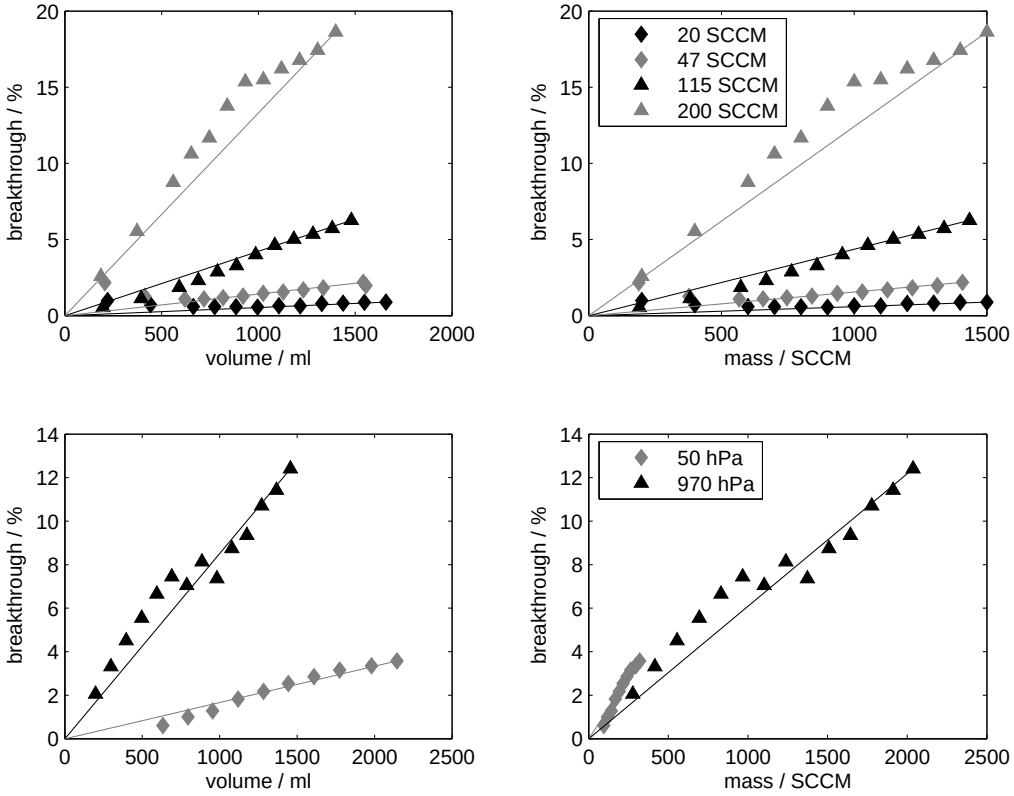

Figure 4.20: Measured breakthrough from double trap experiments. From *Roslin* [2003].

The most striking feature of these plots is that the reference test to the low pressure test, that was taken at ambient pressure, fall out of the picture completely. For the smaller flows the amounts trapped in the second trap are rather small and there are large uncertainties for these small samples. Both the 200 SCCM flow test and 270 hPa pressure test give significant breakthrough that is easily detected. As these values are the cumulative sums of many integrated traps, giving a consistent picture in each calibration, this cannot be explained as detection problems.

The conditions during these samplings vary in several ways:

Sampled air The standard air from pressure bottle is dried.

Driving force The flow from the pressure regulator is very stable compared to the pump that works by pressing out in bursts. This may give an unstable flow in the trap.

Obviously either individual performance of the individual trap or these differences in sample conditions makes such a difference that the two tests are not comparable to each other and traps can, during some circumstances, perform much better than during the flow test.

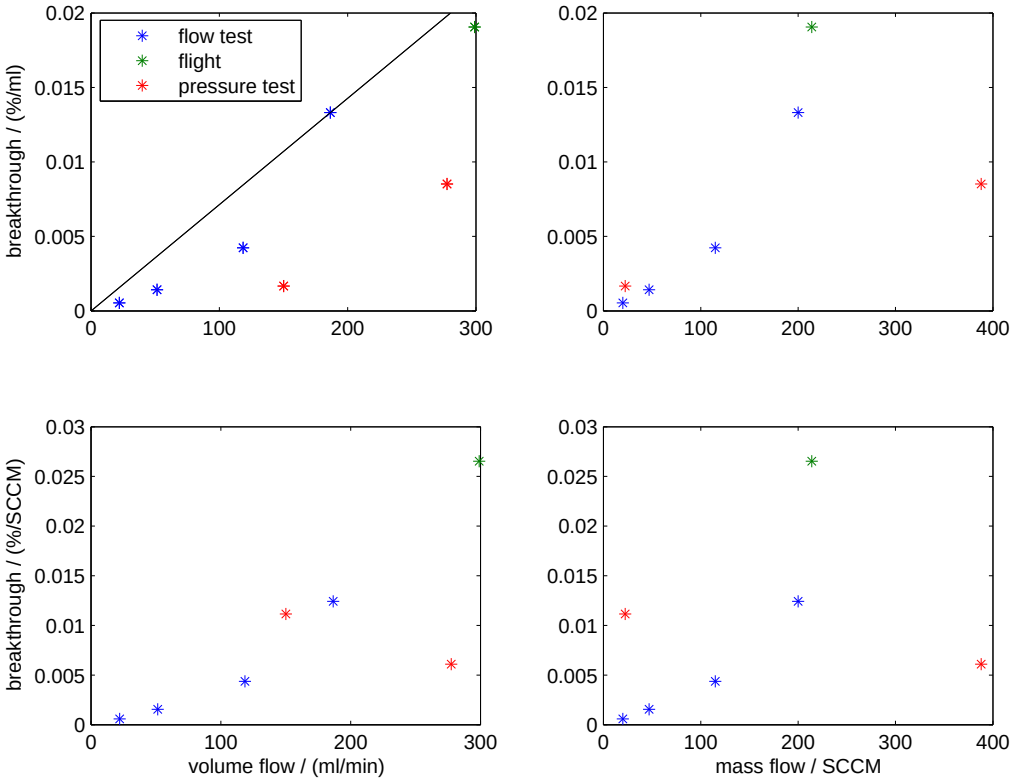

Figure 4.21: Direct proportionality coefficients of breakthrough as a function of sampled mass or volume from double trap experiments assuming direct proportionality of breakthrough to sampled mass or volume.

As the scatter plots in figure 4.21 do not really provide the answer to the question of whether masses or volumes should be used. Chromatographic theory is based on that the volumes should be the important parameter. Ackording to this argument the volume and volume flow, i. e. the top left panel of figure 4.21, is used to give a new direct proportionality coefficient β. As there are few points and no really consistent picture, the proportionality is calculated from the worst case of the points, which is the 200 SCCM flow test,

$$\beta = \frac{\frac{\Delta m_{\mathrm{CFC}}}{m_{\mathrm{CFC}}}}{V}\frac{t_{\mathrm{s}}}{V} = 7.1371 \cdot 10^{-5}\frac{\%\ \mathrm{min}}{\mathrm{ml}^2}. \tag{4.38}$$

The β proportionality function is shown by a line in the top left panel of figure 4.21. As it is shown in the break-through tests that the traps can perform a lot better during some conditions no attempt is made to correct for the break-through, but the possibility that breakthrough can occur is taken into account in the uncertainty estimation. This gives an uncertainty that up to a fraction

$$\Delta m_{\mathrm{CFC}}/m_{\mathrm{CFC}} = \beta\, V^2/t_{\mathrm{s}} = \beta\, \omega^2\, t_{\mathrm{s}} \tag{4.39}$$

of the sample is lost during the sampling due to breakthrough.

4.11.1 Sample volume estimation

The sample volume V and volume flow ω can be calculated from the sampled mass m and mass flow μ according to the ideal gas law (equation 4.8 on page 58) with knowledge of the temperature and pressure in the trap. Neither of these parameters are directly measured, making precise measures impossible. As the expansion of the gas is made in intimate contact with the filling of the trap it is assumed that it is iso-thermal at a fixed temperature of $T_0 = 273.15$ K. The volume is then

$$V = \frac{m\, T_0}{K\, p_{\mathrm{t}}} = \frac{m}{p_{\mathrm{t}}}\ \frac{\mathrm{cm}^3\ \mathrm{atm}}{\mathrm{SCC}}. \tag{4.40}$$

There are two pressure gauges available on board DESCARTES. The line pressure p_{l} over-pressure (compared to ambient) is read out in the sample line (as seen in figure 2.5) and the ambient pressure p_{a} is measured in the instrument box. Unfortunately, as previously mentioned in section 2.1.1, the pressures are not measured during the flight for DESCARTES III. The line pressures are read out while purging the instrument between the samples, to decide whether to use the overflow valve and during the pressurisation of the traps. The ambient pressure has reliable readings right before and after sampling. For the breakthrough tests presented in section 4.3 a special program based on the flight software was written that measured the pressures while sampling through the trap.

The strategy used here to estimate the volume flow during the sampling is to use flights with DESCARTES II that measure both pressures while sampling, to estimate the trap pressure and investigate the relationship between the flow, ambient pressure and trap pressure. As almost the whole pressure drop appears over the sample box, and the same boxes are used in the two instruments, this relationship is used to estimate the trap pressure from ambient pressure and measured mass flow.

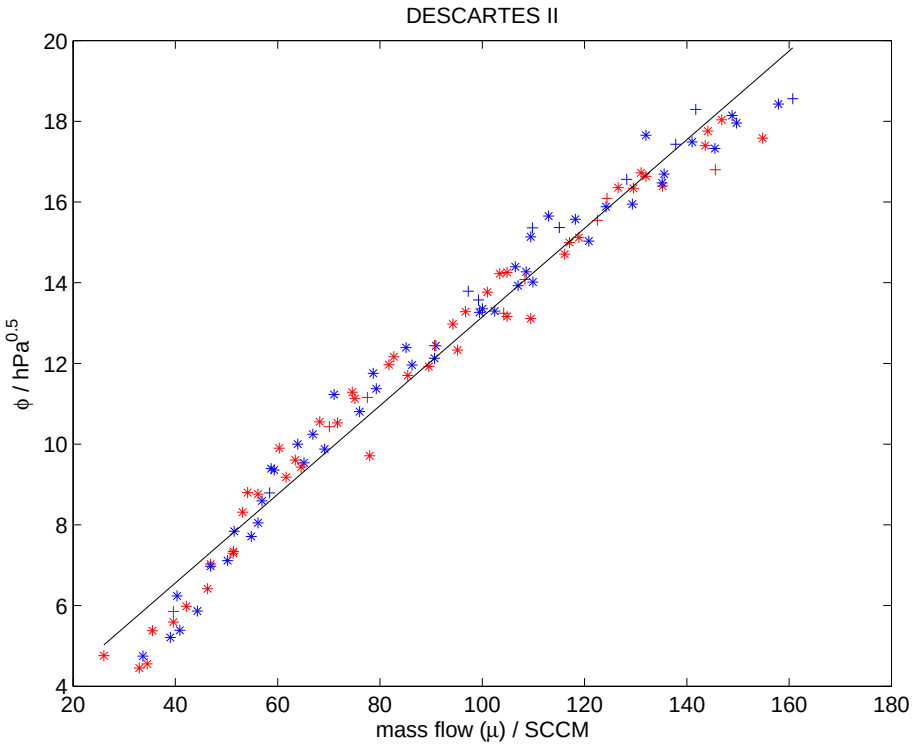

Figure 4.22: Pressure parameter ϕ as a function of mass flow for DESCARTES II flights. Colours separate the first and second readout during a sample. Samples taken with the overflow valve open are marked by plus signs. Black line is the fitted function Φ.

The sample box is built up with similar input and output tubes. The two switches letting the air into the trap are similar and the connections for inflow and outflow between these and the trap itself are similar dimension tubing. This configuration is almost symmetric around the trap and it is assumed that the pressure drop before and after the trap is similar. Thus the trap pressure is estimated to be

$$p_{\mathrm{t}} = \frac{p_{\mathrm{l}}}{2} + p_{\mathrm{a}}, \tag{4.41}$$

similar to the estimations used in the breakthrough tests [*Roslin*, 2003].

Looking for a parameter of the pressure that is possible to estimate from the flow estimation, it has been found that

$$\phi \equiv \frac{p_{\mathrm{l}}}{\sqrt{p_{\mathrm{t}}}} = \frac{p_{\mathrm{l}}}{\sqrt{\frac{p_{\mathrm{l}}}{2} + p_{\mathrm{a}}}} \tag{4.42}$$

gives a reasonable correlation with estimated flow, as shown in figure 4.22. There is also plotted a linear regression of this relationship $\Phi(\mu)$ that fits μ to ϕ in a least square fit. There are two readings of the pressures and flows during each sample. These are separated by colour in the figure. The markers indicates whether the overflow valve was opened. As seen in the figure neither of these differences influences the result.

From equation 4.42 the line pressure can be estimated

$$\begin{aligned} \frac{p_\mathrm{l}}{\frac{p_\mathrm{l}}{2} + p_\mathrm{a}} &= \phi \\ p_\mathrm{l} &= \frac{\phi^2}{4} \underset{(-)}{+} \sqrt{\phi^2\, p_\mathrm{a} + \frac{\phi^4}{16}} \end{aligned} \tag{4.43}$$

and then the trap pressure can also be estimated as

$$p_\mathrm{t} = \left(\frac{p_\mathrm{l}}{\phi}\right)^2 = \left(\frac{\phi}{4} \underset{(-)}{+} \sqrt{p_\mathrm{a} + \frac{\phi^2}{16}}\right)^2 . \tag{4.44}$$

Finally, as $\Phi(\mu)$ is an estimation of ϕ, p_t can be estimated from μ and p_a according to

$$p_\mathrm{t} = \left(\frac{\Phi(\mu)}{4} \underset{(-)}{+} \sqrt{p_\mathrm{a} + \frac{\Phi^2(\mu)}{16}}\right)^2 . \tag{4.45}$$

To give an idea of the size of these variables during ordinary flights and calibrations, compared to the double trap tests that have been used to estimate the potential breakthrough, figure 4.23 shows a scatter plot of V and ω of most of these data points. The figure also shows iso-lines of the uncertainty, estimated according to equation 4.39 (plotted in black). From this figure it is obvious that the calibrations are in a region where breakthrough is very small. The calibrations for the indirect calibration method sampled by the GC are not plotted but those are made at a mass flow of about 20 SCCM compared to the direct absolute calibrations with DESCARTES that have been varying up to about 80 SCCM.

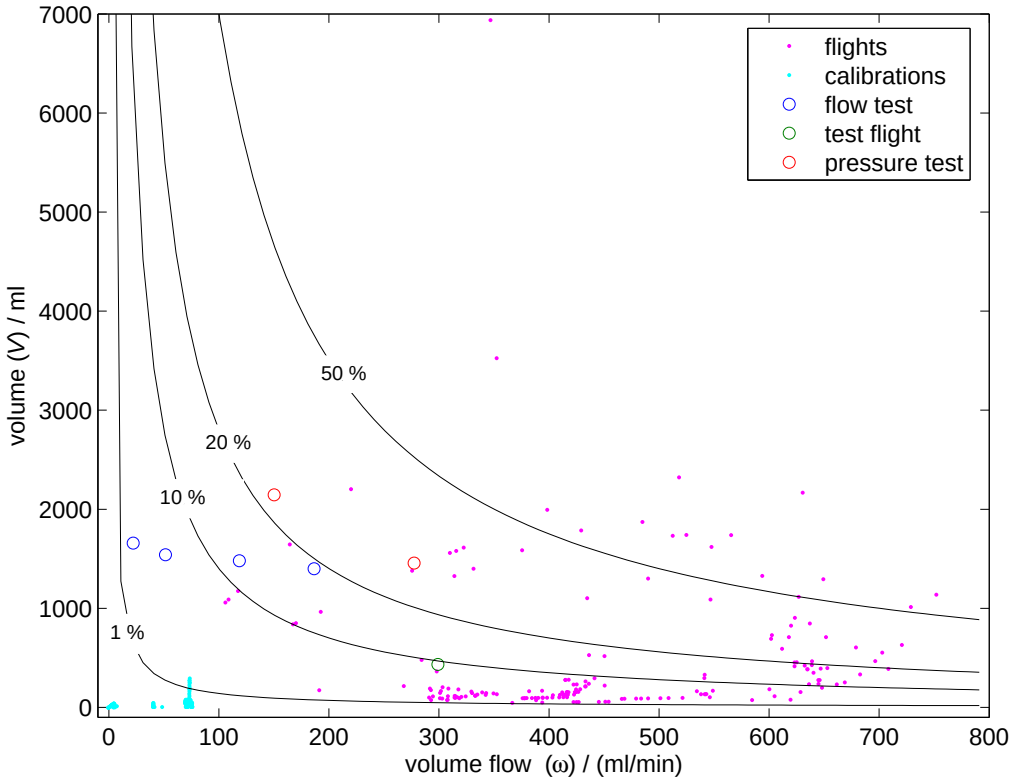

Figure 4.23: Sample volumes and volume flows for tests, calibrations and flights. Circles indicate the tests similar to figure 4.21, magenta dots show flight samples and cyan dots show direct air standard calibrations through DESCARTES. The black lines are iso-lines of the uncertainty due to breakthrough.

Chapter 5

Uncertainty estimations

Generally uncertainty estimations for this work are of three different types. From statistical methods it is possible to see the precision of the instrument during calibrations in the laboratory. Measurements are made in the stratosphere where no calibrations are performed, with rather different environmental variables than in the lab. This may influence the measurements from effects due to the sampling being done in a part of the parameter space of flow, pressure and mixing-ratio that has not been possible to reach during the calibrations. There is also a possibility that the sensors or the adsorption process response changes due to other environmental parameters, for example temperature. The other and less trivial estimation is what extra uncertainty arised due to the fact that the calibration values taken in the laboratory are used for stratospheric flights. This is especially true for the possible breakthrough during sampling.

5.1 Flow estimation

As pointed out in section 3.3.2 the flows during sampling according to the direct calibration method are measured by the DESCARTES on-board flow meters and that calibration is not as sensitive to the flow-meter calibration as the indirect method.

Built in flow meters perform in a stable manner on single lab occations but drift of the zero point is an observed problem. In the lab environment, the flow meters have proved to be sensitive to disturbances. For example if the computer used for manual readings of the flow during flow meter calibrations is connected to the 50 Hz Alternating Current (AC) net, this can give disturbances to the measurements.

The statistical uncertainty corresponding to the 95% confidence interval for a single new measurement of the flow meter calibration function is used as the flow meter calibration function. As described in section 3.2, the flow meter calibration function fits the function $u_n(\mu)$ to the flowmeter readout voltage U_f which is then inverted (and modified with correction for flow meter zero reading) to the function $f_n(U_\mathrm{f}, z_\mathrm{f})$. The estimation of the flow for a sample is made by $\mu = f_n(U_\mathrm{f}, z_\mathrm{f})$ and the confidence limits of $u_n(\mu)$, $\Delta u_n(\mu)$ are calculated. This estimation is then

devided by the derivative of the function to give

$$\Delta\mu = \frac{\Delta u_n(\mu)}{\frac{\mathrm{d}u_n(\mu)}{\mathrm{d}\mu}}. \tag{5.1}$$

The working conditions during stratospheric sampling are very different for both the pump and the flow meters, which are then working in other temperatures and pressures than in the laboratory. Even the fact that the pump is running and thereby possibly can give electrical or elecro magnetic disturbances to the flow meters can possibly contribute to larger errors in the flow estimations. These conditions are difficult to recreate in the calibration proceedure and no such approach has been tested. To some extent the flow meter calibrations performed in the lab are possible to test. Two types of such tests has been performed, one sampling troposperic air in outdoor conditions and the other sampling the air in a low pressure tank covering the range of the relevant pressure region. These tests are presented in section 5.7.1.

5.2 Representativeness of samples

The DESCARTES instrument is in many aspects similar to its sister instrument Determination In situ by Rapid Analytical Chromatography (DIRAC), developed in parallell by the same research group, described in *Robinson et al.* [2000]. During the Stratospheric Aerosol and Gas Experiment (SAGE) III Ozone Loss and Validation Experiment (SOLVE)/Third European Stratospheric Experiment on Ozone (THESEO) campaign in the winter 1999/2000 the DIRAC instrument experienced two problems with the sample line. Due to low flow rates at high altitudes there was a delay in the sampling for the exchange of air in the sample line and non-plug flow effects, mainly in the pump chambers, caused contamination of air with earlier samples. This is described in detail in the appendix of *Robinson et al.* [2005]. DESCARTES version III as described here has a similar pump to the version of DIRAC for which this problem is described.

DIRAC had at the time much lower flows than DESCARTES [A. Robinson personal communication] and there is no reason to beleve the that the same contamination has affected DESCARTES.

5.3 Chromatogram peak integration

As mentioned in section 2.4 the integration of the chromatogram is not fully automatic. The random error from one operator integrating the chromatograms is part of the uncertainty in the calibration curves taken for the direct absolute calibration. The ECD response function and the estimation of the relations between concentrations in standards will be discussed in the following sections. There are however several operators that have been involved in the integration of the chromatograms and one might expect that a systematic error from the subjective evaluations by the different operators may appear. Therefor a blind test was performed where three operators integrated chromatograms from the same flight. Results from that test is presented in figure 5.1.

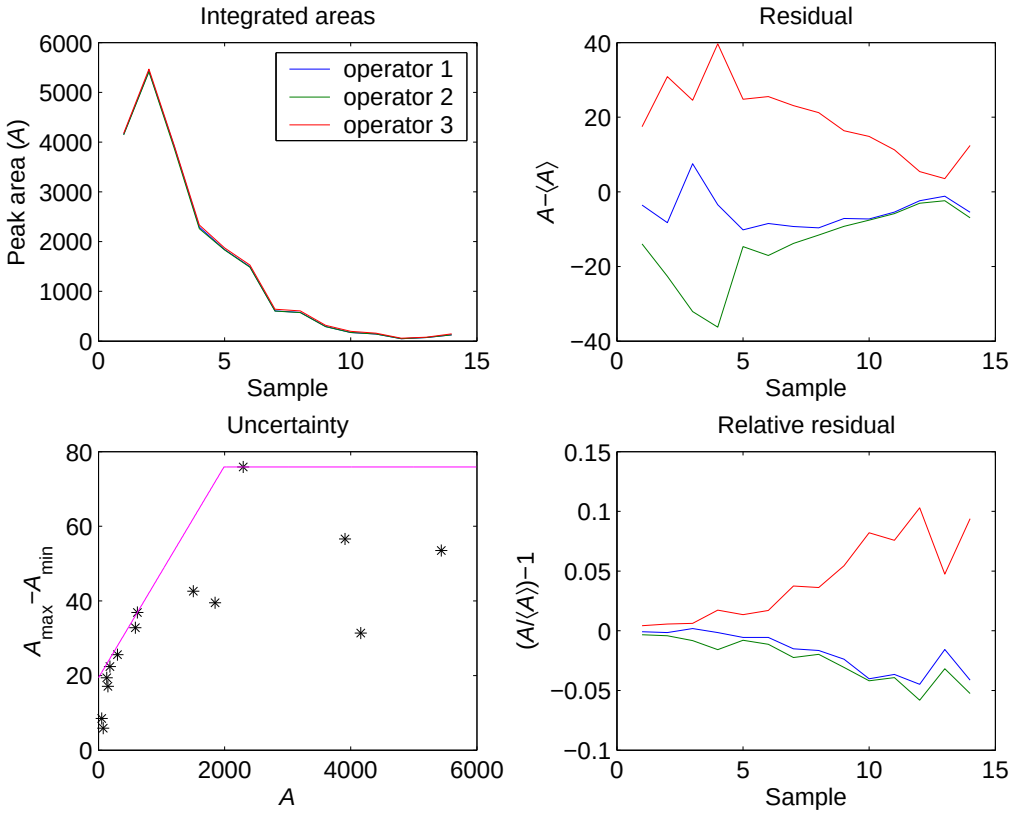

Figure 5.1: Integration test made manually and independently by three operators. The top left panel shows the integration result from all three operators in the order sampled during the flight. The right figures shows the residuals to the mean of the three measures, in absolute values in the top panel and in relative values in the bottom. The larger samples in the beginning showing larger absolute but smaller relative deviations than the smaller samples in the end. The bottom left plot shows the largest difference between two measurements for each point as a function of the mean of the measurements marked by black stars. The magenta line is the uncertainty envelope function as described in the text.

In theory this factor should cancel if the same operator has done the integrations both for the calibration and the flight. This is often the case and anyway the vast majority of the integrations have been done the two by operators denoted 1 and 2 in figure 5.1. However as this is only one test and the subjective sense for integration might change over time even for one operator the uncertainty function inferred from this test is decided to be an envelop covering the difference between the highest and the lowest value for each point in the test. The bottom left panel of the figure shows this difference marked by stars.

The envelop uncertainty function, E_{i}, is calculated according to a function including all these values. Let's for the moment denote the measures of A, A_{kl} where k denotes the operator in the set of operators $\mathcal{K}$ and l is the sample among the samples $\mathcal{L}$. For each sample we denote the difference between the estimations

$$D_l \equiv \max_{k\in\mathcal{K}}(A_{kl}) - \min_{k\in\mathcal{K}}(A_{kl}). \tag{5.2}$$

The uncertainty is at least as large as the difference in the worst case of the three smallest samples

$$D_m \equiv \max_{l\in\{12,13,14\}}(D_l). \tag{5.3}$$

To get the envelop of all D_l values we continue from this minimum for small values by a straight line growth

$$E_{\mathrm{i}}{}'(A) \equiv D_m + \max_{l\in\mathcal{L}}\left(D_l - \frac{D_m}{\langle A_l\rangle}\right) A, \tag{5.4}$$

where $\langle A_l\rangle$ is the mean of the observers estimation of A_l. As seen in the figure the larger values do not have large relative differences so we can set an upper limit to the largest difference

$$E_{\mathrm{i}}{}'' \equiv \max_{l\in\mathcal{L}}(D_l). \tag{5.5}$$

This means that the envelope function is

$$E_{\mathrm{i}}(A) \equiv \min(E_{\mathrm{i}}{}'(A), E_{\mathrm{i}}{}''). \tag{5.6}$$

This function is plotted by a magenta line in the bottom left panel of figure 5.1.

5.4 Breakthrough

All the efforts to quantify the breakthrough in chapter 4 ended up in an estimation of the uncertainty of the breakthrough rather than an estimation of the breakthrough itself. The uncertainty due to breakthrough is calculated according to equation 4.39. As the breakthrough during calibrations is found to be negliable all the time the only uncertainty due to breakthrough is during the sampling in the stratosphere. This can only give rise to a sample loss. The uncertainty due to breakthrough according to equation 4.39 is therefore added to only the upper confidence limit of the results. It is thereby easy to see for which samples this uncertainty is dominating in the resulting profiles from the nonsymmetric error bars. It is added according to Gauss approximation.

5.5 Direct calibration method

In the direct calibration method all systems are calibrated simultaneously. The precision of these calibration is easily read out as the standard deviation of all the calibration data plotted in figure 3.4. The calibration curve for data from all the boxes together and it's standard deviation is shown in figure 5.2. As the calibration standard is well known and is a dry air standard it is reasonable to believe that the uncertainty is equally god as the precision for an imaginary compressed stratospheric sample taken during similar circumstances.

The estimation of the mixing ratio in this case is as showed earlier

$$c = \frac{h(A)}{f_n(U_\mathrm{f}, z_\mathrm{f})\, t_\mathrm{s}}. \tag{3.5}$$

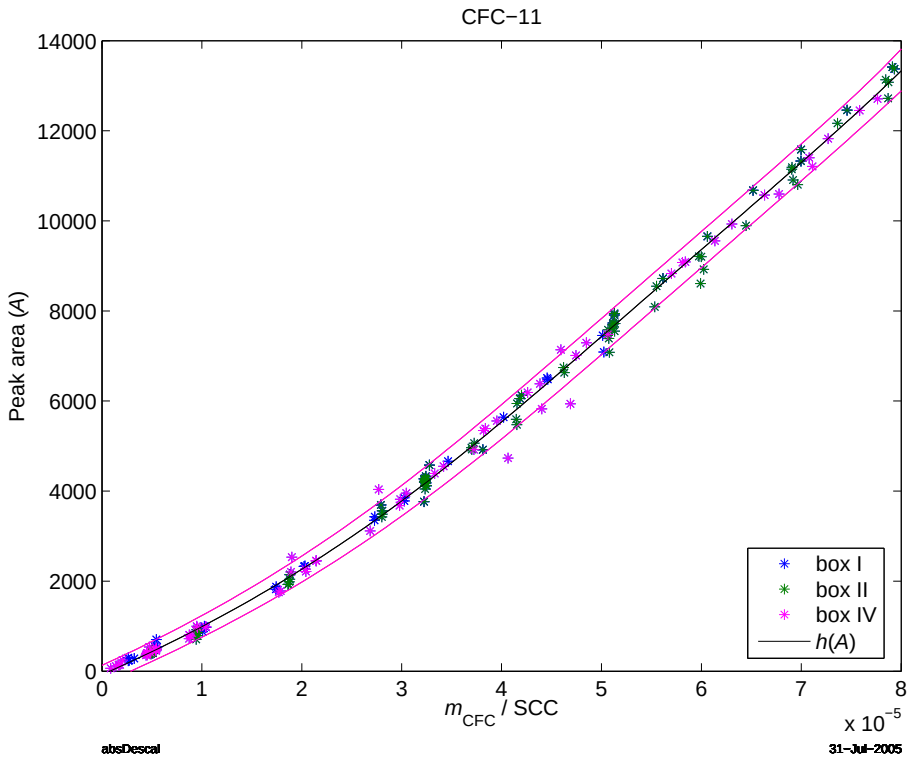

Figure 5.2: Direct absolute calibration curve, $h(A)$, for CFC-11 common to all boxes. This time plotted with 95% confidence limits for new datapoints in magenta.

5.5.1 Precision

The measurement of the peak area A, the flow meter readouts U_f and z_f, and the time t_s, is independent and the stochastic errors from these measurements can be treated according to Gauss approximation. For the two functions $h(A)$ and $f_n(U_\mathrm{f}, z_\mathrm{f})$ we have calibration curves and the stochastic error is thought to be similar during flight as during calibrations. The confidence limits of f_n are

calculated from u_n according to equation 5.1. The confidence limits of these measurements are good estimates for the precision of the estimation of these functional values. With the estimation of the CFC content

$$m_{\mathrm{CFC}} = h(A), \tag{5.7}$$

with the confidence limits Δm_{CFC} as indicated in figure 5.2, and the estimation of the flow

$$\mu = f_n(U_{\mathrm{f}}, z_{\mathrm{f}}), \tag{5.8}$$

with the confidence limits Δf_n, equation 3.5 can be written

$$c = \frac{m_{\mathrm{CFC}}}{\mu\, t_{\mathrm{s}}}. \tag{5.9}$$

The precision of the mixing ratio estimation can now be estimated according to Gauss approximation as

$$\begin{aligned} \Delta c &= \sqrt{\left(\frac{\partial c}{\partial m_{\mathrm{CFC}}}\,\Delta m_{\mathrm{CFC}}\right)^2 + \left(\frac{\partial c}{\partial \mu}\,\Delta \mu\right)^2 + \left(\frac{\partial c}{\partial t_{\mathrm{s}}}\,\Delta t_{\mathrm{s}}\right)^2} \\ &= c\sqrt{\left(\frac{\Delta m_{\mathrm{CFC}}}{m_{\mathrm{CFC}}}\right)^2 + \left(\frac{\Delta \mu}{\mu}\right)^2 + \left(\frac{\Delta t_{\mathrm{s}}}{t_{\mathrm{s}}}\right)^2}. \end{aligned} \tag{5.10}$$

5.5.2 Absolute uncertainty

Besides the uncertainty identified by this calibration method, there is a possible systematic change in flow-meter response discussed in section 5.1 and the possible breakthrough discussed in section 5.4.

In the calibration of the detector response the value of the content of CFC in the trap m_{CFC} was estimated according to equation 3.3

$$m_{\mathrm{CFC}} = f_n(U_{\mathrm{f}}, z_{\mathrm{f}})\, t_{\mathrm{s}}\, c_{\mathrm{a}}. \tag{3.3}$$

Of these parameters, the flow and time is estimated the same way during the flight, and is already accounted for, while the uncertainty of c_{a} is directly influencing the absolute uncertainty of the measurement.

5.6 Indirect calibration method

In the indirect calibration method the calibration is taken in two steps. First the ECD response function is taken on a poorly known standard and then the absolute response is given by relation to a well known standard. This is described in detail in section 3.4. The final expression for the estimation of the mixing-ratio from there is given in equation 3.13

$$c = \frac{g(A)}{\alpha\,\mu\, t_{\mathrm{s}}} = \begin{cases} \dfrac{\gamma_{\mathrm{l}} + e^{g_{\mathrm{l}}(\ln A)}\, t_0}{\alpha\, f_n(U_{\mathrm{f}}, z_{\mathrm{f}})\, t_{\mathrm{s}}} & \text{for } A \le A_{\mathrm{lim}}, \\ \dfrac{g_{\mathrm{h}}(A)}{\alpha\, f_n(U_{\mathrm{f}}, z_{\mathrm{f}})\, t_{\mathrm{s}}} & \text{for } A > A_{\mathrm{lim}}. \end{cases} \tag{3.13}$$

5.6.1 ECD response function

During these calibrations the standard deviation of the curves is a lot larger than during the direct method as indicated in figure 3.7. Most of this spread is thought to come from the sampling procedure during the calibration as discussed in section 3.4.2. For the measured values of real samples, the flow is measured by the on-board flow meters and integrated by DESCARTES flight software which has a lot smaller uncertainty. Single values are therefore not to be estimated by the ECD response function g to the standard deviation indicated in figure figure 3.7. For the precision rather the precision of the chromatogram peak areas should be used.

For estimations of the absolute uncertainty, the uncertainty of the curve fit should be included in the uncertainty estimation. The interval estimation in simple linear regression is easily calculated [e.g. *Hines and Montgomery*, 1980, pages 370–372]. If we call the half width of the resulting confidence interval of g, Δg and the half width of the confidence interval of a linear regression, δ, the upper part of the function is trivial $\Delta g = \delta g_{\mathrm{h}}$. For the lower part, on the other hand, we get an uncertainty in the estimation of $g_{\mathrm{l}}(\ln A)$ that is $\delta g_{\mathrm{l}}(\ln A)$. The uncertainty of the function g in this region is then

$$\begin{aligned} g(A) &= e^{g_{\mathrm{l}}(\ln A) \pm \delta g_{\mathrm{l}}(\ln A)}\, t_0 + \gamma_{\mathrm{l}} \\ &= e^{g_{\mathrm{l}}(\ln A)} e^{\pm \delta g_{\mathrm{l}}(\ln A)}\, t_0 + \gamma_{\mathrm{l}} \\ &\approx e^{g_{\mathrm{l}}(\ln A)} (1 \pm \delta g_{\mathrm{l}}(\ln A))\, t_0 + \gamma_{\mathrm{l}}, \end{aligned} \tag{5.11}$$

where the last step is the first order of the Taylor expansion of the error as $\delta g_{\mathrm{l}}(\ln A) \ll 1$. Thereby

$$\Delta g(A) = \begin{cases} e^{g_{\mathrm{l}}(\ln A)} \cdot \delta g_{\mathrm{l}}(\ln A)\, t_0 & \text{for } A \leq A_{\mathrm{lim}} \\ \delta g_{\mathrm{h}}(A) & \text{for } A > A_{\mathrm{lim}}. \end{cases} \tag{5.12}$$

Figure 5.3 shows the same calibration curve as figure 3.7 (for the last time now, I promise) but this time with the 95% confidence interval of the curve fit in magenta.

5.6.2 Precision

From equation 3.13 one of the variables can be identified not to contribute to the precision; α that is a constant. Opposite to the case with the direct absolute calibration discussed in section 5.5, the spread of the calibration curves of the ECD response is not similar to the flight measurements. Therefore the function g is considered fixed and an estimation of the precision of the estimations of the chromatogram peak areas are needed. The precision of the flow estimation is completely similar however and the confidence limits of the estimation can be used. From this we conclude that the error is made up of three terms in the

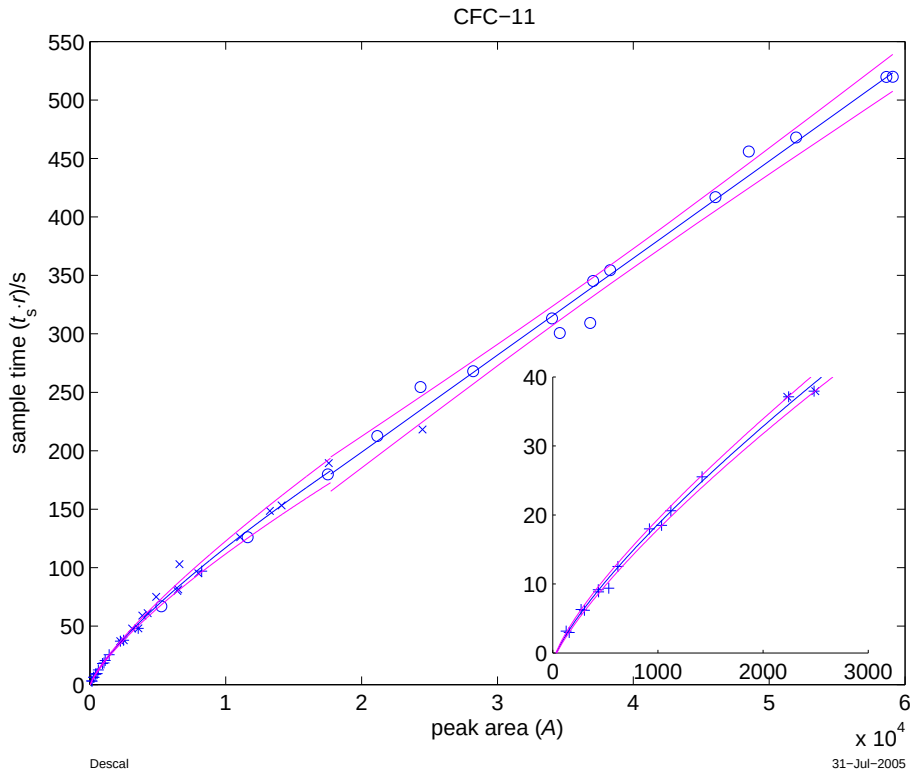

Figure 5.3: ECD response function similar to figure 3.7 this time with 95% confidence interval of the curve fit indicated in magenta.

Gauss approximation

$$\begin{aligned}\Delta c &= \sqrt{\left(\frac{\partial c}{\partial A}\,\Delta A\right)^2 + \left(\frac{\partial c}{\partial \mu}\,\Delta \mu\right)^2 + \left(\frac{\partial c}{\partial t_\mathrm{s}}\,\Delta t_\mathrm{s}\right)^2} \\ &= c\sqrt{\left(\frac{\partial c}{\partial A}\,\frac{\Delta A}{c}\right)^2 + \left(\frac{\Delta \mu}{\mu}\right)^2 + \left(\frac{\Delta t_\mathrm{s}}{t_\mathrm{s}}\right)^2},\end{aligned} \tag{5.13}$$

where

$$\frac{\partial c}{\partial A}\,\frac{\Delta A}{c} = \begin{cases} \dfrac{\Delta A}{g_{\mathrm{l}1}\,A\left(1+\dfrac{\gamma_\mathrm{l}}{A^{g_{\mathrm{l}1}}e^{g_{\mathrm{l}2}}\,t_0}\right)} & \text{for } A \le A_\mathrm{lim}, \\ \dfrac{g_{\mathrm{h}1}\,\Delta A}{g_\mathrm{h}(A)} & \text{for } A > A_\mathrm{lim}. \end{cases} \tag{5.14}$$

5.6.3 Absolute uncertainty

For the uncertainty of the absolute values of the measurements, besides the uncertainties mentioned in direct absolute calibration method, even the uncertainties involved in the fitting of the function g and the absolute calibration coefficient α must be taken into account. In principle also the fitting of function f_n should be taken into account but this error is much smaller than the uncertainty of the flow estimation using the onboard flow meters with the pump during sampling as discussed in section 5.1. The total expression for the absolute uncertainty is then

$$\begin{aligned}\Delta c &= \sqrt{\left(\frac{\partial c}{\partial A}\,\Delta A\right)^2 + \left(\frac{\partial c}{\partial g}\,\Delta g\right)^2 + \left(\frac{\partial c}{\partial \alpha}\,\Delta \alpha\right)^2 + \left(\frac{\partial c}{\partial \mu}\,\Delta \mu\right)^2 + \left(\frac{\partial c}{\partial t_\mathrm{s}}\,\Delta t_\mathrm{s}\right)^2} \\ &= c\sqrt{\left(\frac{\partial c}{\partial A}\,\frac{\Delta A}{c}\right)^2 + \left(\frac{\Delta g(A)}{g(A)}\right)^2 + \left(\frac{\Delta \alpha}{\alpha}\right)^2 + \left(\frac{\Delta \mu}{\mu}\right)^2 + \left(\frac{\Delta t_\mathrm{s}}{t_\mathrm{s}}\right)^2},\end{aligned} \tag{5.15}$$

where $\frac{\partial c}{\partial A}\,\frac{\Delta A}{c}$ is given in equation 5.14 and $\frac{\Delta g(A)}{g(A)}$ is given by dividing equation 5.12 with $g(A)$

$$\frac{\Delta g(A)}{g(A)} = \begin{cases} \dfrac{e^{g_\mathrm{l}(\ln A)}\cdot \delta g_\mathrm{l}(\ln A)\,t_0}{e^{g_\mathrm{l}(\ln A)}\,t_0 + \gamma_\mathrm{l}} = \dfrac{\delta g_\mathrm{l}(\ln A)}{1+\dfrac{\gamma_\mathrm{l}}{e^{g_\mathrm{l}(\ln A)}\,t_0}} & \text{for } A \le A_\mathrm{lim} \\ \dfrac{\delta g_\mathrm{h}(A)}{g_\mathrm{h}(A)} & \text{for } A > A_\mathrm{lim}. \end{cases} \tag{5.16}$$

5.7 Tests of uncertainties

The uncertainties are estimated from the calibrations. Whether these are really representative of flight conditions is hard to test. This section presents some tests that may be done to indicate if the uncertainty estimations are reasonable. The first is just a check that the estimated uncertainty really covers the total variability of the calibration data itself. Then some independent methods are presented.

5.7.1 Test on calibrations

A test to see if the uncertainty estimations are reasonable can be done with the same calibration runs sampling with the instrument as used to test the calibrations in section 3.5. The plots of the calibration runs presented in figures 3.17 and 3.18 are shown again with error estimations in figures 5.4 on the next page and 5.5 on the facing page. As already mentioned in section 3.5 this is not an independent test of the performance of the calibrations as it is the same data as used for the direct absolute calibration described in section 3.3. Worth to notice from figure 5.4 is that the uncertainty estimations are really much smaller for the large samples with high sample flow but still include the known target value while the already indentified problem areas with small flows and small samples is reflected in larger confidence limits.

5.7.2 Low pressure

While DESCARTES II was in Kiruna for the SOLVE/THESEO 2000 campaign, an inter-comparison test "flight" in a low pressure tank was performed. Sampling was controlled by standard flight software in the instruments. Pressure was slowly decreased in the tank until all traps were sampled. The sampled air was the natural air in the tank. The concentrations in this air are unknown. In figures 5.6 and 5.7 the results are shown in the same way as in figures 3.17 and 3.18. The last sample in DESCARTES III.2 was taken during too low pressure and the flow is not measurable. This sample is removed from the plots except in the lower left panel.

Flow meter calibrations were made using the same method for both instruments. For the indirect calibration method the rest of the calibrations are box-specific while for the direct calibration method, calibrations performed by DESCARTES III.2 have been used for both instruments. The spread in the points for each instrument is roughly similar as can be expected as it comes from the efficiency of the instrument and both calibrations are applied to the same measurements. Interesting to see is that the results shows better agreement between the instruments when using the direct calibration method, implying that it is more reliable than the indirect.

5.7.3 Double flights

The best test for the real precision of the measurements is of course to make independent measurements of the same stratospheric air with two instruments. The opportunity to make such tests came during the Spring-to-Autumn Measurements and Modelling of Ozone and Active species (SAMMOA) campaign [*Orsolini et al.*, 2002] and the last flights in the SKERRIES campaign. Low precision of the on board pressure gauges as well as different sampling times made it impossible to take simultaneous samples with two DESCARTES instruments at exactly the same heights but the overall impression from comparing two profiles is that they agree quite well as seen in figures 5.8 and 5.9. The eighth sample of DESCARTES III.2 plotted in green in figure 5.9 on page 102 is indeed two samples reconstructed to one, that might have additional error and may not be

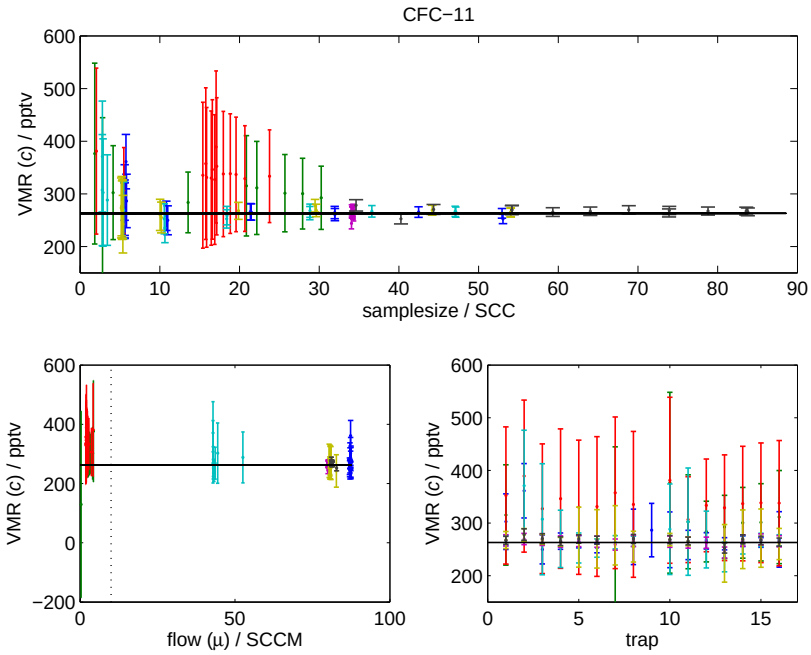

Figure 5.4: Uncertainty estimations of the direct absolute calibration approach applied to calibration runs as presented in figure 3.17.

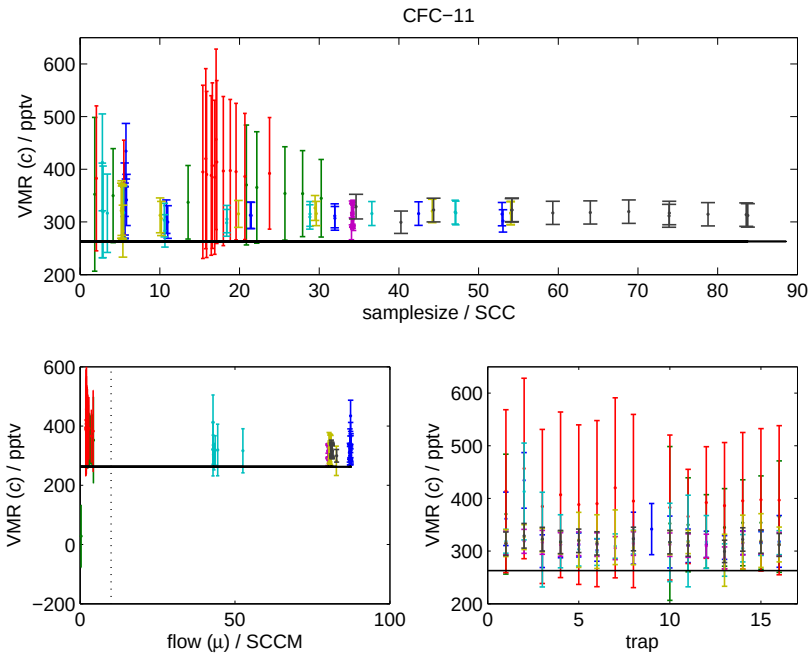

Figure 5.5: Uncertainty estimations of the indirect calibration approach applied to calibrations as presented in figure 3.18.

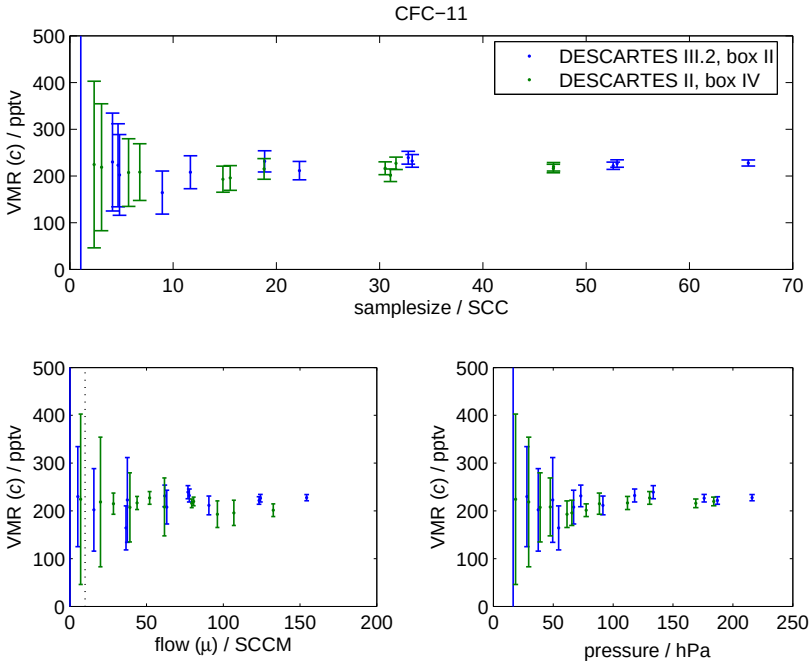

Figure 5.6: Results of low pressure test from the direct absolute calibration method described in section 3.3. Note that the y-axis covers half the interval size compared to figure 3.17. The lines indicates the mean response the single outlayer removed.

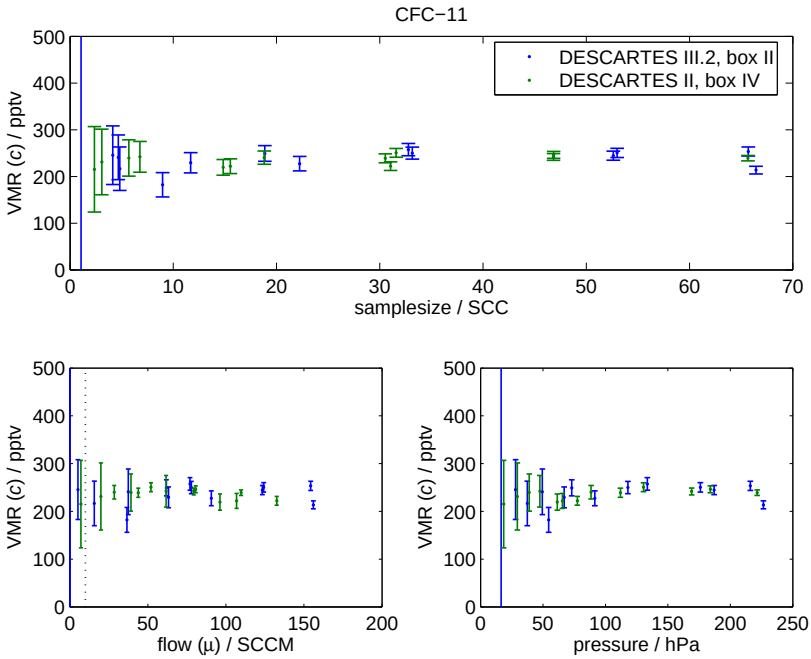

Figure 5.7: Results of low pressure test from the indirect absolute calibration method described in section 3.4. Similar to figure 5.6. The y-axis covers equally sized intervals as in figure 5.6.

really representative for the height where it is plotted, see further in the flight notes on page 122. As the calibration is performed in the same way for both instruments this is only a relative comparison.

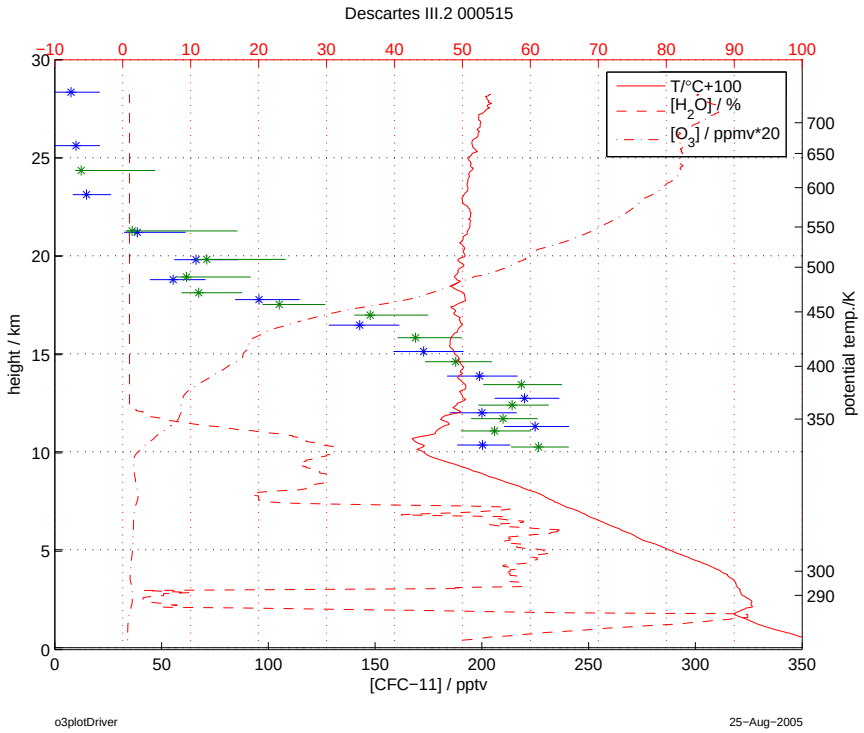

Figure 5.8: Flight profiles from flight 000515. DESCARTES III.2 profile in blue and DESCARTES II in green.

5.7.4 Tropospheric samples on ground

The tropospheric mixing ratio of CFC-11 is known to be fairly similar all over the globe. Measurements made in the troposphere could thereby be a way of estimating the absolute uncertainty.

Sampling at ground level in a clean environment has been tried. The sampling system is designed for stratospheric samples, though, which means that it was hard to make reasonable sampling at this high pressure.

In the flight log files as described in section 2.1.1 two flow readouts during the samples are written to the flight log, using both flow-meters. This gives four short samples of the flow during the air sampling. During normal flight conditions these are in good agreement with the integrated mean flow. During the tropospheric sampling on ground the flow was regulated with an external needle valve to give a reasonable comparison to the flights. In these flights the four short flow readings in the flight log show much more variability and not even internal consistency between the two flow meters indicating that there are either stronger disturbances to the flow meters than during flight or a rapidly varying flow.

Some samples were taken with a special version of the flight software that

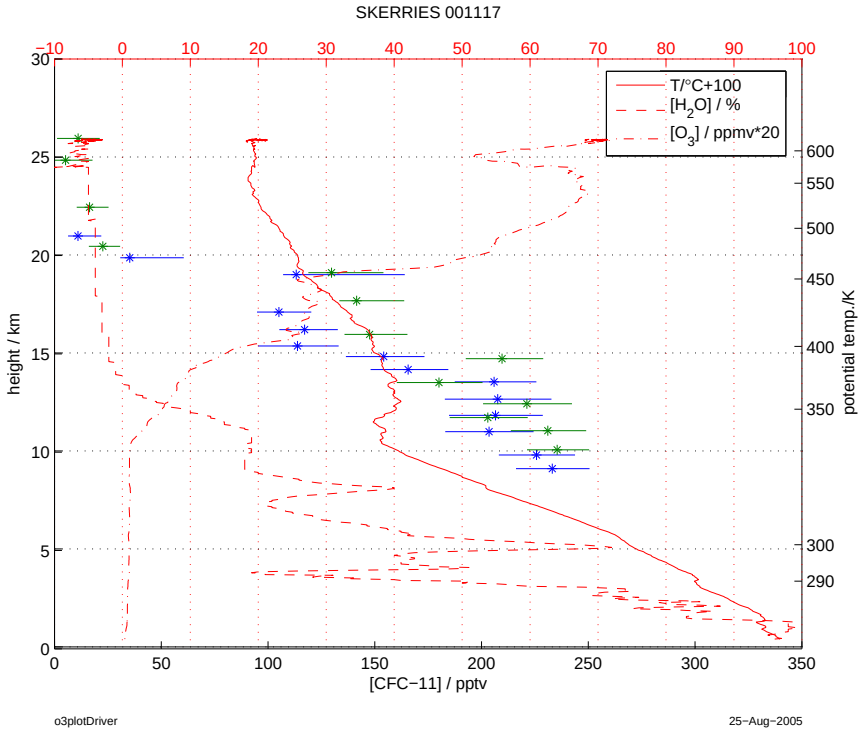

Figure 5.9: Flight profile from flight 001117.

did not take the ordinary zero readings of the flow meters. These show also very strange results. The two tests ran with ordinary flight software and were analysed with the direct and indirect calibration methods. Results are presented in figures 5.10 and 5.11 respectively. The uncertainties shown in the figure are calculated by the normal algorithm. As seen in the figure, the samples are almost internally consistent within uncertainties for each calibration method despite the problems with the unstable flow or flow meter reading. The two outliers with drastically lower concentrations are due to desorption problems. On some occasions the heating doesn't perform nominally and does not give quantitative desorption. This is seen in the second heating of the traps and, when this is seen in the second heating of a real flight sample, the sample is discarded.

5.7.5 Tropospheric samples during flights

The first samples are thought to be tropospheric in some flights. They are taken close to the tropopause anyway and there is always a risk that there might be dilution from stratospheric air. The mixing ratio of CFC-11 in the northern hemisphere troposphere is monitored by HATS to about 265 pptv for the period of flight measurements [*Thompson et al.*, 2004]. No sample results from DESCARTES has ever exceeded 265 pptv CFC-11. Samples taken in the troposphere includes a clear case in 2000-08-14, (figure 7.20 on page 128) where several samples were taken in the tropopause ranging between 200 and 230 pptv CFC-11, 2000-11-17 (figure 5.9) also significantly lower than expected in pure tropospheric air and 2000-12-11 (figure 7.22) that is close to the tropospheric value and could

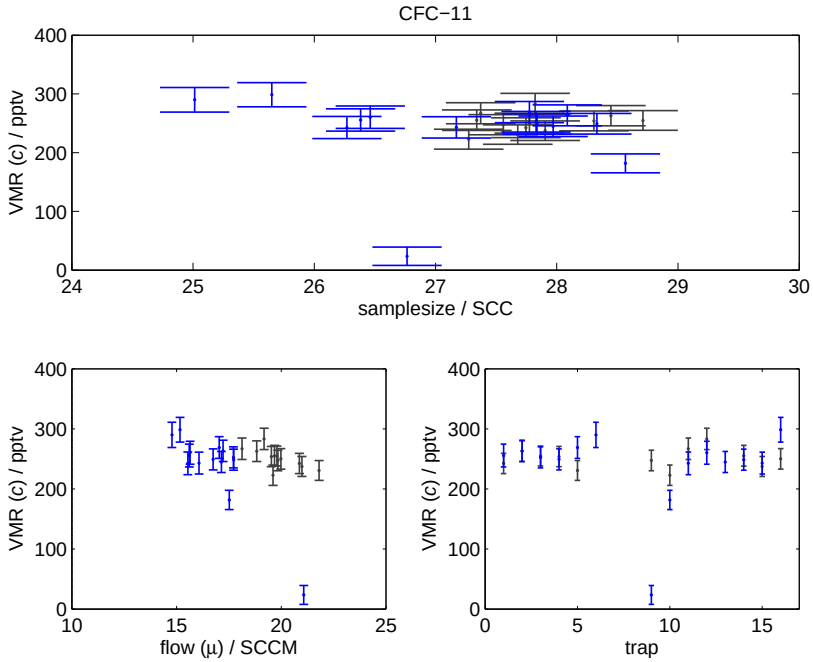

Figure 5.10: Results from samplings done with DESCARTES of ambient air on ground analyzed with the direct absolute calibration method.

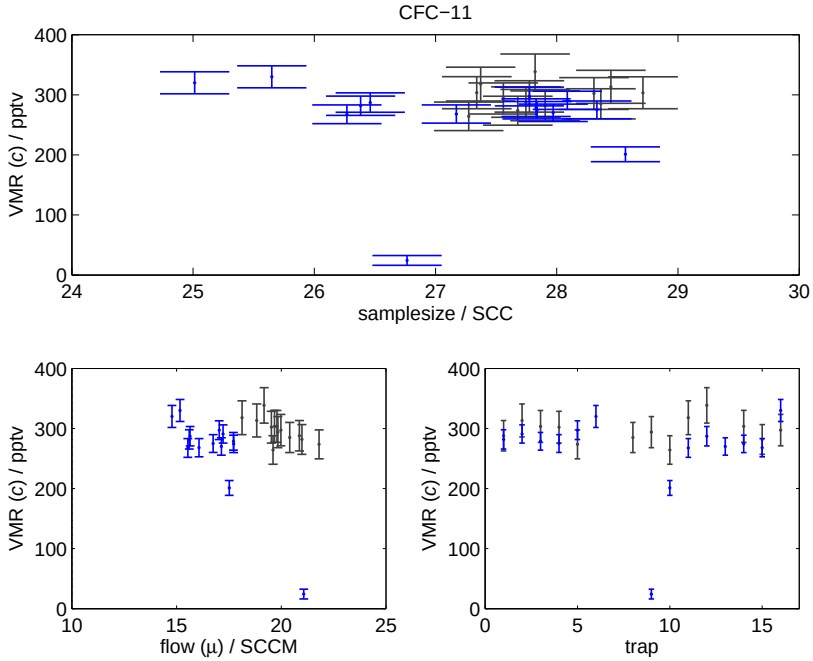

Figure 5.11: Same tests as in figure 5.10 analyzed with the indirect calibration method.

be thought to be almost free from stratospheric dilution.

5.8 Conclusions

The tropospheric trend measured from several ground stations (by CMDL at NOAA [*Thompson et al.*, 2004]) is at the moment approx -2.6 pptv/a (1 % /a). As this time scale is comparable with the stratospheric lifetime of CFC-11 (estimated to 45 a [on Climate Change , IPCC]) and the tropospheric maximum was reached in 1993, the trend in the stratosphere is thought to be slower. As the instrument has undergone some changes and, if it is going to be used in the future more changes is recommended, there might be some changes in the absolute values in the measurements. In this context comparisons of absolute measurements performed with DESCARTES will not be able to give good enough accuracy to detect absolute changes in the near future.

Chapter 6

Possible future improvements

First of all it must be said that lightweight in-situ systems using pre-concentration on a micro-trap and chromatographic analysis in flight, have been developed a great deal since the time when the DESCARTES versions discussed in this work were built. In this process many aspects that would be of interest for a new generation micro trap grab-sampler has been implemented, such as lighter and more flexible plastic based materials.

6.1 Choice of material

The pump on board DESCARTES contains rubber diaphragms as mentioned in section 3.3. From the adsorption point of view this is a potential problem. All other surfaces that are exposed to the sampling air consist of stainless steel and aluminium with a few brass and graphite ferrules. The pump is not tested for desorption of the CFCs in this study but a change to a pump with surfaces in Teflon and stainless steel is probably better.

Even in other parts of the sample line than the pump, unwanted adsorption effects in the instrument can be seen and the materials used in the sample line should be tested more carefully for adsorption effects of the species to measure. As seen in the calibrations of CFC-113 (section 3.6.1), such effects can be seen by sampling calibration samples through the sample line of the instrument. Some kind of full sampling calibration would be an interesting experiment. The ultimate test would be a pressure regulated tank that could fit the whole instrument where the concentrations of the species to measure could be controlled and in some way measured with precision.

6.2 Traps

The breakthrough study in *Roslin* [2003] and this work shows that the traps are not fully satisfactory even for one species. A future grab-sampler must be able to measure a set of several species in order to compete with the lightweight in-situ instruments. Then the traps must be more effective, probably of multi-bed type. In order to get better efficiency traps their flow resistance must be higher and thereby a more efficient pump is needed.

6.3 Heating system

The heating system as described in section 2.3 is, with the present design, trying to estimate the temperature of the trap by measuring the resistance of the trap. As the resistance of the trap is small and the dependence on temperature is low the signal to look for is weak. No other measurements has been performed to investigate the precision of this method. There are possibilities that small changes in the system can change these measurements significantly. There are also some examples of traps that have changed their behaviour in the history of DESCARTES as well as some examples of traps that have, for single occasions, been heated to much higher temperatures than usual.

One way to get away from the uncertainty of this temperature measurement would be to not measure the temperature at all. As there is now a system that we think is working very well on the average, it could be tested for the characteristics of the current heating the traps. Measuring the current going through the system can be done with better precision than estimating the trap resistance. As long as the traps have the same resistance per unit length the thermal effect in the trap should be the same. As there are no significant differences in the cooling of the traps there is no reason to fear large temperature differences.

6.4 Calibration

Test sample filling and analysis is performed for the waiting position in each flight as discussed in section 3.4.3. Filling of each trap after the analysis of the trap was discussed but rejected to leave the possibility for a second heating round if desorption problems arise. In practice, data from flights with problems of such severity are so bad that they are in practice useless. Test samples after each heating are thought to be of value to the analysis and are recommended. These fillings could be of the absolute calibration air standard and their sizes made to match the sampled flight profile. In this way each analysis should contain its own absolute calibration and each trap should have a calibration sample of the same order of magnitude that should decrease individual uncertainty of the samples.

The sampling procedure used in the indirect calibration method described in section 3.4 where the GC is set to control the flow by regulating the pressure is not good enough for calibration purposes. All future calibration sampling should be done with measures of the flow by the instruments flow meters and flow sampling algorithm such as the direct absolute calibration method described in section 3.3.

6.5 Determination of sample sizes

In the present instrument the sampling flow estimation is the dominating error for samples taken on low pressure levels where the flow is low. The flow meters do not have a properly stable zero reading. The readout in the flight log of the zero is a byproduct of the reading of the pressurisation pressure of the trap. With minor changes the flight software could be rewritten to give more and more reliable zero readings.

Better yet would be a completely new approach to determine the sample size. A fixed volume on board that can contain the sample before injection to the traps, where the sample size can be determined from temperature and pressure readings, would give a good estimation independent of the time it takes to do the sampling.

6.6 Breakthrough control

As seen in the study of breakthrough in chapter 4, the breakthrough of the traps is strongly dependent on the flow during sampling. A system to determine the pressure in the trap, for example by pressure monitoring before and after the trap, could be used together with an interactive flow control system where this pressure and continuous flow measuring can be used to regulate the flow through the trap to a level safe for breakthrough.

There is a trade-off between the risk of breakthrough and the depth of the adsorption bed and thereby the flow resistance of the trap. This problem will increase if the same traps are to be used for many different species with different adsorption properties. A system that could be used to get closer to the limits of breakthrough, while keeping good control, is to divide the adsorption bed into two traps in series as used in the double trap experiments of chapter 4. The total sample could then be estimated from the sum of the trapped species of the two traps. With a calibration effort to see the breakthrough behaviour of the double trap system, the risk of breakthrough of even the second trap could be estimated in a much more reliable way than the present. With this kind of system, sampling may even be done beyond the limit where breakthrough occurs and a safe compensation for the breakthrough can be applied from the ratio of concentrations in the two traps. The drawbacks of this kind of system are the larger uncertainties due to double chromatographic peak integration and the more complicated mechanical structure for the instrument with two multi-trap valves.

Chapter 7

Measurement activities

The Kiruna DESCARTES team has been involved in several campaigns, as well as some flights with no connection to scientific campaigns, mostly as a piggy back load on balloons carrying out technical tests. The major campaign contributions are Improved Limb Atmospheric Spectrometer (ILAS) validation campaign 1997, THESEO [*Harris et al.*, 2000b] 1998–1999, SKERRIES 1998–2000, SOLVE/THESEO 2000 [*Newman et al.*, 2002] and SAMMOA [*Orsolini et al.*, 2002] 2000. The ILAS validation campaign was performed with the instrument version II.

All flights performed are listed in tables 7.1 and 7.2.

Date	Time	Flight
970129	12:50 LT	SAOZ
970211	09:25 UT	Triple
970222	09:16 UT	Sakura
970225	09:16 UT	CLD
970228	13:45 UT	SAOZ
970318	07:26 UT	Sakura

Table 7.1: Flights during the ILAS Validation Campaign 1997

Most flights are from Esrange (67.9° N, 21.1° E), a few flights noted in table 7.2 was made from Andøya Rocket Range (ARR) on Andøya (69.3° N, 16.2° E).

In the figures throughout the chapter the notation $[x]$ will be used for the mixing ratio of species x (i. e. $[x] = c_x$), not to confuse with the normal use of the similar notaton for the concentration in terms of amount of substance per unit volume.

7.1 1997, ILAS validation campaign

Six flights were made with the DESCARTES version II instrument during the validation campaign for the ILAS instrument [*Sasano et al.*, 1999] on the Advanced Earth Observing Satellite (ADEOS) from late January to mid Mars. The flights was performed from the ARR and Esrange balloon launch facilities, together with the Systeme d'Analyse par Observation Zenithale (SAOZ), Triple

Date	Time[a]	Flight[b]	Base	Comments
980825	22:05 UT	SKERRIES	Esrange	software problem
981117	10:20 UT	SAOZ	Andøya	poor desorption
981208	16:15 UT	SKERRIES	Esrange	poor desorption
990127	11:54 UT	SAOZ / BrO	Esrange	
990212	10:33 UT	Technical (SSC)	Esrange	
990218	13:30 UT	Technical (CNES)	Esrange	
990420	09:50 UT	Technical (SSC)	Esrange	
990826	12:30 UT	SKERRIES	Esrange	
990906	07:12 UT	Technical (SSC)	Esrange	Low peak altitude, desorption problems
991109	10:30 UT	SKERRIES	Esrange	Poor desorption
991117	10:30 UT	SAOZ	Andøya	Analyzed at UCamb
991203	09:00	OMS remote	Esrange	
991215	11:00 UT	SKERRIES	Esrange	
000128	11:20 UT	SAOZ	Esrange	
000209	13:00 UT	SAOZ	Esrange	
000213	13:00	SAOZ	Esrange	Technical failure.
000301	10:00 UT	HALOZ	Esrange	
000305	15:30 LT	OMS in-situ	Esrange	
000307	14:25 UT	SAOZ	Esrange	
000403	18:30	SAOZ	Andøya	
000404	11:00 UT	HALOZ	Esrange	
000515	11:30 UT	SAMMOA	Esrange	
000616	10:00 UT	SAMMOA	Esrange	
000815	09:30 UT	SAMMOA	Esrange	
000922	16:00 LT	SKERRIES	Esrange	
001117	13:00 UT	SKERRIES	Esrange	
001211	14:00 UT	SKERRIES	Esrange	

[a]The launch time is not registered by the instrument and usually no special notes has been taken, these approximate launchtimes is in most cases estimated from the detected pressure drop.

[b]In the SAMMOA and SKERRIES campaigns DESCARTES is one of the priary payloads on each flight, for the other campaigns DESCARTES is the host payload is given.

Table 7.2: Flights during the THESEO, SOLVE/THESEO 2000, SAMMOA and SKERRIES Campaigns 1998 to 2000

(including the Bonbon grabsampler [*Schmidt et al.*, 1991]), Sakura [*Honda et al.*, 1996] and CLD (including the Astrid grabsampler) payloads. CFC-12 data from Bonbon, Sakura and Astrid from these flights are presented in *Khosrawi et al.* [2004].

Analysis of these flights was perfomed at Universtiy of Cambridge and the measurements are presented and discussed in *Nilsson et al.* [1997] and *Danis et al.* [1998].

7.2 1999, THESEO and SKERRIES campaigns

During the one year period from late August 1998 to early September 1999 DESCARTES participated in 9 flights. These were participations in the THESEO and SKERRIES campaigns as well as several chances for piggy back flights on technnical test balloons mainly from Swedish Space Corporation (SSC) but also Centre National d'Etudes Spatiales (CNES). Due to several different technical problems with the (by then) new version III.2 DESCARTES instrument, there are reliable results only from the 5 flights spread out during half of the period from late January to late August 1999 as seen in table 7.2 on the facing page. The data from this season has previously been presented in a preliminary form in *Arvelius et al.* [1999] and *Arvelius et al.* [2000].

Especially the improvement of the desorption system to move a temperature dependent diode away from transistors that got warm during the heating (discussed in section 2.3) were done during this season. The heating system was hard to tune before this improvement and the first flight profiles showed, that for some reason, the samples taken during a real flight were harder to desorb. An example of a chromatogram taken on the november flight from Andøya with six consecutive heatings is shown in figure 7.1 to be compared to figure 2.8 on page 16 from the spring. Of course any estimate of the concentrations from such chromatograms are very uncertain. As the behaivour of the flights are different from the calibrations, and the hardware was modified to give more reliable response during the campaign, there is no way to investigate this further and these two flights are left without results.

980825, 22:05 UT, flight with SKERRIES. A software error, where the response difference of the new flow meters in DESCARTES was not accounted for, made the flight software believe there were problems with the stepping of the box, thus stepping the trap position two revolutions resulting in two samples in every second trap. Not analyzed.

981117, flight with SAOZ from Andøya. Flight under good conditions but the heating was not working well as discussed above (see figure 7.1 on the following page).

981208, flight with SKERRIES from Esrange. Flight with the same heating system as above.

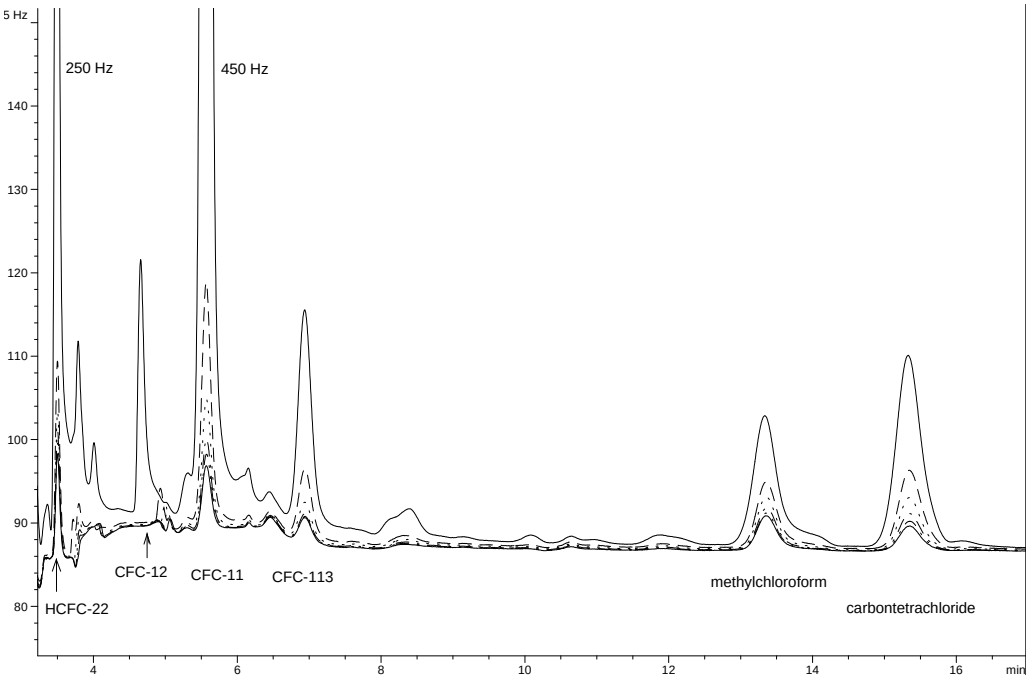

Figure 7.1: Example of chromatogram from the flight 981117 from Andøya.

990127, flight with SAOZ/BrO from Esrange. The flight was done under very cold conditions, $-40\,^{\circ}\mathrm{C}$ during the release and even colder after landing. The instrument was left out for more than 24 hours as the recovery team did not work in the field due to the low temperature. This might have caused leaks in the traps. The fact that no other peaks than usual are seen in the chromatograms from this flight indicates that there were no leaks. The parameters set for the flight program were adopted for flights in tropical conditions. The last samples became far too small to give good estimations. Worth to notice is that the uncertainty estimation seems reasonable as it is expected to find very low levels of CFC-11 in the height region above 25 km. Profile plotted in figure 7.2 on the next page. Ozone data taken from accompanying Electrochemical Concentration Cell (ECC) ozone sonde.

990212, technical flight from Esrange. This flight had the slowest ascent during the campaign. The quality of these measurements seems better than the rest. With this in mind it might be best for future flights to have a slow ascent however this might be at odds with achieving a high float. A slower ascent also makes the samples better defined in height. The same parameter file used for the sample program as for the flight 990127. Profile shown in figure 7.3 on page 114.

990218, technical flight from Esrange. The same parameter file used for the sample program as for the flight 990127 resulting in too small samples at high altitudes. Profile shown in figure 7.4 on page 114.

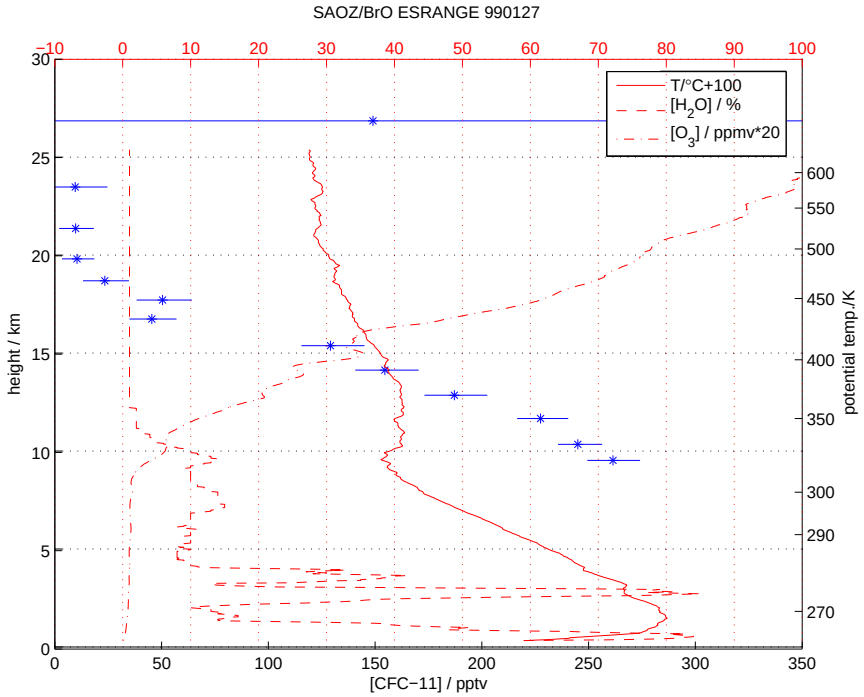

Figure 7.2: Flight profile from flight 990127.

990420, technical flight from Esrange. Flight done after turnaround (i. e. summer wind direction in the stratosphere). Instrument performance appears nominal. Profile shown in figure 7.5 on page 115.

990826, flight in SKERRIES campaign. Instrument performance appears nominal. Profile shown in figure 7.6 on page 115.

990906, technical flight from Esrange. Desorption problems during the analysis, no data presented.

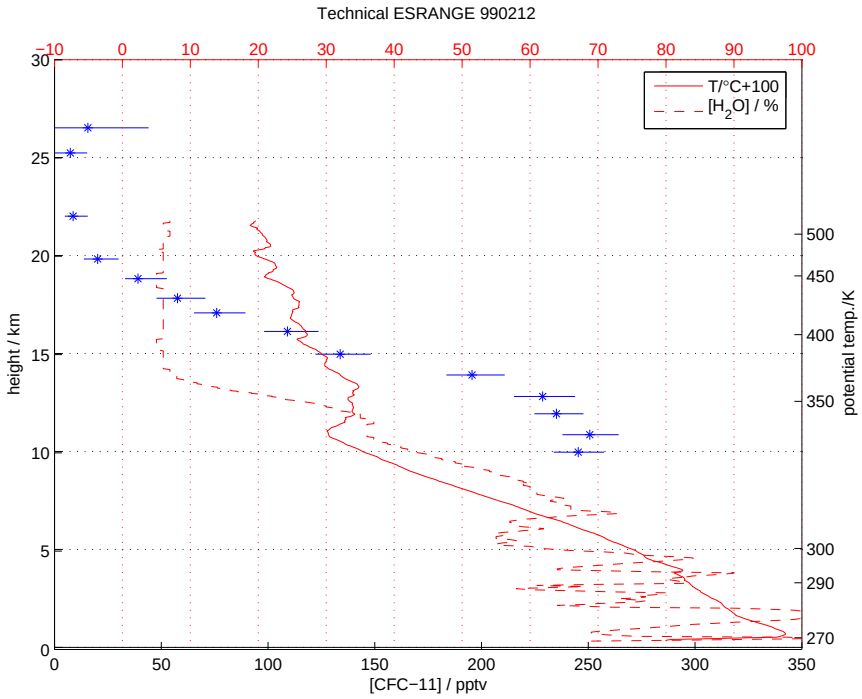

Figure 7.3: Flight profile from flight 990212

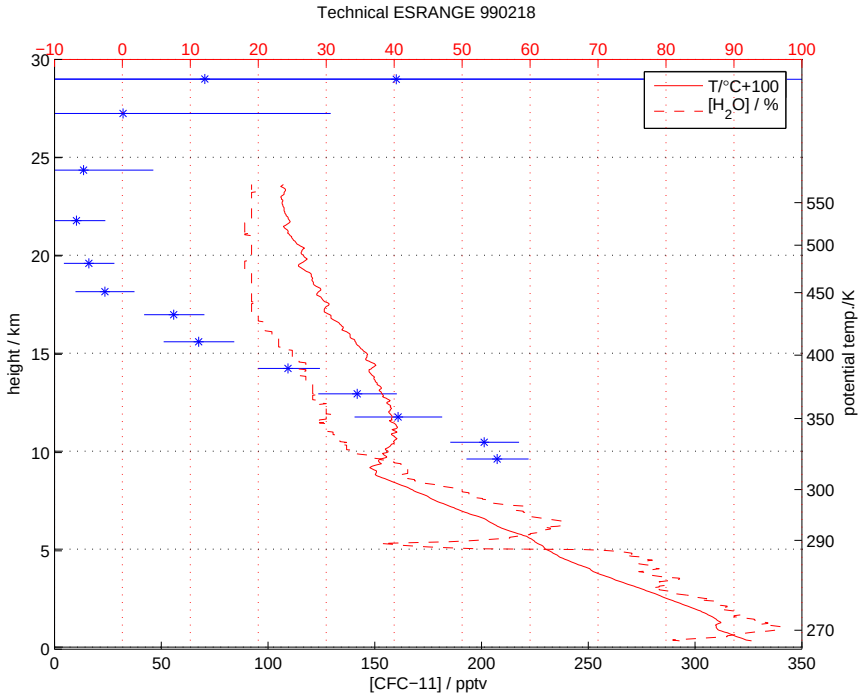

Figure 7.4: Flight profile from flight 990218.

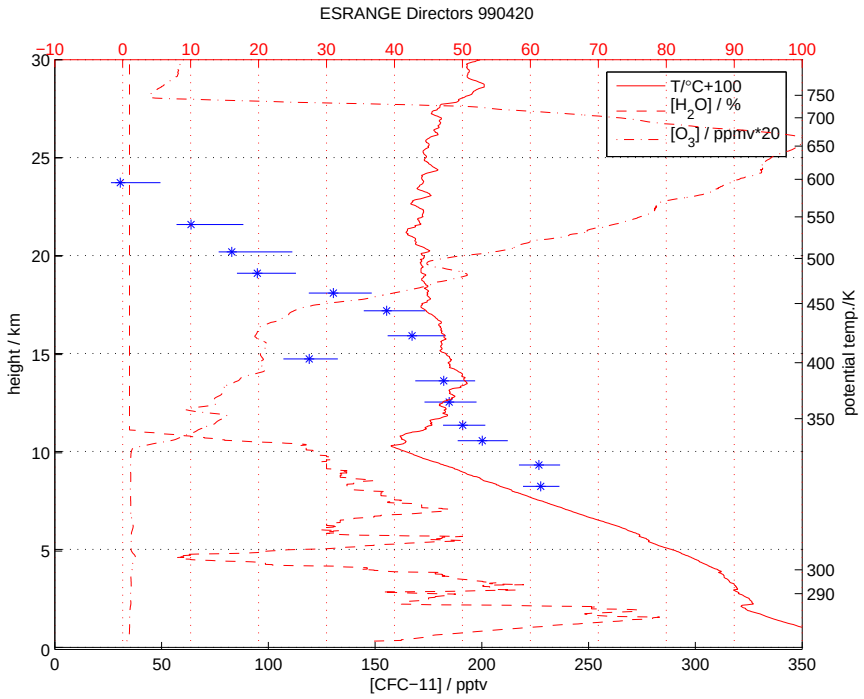

Figure 7.5: Flight profile from flight 990420

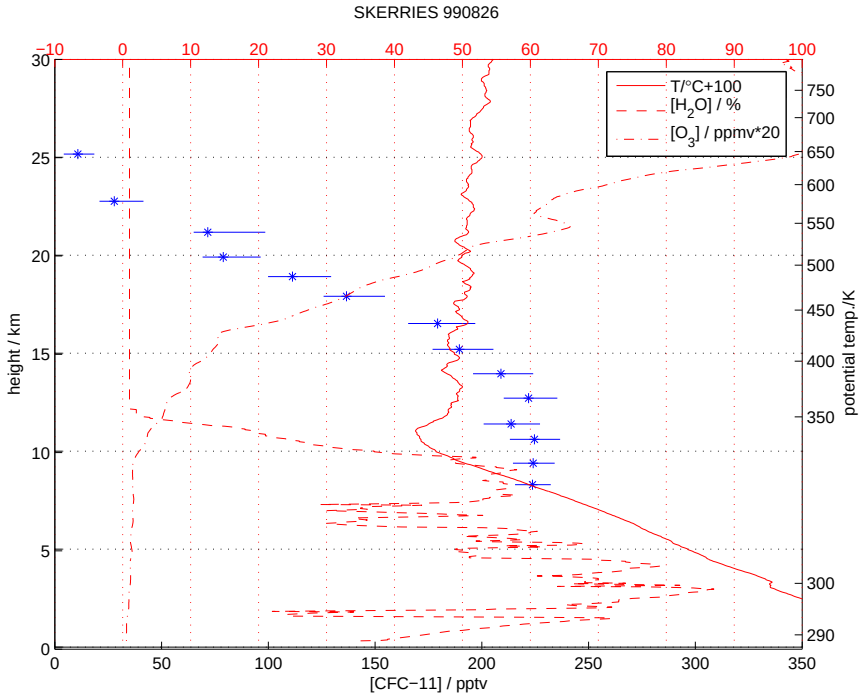

Figure 7.6: Flight profile from flight 990826.

7.3 1999–2000, SOLVE/THESEO 2000, SAMMOA and SKERRIES campaigns

During the year from mid November 1999 to mid December 2000, DESCARTES participated in the SOLVE/THESEO 2000, SAMMOA and SKERRIES campaigns. This resulted in 18 flights of which there are reliable results from 15. The flights in the SOLVE/THESEO 2000 campaign was done piggy back to the SAOZ, HALogens and OZone loss (HALOZ), Observations of the Middle Stratosphere (OMS) remote and OMS in-situ payloads. Due to the compact schedule during the spring both versions II and III.2 of the DESCARTES instrument was used during those flights. Both versions of the instrument used the same inter changeable sample boxes, developed with the version III.2 instrument, during this time in contrast to the ILAS validation campaign where the previous sample boxes using nichrome wire heating was used with the version II instrument.

Measurements were performed throughout the year 2000. By these measurements it is possible to follow the evolution of the stratosphere during the whole year. Figure 7.7 shows the ozone and potential temperature for all fully successful flights during the year with accompanying data of temperature, pressure and oxone mixing ratio from other payloads, interpolated to isopleths of CFC-11. Interpolation has been done by first integrating the measurements over the sampling-time of the closest DESCARTES samplings and then linear interpolation between these points to get corresponding measurements. Direct interpolation of the closest DESCARTES samples without any smoothing of the profile has been used. On a couple of occations, where the profile is turning in such a way that two possible solutions have been possible, the one referring to the part of the profile where the CFC-11 mixing ratio is decreasing with increasing potential temperature has been chosen. All potential temperature values are calculated from ptu units. For the flights 000128, 000209, 000307 and 000403 ozone are derived from SAOZ [*Pommereau and Piquard*, 1994] measurements, and for the rest from Vaisala ECC ozone sondes. Ozone values are missing from flight 000922 due to a malfunctioning ozone sond. Vortex classifications are made by an upper and a lower Potential Vorticity (PV) threshold where over the upper threshold means in-vortex, in between means on the edge, and under the lower threshold means out-of-vortex. These thresholds increase from 30 to 42 pvu at 475 K from first of November to 1 January for the upper and from 20 to 25 pvu for the lower. PV data are taken from the European Centre for Medium-Range Weather Forecasts (ECMWF) analysis. A preliminary version of this study was presented in *Arvelius et al.* [2002].

7.3.1 In vortex flights

During the winter and spring 1999–2000, in total five flights were performed in the polar vortex. From these profiles the vortex subsidence can be seen directly in figure 7.8. Ozone concentrations from accompanying ozone sondes can be effectively corrected for subsidence by plotting against CFC-11 concentrations so that the chemical ozone depletion can also be illustrated as in figure 7.9. From figure 7.8 on page 118 is seen that there is a cooling on the order of 50 K in

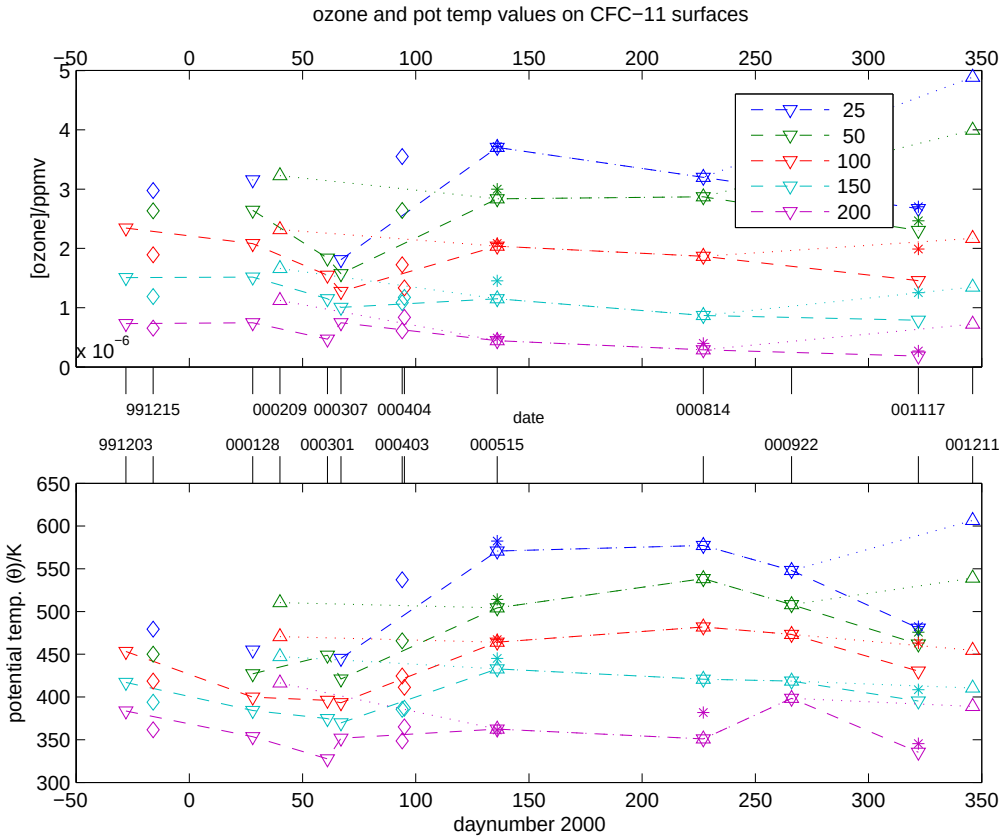

Figure 7.7: Ozone and potential temperature measurements interpolated to CFC levels from DESCARTES measurements. Downward facing triangles are in-vortex flights, upward facing are out of vortex flights, diamonds are vortex edge and stars are for double flights interpolations to the second DESCARTES profile and otherwise vortex edge. Flights in summer (May to October) are plotted with both the in and out of vortex series.

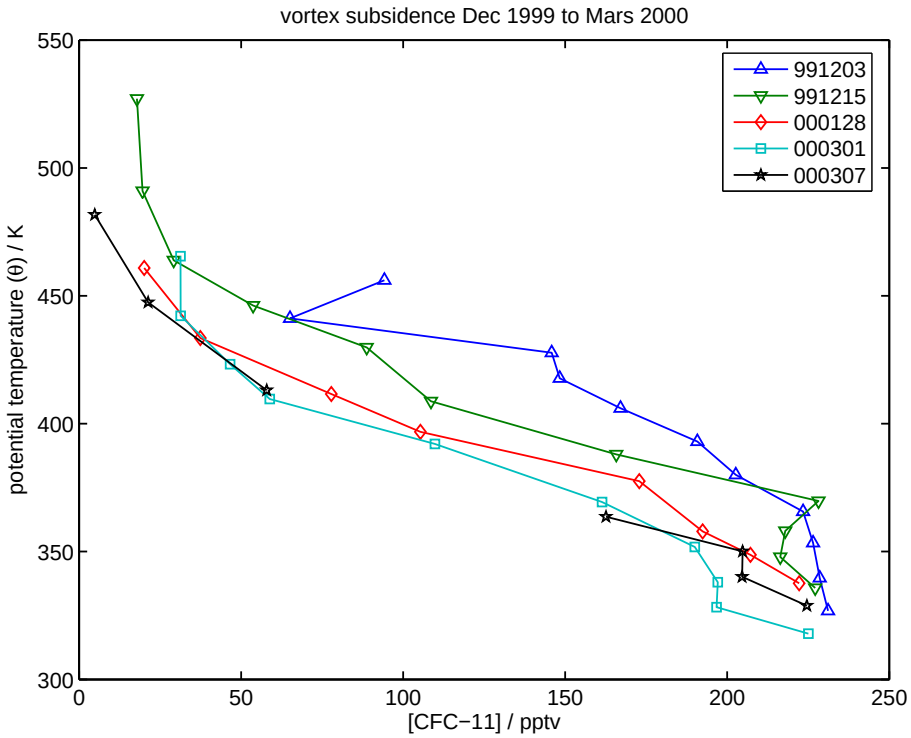

Figure 7.8: Flight profiles of CFC-11 inside vortex winter and spring 1999–2000.

the middle stratosphere (CFC-11 concentration levels ca 150 pptv), and that this mainly takes place early in the winter, between the first flight early December and the third in late January. In figure 7.9 on the next page we can see that the chemical ozone depletion mainly takes place later in the season, in the time period from late January to the last measurement in March. This short series of DESCARTES flights, with only a subjective 'inside vortex' estimation from potential vorticity maps gives only are crude estimate of the ozone loss. More extended studies involving comparisons to other tracer flight profiles, satellite measurements and model studies has been made by *Robinson et al.* [2005] and *Müller et al.* [2002].

7.3.2 Comparisons to other instruments

During the SOLVE/THESEO 2000 campaign two possibilities to make comparisons to in-situ instruments that measure CFC-11 became available.

DESCARTES was flying on 2000-01-28 one day and under similar circumstances as the flight carrying Bonbon and DIRAC one day earlier.

On 2000-03-05 DESCARTES II, with box IV flew together with both DIRAC [*Robinson et al.*, 2000] and Lightweight Airborne Chromatograph Experiment (LACE) [*Moore et al.*, 2003]. The analysis of this flight showed, however, some problems with the desorption (see further notes in the next section). Two days later the normal configuration DESCARTES III.2 and box II used during most of the campaign was flying under similar circumstances giving a better opportunity

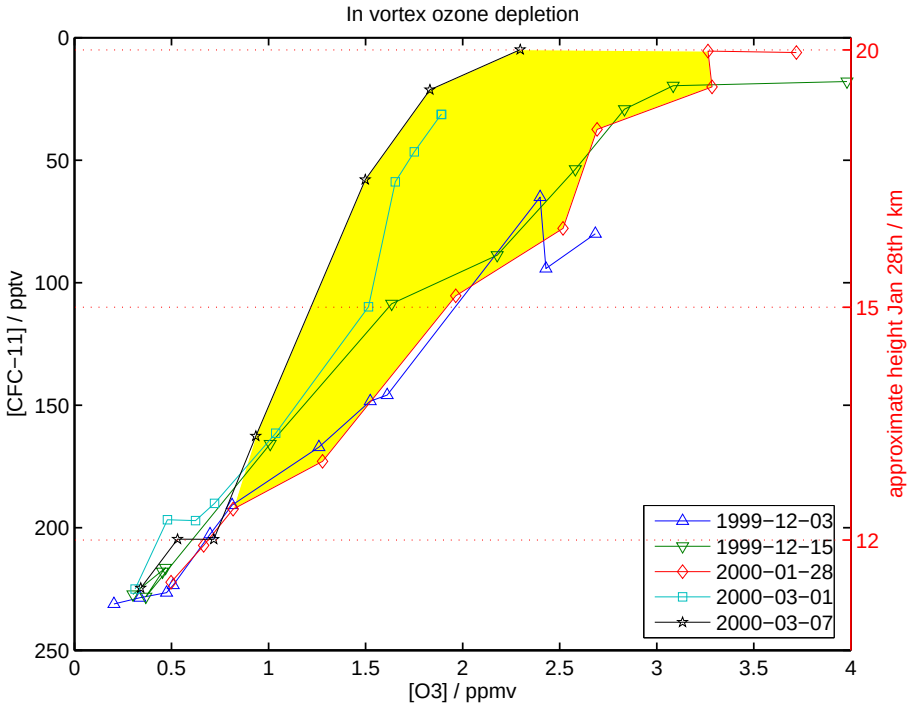

Figure 7.9: Tracer-tracer correlations of CFC-11 and ozone inside vortex winter and spring 1999–2000. The shaded area in this figure shows the chemical depletion of ozone from late January to early Mars.

for a comparison to DESCARTES working nominally.

Both these cases are already studied in detail comparing the profiles from all the instruments in *Robinson et al.* [2005]. For the Robinson study the most important factor was to give the most internally consistent data set with DESCARTES and DIRAC. From this perspective the indirect calibration method of DESCARTES was chosen. The two calibration methods show about 12% absolute calibration difference, the direct being the lower of the two. As seen in figure 3 of *Robinson et al.* [2005] this is about the fraction that differs in the comparison to Bonbon for DESCARTES, making the direct calibration method give an almost perfect comparison to Bonbon but worse to DIRAC for the January case. In the comparison to LACE and DIRAC in Mars on the other hand, DESCARTES already show lower estimations than both the in-situ instruments making this comparison worse (when using the direct absolute calibration method is used).

7.3.3 Comments to flights

The most frequently used sample box during the campaign was box II. One trap (no 8) in that box gave very strange values regularly, much lower than the others during the campaign. The samples contained in this trap that is not reliable have therefore been removed in all profiles presented.

991109, Flight with SKERRIES. The analysis of the flight showed unexpected poor desorption after the last analysis with good performance. No analyzed data presented. The rest of the month a large effort was made to tune the heating parameters to reestablish good desorption.

991117, Flight with SAOZ from Andøya. Due to uncertainties about performance of the analysis equipment after the last flight the sample box was sent to University of Cambridge for analysis. As the box was not calibrated there earlier, some problems with the tuning of the heater current were present and some samples were lost.

991203, Flight with OMS remote with the Jet Propulsion Laboratory (JPL) Mark IV interferometer [*Toon*, 1991]. Profile shown in figure 7.10 on page 123.

991215, Flight with SKERRIES, operation appears nominal. Profile shown in figure 7.11 on page 123.

000128, Flight with SAOZ. The flight was performed one day after two flights on the 27th of January carrying the DIRAC and Bonbon tracer instruments, both measuring CFC-11. These flights gives a good opportunity for a comparison between the instruments, this is done by *Robinson et al.* [2005] showing similar results within uncertainty. Profile shown in figure 7.12 on page 124.

000209, Flight with SAOZ. Flight profile nominal. Profile shown in figure 7.13 on page 124.

000213, Flight with SAOZ. Battery shortcircuit before takeoff, no measurements at all.

000301, Flight with HALOZ. Profile shown in figure 7.14 on page 125.

000305, Flight with OMS in-situ including LACE and DIRAC in-situ trace gas instruments. The flight was performed with DESCARTES version II, and box IV, that was not previously used or analyzed by the Kiruna DESCARTES team. Heating problems in the analysis makes the analysis more uncertain than others. Some samples are removed from the profile presented in figure 7.15 on page 125 due to bad desorption.

000307, Flight with SAOZ. This flight was done under similar conditions to the flight 000305. Instrument performance nominal. As this profile is more reliable than the one 000305 (that experienced some heating problems) it is better to compare to the profiles of LACE and DIRAC of the 000305 flight. This has been done by *Robinson et al.* [2005] and shows good agreement between all three instruments. Profile shown in figure 7.16 on page 126.

000403, Flight with SAOZ from Andøya. DESCARTES II was used for this flight, together with box IV. Profile shown in figure 7.17 on page 126.

000404, Flight with HALOZ. Very slow ascent for this flight. This was not known in advance and the parameters in the flight software were not adjusted for this resulting in larger than usual samples at similar heights. Leakage found in box during analysis of first sample, (see note on page 141) this may have influenced the sampling but no extra uncertainty added to profile shown in figure 7.18 on page 127.

000515, Flight in the SAMMOA campaign. Double flight with two DESCARTES instruments. There was a long wait for recovery of this flight and the DESCARTES II instrument ran out of batteries before recovery. As the instrument stores most flight data in computer memory only, there is only a limited backup storage data file available. The most important parameter missing is the zero reading from the flow meters, this means no zero reading correction is performed and the flow reading uncertainty may be underestimated. Profile shown in figure 5.8 on page 101.

000616, Flight in the SAMMOA campaign. Due to a technical problem none of the switches were functioning during this flight. The profile is reconstructed from the times each trap was open and the pump running. These times could be fully calculated from times given in the source code for the flight software. The flow is reconstucted by interpolation of the flows measured during the normal time. The samples are extremly large and the indirect calibration method described in section 3.4 is used for the analysis, as such large sample sizes are not covered by the direct absolute calibration method described in section 3.3. The

profile presented in figure 7.19 on page 127 has uncertainties estimated according to the normal algorithm. Obviously, from the very strange profile, this kind of rescue of the data from such a malfunctioning instrument does not work very well. No extra uncerainty has been inferred due to the fact that the flow during the sampling is estimated from a flow measurement made during only a part of the sampling time. Also, errors are probably caused by mixing of the samples as the purging of the instrument has not worked nominally, which has not been accounted for. Last but not least, this is the only profile for which the indirect calibrations have been used. As seen in section 3.5 this gives an absolute response difference of about 12%.

000814, Flight in the SAMMOA campaign. Double flight with two DESCARTES instruments. Both instruments operated nominally, two samples showed desorption problem during analysis of box I. These are removed from the profiles shown in figure 7.20 on page 128. The parameters of the sample software were chosen to give a better than usual height resolution of the tropopause region with DESCARTES III.2.

000922, Flight in the SKERRIES campaign. Instrument performance appears nominal. Profile shown in figure 7.21 on page 128.

001117, Flight in the SKERRIES campaign. Double flight with two DESCARTES instruments. Zero readouts from the flow meters are missing for DESCARTES III.2 from this flight. This means no zero reading correction is performed and the flow reading uncertainty may be underestimated. Due to a malfunction in the sampling proceedure the same trap was opened twice and contains two samples. This is the eighth sample of DESCARTES III.2 plotted in green in figure 5.9 on page 102 which is plotted at a weighted mean height between the samples according to their sample sizes. The mixing ratio in this sample is calculated using the sum of the sampled airmasses.

001211, Flight in the SKERRIES campaign. Instrument performance appears nominal. Profile shown in figure 7.22 on page 129.

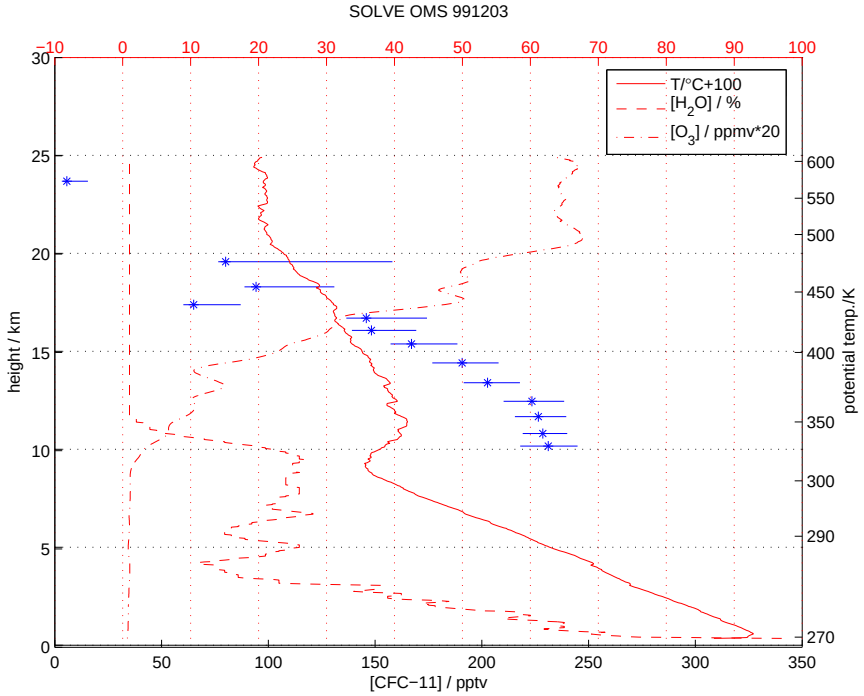

Figure 7.10: Flight profile from flight 991203. Comparison parameters measured by accompanying radio sonde and ozone sonde.

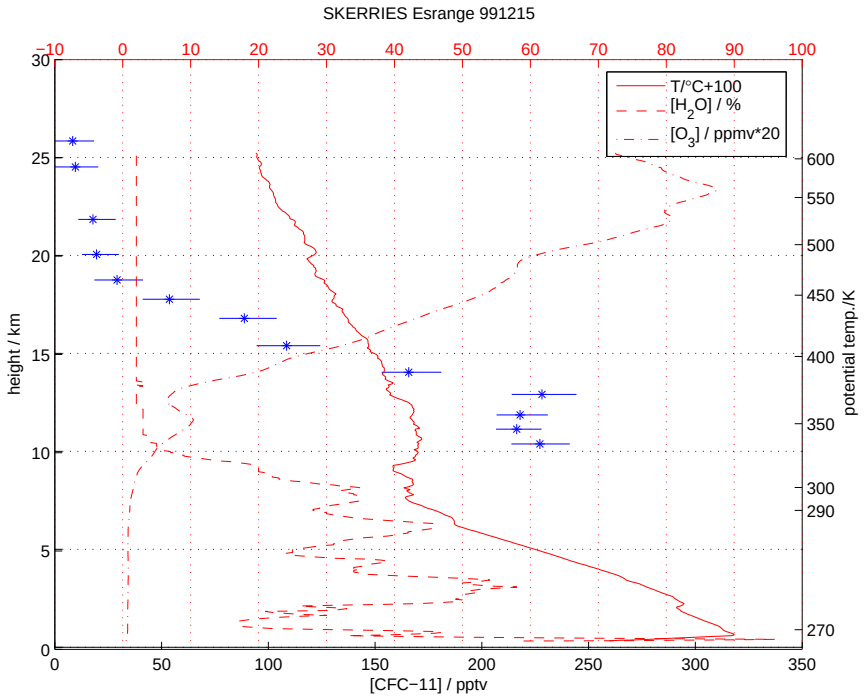

Figure 7.11: Flight profile from flight 991215.

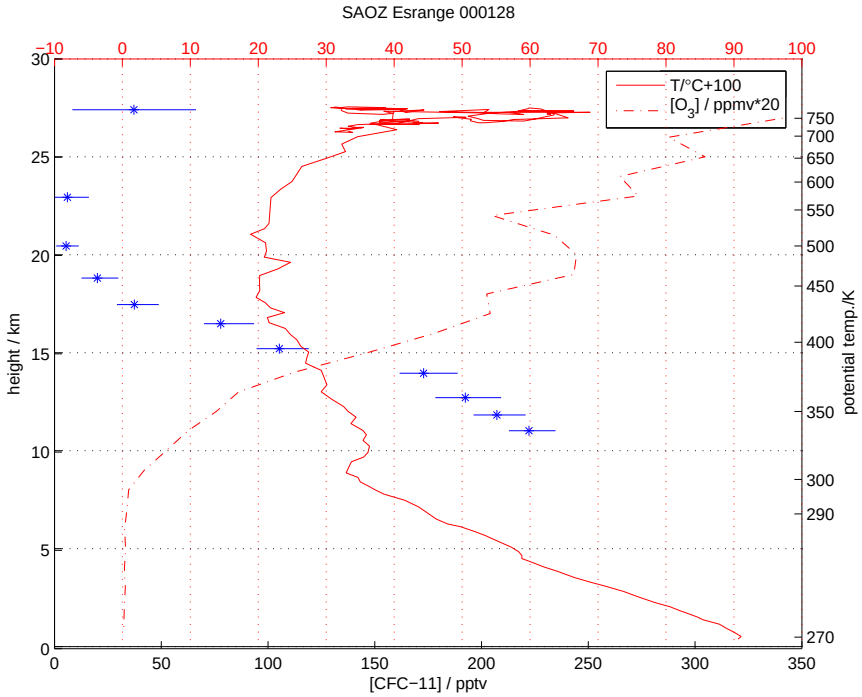

Figure 7.12: Flight profile from flight 000128. Pressure and temperature measurements from radio sonde and ozone from SAOZ.

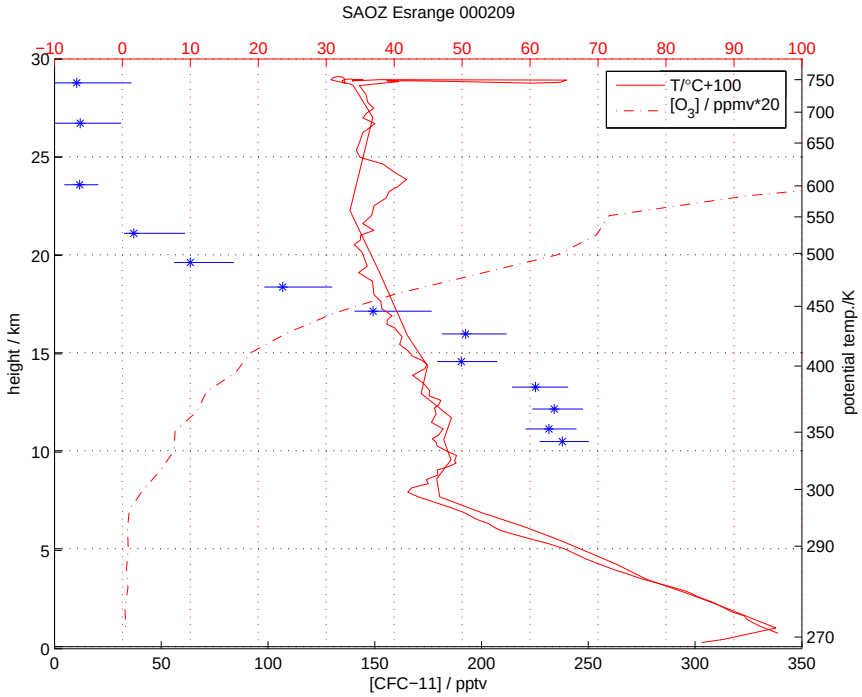

Figure 7.13: Flight profile from flight 000209. Pressure and temperature measurements from radio sonde and ozone from SAOZ.

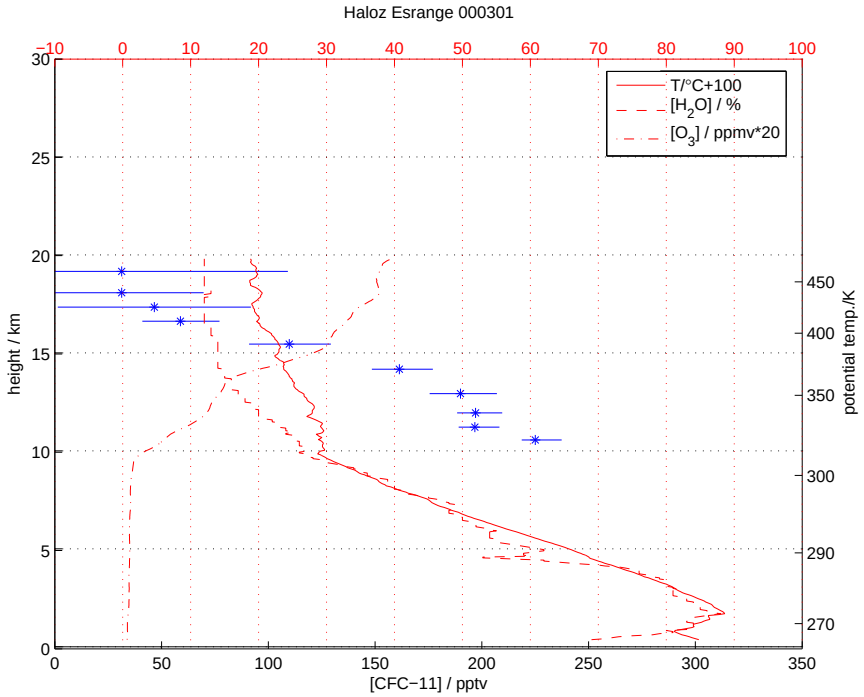

Figure 7.14: Flight profile from flight 000301.

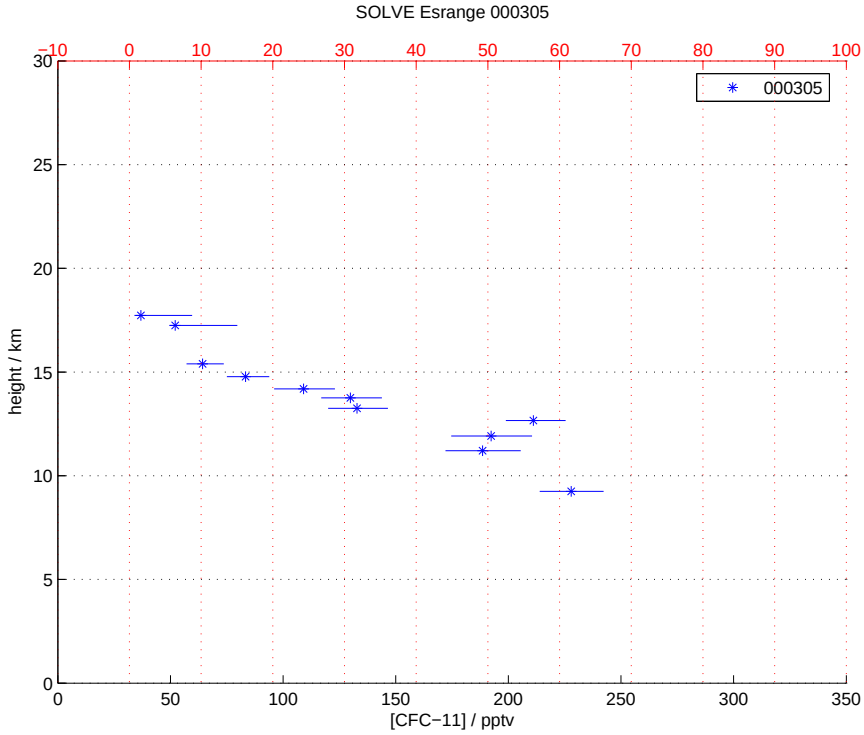

Figure 7.15: Flight profile from flight 000305.

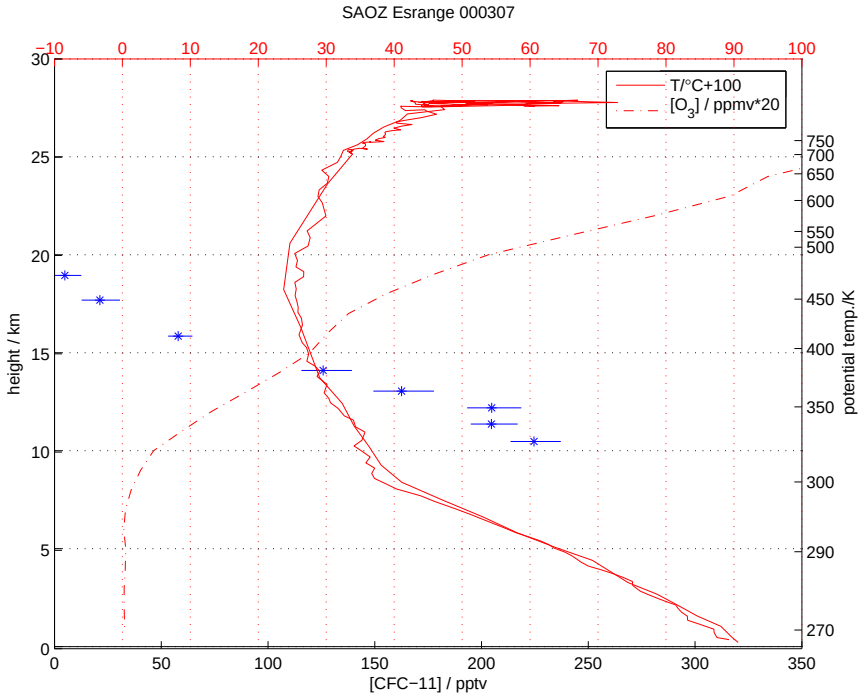

Figure 7.16: Flight profile from flight 000307. Pressure and temperature measurements from radio sonde and ozone from SAOZ.

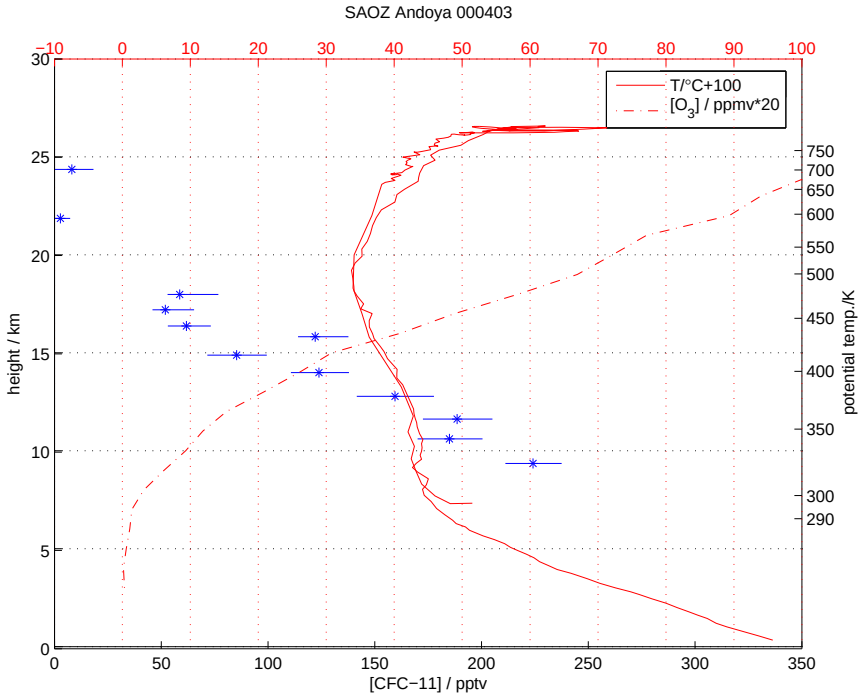

Figure 7.17: Flight profile from flight 000403. Pressure and temperature measurements from radio sonde and ozone from SAOZ.

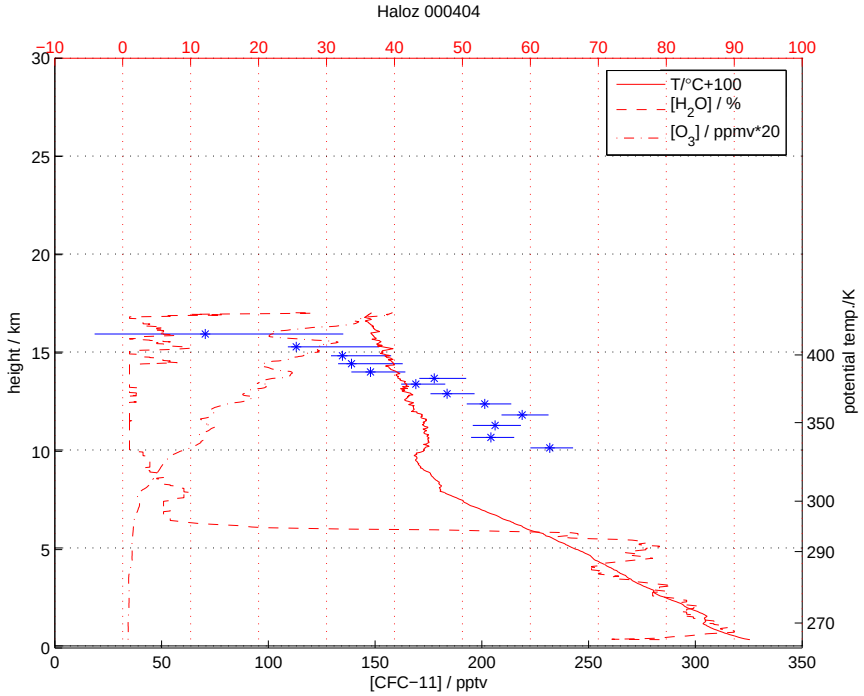

Figure 7.18: Flight profile from flight 000404.

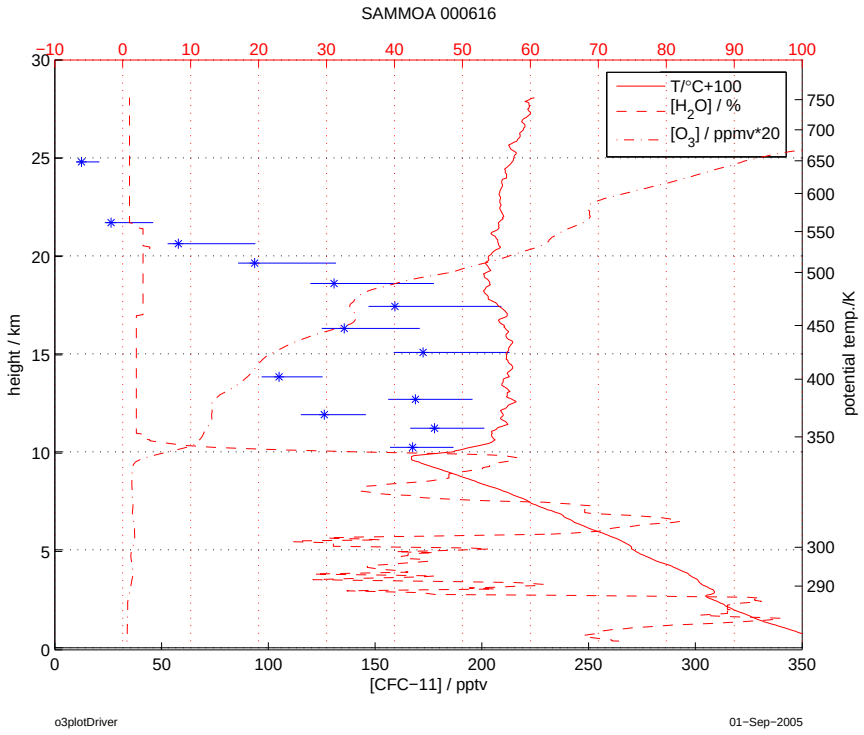

Figure 7.19: Flight profiles from flight 000616. Instrument flew with malfunctioning switches. Uncertainty probably underestimated, see text for details.

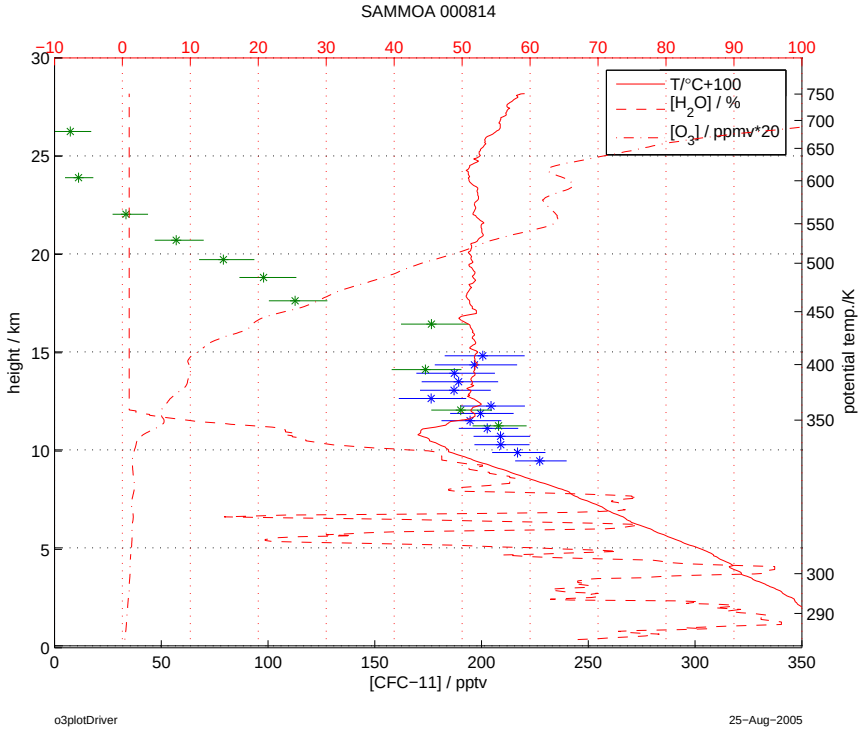

Figure 7.20: Flight profile from flight 000814. DESCARTES III.2 in blue and DESCARTES II in green.

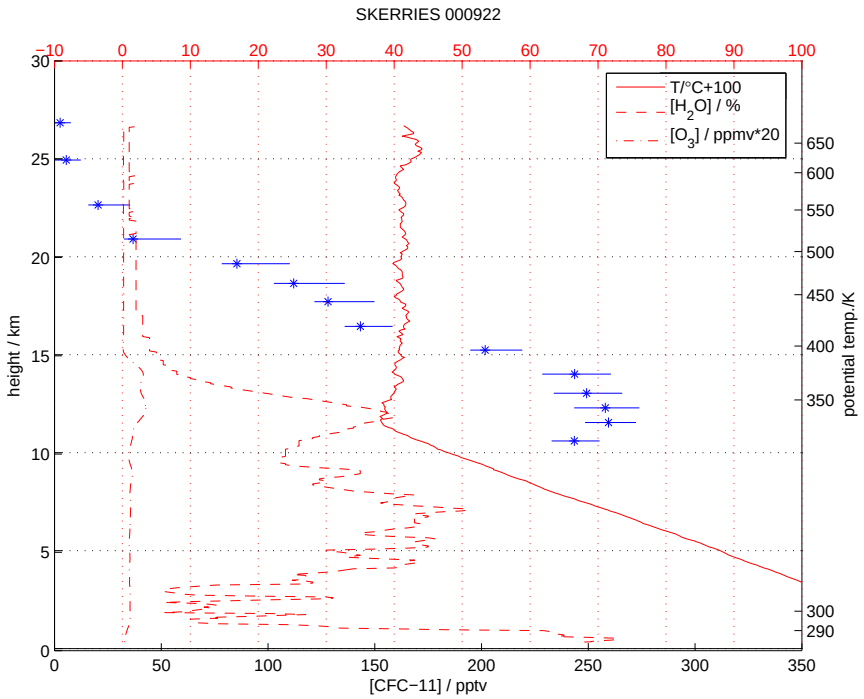

Figure 7.21: Flight profile from flight 000922.

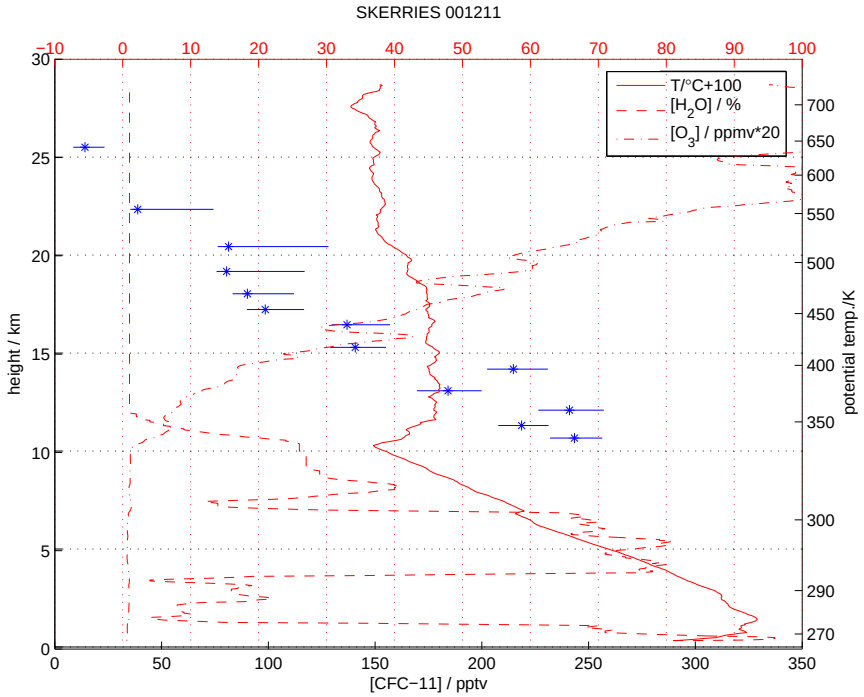

Figure 7.22: Flight profile from flight 001211.

7.4 Published data

This is a list of the publications that have made use of tracer data measured by the Kiruna DESCARTES team. The complete bibliography is found in the end of the thesis.

Arvelius, J., H. Nilsson, S. Kirkwood, F. Danis, N. R. P. Harris, and J. A. Pyle, CFC measurements with DESCARTES during the THESEO campaign in Kiruna spring 1999 — early results, in *Proceedings 14th ESA Symposium on Rocket and Balloon Programmes and Related Research*, edited by B. Kaldeich-Schürmann, no. 437 in SP, pp. 353–358, Eurpoean Space Agency, ESA Publications Division, 1999.

Arvelius, J., H. Nilsson, S. Kirkwood, F. Danis, N. R. Harris, and J. A. Pyle, CFC measurements with DESCARTES during the THESEO campaign in Kiruna spring 1999, in *Harris et al.* [2000a], pp. 459–462.

Arvelius, J., H. Nilsson, S. Kirkwood, A. Robinson, N. Harris, J. Pyle, O. Morgenstern, F. Goutail, and J.-P. Pommereau, Measured tracer profiles from the polar stratosphere covering all seasons 2000, in *Proceedings of the Sixth European workshop on stratospheric ozone*, edited by N. R. P. Harris, G. T. Amanatidis, and J. G. Levine, no. 79 in Air Pollution Research Report, pp. 217–220, European Commission, 2002.

Danis, F., K. Persson, H. Nilsson, A. D. Robinson, M. P. Chipperfield, J. D. McIntyre, P. G. Simmonds, N. R. P. Harris, and J. A. Pyle, Tracer mea-

surements with DESCARTES during ILAS in early 1997, in *Polar stratospheric ozone 1997, Proceedings of the fourth European symposium 22 to 26 September 1997, Schliersee, Bavaria, Germany*, edited by N. R. P. Harris, I. Kilbane-Dawe, and G. T. Amanatidis, no. 66 in Air Pollution Research Report, pp. 423–426, European Commission, 1998.

Danis, F., N. R. P. Harris, W. H. Taylor, J. D. McIntyre, P. G. Simmonds, and J. A. Pyle, DESCARTES: A novel lightweight balloon-borne instrument for measurement of Halocarbons, *Review of Scientific Instruments*, *71*, 271–280, 2000.

Müller, R., S. Tilmes, J.-U. Groß, D. S. McKenna, M. Müller, U. Schmidt, G. C. Toon, R. A. Stachnik, J. J. Margitan, J. W. Elkins, J. Arvelius, and J. M. Russel III, Chlorine activation and chemical ozone loss deduced from HALOE and balloon measurments in the arctic during the winter of 1999–2000, *J. Geophys. Res.*, *108*, 2002, DOI:10.1029/2001JD001423.

Nilsson, H., K. Persson, F. Danis, N. R. P. Harris, and J. A. Pyle, CFC measurements with DESCARTES during the ILAS validation campaign early results, in *Proceedings 13th ESA Symposium on Rocket and Balloon Programmes and Related Research*, 1997.

Robinson, A. D., G. A. Millard, F. Danis, M. Guirlet, N. R. P. Harris, A. M. Lee, J. D. McIntyre, J. A. Pyle, J. Arvelius, S. Dagnesjo, S. Kirkwood, H. Nilsson, D. W. Toohey, T. Deshler, F. Goutail, J.-P. Pommereau, J. W. Elkins, F. Moore, E. Ray, U. Schmidt, A. Engel, and M. Müller, Ozone loss derived from balloon-borne tracer measurements in the 1999/2000 arctic winter, *Atmos. Chem. Phys.*, *5*, 1423–1436, 2005, sRef-ID: 1680-7324/acp/2005-5-1423.

Appendix A

Practical treatment of DESCARTES

The analysis equipment basically consistsof four pieces that, with some peripherals, should work together. These are a computer with installed software Chemstation, one electronics box for the heating system called "heater box", one GC and DESCARTES sample boxes.

A.1 Sample box

The sample box is the core part of the instrument. It contains mainly a 16 position Valco valve to switch the gasflow to 16 carboxen traps. Gas flow can go through the box either through a sample trap or a bypass line. There are two electrical switches to change this flow. The 16 position valve is changed in position by nitrogen pressure and there are two electrical switches for nitrogen pressure to step the valve forward and to reset the valve to be ready for another step. These two switches can be activated from the `pc_man` program commands `S` and `R` when mounted to DESCARTES and from the switches on the front of the heater box when mounted to that. Box IV has the switches mounted the other way and will perform the opposite actions.

A task of special concern is to determine the position of the 16 position switch. For this purpose an electrical system is incorporated in the sample box. This is a very simple design with a series of resistors connecting 16 points to which a switch following the movement of the valve is connected. The resistance of this circuit is read out by DESCARTES and written to the log during flight and can be seen by the `pc_man` program command `V`, but is not connected to the analysis system i. e. the position must be determined by visual inspection. The trap heater switch can be seen at the end of axis through the valve on the opposite side from the traps (to the right in figure 2.2 on page 8). The positions can be determined by looking at the series of resistors, as the red cord with a resistor is connected to the point matching trap 16. Figure A.1 show what this looks like when the trap is in position 11. The trap heater switch is in contact with a point five positions after position 16 where the read cord is connected. The position of the valve at delivery for flight is not used for sampling but for performance tests during analysis. It is called the waiting position.

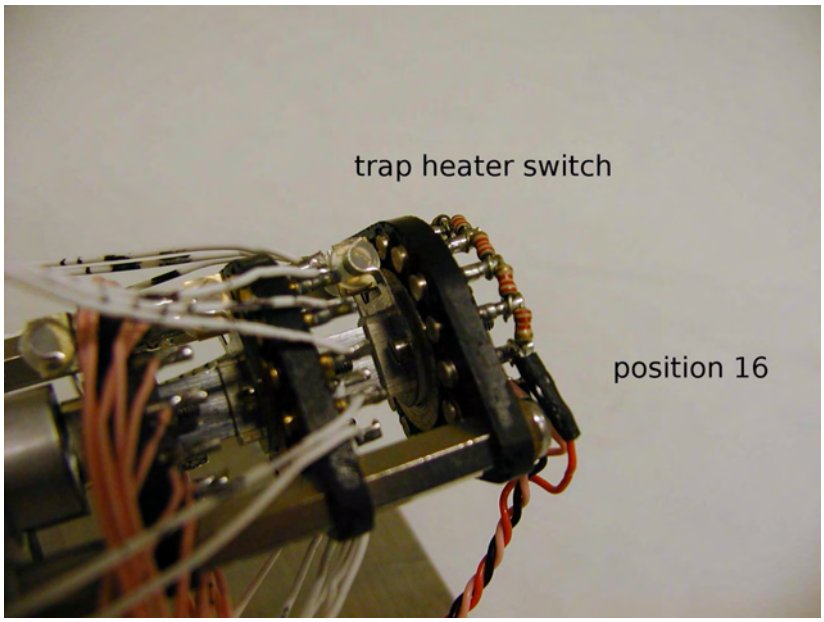

Figure A.1: Trap heater switch, when valco valve is in trap position 11.

A.2 Analysis software

The software used on the desk top computer for the analysis is HP GC Chemstation Rev. A.04.02. For questions concerning the handling of this software in general the reader is referred to the manual [Hewlett-Packard, 1995a]. To run the DESCARTES analysis with the program some macro files, method files and sequence files are needed. The macros are installed on the desktop computer connected to the GC in the directory `c:\hpchem\core`,* the sequences in `c:\hpchem\1\sequence\ucam` and the methods in `c:\hpchem\1\methods\ucam`*box*, where *box* is the number of the current sample box (1, 2 or 4).

In this context, "macro" is a low-level file used to send commands to external parts, mainly the heater box. "Methods" are files that keep all parameters for one action of the GC. These can be run individually from the Chemstation software. One method typically gives one file of data output. "Sequences" are files basically running a list of methods and ordering the output files in an own directory.

The methods for heating traps differ in the numbers sent to the heater box. There is one method for each trap of the heating types due to this and it is important to make sure to load methods from the right directory.† Explanations of the methods and sequences are given in tables A.1 and A.2.

*In this section the following typograpic conventions are used: Filenames, paths and commandline in- and out-put are set in `typewriter font`. Multichoice parts of these are set in *italic* text, the italic part should most often be exchanged to a number and is hopfully self explained. Menu names and items, checkboxes, fields and similar in the windows environment are set in *slanted* text.

†It has actually been found important also to load a method that will be present the next time the program will start, before quitting. If a method from a removable media is loaded when the program is shut down it will just hang on startup with a strange error message if the searchpath is not present. The solution is to edit the path in `win.ini` by hand.

Method	Description
`air96.m`	Used to fill trap with ambient air and change to next trap. External pump used.
`baseline.m`	Only saving of baseline to file.
`chtrap.m`	Step the 16 port valve in the sample box to the next position.
`cleant`*trap*`.m`	Heating of trap with a temperature parameter setting 50 lower than for `trap`*trap*`.m` but for 5 minutes, for cleaning purpose. This method does not wait for all species to pass the column and does not give a valuable chromatogram.
`endspl.m`	In sampling sequences when back in waiting position to pass the standard in the dead volume before trap to compensate for the nitrogen in this volume in the beginning of sample.
`newbypas.m`	Purging standard through bypass loop for 2 min, switch valve 1 and analyse. Response check not dependent on adsorbtion/desorbtion see section 3.4.2 page 30.
`newshutd.m`	Reduce flows and temperatures in GC to standby levels. The normal state of the GC when not in use.
`purge.m`	Purge system with standard 2 min used before standard sampling.
`sampl`*time*`.m`	Pass a sample of standard for *time* s through the trap and change to next trap position.
`schtrap.m`	Change trap with standard flushing trough bypass.
`stand`*time*`.m`	Filling methods with uneven times to match the estimated ratio of CFC-11 concentrations between syntetic and air standards. For sampling absolute calibration air standard corresponding to sizes of `sampl`*time*`.m`.
`start.m`	Reminder to set printer before heating.
`trap`*trap*`.m`	The normal heating and analysis method. Heats the trap for 30 s by specified temp parameter. This also takes up the chromatogram of the analysis.[a]
`wait.m`	Waiting for 60 min with the same parameter settings as `trap`*trap*`.m`, used in `analys7w.s` for the baseline to stabilize

[a]Described furter in section2.3.

Table A.1: Explanations of Chemstation methods for use with DESCARTES

Sequence	Description
`air16-96.s`	Fills all traps with method `air96.m`
`analys`*wp*`.s`	The normal analysis sequence to analyze all traps in one sample box with `trap`*trap*`.m`. Calibration samples with standard are taken and analyzed in waiting position first and last.
`analys7w.s`	Similar to `analys7.s` but includes waiting at the start for baseline to stabilize
`anp7stnd.s`	For all traps: analyse, fill with `sampl1.s` and analyse again.
`cleanp`*wp*`.s`	Cleaning of all traps with `cleant`*trap*`.m` and validating with `trap`*trap*`.m` to see that no remnants are left in trap.
`clp7we.s`	Really hard cleaning, runs `cleant`*trap*`.m` 19 times for each trap and analyses.
`fcleanp`*wp*`.s`	Cleaning of all traps with `cleant`*trap*`.m`.
`newpos`*wp*`.s`	Older analysis sequense, as `analys`*wp*`.s` but includes `newbypas.m` after each trap.
`s1by16.s`	Fills all traps with `sampl16.m`
`s1of2.s`	Fills every second trap with `sampl216.m` and steps trough every second with `schtrap.m`.
`s2by16.s`	Fills all traps with `sampl96.m`
`s2by8.s`	Fills the first 8 traps with `sampl16.m` and steps through the rest.
`s3by16.s`	Fills all traps with `sampl48.m`
`sampl`*time*`.s`	Fills all traps with `sampl`*time*`.m` for linearity or absolute calibration.
`stand32.s`	Try to match the same sample sizes with synthetic standard sampled with air standard and `sampl32.s`. Using specially written `stand`*time*`.m` with uneven times to match the estimated ratio of CFC-11 concentrations.

Table A.2: Descriptions of Chemstation sequences to use for DESCARTES analysis.

The heating of the traps is managed by the heater box. This takes two input parameters from the computer, the time and the temperature setting. The communication is handled by the macro "heater" and a RS232 connection between "Serial A" on the back of the computer and the port marked "RS232 to Chemstation" on the back of the heater box. To be able to send signals to the heater box, the macro "heater" must be loaded and the printer be set to *Generic / text only on COM 1:*[‡]. Due to the fact that temperatures differ between the traps, there is one analysis method as well as one cleaning method file for each trap. These temperature settings is stored in the respective method files and can be changed through the Chemstation software. The menu *Methods – Run Time Checklist...* will give a dialog box where the field *Pre-Run Command / Macro* should be marked and the command `temptime` *temp*`,`*time* inserted. Here *temp* is a number sent to the heater control box, typically in the range 1800–2100. The final values used for this parameter for the different traps in the different boxes are given in table A.3. *time* is the time in seconds to heat the trap, 30 s has been used for analyses. The macro command `temptime` can also be run manually: just enter the command `temptime` *temp*`,`*time* on the command line at the bottom of the program window. Manual heating can then be initiated by pushing the heater knob on the heater box (see section A.3).

Trap	box I	box II	box IV
1	1925	2125	1925
2	1825	2100	1900
3	1850	2000	2000
4	1850	2025	1925
5	1950	2050	1925
6	1850	1925	1950
7	1975	1950	1900
8	1900	2025	1925
9	1925	1925	1850
10	1925	2000	1825
11	1800	1975	1825
12	1950	2000	1900
13	1825	1900	1900
14	1850	2075	1825
15	1975	1950	1850
16	1875	2100	1975

Table A.3: Temperature parameters for heating methods.

Analysis data is stored in a file structure containing small files divided into very many folders in multiple layers. This gives practical problems for backup of the hard disc and storage of data to compact discs. This has been solved by compressing the folders from top level of analysis to files. These files have been moved to partition `E:` on the second hard disc that has been in the backup system.

[‡]To add the printer, if not present on system, do the following: In the printer folder choose *add printer*, in the manufacturers list, choose *Generic / Text only* then choose the port *COM 1*

The storage of data to compact discs has also been made in the compressed format.

A.2.1 Quick start

To run the analysis of a DESCARTES sample box the following steps should be followed on the computer. There are several more steps to control hardware, see section B.6.

1. Make sure the GC is on and connected to the computer.
2. Start up the program "HPGC 6890 Online".
3. Load the heater macro by typing `macro heater.mac` by the command line.
4. Set printer to serial to get signal to heater box by pulling *File – Printer Setup...* from the menu and choose *Specific Printer: Generic / Text Only on COM1*
5. Load a `trap`*trap*`.m` method by pulling *Method – Load Method...* from the menu to get the right temperatures to stabilize in the GC. *Make sure to load a method for the right box (the box name is in the search path) as this will be the path used for all methods loaded in the sequence.*
6. Load an `analys`*position*`.s` (or `analys7w.s`) sequence for the right waiting position by pulling the *Sequence – Load Sequence* menu.
7. Create a new directory to store the data files by pulling *Sequence – Sequence Parameters* in the menu, set your name in the *Operator Name:* field[§], check the *Prefix/Counter* and write the directory name in *Subdirectory:* field. The name convention used has been `ABYYMMDD` where `A` is the type of samples analyzed F – flight, T – test sampling with DESCARTES, B – box filled directly trough GC (and C for cleaning sequences), `B` is the box number and `YYMMDD` date in normal year-month-day form.
8. Make sure the sample box is connected properly.
9. Start the sequence by pulling *RunControl – Run Sequence* in the menu.

A.3 Heater box

The heating of the traps is managed by the heater box. The signal for stepping of the Valco valve in the sample box is also going throug the box with possibilities for manual treatment.

The box is connected to the computer according to section A.2, to the sample box and to the GC. The sample box is connected by the black and red connection on the front of the heater box to the 2 pole Lemo and the connection marked

[§]This kind of silly thing no one ever cares about has actually been used by the Kiruna DESCARTES team during the project and is the way to figure out who was operating the instrument.

"VALCO Box" to the 19 pole Lemo connection on the sample box. The GC is connected via RS232 to the connection on the heater box marked "GC HP 6890" and the connection on the GC marked "EXT". A direct connection coming out under the lid of the heater box and in through the shell of the GC connected to a connector marked "3" (see figure A.2) in the GC shall also be apparent. Originally there was only one connection to the GC. The direct connection to valve 3 is made due to a malfunction of valve 7 in the GC, see sec A.5. A temperature sensitive diode in the circuit of the heater box is placed in the oven (see sec A.5 on page 139). This has no electrical connection to the GC.

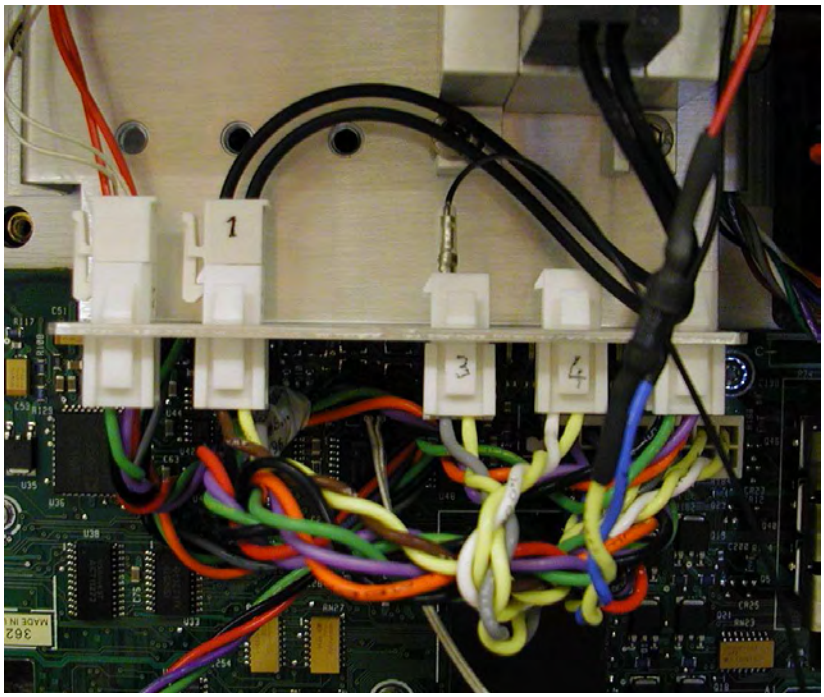

Figure A.2: Connection to valve 3 in the GC

The switching of the Valco valve to change trap position uses simple relays to switch the valves in the sample box by signals from the GC. There are also two manual switches to do the same thing on the front panel of the heater box marked "Reset Valco" and "Step Valco". Between each step the reset must be activated¶.

The heating of the traps is based on a basic stamp. The stamp waits for a paricular sequence containing two numbers from the desk top computer via RS232. This sequence is sent by the macro `heater.mac`. Directly when received, these numbers are shown at the LCD display. Then it waits for a signal from the GC to start the heating. This signal can also be given manually by pressing the black knob marked "Heat" on the front panel of the heater box.

The heater box needs 12 V DC power supply. This was originally performed by a lead battery, later changed to a switching power supply. The power supply needs to be able to give about 4 ampere.

¶Sample box IV has step and reset reversed

A.4 Gas chromatograph

Input to the system are one N_2 carrier gas[‖], two calibration standards and the DESCARTES sample box. Electrically it is connected to the heater box and the desk top computer.

The carrier gas is split in two flows, one is fed directly to the ECD through a plastic tube, the other is cleaned first from oxygen and then from organic constituents by a Hewlett-Packard 5060-9096 activated charcoal trap. Earlier there has also been a Nafion drier after the charcoal trap, see sec A.5. The cleaned gas is divided into flows regulated by the GC to flush the columns, box and detector and one flow regulated by a separate regulator for purging the sample box between test samples. Flows to the pre and main columns as well as the sample box, dependent on the position of valve 1 are regulated by the GC valves AUX 3 and AUX 5. Makeup flow for the detector is connected to the input marked so. The flow for purging the sample box between test samples should be set to match the sampling flow from the standard.

There are input for two standards for test sampling regulated by the GC on the back of the GC. These are switched manually. After the manual switch, the flow goes to a regulator to match this flow to the carrier gas flow and is then connected to the automatic switch that distinguishes these flows and is passed to the GC input AUX 4. As the standards contain CFCs, there are potential adsorption problems in the equipment. To minimize these problems connections involving the standard samples are in stainless steel as far as possible. The exception is the regulator for the synthetic standard in brass. The nitrogen is free from CFCs and these couplings are mainly in copper and brass.

Under the top of the GC is a ten port valve, valve 1. This valve connects the regulated flows from the inputs to the GC with the sample box and the columns.

Apart from AC power there are three electrical connections to the GC, two to the heater box (see section A.3) and HP-IB connection to the desk top computer. The GC is normally handled by the computer trough the Chemstation software but for some, (especially monitoring) reasons it might be useful to do this through the interface on the front side. See the manual [Hewlett-Packard, 1995b] for details.

A.5 Updates on instrument

960619 Agreement of collaboration between University of Cambridge and IRF for DESCARTES project signed.

970108 Installation of GC system with computer at Esrange.

971212 Flow controller Aera FC-2600 0–60 SCCM flow calibrated in factory before delivery.

981014–981110 Intense period of tests to get temperature signals for all traps in box I and II.

[‖]Changed between the purity grades Plus, 5.0, 5.5 and detector OTC-50, all supplied by AGA.

981111 Nitrogen carrier gas exchanged from grade Plus to 5.0.

981112 Measured the resistances of the switch position reading on box I and II. Changed voltage limits in `PC_man` and `GCAT`.

981214–981217 Johan with box II in Cambridge. Changed Valco valve, leak tested box.

990116–990120 François Danis in Kiruna. Change in the heating system. The temperature sensitive diodes controlling heater current, one for each trap mounted in the sample box next to the transistors exchanged for one single diode mounted in the heater box. This new diode will not be heated by the transistors during heating and thereby the controll of the heating is improved. See further change 991117.

990210 Changed temperatures box II.

990223 Flow meter calibration.

990311 Changed temperatures box II.

990326 Changed temperatures box I.

990420 Re-calibration of our Aera FC-2600 flow controller performed in range 0–60 SCCM with N_2 for air. Performed at factory.

990422 Calibration of a new Aera FC-2600 flow controller performed in range 0–200 SCCM with N_2 for air.

990817 Found an error in the flight software. The loop integrating the flow in the software sums up averages of flow meter reading from each time the loop is executed and ends by dividing this with the number of loopings. This divisor has had a value of 1 too high. This means that for all previous flights the number of loops n must be estimated and flow multiplied by $n/(n+1)$. Luckily the number of loops i easily estimated by $n = (t - 387 \text{ cs})/364 \text{ cs} - 1$, where t is the sampling time written in the flight log file, as the loop has a well defined length. The error in the code was corrected.

991012–991015 DESCARTES III.2 and one box in Cambridge with Saga. One flow meter found to be leaking. Flow meters calibrated up to 1000 SCCM by a Tylan FC-2900 flow controller. The leaking flow meter exchanged and the new one also calibrated.

991018 Tests to exclude ramp function.

991108 GC valve 7 broke down. Valve 7 is the switching valve in the sample box for choosing between gasflow through bypass or trap. The signal from valve 7 was going to the RS232 connection to the heater box and from there to the sample box. This signal causes malfunction in the GC and a new valve had to be connected. Valve 3 was not connected to the RS232 interface but had to be directly connected to the heater box. The valve signal is in a contact marked “3” under the panel on the right of the GC,

as shown in figure A.2 on page 137. The left pin of this directly connected to RS232 pin 3 in the output from the heater box. Methods *trap*trap.m changed to use valve 3 instead of valve 7.

991109 Dilution of new synthetic standard. A high concentration synthetic standard was diluted with nitrogen 5.0. The cylinder was evacuated and flushed with nitrogen, filled with standard to 80 psi ($\approx$ 5.5 bar) through a fitting with a regulator purged by a controlled leakage at the end point. The bottle was then filled up to 56 bar with nitrogen the same way, with a steady flow to avoid contamination of the N_2 cylinder.

991112 Desorption problems in analysis of flight 991109.

991117 The temperature sensitive diode earlier moved to the heater box seems more temperature dependent than expected and is moved inside the oven of the GC that is temperature regulated. Changes of the oven temperature in the methods for the previous `UCAM2` saved in `D:\old methods`. A stable temperature of 40 °C without ramping is now used for all methods. All methods resolved for this new temperature. Longer retention times forced enlongation of the methods to 24 min.

991120 Changed temperatures box II.

000119 Box I converted to new heating system and got gold plated circlips for the trap heating at the same time. Previous methods for box I saved to `D:/oldmethods`, new methods by copying methods for box II and changing temperature.

000119 Adjusted N_2 flow on board DESCARTES. Initial flow (N_2 on) was 15 SCCM after adjustment 90 SCCM.

000119–000126 Intense period of finding new temp settings for box I

000201 Power break during flight analysis.

000202 Changed N_2 cylinder.

000203 Leak test box I.

000203 Changed temperature box I.

000204 Box IV appears first time in Kiruna.

000207 Finding temp for box IV.

000207 Leak test box II.

000209 Box IV makes strange noises during heating. A ground cable in heater box re-soldered over a 1 Ω resistor. The noise comes from not completely fastened connectors.

000222 Changed temperature box IV.

000409 Analysis of flight, box II stopped due to longer retention time (7.5 instead of 7 min for CFC-11). Found significant leak on out connection to the Valco valve. The nut was impossible to turn in that position so the leakage was tightened using Araldit epoxy. Tested to be reasonably tight. Analysis continued.

000418 Changed N_2 cylinder.

000520 Changed the circuits in DESCARTES III.2 malfunctioning after flight.

000622 Problems with analysis of box IV in Cambridge. Development of a new trap heating system was going on with their analysis system. Not all changes was removed before analysis so there was in fact no control of the trap heating and the flow was going in reverse direction (same as during sampling).

000713 Technical mistake in Cambridge in practice short circuited a lead battery over trap 7 in box IV. The trap melted.

000717 Found that switches had no voltage from the new circuit board installed 000520. Since then the switches in DESCARTES III.2 has not worked and the traps has been filled even during the pressurization process. Problem solved.

0010 Moved GC from radio lab to atmospheric lab. Set up system and changed the N_2 cylinder at the same time.

001115 Changed temperatures for box II.

0012–0101 Changed tubing for all standard sampling from copper and brass to stainless steel.

010115 New dried air absolute calibration standard from NOAA delivered.

010129 Changed N_2 cylinder to grade "detektor, OTC-50".

010206 Leak tested N_2 circuit with He. Found major leaks by Nafion drier. Checked flow trough Nafion drier and found out that the drying gas flow was not detectable and that there can not be any drying effect of the drier. The Nafion drier was permanently removed.

010214 First linearity test performed by running a special `gcat.exe` in DESCARTES taking standard samples from 1 to 50 SCC.

Appendix B

Detailed flight instructions

This section is the recipe for a successful DESCARTES flight. It is step by step following the flight checklist in appendix D that is meant to be a help enough for people who have made DESCARTES flights earlier and at the same time be a log to save for the flight.

B.1 Before leaving

- Well in advance for the flight make a cleaning of the box to be used by running `cleanp`*wp*`.s`. Look through the chromatograms from the analysis methods ran in the sequence, `analys`*trap*`.m`, to see that box is clean and make a note of where the data is stored for later use.
- Compile the flight software `gcat.exe`. Change sample sizes and heights in `fr_prms.h` and save a copy for later reference.
- Backup `gcat.exe` on a floppy disc.
- Load batteries. There are batteries with and without fuses. Load one of each kind, with fuse for computer and without for the pump plus one spare of each.

B.2 Bring to flight

- Descartes complete (with sample box), in the polystyrene box with the slings.
- Batteries and spare batteries. With and without fuse on each.
- Inlet tube (a bent tube of the same dimension as the tube to the pump) with connection piece (a piece of rubber tube to connect it).
- Silver tape
- Laptop with the newly compiled `gcat.exe` and kermit to communicate with the GCAT computer.
- RS232 cable

- Dummy RS232 plug (an 9 pole D-sub connector that connects some pins, for the GCAT to be able to run the program).
- Multimeter with fresh batteries
- Long phillips screwdriver to fix the sample box.
- Screwdriver to mount the outside box.
- Nitrogen cylinder.
- Regulator for the nitrogen cylinder.
- Copper tube to connect the nitrogen cylinder to DESCARTES.
- Vacuum pump to evacuate the connection.
- Fixed spanners for mounting the sample box.
- Adjustable spanners to cover all sizes of nuts used in DESCARTES.
- Power supply for DC 12 V
- Connection cords for batteries, computer and pump.
- GPS
- Backup programs `gcat.exe` `fr_prms.h` and kermit.
- Extension cable.
- Fuses to batteries.
- Screws to batteries.
- Screws to box.
- Snoop.
- Teflon tape.
- If flight mission might be more than over the day bring also battery charger.

B.3 Before flight

- Start up laptop in DOS-mode or a DOS command interpreter and change to the dirctory containing the programs for the gcat on board computer, in this example `C:\home\gcat\`.
- Start kermit

  ```
  C:\home\gcat\> kermit
  ```

- Open connection to serial port

```
MS-Kermit> c
```

- Connect RS232 cable connection between laptop and gcat.
- Start GCAT by powering 12 V from power supply to connection marked "Computer".
- While prompted copy a file for namechange

  ```
  E:\> copy readall.exe atodall.exe
  ```

- Start the monitoring program `pc_man`

  ```
  E:\> pc_man
  ```

- Connect the nitrogen cylinder to DESCARTES with a copper tube. The vaccum pump should be connected to this tube trough a valve.
- Evacuate connection three times: *NB be careful not to release the over pressure security plug on the pump by either letting high pressure to the pump or by stopping the outflow from the outflow tube.*

  1. Start the pump and open the valve on the tube to the pump with valves to regulator and DESCARTES flask shut.
  2. Carefully switch the red three port valve onboard DESCARTES to connect the pump to the on board pressure flask until it is evacuated and shut the valve again.
  3. Make sure the external high pressure nitrogen cylinder is shut and the regulator open. Carefully open the valve to the regulator and evacuate it.
  4. Shut the valve to the pump.
  5. Temporarily open the high pressure cylinder to pressurize connection and shut again.
  6. Evacuate connection again by opening the valve to the pump and shut it again.
  7. Repeat step 5–6.
  8. Stop the pump and open the cylinder.

- Fill the onboard cylinder by switching the onboard valve to connect the external to the onboard N_2flask. The pressure should be 190 psi, read out by the onboard pressure guage with the `pc_man` command `2` (Read pressures), this corresponds to ˜12 bar.
- Connect the sample box. Lemo 19 pole connector, inlet and outlet for sampling and two connections to plastic tubes for stepping and pressurization. The plastic tube from the first small brass regulator should be connected to the stepping i. e. the connection on the box that continues with a plastic tube on the inside while the plastic tube that has gone through two regulator steps should be connected to the other inlet for pressurization to the box.

- Switch the valve to connect onboard cylinder to box.
- Leak-test all connections on the pressurized circuit with snoop.
- Read out waiting position by `pc_man` command `V` and by eye by looking at the electrical 16 position switch in the sample box as described in section A.1.
- Control battery charge, voltage at least 12.5 V.
- Fasten batteries in lid of DESCARTES box.

B.4 Delivery time

- Check cylinder pressure with `pc_man` and calculate the loss-rate. The remaining pressure should be at least 160 psi and the loss rate maximum 5 psi/hour.
- Disconnect nitrogen cylinder.
- Reboot gcat by connecting to battery with fuse.

```
E:\> copy readall.exe atodall.exe
E:\> pc_man
```

- Connect battery without fuse to connector marked "pump".
- Read out pressure once more.
- Exit `pc_man` with the `X` command.
- Transfer the right version of the flight program `gcat.exe`.

```
E:\> runrec
E:\> <alt>-x
MS-Kermit> run compsend
```

answer questions use port 1.

```
filename: gcat.exe
file length in bytes: 50493
```

wait

```
MS-Kermit> c
```

- Start the flight program
  `E:\> gcat`.
  `Enter new date: ????` Enter date in mm-dd-yy form. The program is not 2k compatible and a date in the 21st century must be entered as an earlier date. Present date -20 years has been used.

`Enter new time: ????` Enter date in hh:mm:ss format. Set the time from a source that gives good GPS time.
Normal pressures `External` ≈ 1000, `N2` same as earlier, `N2E_box` ≈ 1000.
Battery power > 12000.

- Disconnect RS232 cable.
- Connect dummy plug.
- Put on the lid on DESCARTES.
- Put DESCARTES in polystyrene box and put on the end of the box. Be careful to protect the inlet for dirt and especially polystyrene from the box by protecting it.
- Connect inlet tube.
- Deliver DECARTES for flight.

B.5 After recovery

- Start up laptop and open connection for serial communication.

```
C:\home\gcat\> kermit
MS-Kermit> c
```

- Connect RS232 cable to laptop and gcat.
- Start GCAT from power supply 12 V

```
E:\> copy readall.exe atodall.exe
E:\> pc_man
```

- Read out onboard cylinder pressure.
- Read out trap position with `pc_man` and observe it manually.
- Exit `pc_man`.
- `E:\> <Alt>-x`
- Compile `readee.exe` with current `fr_prms.h` on the laptop.
- Transfer freshly compiled `readee.exe`

```
MS-Kermit> c
E:\> runrec
E:\> <alt>-x
MS-Kermit> run compsend
```

port 1

```
filename: readee.exe
file length in bytes: 16845
```

wait.

- Readout the raw data in the eeprom to the file `data.dat`

```
MS-Kermit> c
E:\> readee
```

- Transfer `data.dat` to the laptop. If there is an existing file named `data.dat` in the current directory it will be overwritten. The `from_pc` command starts to send the file after ten seconds and the `<Alt>-x` and `run to_term` commands must be given in this time.

```
E:\> from_pc
<alt>-x
MS-Kermit> run to_term
```

wait

- If messages come on the screen during transmission there are trasmission errors, try to redo this step with the computers running on battery to avoid disturbance from the net AC.

- Exit kermit

```
MS-Kermit> exit
C:\dgcat\>
```

- Shut down the onboard computer.

- Store the files `data.dat`, `fr_prms.h` and `gcat.cpp` for the flight for future reference.

- Print out and store hard copies of `data.dat` and `fr_prms.h`.

B.6 Analysis

- Start up the program "HPGC 6890 Online".

- Load the heater macro by typing `macro heater.mac` by the command line.

- Set printer to serial to get signal to heater box by pulling *File – Printer Setup...* from the menu and choose *Specific Printer: Generic / Text Only on COM1*

- Load an arbitary `trap`*trap*`.m` method by pulling *Method – Load Method...* from the menu to get the right temperatures to stabilize in the GC. *Make sure to load a method for the right box (the box number is in the search path, see section A.2) as this will be the path used for all methods loaded in the sequence.*

- Load an `analys`*position*`.s` (or `analys7w.s`) sequence for the right waiting position by pulling the *Sequence – Load Sequence* menu.
- Create a new directory to store the data files by pulling *Sequence – Sequence Parameters* in the menu, set your name in the *Operator Name:* field*, check the *Prefix/Counter* and write the directory name in *Subdirectory:* field. The name convention used has been `ABYYMMDD` where `A` is the type of samples analyzed F – flight, T – test sampling with DESCARTES, B – box filled directly trough GC (and C for cleaning sequences), `B` is the box number and `YYMMDD` date in normal year-month-day form.
- Disconnect the sample box from DESCARTES.
- Connect sample box for analysis. Inlet and outlet flow, nitrogen for stepping, Lemo 19 pole and 2 pole connectors from heater box.
- Check that nitrogen cylinder and the valve to step valves is open.
- Check that standard cylinder is open and the manual switch on the back of the GC is taking standard from the cylinder with syntetic standard.
- Leak-test connection to box by stopping the flow from the output marked "to flowmeter" and testing connections with snoop. Remove the stopper again.
- Step the valve to the desired position for analysis using the switches "step" and "reset" on the front of the heaterbox.
- Manually reset valco valve by the switch marked "reset" on the heater box. *remember that box IV has step and reset opposite.*
- Manually reset heater box by disconnecting power supply.
- Check position of trap manually.
- Wait till GC is ready and baseline stable
- Start the sequence by pulling *RunControl – Run Sequence* in the menu.
- Check that heating works. There should be a sound when the heating turns on after 0.7 min of method `trap`*trap*`.m`.

B.7 After analysis

- Compress the data directory to a file and move this to partition `E:`. Make sure that partition `E:` is back in the backup program again.

*This kind of silly thing no one ever cares of has actually been used by the Kiruna DESCARTES team during the project

Appendix C

Calibration constants

The response function for the flow-meter calibration is as we have seen in equation 3.1 on page 23

$$f_n(U_\mathrm{f}, z_\mathrm{f}) = -\frac{1}{2u_{n3}}\left(u_{n2} - \sqrt{u_{n2}^2 - 4(u_{n1} - u_{11} + z_\mathrm{f})u_{n3} + 4u_{n3}U_\mathrm{f}}\right). \qquad \text{(C.1)}$$

Calibration constants for this function as well as the voltage readouts for the switch points between the parts of the function is given in tables C.1 to C.3.

		flowmeter 200 SCCM			flowmeter 60 SCCM		
n	$U_{\max,n}$	u_{n1}	$\frac{u_{n2}}{\mathrm{SCCM}}$	$\frac{u_{n3}}{\mathrm{SCCM}^2}$	u_{n1}	$\frac{u_{n2}}{\mathrm{SCCM}}$	$\frac{u_{n3}}{\mathrm{SCCM}^2}$
1	8751.2	3109.5	129.45	−0.63650	3143.5	247.61	−1.1118
2	14828.	4766.4	73.294	−0.11470	6276.9	146.33	−0.24796
3	18329.	8930.4	35.462	−0.029863			
4	19636.	12735.	19.049	−0.012660			
5	20603.	14734.	11.464	−0.0054925			

Table C.1: Calibration constants for flow meter calibration 1999-10-13 used for flights to that date.

		flowmeter 200 SCCM			flowmeter 60 SCCM		
n	$U_{\max,n}$	u_{n1}	$\frac{u_{n2}}{\mathrm{SCCM}}$	$\frac{u_{n3}}{\mathrm{SCCM}^2}$	u_{n1}	$\frac{u_{n2}}{\mathrm{SCCM}}$	$\frac{u_{n3}}{\mathrm{SCCM}^2}$
1	10948.	2841.1	122.15	−0.42746	2551.1	235.30	−0.81058
2	14841.	4694.3	74.707	−0.12172	6015.0	148.66	−0.26030
3	18466.	8439.0	39.090	−0.035399			
4	19836.	13283.	15.736	−0.0069435			
5	21441.	14310.	13.383	−0.0060664			

Table C.2: Calibration constants for flow meter calibration 1999-10-14 used for flights after that date.

The the direct absolute calibration function defined in equation 3.4 on page 24 when fitted to the time in 1/100 s (as in the flight log), the flow in standard cubic

n	$U_{\max,n}$	flowmeter 200 SCCM u_{n1}	$\frac{u_{n2}}{\text{SCCM}}$	$\frac{u_{n3}}{\text{SCCM}^2}$	flowmeter 60 SCCM u_{n1}	$\frac{u_{n2}}{\text{SCCM}}$	$\frac{u_{n3}}{\text{SCCM}^2}$
1	1322.0	336.44	18.131	−0.083620	427.33	30.411	−0.10866
2	1785.4	815.98	6.2566	−0.0070488	794.79	20.072	−0.036215

Table C.3: Calibration constants for flow meter calibration of DESCARTES II 2000-09-19.

centimeter per minute (SCCM) and concentration of the standard in pptv is

$$\begin{aligned} m_{\text{CFC}} &= h(A) \\ &= (1.2720 \cdot 10^6 + 16829\,A - 1.3989\,A^2 + 1.0546 \cdot 10^{-4}\,A^3 \\ &\quad - 2.9613 \cdot 10^{-9}\,A^4)\,\frac{\text{s SCCM pptv}}{100}. \end{aligned} \tag{C.2}$$

To get the result in SCC as discussed in the footnote on page 24 (and plotted in figure 3.3) the result (or the coefficients) has to be multiplied by $6 \cdot 10^{-13}$.

For the Indrect calibration method the equation 3.13 on page 42 with expansion of g becomes

$$c = \begin{cases} \dfrac{\gamma_{\text{l}} + A^{g_{\text{l}1}} e^{g_{\text{l}2}}\, t_0}{\alpha\, f_n(U_{\text{f}}, z_{\text{f}})\, t_{\text{s}}} & \text{for } A \le A_{\text{lim}}, \\ \dfrac{g_{\text{h}1} A + g_{\text{h}2}}{\alpha\, f_n(U_{\text{f}}, z_{\text{f}})\, t_{\text{s}}} & \text{for } A > A_{\text{lim}}, \end{cases} \tag{C.3}$$

and as seen in the equation the calibration constants needed to calculate the mixing ratio are besides the flow meters the absolute calibration constant α and the ECD response function. The absolute calibration constant is calculated for all boxes together to the value

$$\alpha = 91.7 \cdot 10^{-6}\,\frac{100}{\text{pptv SCCM}} \tag{C.4}$$

while the response functions are calculated individually for each box to values given in table C.4.

box	$g_{\text{l}1}$	$g_{\text{l}2}$	γ_{l}/s	$g_{\text{h}1}$ /s	$g_{\text{h}2}$ /s	A_{lim}
1	0.78110	−2.4061	−1.5	0.0080082	38.099	17719.
2	0.77087	−2.4233	−1.5			
4	0.76689	−2.3667	−1.4	0.0079208	39.081	17791.

Table C.4: Calibration constants for ECD response functions g.

Appendix D

Flight checklist

```
    Flight report        Date:..........

    Sample box No: ...  Flight planned with: ..................

    Before leaving
    --------------

(_) Look through and save latest cleaning on directory:.....................

(_) gcat.exe compiled with fr_prms.h on file:...................
(_) Backup gcat.exe
(_) Batteries and spare batteries loaded

DESCARTES ready for flight date:.......... Signature.........

    Bring to flight
    ---------------

(_) Descartes complete (with sample box), in the polystyrene box
     with the slings
(_) Batteries and spare batteries. With and without fuse on each.
(_) Inlet tube with connection piece
(_) Silver tape
(_) Laptop
(_) RS232 cable
(_) Dummy RS232 plug
(_) Multimeter with fresh batteries
(_) Screwdriver to fix the sample box
(_) Screwdriver to mount the outside box
(_) Nitrogen cylinder
(_) Regulator
(_) Copper tube
(_) Pump
(_) Fixed spanners
```

```
(_) Adjustable spanners
(_) Power supply
(_) Connection cords for batteries, computer and pump.
(_) GPS
(_) Backup programs
(_) Extension cable
(_) Fuses
(_) Screws to batteries
(_) Screws to box
(_) Snoop
(_) Teflon tape

Long trip:
(_) Batterie charger

DECARTES ready to leave the building. Signature.........


    Before flight
    -------------

Launch time set to ...:... UT/LT. DESCARTES ready latest .......
    Start up laptop C:\home\gcat\>
      C:\home\gcat\> kermit
      MS-Kermit> c
    Connect RS232
    Start GCAT from power supply
      E:\> copy readall.exe atodall.exe
      E:\> pc_man
    Connect cylinder
(_) Evacuate connection three times

(_) Filled onboard cylinder pressure:........ time:.........
(_) Connect box (5 connections)
(_) Pressurise box
(_) Leaktest
(_) Read out waiting position ........ observed .........
(_) Control batteries charge
(_) Fasten batteries
DESCARTES ready and waiting for delivery time. Sign..............

    Delivery time
    -------------

(_) Check cylinder pressure:.......psi time:....... loss:.......psi/h
(_) Disconnect Nitrogen cylinder
    Reboot gcat on batteries with fuse
```

```
      E:\> copy readall.exe atodall.exe
      E:\> pc_man
(_) Connect pump battery without fuse

(_) readout pressure:.............
(_) Transfer gcat.exe
      E:\> runrec
      E:\> <alt>-x
      MS-Kermit> run compsend
        port 1
      filename: gcat.exe
      file length in bytes: 50493
      <wait>
      MS-Kermit> c
(_)   E:\> gcat (listen for pump)

    Time set to UT/LT from source:.............
    disconnect RS232
(_) connect dummyplug
    Put DESCARTES together
    Put DESCARTES in polystyrene box
(_) Connect inlet tube
(_) Deliver DECARTES for flight
DESCARTES delivered and working. Sign..........


    After recovery
    --------------
    Start up laptop C:\home\gcat\>
      C:\home\gcat\> kermit
      MS-Kermit> c
    Connect RS232
    Start GCAT from power supply
      E:\> copy readall.exe atodall.exe
      E:\> pc_man
(_) Readout pressure.........
(_) Readout trap position:......... observed .........
(_) Compile readee.exe with current fr_prms.h
(_) Transfer freshly compiled readee.exe
      MS-Kermit> c
      E:\> runrec
      E:\> <alt>-x
      MS-Kermit> run compsend
        port 1
      filename: readee.exe
      file length in bytes: 16845
      <wait>
```

```
(_) Produce data.dat
      MS-Kermit> c
      E:\> readee
(_) Transfer data.dat
      E:\> from_pc
       <alt>-x
      MS-Kermit> run to_term
(_) Printout and store hardcopy of data.dat.  Softcopy at ..................

(_) Printout and store hardcopy of fr_prms.h. Softcopy at ..................

(_) Softcopy of gcat.cpp at ........................

Flight data stored. Sign...........


    Analysis
    --------
(_) Connect sample box (5 connections)
(_) Load right sequence (starting from waiting pos)

(_) Set sequence parameters file:.................
(_) Load first trap method (for appropriate box)
(_) Check that macro is loaded
(_) Check that N2 to step is on and cylinder open. Pressure: ....../.....bar

(_) Check that standard cylinder is open. Pressure:.........psi

(_) Leaktest connection to box
(_) Manually reset valco valve
(_) Manually reset heater box

(_) Check position of trap:..........
(_) Wait till GC is ready and baseline stable

Flight samplebox ready for Analysis. Sign.............
(_) Start sequence
(_) Check that heating works

Analysis started. Sign............
    Check during analysis

    trap position:..... method:............ heaterbox temp:...........

    trap position:..... method:............ heaterbox temp:...........

    trap position:..... method:............ heaterbox temp:...........
```

```
    After analysis
    --------------
(_) Datadirectory backup at:.....................
(_) Send to Francois: Sig directory
                      data.dat
                      fr_prms.h

Backup done date......... sign ..........

This file is approachable from balva:/home/johan/pub/checklist.txt
and latest edited by Johan 991217 if you edit make read and writable again
balva% chmod 666 checklist.txt
```

Bibliography

Arvelius, J., H. Nilsson, S. Kirkwood, F. Danis, N. R. P. Harris, and J. A. Pyle, CFC measurements with DESCARTES during the THESEO campaign in Kiruna spring 1999 — early results, in *Proceedings 14th ESA Symposium on Rocket and Balloon Programmes and Related Research*, edited by B. Kaldeich-Schürmann, no. 437 in SP, pp. 353–358, Eurpoean Space Agency, ESA Publications Division, 1999.

Arvelius, J., H. Nilsson, S. Kirkwood, F. Danis, N. R. Harris, and J. A. Pyle, CFC measurements with DESCARTES during the THESEO campaign in Kiruna spring 1999, in *Proceedings of the Fifth European workshop on stratospheric ozone*, edited by N. R. P. Harris, M. Guirlet, and G. T. Amanatidis, no. 73 in Air Pollution Research Report, pp. 459–462, European Commission, 2000, ISBN 92-827-5672-6.

Arvelius, J., H. Nilsson, S. Kirkwood, A. Robinson, N. Harris, J. Pyle, O. Morgenstern, F. Goutail, and J.-P. Pommereau, Measured tracer profiles from the polar stratosphere covering all seasons 2000, in *Proceedings of the Sixth European workshop on stratospheric ozone*, edited by N. R. P. Harris, G. T. Amanatidis, and J. G. Levine, no. 79 in Air Pollution Research Report, pp. 217–220, European Commission, 2002.

Arvelius, J., S. Roslin, H. Nilsson, and S. Kirkwood, Adsorption efficiency of a molecular sieve in low pressure, in *Proceedings of the XX quadrennial ozone symposium*, edited by C. Zerefos, pp. 515–516, International Ozone Commission, 2004.

Bauer, R., A. Engel, H. Franken, E. Klein, G. Kulessa, C. Schiller, U. Schmidt, R. Borchers, and J. Lee, Monitoring the vertical structure of the arctic polar vortex over northern Scandinavia during EASOE: Regular N_2O profile observations, *Geophys. Res. Lett.*, *21*, 1211–1214, 1994.

Bertoni, G., and R. Tappa, Improvement in breakthrough volume evaluation methods for light adsorbent traps employed for volatile organic compounds determination at atmospheric concentration levels, *J. Chromatogr. A*, *767*, 153–161, 1997.

Bertoni, G., F. Bruner, A. Liberti, and C. Perrino, Some critical parameters in collection, recovery and gas chromatographic analysis of organic pollutants in ambient air using light adsorbents, *J. Chromatogr.*, *203*, 263–270, 1981.

Betz, W. R., S. G. Maroldo, G. D. Wachob, and M. C. Firth, Characterization of carbon molecular sieves and activated charcoal for use in airborne contaminant sampling, *Am. Ind. Hyg. Assoc. J.*, *50*, 181–187, 1989.

Bregman, A., J. Lelieveld, M. M. P. van den Broek, P. C. Siegmund, H. Fischer, and O. Bujok, N_2O and O_3 relationship in the lowermost stratosphere: A diagnostic for mixing processes as represented by a three-dimenstional chemistry-transport model, *J. Geophys. Res.*, *105*, 17,279–17,290, 2000.

Bujok, O., V. Tan, E. Klein, R. Nopper, R. Bauer, A. Engel, M.-T. Gerhards, A. Afchine, D. S. McKenna, U. Schmidt, F. G. Weinhold, and H. Fischer, GHOST – A novel airborne gas chromatograph for in situ measurements of long-lived tracers in the lower stratosphere: Method and applications, *J. Atm. Chem.*, *39*, 37–64, 2001, dOI: 10.1023/A:1010789715871.

Comes, P., N. Gonzalez-Flesca, T. Menard, and J. O. Grimalt, Langmuir-derived equations for the prediction of solid adsorbent breakthrough volumes of volatile organic compounds in atmospheric emission effluents, *Anal. Chem.*, *65*, 1048–1053, 1993.

Comes, P., N. Gonzalez-Flesca, F. Bader, and J. O. Grimalt, Langmurian behaviour of smelly volatile organic compounds on air sampling with solid adsorbents, *J. Chromatogr. A*, *723*, 293–299, 1996.

Cronn, D. R., R. A. Rasmussen, E. Robinson, and D. E. Harsch, Halogenated compound identification and measurement in the troposphere and lower stratospere, *J. Geophys. Res.*, *82*, 5935–5944, 1977.

Cunnold, D. M., R. F. Weiss, R. G. Prinn, D. Hartley, P. G. Simmonds, P. J. Fraser, B. Miller, F. N. Alyea, and L. Porter, GAGE/AGAGE measurements indicating reductions in global emissions of CCl_3 and CCl_2F_2, *J. Geophys. Res.*, *102*, 1259–1269, 1997.

Danis, F., K. Persson, H. Nilsson, A. D. Robinson, M. P. Chipperfield, J. D. McIntyre, P. G. Simmonds, N. R. P. Harris, and J. A. Pyle, Tracer measurements with DESCARTES during ILAS in early 1997, in *Polar stratospheric ozone 1997, Proceedings of the fourth European symposium 22 to 26 September 1997, Schliersee, Bavaria, Germany*, edited by N. R. P. Harris, I. Kilbane-Dawe, and G. T. Amanatidis, no. 66 in Air Pollution Research Report, pp. 423–426, European Commission, 1998.

Danis, F., N. R. P. Harris, W. H. Taylor, J. D. McIntyre, P. G. Simmonds, and J. A. Pyle, DESCARTES: A novel lightweight balloon-borne instrument for measurement of Halocarbons, *Review of Scientific Instruments*, *71*, 271–280, 2000.

Elkins, J. W., D. W. Fahey, J. Gilligan, G. S. Dutton, T. J. Baring, C. M. Volk, R. E. Dunn, R. C. Myers, S. A. Montzka, P. R. Wamsley, A. H. Hayden, J. H. Butler, T. L. Thompson, T. H. Swanson, E. J. Dlugokencky, P. C. Novelli, D. F. Hurst, J. M. Lobert, S. J. Cicora, R. J. McLaughlin, T. L. Thompson, R. H. Winkler, P. J. Fraser, L. P. Steele, and M. P. Lucarelli, Airborne gas

chromatograph for in situ measurements of long-lived species in the upper troposphere and lower stratosphere, *Geophys. Res. Lett.*, *23*, 347–350, 1996.

Fabian, P., R. Borchers, K. H. Weiler, U. Schmidt, A. Volz, D. E. Ehhalt, W. Seiler, and F. Müller, Simultaneously measured vertical profiles of H_2, CH_4, CO, N_2O, $CFCl_3$ and CF_2CCl_2 in the mid-latitude stratosphere and troposphere, *J. Geophys. Res.*, *84*, 3149, 1979.

Greenblatt, J. B., H.-J. Jost, M. Loewenstein, J. R. Podolske, D. F. Hurst, J. W. Elkins, S. M. Schauffler, E. L. Atlas, R. L. Herman, C. R. Webster, T. P. Bui, F. L. Moore, E. A. Ray, S. Oltmans, H. Vömel, J.-F. Blavier, B. Sen, R. A. Stachnik, G. C. Toon, A. Engel, M. Müller, U. Schmidt, H. Bremer, R. B. Pierce, B.-M. Sinnhuber, M. Chipperfield, and F. Lefèvre, Tracer-based determination of vortex descent in the 1999-2000 arctic winter, *J. Geophys. Res.*, *107*, DOI 10.1029/2001JD000,937, 2002.

Hall, B. D., et al., Halocarbons and other atmospheric trace species, in *Climate Monitoring and Diagnostics Laboratory Summary Report No. 26 2000–2001*, edited by D. B. King and R. C. Schnell, chap. 5, National Oceanic and Atmospheric Administration, 2002.

Harper, M., Evaluation of solid sorbent sampling methods by breakthrough volume studies, *Ann. occup. Hyg.*, *37*, 65–88, 1993.

Harper, M., Sorbent trapping on volatile organic compunds from air, *J. Chromatogr. A*, *885*, 129–151, 2000.

Harris, N. R. P., M. Guirlet, and G. T. Amanatidis, eds., *Proceedings of the Fifth European workshop on stratospheric ozone*, no. 73 in Air Pollution Research Report, European Commission, 2000a, ISBN 92-827-5672-6.

Harris, N. R. P., M. Guirlet, G. T. Amandatidis, G. Ancellet, G. Braaten, A. Bregman, A. Engel, P. von der Gathen, A. Goede, F. Goutail, A. Hauchecorne, H. Küllman, N. Larsen, G. Mégie, D. Murtagh, G. Naujokat, J. de La Noë, W. Norton, H. Oelhaf, T. Peter, K. Pfeilsticker, J.-P. Pommereau, J. A. Pyle, M. van Roozendael, H. Schlager, U. Schmidt, L. Stefanutti, and G. Toci, Overview and results of THESEO 1998–1999, in *Harris et al.* [2000a], pp. 33–49.

Harris, N. R. P., M. Rex, F. Goutail, B. M. Knudsen, G. L. Manney, R. Müller, and P. von der Gathen, Comparison of empirically derived ozone losses in the arctic vortex, *J. Geophys. Res.*, *107*, 2002, dOI 10.1029/2001JD000482.

Hartmann, D. L., L. E. Heidt, M. Loewenstein, J. R. Podolske, J. Vedder, W. L. Starr, and S. E. Strahan, Transport into the south polar vortex in early spring, *J. Geophys. Res.*, *94*, 16,779–16,795, 1989.

Heidt, L. E., J. F. Vedder, W. H. Pollock, R. A. Lueb, and B. E. Henry, Trace gases in the antarctic atmosphere, *J. Geophys. Res.*, *94*, 11,599–11,611, 1989.

Hewlett-Packard, *Understanding your Chemstation*, Hewlett-Packard, 3rd ed., 1995a.

Hewlett-Packard, *HP 6890 Series Gas Chromatograph Operating Manual*, Hewlett-Packard, 2nd ed., 1995b.

Hines, W. W., and D. C. Montgomery, *Probability and Statistics in Engineering and Management Science*, 2nd ed., John Wiley and Sons, Inc., 1980, ISBN 0-471-09409-9.

Holton, J. R., A dynamically based transport parameterization for one-dimensional photochemical models of the stratosphere, *J. Geophys. Res.*, *91*, 2681–2686, 1986.

Honda, H., S. Aoki, T. Nakazawa, S. Morimoto, and N. Yajima, Crygemic air sampling system for measurements of the concentrations of stratospheric trace gases and their isotopic ratios over antarctica, *J. Geomag. Geoelectr.*, *48*, 1145–1155, 1996.

Houghton, J. T., Y. Ding, D. J. Griggs, M. Noguer, P. J. van der Linden, X. Dai, K. Maskell, and C. A. Johnson, eds., *Climate Change 2001: The Scientific Basis. Contribution of Working Group I to the Third Assessment Report of the Intergovernmental Panel on Climate Change*, Cambridge University Press, 2001.

Khosrawi, F., R. Müller, H. Irie, A. Engel, G. C. Toon, B. Sen, S. Aoki, T. Nakazawa, W. A. Traub, K. W. Jucks, D. G. Johnson, H. Oelhaf, G. Wetzel, T. Sugita, H. Kanzawa, T. Yokota, H. Nakajima, and Y. Sasano, Validation of CFC-12 measurements from the Improved Limb Atmospheric Spectrometer (ILAS) with the version 6.0 retrieval algorithm, *J. Geophys. Res.*, *109*, 2004, doi:10.1029/2003JD004325.

Lait, L. R., M. R. Schoeberl, P. A. Newman, M. H. Proffitt, M. Loewenstein, J. R. Podolske, S. E. Strahan, K. R. Chan, B. Gary, J. J. Margitan, E. Browell, M. P. McCormick, and A. Torres, Reconstrucion of O_3 and N_2O fields from ER-2, DC-8 and balloon observations, *Geophys. Res. Lett.*, *17*, 521–524, 1990.

Loewenstein, M., J. R. Podolske, K. R. Chan, and S. E. Strahan, Nitrous oxide as a dynamical tracer in the 1987 airborne antarctic ozone experiment, *J. Geophys. Res.*, *94*, 11,589–11,598, 1989.

MacElroy, J. M. D., N. A. Seaton, and S. P. Friedman, Sorption rate processes in carbon molecular sieves, in *Equilibria and Dynamics of Gas Adsorption on Heterogeneous Solid Surfaces*, edited by W. Rudzinski, W. A. Steele, and G. Zgrablich, vol. 104 of *Studies in Surface Science and Catalysis*, pp. 837–880, Elsevier, 1997, ISBN 0-444-82243-7.

Mahlman, J. D., H. L. II, and W. J. Moxim, Three-dimensional simulations of stratospheric N_2O: Predictions for other trace constituents., *J. Geophys. Res.*, *91*, 2687–2707, 1986.

Molina, M. J., and F. S. Rowland, Stratospheric sink for chlorofluoromethanes : chlorine atom-catalysed destruction of ozone, *Nature*, *249*, 810–812, 1974.

Montzka, S. A., P. J. Fraser, et al., eds., *Controlled Substances and Other Source Gases*, chap. 1, in World Meterological Organization (WMO) 2002 [2002], 2002, global Ozone Research and Monitoring Project—Report No. 47.

Moore, F. L., J. W. Elkins, E. A. Ray, G. S. Dutton, R. E. Dunn, D. W. Fahey, R. J. McLaughlin, T. L. Thompson, P. A. Romashkin, D. F. Hurst, and P. R. Wamsley, Balloonborne in situ gas chromatograph for measurements in the troposphere and stratosphere, *J. Geophys. Res.*, *108*, 2003, 8330, doi:10.1029/2001JD000891.

Morgenstern, O., and J. A. Pyle, Strategies for measuring canonical tracer relationships in the stratosphere, *Atmos. Chem. Phys.*, *3*, 259–266, 2003.

Müller, R., U. Schmidt, A. Engel, D. S. McKenna, and M. H. Proffitt, The O_3–N_2O relation from balloon-borne observations as a measure of Arctic ozone loss in 1991/92, *Quarterly Journal of the Royal Meteorological Society*, *127*, 1389–1412, 2001.

Müller, R., S. Tilmes, J.-U. Groß, D. S. McKenna, M. Müller, U. Schmidt, G. C. Toon, R. A. Stachnik, J. J. Margitan, J. W. Elkins, J. Arvelius, and J. M. Russel III, Chlorine activation and chemical ozone loss deduced from HALOE and balloon measurments in the arctic during the winter of 1999–2000, *J. Geophys. Res.*, *108*, 2002, dOI:10.1029/2001JD001423.

Namiesnik, J., L. Torres, E. Kozlowski, and J. Mathieu, Evaluation fo the suitability of selected porous polymers for preconcentration of voltile organic compounds, *J. Chromatogr.*, *208*, 239–252, 1981.

Newman, P. A., N. R. P. Harris, A. Adriani, G. T. Amandatidis, J. G. Anderson, G. O. Graaten, W. H. Brune, K. S. Carslaw, M. S. Craig, P. L. DeCola, M. Guirlet, R. S. Hipskind, M. J. Kurylo, H. Küllmann, N. Larsen, G. J. Mégie, J.-P. Pommereau, L. R. Poole, M. R. Schoeberl, F. Stroh, O. B. Toon, C. R. Trepte, and M. V. Roozendael, An overview of the SOLVE/THESEO 2000 campaign, *J. Geophys. Res.*, *107*, 8259, 2002, doi:10.1029/2001JD001303.

Nilsson, H., K. Persson, F. Danis, N. R. P. Harris, and J. A. Pyle, CFC measurements with DESCARTES during the ILAS validation campaign early results, in *Proceedings 13th ESA Symposium on Rocket and Balloon Programmes and Related Research*, 1997.

O'Doherty, S. J., P. G. Simmonds, and G. Nickless, Evaluation of carboxen carbon molecular sieves for trapping replacement chloroflourocarbons, *J. Chromatogr.*, *630*, 265–274, 1993a.

O'Doherty, S. J., P. G. Simmonds, and G. Nickless, Analysis of replacement chlorofluorocarbons using carboxen microtraps for isolation and preconcentration in gas chromatography—mass spectrometry, *J. Chromatogr. A*, *657*, 123–129, 1993b.

on Climate Change (IPCC), I. P., ed., *Climate Change 1994*, Cambridge University Press, 1995.

Orsolini, Y., et al., Final report, Spring-to-Autumn Measurements and Modelling of Ozone and Active species, 2002.

Pankow, J. F., Error magnitudes in extrapolated approximations of sorbent retention volumes obtained by using tempereature-dependent vapor pressures, *Atmos. Environ.*, *23*, 1113–1115, 1989.

Pierotti, D., R. A. Rasmussen, and R. Dalluge, Measurements of N_2O, CF_2Cl_2, $CFCl_3$, CH_3CCl_3, CCl_4 and CH_3Cl in troposphere and lower stratosphere over north america, *J. Geomag. Geoelectr.*, *32*, 181–205, 1980.

Plumb, R. A., A "tropical pipe" model of stratopheric transport, *J. Geophys. Res.*, *101*, 3957–3972, 1996.

Plumb, R. A., and M. K. W. Ko, Interrelationships between mixing ratios of long-lived stratospheric constituents, *J. Geophys. Res.*, *97*, 10,145–10,156, 1992.

Plumb, R. A., D. W. Waugh, and M. P. Chipperfield, The effects of mixing on tracer relationships in the polar vortices, *J. Geophys. Res.*, *105*, 10,047–10,062, 2000.

Pommereau, J.-P., and J. Piquard, Ozone, nitrogen dioxide and aerosol vertical distributions by uv-visible solar occultation from balloons, *Geophys. Res. Lett.*, *13*, 1227–1230, 1994.

Proffitt, M. H., K. K. Kelly, J. A. Powell, B. L. Gary, M. Loewenstein, J. R. Podolske, S. E. Strahan, and K. R. Chan, Evidence for diabatic cooling and poleward transport within and around the 1987 antarctic ozone hole, *J. Geophys. Res.*, *94*, 16,797–16,813, 1989.

Proffitt, M. H., J. J. Margitan, K. K. Kelly, M. Loewenstein, J. R. Podolske, and K. R. Chan, Ozone loss in the arctic polar vortex inferred from high-altitude aircraft measurements, *Nature*, *347*, 31–36, 1990.

Proffitt, M. H., K. Aikin, J. J. Margitan, M. Loewenstein, J. R. Podolske, A. Weaver, K. R. Chan, H. Fast, and J. W. Elkins, Ozone loss inside the northern polar vortex during the 1991–1992 winter, *Science*, *261*, 1150–1154, 1993.

Ray, E. A., F. L. Moore, J. W. Elkins, G. S. Dutton, D. W. Fahey, H. Vömel, S. J.Oltmans, and K. H. Rosenlof, Transport into the northern hemisphere lowermost stratosphere revealed by in situ tracer measurements, *J. Geophys. Res.*, *104*, 26,565–26,580, 1999.

Ray, E. A., F. L. Moore, J. W. Elkins, D. F. Hurst, P. A. Romanshkin, G. S. Dutton, and D. W. Fahey, Descent and mixing in the 1999–2000 northern polar vortex inferred from in situ tracer measurements, *J. Geophys. Res.*, *107*, 2002, doi:10.1029/2001JD000961.

Raymond, A., and G. Guiochon, The use of graphitized carbon black as a trapping material for organic compounds in light gases before a gas chromatographic analysis, *J. Chromatogr. Sci.*, *13*, 173–177, 1975.

Reilly, C. N., G. P. Hildebrand, and J. W. Ashley, Jr., Gas chromatograpic response as a function of sample input profile, *Anal. Chem.*, *34*, 1198–1213, 1962.

Riba, M. L., B. Clement, M. Haziza, and L. Torres, Trace analysis. determination of the "breaktrough volume" (B. T. V) of atmospheric isoprene, *Toxicological and Environmental Chemistry*, *31–32*, 235–240, 1991.

Riediger, O., Entwicklung und einsatz eines flugzeuggetragenen instrumentes zur in-situ-messung langlebiger spurengase in der stratosphäre, Ph.D. thesis, Johann Wolfgang Goethe-Universität, Frankfurt am Main, 2000.

Robinson, A. D., J. D. McIntyre, N. R. P. Harris, J. A. Pyle, P. G. Simmonds, and F. Danis, A lightweight balloon-borne gas chromatograph for in situ measurements of atmospheric halocarbons, *Review of Scientific Instruments*, *71*, 4553–4560, 2000.

Robinson, A. D., G. A. Millard, F. Danis, M. Guirlet, N. R. P. Harris, A. M. Lee, J. D. McIntyre, J. A. Pyle, J. Arvelius, S. Dagnesjo, S. Kirkwood, H. Nilsson, D. W. Toohey, T. Deshler, F. Goutail, J.-P. Pommereau, J. W. Elkins, F. Moore, E. Ray, U. Schmidt, A. Engel, and M. Müller, Ozone loss derived from balloon-borne tracer measurements in the 1999/2000 arctic winter, *Atmos. Chem. Phys.*, *5*, 1423–1436, 2005, sRef-ID: 1680-7324/acp/2005-5-1423.

Roslin, S., Adsorption of CFC on carboxen during sampling in the stratosphere, Master's thesis, Swedish Institute of Space Physics/Umeå University, 2003.

Sasano, Y., M. Suzuki, T. Yokota, and H. Kanzawa, Improved Limb Atmospheric Spectrometer (ILAS) for stratospheric ozone layer measurements by solar occultation technique, *Geophys. Res. Lett.*, *26*, 197–200, 1999, doi:10.1029/1998GL900276.

Schmeltekopf, A. L., P. D. Goldan, W. R. Henderson, W. J. Harrop, T. L. Thomson, F. C. Fehsenfeld, H. I. Schiff, J. P. Crutzen, I. S. A. Isaksen, and E. E. Ferguson, Measurements of stratospheric $CFCl_3$, CF_2Cl_2 and N_2O, *Geophys. Res. Lett.*, *2*, 393–396, 1975.

Schmeltekopf, A. L., P. D. Goldan, W. J. Harrop, T. L. Thomson, D. L. Albritton, M. MacFarland, A. E. Sapp, and W. R. Henderson, Ballon-borne stratospheric grab-sampling system, *Review of Scientific Instruments*, *47*, 1479–1485, 1976.

Schmidt, U., R. Bauer, A. Khedim, E. Klein, G. Kulessa, and C. Schiller, Profile observations of long-lived trace gases in the artic vortex, *Geophys. Res. Lett.*, *18*, 767–770, 1991.

Schoeberl, M. R., and D. L. Hartmann, The dynamics of the stratospheric polar vortex and its relation to springtime ozone depletions, *Science*, *251*, 46–52, 1991.

Senum, G. I., Theoretical collection efficiencies of adsorbent samplers, *Environ. Sci. Technol.*, *15*, 1073–1075, 1981.

Seshadri, S., and J. W. Bozzelli, Collection of vapors of selected chlorocarbons and benzene on Tenax GC, *Chemosphere*, *12*, 809–820, 1983.

Sing, K. S. W., and R. T. Williams, Review: The use of molecular probes for the characterization of nano-porous adsorbents, *Part. Part. Syst. Charact.*, *21*, 71–79, 2004, dOI:10.1002/ppsc.200400923.

Stacey, E., Characterisation of a lightweight instrument for atmospheric measurement, Master's thesis, Department of Chemistry, Cambridge University, 1996.

Sturges, W. T., and J. W. Elkins, Use of adsorbent to collect selected halocarbons and hydrohalocarbons of environmental interest from large air volumes, *J. Chromatogr.*, *642*, 123–134, 1993.

Thompson, T. M., et al., Halocarbons and other atmospheric trace species, in *Climate Monitoring and Diagnostics Laboratory Summary Report No. 27 2002–2003*, edited by R. C. Schnell, A.-M. Buggle, and R. M. Rosson, chap. 5, National Oceanic and Atmospheric Administration, 2004.

Toon, G. C., JPL Mark IV interferometer, *Optics and Photonics News*, *2*, 19–21, 1991.

Trepte, C. R., and M. H. Hitchman, Tropical stratosphseric circulation deduced from satellite aerosol data, *Nature*, *355*, 626–628, 1992.

Tyson, B. J., J. F. Vedder, J. C. Arvesen, and R. B. Brewer, Stratospheric measurements of CF_2Cl_2 and N_2O, *Geophys. Res. Lett.*, *5*, 369–372, 1978.

United Nations Environment Program (UNEP) 2000, The montreal protocol on substances that deplete the ozone layer, 2000, iSBN: 92-807-1888-6.

Vidal-Madjar, C., M.-F. Gonnord, F. Benchah, and G. Guiochon, Performances of various adsorbents for the trapping and analyses o organohalogenated air pollutants by gas chromatography, *J. Chromatogr. Sci.*, *16*, 190–196, 1978.

Volk, C. M., J. W. Elkins, D. W. Fahey, G. S. Dutton, J. M. Gilligan, M. Loewenstein, J. R. Podolske, K. R. Chan, and M. R. Gunson, Evaluation of source gas lifetimes from stratospheric observations, *J. Geophys. Res.*, *102*, 25,543–25,564, 1997.

Waugh, D. W., R. A. Plumb, J. W. . Elkins, D. W. Fahey, K. A. Boering, G. S. Dutton, C. M. Volk, E. Keim, R.-S. Gao, B. C. Daube, S. C. Wofsy, M. Loewenstein, J. R. Podolske, K. R. Chan, M. H. Proffitt, K. K. Kelly, P. A. Newman, and L. R. Lait, Mixing of polar vortex air into middle latitudes as revealed by tracer–tracer scatterplots, *J. Geophys. Res.*, *102*, 13,119–13,134, 1997.

World Meterological Organization (WMO) 2002, Scientific assessment of ozone depletion: 2002, 2002, global Ozone Research and Monitoring Project—Report No. 47.

Yoon, Y. H., and J. H. Nelson, Application of gas adsorption kinetics I. a theoretical model for respirator cartridge service life, *Am. Ind. Hyg. Assoc. J.*, *45*, 509–516, 1984.

Yoon, Y. H., and J. H. Nelson, Contaminant breakthrough: A theoretical study of charcoal sampling tubes, *Am. Ind. Hyg. Assoc. J.*, *51*, 319–325, 1990.

Index of acronyms

AAOE, Airborne Antarctic Ozone Experiment, 5
AASE, Airborne Arctic Stratospheric Expedition, 5
AC, Alternating Current, 22, 89
ADEOS, Advanced Earth Observing Satellite, 109
AGAGE, Advanced Global Atmospheric Gases Experiment, 20
ARR, Andøya Rocket Range, 109

CFC, Chloro Fluoro Carbon, 2, 3, 5–7, 21, 24, 26, 35, 40, 53, 58–60, 62, 64, 66–69, *70*, 72–75, 138
CFC-11, CCl_3F, 19, 20, *20*, 21, *40*, 42, *46*, 58, 62, 101, 102, 104, 112, 116, 118
CFC-113, CCl_2F-$CClF_2$, 19, 20, *20*, 42, 44, **44**, *44–46*, 47, 105
CFC-115, CF_3-CF_2Cl, 3
CFC-12, CCl_2F_2, 20, *20*, 111
CMDL, Climate Monitoring and Diagnostic Laboratory, 20, 104
CNES, Centre National d'Etudes Spatiales, *110*, 111
CTM, Chemical Transfer Model, 6

DIRAC, Determination In situ by Rapid Analytical Chromatography, 90, 118, 120, 121

ECC, Electrochemical Concentration Cell, 112, 116
ECD, Electron Capture Detector, 19, 20, 26, 27, *28*, 30, *31*, 35, 36, *36*, 37, *38*, 39, *39*, 40, 90, 94, 95, *152*
ECMWF, European Centre for Medium-Range Weather Forecasts, 116

FTD, Flight Trajectory Data, 17

GC, Gas Chromatograph, 7, *9*, 14, *15*, 16, 19, 26, 29, 30, 44, 51, 86, 106, 131, 132, 136–138, 141
GPS, Global Positioning System, 16

HALOZ, HALogens and OZone loss, *110*, 116, 121
HATS, Halocarbons and other Atmospheric Trace Species, 59, 102
HP, Hewlett Packard, 14

ILAS, Improved Limb Atmospheric Spectrometer, 109, *109*, 116
IRF, Swedish Institute of Space Physics, 7, 138

JPL, Jet Propulsion Laboratory, 120

LACE, Lightweight Airborne Chromatograph Experiment, 118, 120, 121

NOAA, National Oceanic and Atmospheric Administration, 20, 44, 47, 51, 59, 104, 141

OMS, Observations of the Middle Stratosphere, *110*, 116, 120, 121

PV, Potential Vorticity, 116

SAGE, Stratospheric Aerosol and Gas Experiment, 90
SAMMOA, Spring-to-Autumn Measurements and Modelling of Ozone and Active species, 98, 109, *110*, 116, 121, 122
SAOZ, Systeme d'Analyse par Observation Zenithale, 109, *109, 110*, 116, 120, 121, *124*, *126*
SCC, standard cubic centimeter, 24, 58, 152
SCCM, standard cubic centimeter per minute, **22**, 23, 58, 60, 62, 76, *77*, 152
SOLVE, SAGE III Ozone Loss and Validation Experiment, 90, 98, 109, *110*, 116, 118
SSC, Swedish Space Corporation, *110*, 111

THESEO, Third European Stratospheric Experiment on Ozone, 90, 98, 109, *110*, 111, 116, 118

UEA, University of East Anglia, 20, 44

WCOT, Wall-Coated Open Tubular, 14

Index of notation

A, peak area, 24, *24, 25*, 27, *28*, 29, 30, 35, 36, 39, 40, 42, *45*, *48, 49*, 92, 93, *93*, 94, 95, 97, 152
A_{lim}, peak area limit, 27, 42, 94, 95, 97, 152, *152*
α, absolute calibration proportionality coefficient, 21, 40, **40**, *40, 41*, 42, 94, 95, 97, 152

b, total number of model bins, 62, **62**, 63, *63*, 67–70
β, breakthrough coefficient, 84, **84**

c, mixing ratio, 24, 32, *34*, 40, 42, 93, 94, 97, 109, 152
c_{a}, absolute standard mixing ratio, 21, 24, 42, *43*, 94
χ, mixing ratio, 3

ΔN, exchange of CFC during a model timestep, 66, 70, 72
ΔN_{a}, adsorption during one model timestep, *65*, 66, 69–72
ΔN_{d}, desorption during one model timestep, 62, 66–68, 70–72
ΔN_{in}, inflow to trap during one model timestep, 66–68, 70
ΔN_{out}, outflow from second trap during one model timestep, 67, 68, 70
ΔN_{r}, redistribution during one model timestep, 66, 67
ΔN_{s}, self readsorption during one model timestep, 67, 70, 72
Δt, length of timestep in Dessim, 62, 63, 66–68, 70–72
Δx, width of bin in Dessim, 62, **62**, *63*, 66, 67, 69, 71, 72
D_l, difference in area estimation, 92
D_m, min error from area estimation, 92

$\mathbf{E}$, vector in algorithm, 68, **68**, 69
E_{i}, integration uncertainty function, 92

f_n, flow meter respons function, 23, **23**, 24, 25, 42, 89, 93, 94, 97, 151, 152

g, ECD respons function, **27**, *28*, 29, 30, 35, 36, 39, 40, 42, 94, 95, 97, 152, *152*
Γ, net export of tracer, 4, 5
$\bar{\Gamma}$, mean age of airmass, 3
γ_{l}, ECD respons offset term, 27, 42, 94, 95, 97, 152, *152*
g_{h}, ECD respons function high part, 27, **27**, 42, 94, 95, 97, 152, *152*
g_{l}, ECD respons function low part, 26, 27, **27**, 42, 94, 95, 97, 152, *152*

h, absolute calibration response function, 24, *24*, 25, *25*, *45*, *48, 49*, 93, *93*, 94, 152

K, ideal gas law proportionality coefficient, 58, 84
$\mathcal{K}$, set of operators, 92
k', rate constant, 55, *56*
K_{a}, adsorption coefficient, **62**, 63, 66–70, 72
κ_{a}, adsorption coefficient, 53, 62, 63, 66–69, 72, 74
κ_{d}, desorption coefficient, 53, 62, 63, 66, 71, 72, 74

K_d, desorption coefficient, **62**, 63, 66–68, 70

$\mathcal{L}$, set of samples, 92

m, part of simulation bin, 57, 58, 70–72, *73*
m, mass, 58, 84
M_a, dry mass of the atmosphere, 3
m_c, mass Carboxen in trap, 58
m_CFC, mass CFC in sample, 24, *24*, *25*, 40, *45*, *48*, *49*, 84, *93*, 94, 152
m_max, maximum allowed sample mass, 58
M_u, dry mass of the atmosphere above the tropopause, 3
μ, mass flow, 23, **23**, 40, 42, 84, 85, *85*, 86, 89, 90, 94, 97
μ_max, maximum allowed mass-flow, 57, 58
$\mu_{\mathrm{max},n}$, switch point in mass flow calibration fitting, 23, **23**

N, amount of CFC in model, 23, 62, 63, *63*, 66–70, *70*, 71, *71*, 72
n, bin number, 62, *63*, 65, *65*, 66–70, *70*, 71, *71*, 72, *73*
N, number of theoretical plates, 56, **56**, 57, *57*
N, amount of CFC in model, 63, 68, 69
N_g, inflow to model bin, 69, 70, *70*, 71, *71*, 72, *73*
N_L, number of adsorption cites in a model bin, 72, **72**, *73*
$N_\mathrm{L,tot}$, number of adsorption cites in trap, 72

ω, volume flow rate, 84, 86

P, concentration ratio between trap outflow and inflow, 55, 56, 75, 76
p, pressure, 58
p_a, ambient pressure, 84–86
Φ, estimation of pressure parameter from μ, 85, *85*, 86
ϕ, pressure parameter, 85, **85**, *85*, 86
p_l, line over pressure, **84**, 85, 86
p_t, trap pressure, 84–86

q, potential vorticity, 5, 6

R, analysis run respons factor, 32, **32**, *34*
r, trap individual respons factor, **29**, 30, *40*, 42

σ, steady state mixing ratio, 4, 5
σ, standard deviation of gaussian distribution, 56
$\bar{\sigma}$, mass weight average mean atmospheric mixing ratio, 3, 4

T, temperature, 17, 58
t, time, 55, 56, 68, 70, 75
T_0, 273.15 K, 84, **84**
t_0, 1 second, 27, **27**, 42, 94, 95, 97, 152
τ, life time, 3–5
τ, time of 50% breakthrough, 55, 56
θ, potential temperature, 1–3, 5, 6, 17
t_R, retention time, 56
t_s, sampling time, 24, 26, 27, 40, 42, 84, 93, 94, 97, 152

U_f, flow meter voltage readout, 23, 24, 42, 89, 93, 94, 151, 152
U_max, flowmeter voltage of switch point, **23**, *151*, *152*
u_n, flow meter respons function, 23, **23**, 89, 90, 94, 151, *151*, *152*

V, sampled volume, 35, 56–58, 84, 86
v, flow linear velocity, 57, 58, 62, **62**, 63, 66–69, 71, 72
V_b, breakthrough volume, 54, 58
V_max, maximum allowed sample volume, 57, 58
V_R, retention volume, 56, 57

x, depth in adsorption bed, **62**, 66–69, 71, 72
Ξ_a, adsorption coefficient, 71, **71**, 72
ξ_a, adsorption coefficient, 71, 72
x_n, center of bin n x-value, 66

x_t, length of trap, 62, **62**, 67, 68

z_f, zero reading from flowmeter, 22, 23, **23**, 24, 42, 89, 93, 94, 151, 152

Index

SAGE III Ozone Loss and Validation Experiment (SOLVE), 90, 98, 109, *110*, 116, 118
CCl_2F-$CClF_2$ (CFC-113), 19, 20, *20*, 42, 44, **44**, *44–46*, 47, 105
CF_3-CF_2Cl (CFC-115), 3
CCl_3F (CFC-11), 19, 20, *20*, 21, *40*, 42, *46*, 58, 62, 101, 102, 104, 112, 116, 118
CCl_2F_2 (CFC-12), 20, *20*, 111
1 second (t_0), **27**
273.15 K (T_0), **84**

absolute calibration proportionality coefficient (α), 21, **40**, *40, 41*, 42, 97, 152
absolute calibration response function (h), 24, *24*, 25, *25*, *45*, *48, 49*, *93*, 152
absolute standard mixing ratio (c_a), 21, 24, 42, *43*
absolute calibration, **23–42**
adsorbent, 7, **13**
adsorber, 25
adsorption, 19, 25, 105, 138
adsorption coefficient (K_a), **62**, 63, 66–69
adsorption coefficient (Ξ_a), **71**
adsorption coefficient (κ_a), 53, 62, 63, 66–69, 72, 74
adsorption coefficient (ξ_a), 71
adsorption during one model timestep (ΔN_a), *65*, 66
Advanced Earth Observing Satellite (ADEOS), 109
Advanced Global Atmospheric Gases Experiment (AGAGE), 20
`air16-96.s`, *134*
`air96.m`, *133, 134*
Airborne Antarctic Ozone Experiment (AAOE), 5
Airborne Arctic Stratospheric Expedition (AASE), 5
Alternating Current (AC), 22, 89
aluminium, 25, 105
ambient pressure (p_a), 84
amount of CFC in model (**N**), 63, 68, 69
amount of CFC in model (N), 23, 63, *63*, 66, 68, *70, 71*
`analys`*`trap`*`.m`, 143
`analys`*`position`*`.s`, 136, 149
`analys`*`trap`*`.s`, *134*
`analys`*`wp`*`.s`, 30, *134*
`analys7w.s`, *133, 134*, 136, 149
analysis, 26, 27, 30, 32, 33, 106, 141
analysis run respons factor (R), **32**
analysis sequence, 132
analysis system, 141
Andøya Rocket Range (ARR), 109
`anp7stnd.s`, *134*
`AtoD_all`, 11
`AtoDall`, 11, 13

backup, 135
`baseline.m`, *133*
basic stamp, 137
bin number (n), *63*, 66, 68, 70, *70, 71*, *73*
brass, 105, 138, 141
breakthrough coefficient (β), **84**
breakthrough volume (V_b), 54, 58
bypass, **9**

calibration, 9, **19–42**
carrier gas, 138
center of bin n x-value (x_n), 66

Centre National d'Etudes Spatiales (CNES), *110*, 111
charcoal, 138
char coal, 138
Chemical Transfer Model (CTM), 6
Chemstation
    version, 132
Chloro Fluoro Carbon (CFC), 2, 3, 5–7, 21, 24, 26, 35, 40, 53, 58–60, 62, 64, 66–69, *70*, 72–75, 138
Chrompac, 14
`chtrap.m`, *133*
circlips, 140
circuit, 141
circuit board, 141
`cleanp`*wp*`.s`, *134*, 143
`cleant`*trap*`.m`, *133, 134*
Climate Monitoring and Diagnostic Laboratory (CMDL), 20, 104
`clp7we.s`, *134*
coefficients, 27
column, 14
compact disc, 135
compression, 135, 136
computer
    for analysis, 131, 132, 136–138
`conc`, 74
concentration ratio between trap outflow and inflow (P), 55, 56, 75, 76
copper, 138, 141

data, 135
`data.dat`, 11, 148
depth in adsorption bed (x), **62**, 66
desorption, **7**, 19, 25, 105, 106, 140
    efficiency, 13
desorption coefficient (K_d), **62**, 63, 68
desorption coefficient (κ_d), 53, 62, 63, 71, 74
desorption during one model timestep (ΔN_d), 66, 68
Determination In situ by Rapid Analytical Chromatography (DIRAC), 90, 118, 120, 121
difference in area estimation (D_l), 92
dilution, 140
diode
    temperature dependence of, 137
diodes, 13
dry mass of the atmosphere (M_a), 3
dry mass of the atmosphere above the tropopause (M_u), 3

`E:`, 135, 149
ECD respons function (g), **27**, *28*, 30, 42, 95, 152, *152*
ECD respons function high part (g_h), **27**, *152*
ECD respons function low part (g_l), 26, **27**, *152*
ECD respons offset term (γ_l), 27, *152*
Electrochemical Concentration Cell (ECC), 112, 116
Electron Capture Detector (ECD), 19, 20, 26, 27, *28*, 30, *31*, 35, 36, *36*, 37, *38*, 39, *39*, 40, 90, 94, 95, *152*
electron capture detector, 138
`endspl.m`, *133*
epoxy, 141
estimation of pressure parameter from μ (Φ), 85, *85*
European Centre for Medium-Range Weather Forecasts (ECMWF), 116
evacuation, 140
exchange of CFC during a model timestep (ΔN), 66

`fcleanp`*wp*`.s`, *134*
ferrules, 25, 105
file, 135
    flight log, 139
    for analysis, 132, 135
    of flow meter reading, 11
    with analysis data, 135
files, 135
fitting, 26, 27
flight, 22, 106, 139–141
Flight Trajectory Data (FTD), 17
flight analysis, 140

flight program, 9–11, 139, 141
flow, 11, 22, 26, 139–141
  integration, 11, **11**, 139
flow linear velocity (v), 57, 58, 62, **62**, 63, 66–68
flow meter respons function (f_n), 23, **23**, 24, 25, 42, 151
flow meter respons function (u_n), 23, **23**, 151, *151, 152*
flow meter voltage readout (U_f), 23, 24, 89, 93, 151
flowmeter voltage of switch point (U_max), **23**, *151, 152*
flow controller, **22**, 22–23, 26, 138, 139
flow meter, 11, 19, 25, 139
  calibration, *22*, **22**–**23**, 139
  reading, 26, 139
  response of, 26
flow meter reading, 11
flushing, 9, 140
`fr_prms.h`, 11, 143, 144, 147, 148
`from_pc`, 148

Gas Chromatograph (GC), 7, *9*, 14, *15*, 16, 19, 26, 29, 30, 44, 51, 86, 106, 131, 132, 136–138, 141
gas chromatograph, **138**, 148
`GCAT`, 139
`gcat.cpp`, 148
`gcat.exe`, 141, 143, 144, 146
Global Positioning System (GPS), 16
gold, 140
graphite, 25, 105

Halocarbons and other Atmospheric Trace Species (HATS), 59, 102
HALogens and OZone loss (HALOZ), *110*, 116, 121
`heater.mac`, 137
heater box, 131, 132, 135, 136, **136**–**137**, 138, 140, 148
heating, 7, 106, 135, 136, 140
  initialization, 137
heating system, **13**–**14**, 106, 131, 140, 141
helium, 141
Hewlett Packard (HP), 14

ideal gas law proportionality coefficient (K), 58
Improved Limb Atmospheric Spectrometer (ILAS), 109, *109*, 116
`IN-OUT`, 13
inflow to model bin (N_g), 69, 70, *70, 71*, 72, *73*
inflow to trap during one model timestep (ΔN_in), 66–68, 70
inlet tube, 11
integration uncertainty function (E_i), 92

Jet Propulsion Laboratory (JPL), 120

lead battery, 141
leak, 139–141
leak test, 139–141
length of timestep in Dessim (Δt), 62, 63
length of trap (x_t), 62, **62**
life time (τ), 4
Lightweight Airborne Chromatograph Experiment (LACE), 118, 120, 121
line over pressure (p_l), **84**
linearity test, **26**–**141**
logarithm, 26

macro, 132, 135
main column, 14, 138
makeup flow, 138
mass (m), 58, 84
mass Carboxen in trap (m_c), 58
mass CFC in sample (m_CFC), 24, 40, 94, 152
mass flow (μ), 23, **23**, 40, 84, *85*, 94, 97
maximum allowed mass-flow (μ_max), 57, 58
maximum allowed sample mass (m_max), 58
maximum allowed sample volume (V_max), 57, 58

mean age of airmass ($\bar{\Gamma}$), 3
melting, 141
method, 132, 140
mixing ratio (χ), 3
mixing ratio (c), 24, 32, 40, 93, 94

Nafion drier, 138, 141
National Oceanic and Atmospheric Administration (NOAA), 20, 44, 47, 51, 59, 104, 141
net export of tracer (Γ), 4, 5
`newbypas.m`, 30, *133, 134*
`newpos`*wp*`.s`, 30, *134*
`newshutd.m`, *133*
nichrome, 14
nitrogen, 14, 26, 138–141, 145
noise, 13, 140
number of adsorption cites in a model bin (N_L), **72**, *73*
number of adsorption cites in trap ($N_\mathrm{L,tot}$), 72
number of theoretical plates (N), 56, **56**, 57, *57*

Observations of the Middle Stratosphere (OMS), *110*, 116, 120, 121
outflow from second trap during one model timestep (ΔN_out), 70
oven, 137
  temperature of, 14
overflow valve, 11
`OvFlw`, 13
oxygen, 138

part of simulation bin (m), 58, 70, 71, *73*
partition, 135
path, 136, 148
`PC_man`, 139
`pc_man`, 131, 145–147
peak area (A), 24, 27, *28*, 30, 35, 39, 93, 95, 97, 152
peak area limit (A_lim), 27, 95, 97, *152*
peak area, 26
potential temperature (θ), 1, 5, 6, 17
Potential Vorticity (PV), 116
potential vorticity (q), 5, 6
pre-column, 14
pressure, 11
  level, 7, 9, 11
pressure (p), 58
pressure parameter (ϕ), **85**, *85*
pressure meter, 9
pre column, 138
printer, 135
program
  analysis, 131, **132**–**136**, 138
`Prss`, 13
pump, 9, 11, 22, 23, 25, 105
pumping, 7, 9
`purge.m`, *133*
purging, 11, 138

ramping, 139
rate constant (k'), 55, *56*
`readee.exe`, 147
regression, 26, 27, 35
regulator, 138
remnants
  of sample, 13
resistance
  trap position, 139
resistor, 140
retention time (t_R), 56
retention volume (V_R), 56, 57
retention time, 141
reverse flow, 141
RS232, 135, 137
rubber, 25, 105
rubber diaphragm, 25

`s1by16.s`, *134*
`s1of2.s`, *134*
`s2by16.s`, *134*
`s2by8.s`, *134*
`s3by16.s`, *134*
`sampl`*time*`.m`, *133, 134*
`sampl`*time*`.s`, *134*
sample, 25–27
sampled volume (V), 35, 56, 58, 84
samples, 26, 27, 30, 32, 138
sample box, **7**, 27, 32, 131, *133*, 136–138
sample size, 11

sampling, 7, **9**–**11**, 22, 27, 141
sampling time (t_s), 24, 27, 93
sampling time, 139
`schtrap.m`, *133, 134*
second heating, 13
Serial A, 135
short circuit, 141
Spring-to-Autumn Measurements and Modelling of Ozone and Active species (SAMMOA), 98, 109, *110*, 116, 121, 122
`stand`*time*`.m`, *133, 134*
`stand32.s`, *134*
standard, 9, 134, 138, 141
  air, 20, 26, 141
  synthetic, 26, 138, 140
standard cubic centimeter (SCC), 24, 58, 152
standard cubic centimeter per minute (SCCM), **22**, 23, 58, 60, 62, 76, *77*, 152
standard deviation of gaussian distribution (σ), 56
`start.m`, *133*
steady state mixing ratio (σ), 4
steel, 25, 105, 138, 141
stepping, 136
`Stnd`, 13
storage, 11
`StoreState`, 13
Stratospheric Aerosol and Gas Experiment (SAGE), 90
subsystems, 26
surface, 105
Swedish Institute of Space Physics (IRF), 7, 138
Swedish Space Corporation (SSC), *110*, 111
switch point in mass flow calibration fitting ($\mu_{\max,n}$), 23, **23**
switches, 141
Systeme d'Analyse par Observation Zenithale (SAOZ), 109, *109, 110*, 116, 120, 121, *124*, *126*

Teflon, 105
temperature, 25
  of traps, 138
temperature (T), 17, 58
temperature dependence
  of diodes, **13**–**14**
`temptime`, 135
test sample, 106
test samples, 106
Third European Stratospheric Experiment on Ozone (THESEO), 90, 98, 109, *110*, 111, 116, 118
time (t), 55, 56, 68, 70, 75
time of 50% breakthrough (τ), 55, 56
total number of model bins (b), 62, **62**, 63, *63*, 68
trap, 106, 141
  resistance of, 106
  temperature of, 106
trap individual respons factor (r), **29**, 30, *40*, 42
trap pressure (p_t), 85
`trap`*trap*`.m`, 14, *133, 134*, 136, 148, 149
traps, 7, **7**, 9, 11, 26, 30, 106, 135, 136, 138
  heating of, 13–14, 132, 140, 141
  individual response of, *28*, **27**–**30**
  resistance of, **13**
  temperature of, 13, 135
  voltage over, 13
trap position, 137
trend, 32

University of East Anglia (UEA), 20, 44

Valco valve, 7, 136, 137, 139, 141
`vel`, 74
version
  of DESCARTES, 7, **7**
  program, 132
`VN2`, 13
`vol`, 74
volume flow rate (ω), 84

`wait.m`, *133*
waiting position, 30, 106
Wall-Coated Open Tubular (WCOT), 14

width of bin in Dessim (Δx), 62, **62**, *63*, 66, 69
`win.ini`, 132

zero reading from flowmeter (z_f), 22, 23, **23**, 24, 93, 151